Metabolic Remodeling of Human B-Cells During Latent Epstein-Barr Virus (EBV) Infection

Metabolic Remodeling of Human B-Cells

During

Latent Epstein-Barr Virus (EBV) Infection

A dissertation presented

by

Liang Wei Wang

to

Division of Medical Sciences

in partial fulfilment of the requirements

for the degree of

Doctor of Philosophy

in the subject of

Virology

Harvard University

Cambridge, Massachusetts

May 2019

Dissertation Advisor: Benjamin E. Gewurz Liang Wei Wang

Metabolic Remodeling of Human B-Cells During Latent Epstein-Barr Virus (EBV) Infection

Abstract

Epstein Barr-virus (EBV) is a ubiquitous herpesvirus that causes infectious mononucleosis and is associated with a variety of human cancers. Ordinarily, EBV persists in healthy individuals by establishing latent infection in the B-cell compartment. Immunosuppression can result in unchecked outgrowth of latently infected cells, culminating in lymphoproliferative disorders and lymphomas. How EBV induces and supports the physiological shift from quiescence to long-term growth and proliferation as modeled by in vitro lymphoblastic transformation is unknown. Multiplexed proteomics on de novo infected primary B-cells was performed to uncover metabolic and signaling pathways that facilitate outgrowth and survival of B-cells latently infected with EBV. By combining chemical inhibitor studies and clustered regularly interspaced short palindromic repeats (CRISPR) genetic perturbation experiments, we discovered viral upregulation of mitochondrial one-carbon (1C) metabolism and de novo synthesis of serine, cholesterol and fatty acids, to be crucial for EBV-positive B-cell proliferation and viability. We demonstrated that mitochondrial 1C metabolism broke down serine to generate formate for nucleotide synthesis, glycine for glutathione production and cellular reducing power in the form of NADPH. We also showed that intramitochondrial NADPH was important for efficient LCL proliferation. De novo serine synthesis (DNSS) may augment 1C metabolism and/or buffer the infected cells from external fluctuations in serine availability. Both mitochondrial 1C metabolism and DNSS depended on EBV-encoded nuclear antigen 2 (EBNA2) and its target MYC for activation. EBV-infected cells also utilized cholesterol and fatty acid synthetic pathways to produce geranylgeranyl pyrophosphate (GGPP) and palmitate, respectively, to reorganize the signaling milieu of the transforming cell. Rab geranylgeranyltransferase was specifically required for EBV-positive B-cell outgrowth and proliferation. We also identified RAB13 as a

potent driver of latently infected cell growth and survival, whose expression was driven by EBNA3C and likely functioned as a chaperone for viral latent membrane proteins (LMPs) to maintain the latter's oncogenic signaling capacities. Taken altogether, our results provide an expansive investigation into the pathways that underlie the transformative change of a B lymphocyte from quiescence to activation and growth and identify vulnerabilities in EBV-driven lymphoblastic disorders that may represent new therapeutic targets.

Table of Contents

Abstract iii
List of Figures and Tables ix
Acknowledgements xiii
Chapter I: Introduction 1
Epstein-Barr Virus (EBV): Genome Structure and Gene Expression 2
EBNA2 is a Viral Regulator of MYC Expression 4
MYC as a Master Regulator of Cellular Metabolism 5
Latent EBV Infection of B-Cells Parallels the Germinal Center Reaction 6
Epidemiological Associations of EBV with Lymphoproliferative Disorders and Cancers 9
Metabolic Reprogramming in Cancers and DNA Virus Infections 10
Induction of Aerobic Glycolysis (the Warburg Effect) 10
Mitochondrial One-Carbon (1C) Metabolism 13
De Novo Serine Synthesis (DNSS) 19
Mevalonate Metabolism and De Novo Lipid Biosynthesis 22
Chapter II: Quantitative temporal viromics reveal dynamic, global changes to the host and viral proteomes during primary B-cell infection with EBV 29
Contributions 30
Abstract 31
Introduction 31
Materials and Methods 32
Culture of established cell lines 32
Primary human B-cell isolation and culture 33
EBV infection of primary B-cells 34
Antibodies, reagents and kits 35
Cell preparation for three biological replicates of TMT proteomic analysis 36
Protein preparation for TMT-based proteomics 37
Peptide fragmentation and detection by LC-MS3 39
Analysis of LC-MS3 data 40
Gene Set Enrichment Analysis (GSEA) 42
Nuclear imaging and cell diameter measurements 42
Immunofluorescence microscopy 43
Immunoblotting 43
Flow cytometry analysis 44

LC-MS metabolite analysis 44
Natural isotope correction 45
Growth curve analysis 47
Mitochondrial stress test 48
Results 48
EBV infection of primary B-cells induces a drastic increase in cell size 48
EBV upregulation of human B-cell metabolic pathways 49
Early induction of aerobic glycolysis in newly infected B-cells 61
EBV remodels the B-cell mitochondrial proteome, dynamically altering respiratory chain complex subunit abundances 65
Discussion 73
Chapter III: EBV upregulates mitochondrial 1C metabolism and DNSS in B-cells to support metabolic demands of transformed cell growth and proliferation 76
Contributions 77
Abstract 78
Introduction 79
Materials and Methods 81
Antibodies, reagents and kits 81
Agonist stimulation of primary B-cells 83
LC-MS metabolite analysis 83
Natural isotope correction 85
Flow cytometry analysis 85
Immunofluorescence microscopy 86
In vitro transformation assays 87
Growth curve analysis 88
CRISPR editing in GM12878 LCL 88
Kit-based quantitation of ATP, NAD(P)H and extracellular lactate 89
Quantitative PCR 89
Mitochondrial stress test 90
Results 91
EBV upregulates mitochondrial one-carbon metabolism via EBNA2 and MYC 91
EBNA2 and MYC upregulate B-cell import and mitochondrial 1C catabolism of serine 97
EBNA2 and MYC upregulate de novo synthesis of the 1C fuel serine 101
Serine catabolism and mitochondrial 1C are critical for EBV-infected B-cell growth 104
EBV-induced mitochondrial 1C metabolism generates compartment-specific NADPH 112

Serine-derived formate fuels infected B-cell nucleotide synthesis 117
Viral activation of mitochondrial 1C generates glutathione for redox and glycine toxicity defense 122
Discussion 129
Chapter IV: EBV upregulates mevalonate metabolism to support protein geranylgeranylation and LMP trafficking 133
Contributions 134
Abstract 134
Introduction 135
Materials and Methods 138
Culture of established cell lines 138
Primary human B-cell isolation and culture 139
EBV infection of primary B-cells 140
Antibodies and reagents 140
Immunoblot analysis for RAB13 141
Flow cytometry 142
Immunofluorescence 142
Growth curve analysis 143
CRISPR editing in GM12878 LCL 143
Quantitative PCR 145
Bioinformatic analysis 145
Results 146
EBV strongly induces cholesterol and fatty acid syntheses in newly infected B-cells 146
SREBPs, EBNA2 and MYC induce cholesterol and fatty acid biosynthesis enzymes 155
The mevalonate pathway product geranylgeranyl pyrophosphate is important for EBV-infected B-cell outgrowth 165
The Rab geranylgeranyltransferase GGT-II complex is important for EBV-driven B-cell outgrowth 170
EBNA3C-induced RAB13 is critical for LMP1/2A trafficking and, LCL growth and survival 176
Discussion 189
Chapter V: Dissertation Perspectives 194
Summary of Results 195
Discussion 196
MYC, NF-κB and mTOR pathways co-regulate EBV-infected cell metabolism 196
Additional roles for mitochondrial 1C and mevalonate metabolism 199

Concluding Remarks 200
Appendices 202
References 220

List of Figures and Tables

Table of Contents.....v

Chapter I: Introduction

Figure I.1 Schematic of one-carbon metabolism. 14
Figure I.2 Schematic of cholesterogenic and lipogenic pathways. 24
Figure I.3 Schematic of SREBP regulation and activation. 26

Chapter II: Quantitative temporal viromics reveal dynamic, global changes to the host and viral proteomes during primary B-cell infection with EBV

Figure II.1 EBV infection induces an early increase in cell size concomitant with mTOR activation.....49
Figure II.2 Outline of the proteomics approach and confirmation of viral gene expression. 50
Figure II.3 Strong concordance between biological replicates. 51
Figure II.4 k-means clustering of quantified B-cell proteins based on averaged relative abundances. 53
Figure II.5 Plot of within-class variance against number of classes. 54
Figure II.6 DDX1 and DDX46 levels remain unchanged over the infection time course. 54
Figure II.7 Term enrichment analysis for proteins significantly upregulated at 4 DPI. 55
Figure II.8 Heatmap temporal proteomic plots of EBV proteins quantified in any of the three WCL replicates.....56
Figure II.9 Temporal proteomic profiles of EBNA and MYC proteins. 57
Figure II.10 Primary sequences of two newly discovered EBV gene products. 58
Figure II.11 Flow cytometric analysis of newly infected B-cells for surface gp350 abundance...59
Figure II.12 EBV remodels the plasma membrane proteome. 60
Figure II.13 Early upregulation of large amino acid transporter subunits. 61
Figure II.14 Heatmap of averaged relative abundances of glycolytic enzymes. 62
Figure II.15 Glucose transporter SLC2A1 expression is upregulated during EBV infection. 63
Figure II.16 EBV induces high rates of glucose consumption and glycolytic flux. 64
Figure II.17 EBNA2 upregulates glycolysis. 65
Figure II.18 Substitution of glucose with galactose inhibits newly infected cell growth. 66
Figure II.19 Heatmap of detected mitochondrial proteins over the infection time course. 67
Figure II.20 Heat map of averaged relative abundances of mitochondrial electron transport chain components. 69
Figure II.21 EBV-induced OXPHOS upregulation is crucial for outgrowth of newly infected cells. 71
Figure II.22 Analysis of changes to the mitochondrial proteome highlights ribosome biogenesis and one-carbon metabolism. 72
Figure II.23 Early upregulation of folate-dependent one-carbon metabolism in newly infected cells. 73

Chapter III: EBV upregulates mitochondrial 1C metabolism and DNSS in B-cells to support metabolic demands of transformed cell growth and proliferation

Figure III.1 ATF4 is dispensable for MTHFD2 expression. 91
Figure III.2 Lytic reactivation does not contribute to enhanced mitochondrial 1C enzyme expression. 92
Figure III.3 Equal infection of primary human B-cells with various EBV strains....93
Figure III.4 B95-8 induces the expression of mitochondrial 1C enzymes. 94
Figure III.5 EBNA2, MYC and their binding partners co-localize at the MTHFD2 promoter....94
Figure III.6 EBNA2 regulates MTHFD2 expression in LCLs. 95
Figure III.7 The EBNA2 target gene MYC controls MTHFD2 expression in LCLs. 96
Figure III.8 Net consumption of serine and glycine by newly infected B-cells. 97
Figure III.9 EBV EBNA2 induces ASCT1 and ASCT2 expression and trafficking to the cell surface. 98
Figure III.10 Serine deprivation leads to a proliferative defect in newly infected B-cells. 99
Figure III.11 Serine is preferentially consumed by the mitochondrial branch of one-carbon metabolism. 100
Figure III.12 EBV induces DNSS enzyme expression in newly infected cells. 101
Figure III.13 PHGDH inhibition leads to proliferative defects in EBV-infected B-cells. 102
Figure III.14 EBV induces DNSS flux which is augmented by serine depletion from media. 103
Figure III.15 EBNA2 and its target MYC regulate DNSS gene expression in LCLs. 104
Figure III.16 Inhibition of mitochondrial 1C metabolism impairs newly infected cell outgrowth. 105
Figure III.17 SHIN1 and MTH-1479 exert on-target effects on mitochondrial 1C metabolism. .106
Figure III.18 Inhibition of one-carbon metabolism reduces proliferation and increases death of EBV-infected B-cells. 107
Figure III.19 Formate supplementation rescues the SHIN1-induced proliferative defects. 108
Figure III.20 SHIN1 decreases transformation efficiency of EBV infection. 109
Figure III.21 MTHFD2 KO in LCLs leads to G1/S arrest. 110
Figure III.22 KO of endogenous MTHFD2 can be rescued with sgRNA-refractory cDNA encoding wild-type MTHFD2. 111
Figure III.23 Primary B-cell stimulation with myriad agonists activates one-carbon metabolism. 112
Figure III.24 EBV downmodulates G6PD protein expression. 113
Figure III.25 EBV selectively increases overall NADPH/NADP ratios in newly infected cells. ..114
Figure III.26 One-carbon metabolism is a significant source of NADPH in newly infected cells. 115
Figure III.27 Expression of a mitochondria-localized NADPH oxidase (TPNOX) impairs LCL growth and/or survival. 116
Figure III.28 EBNA2-regulated MTHFD2 expression increases whole cell NADPH/NADP ratios. 117
Figure III.29 Serine depletion-induced proliferative defects in newly infected cells can be rescued by formate supplementation. 118
Figure III.30 Inhibition of one-carbon metabolism does not provoke the DNA damage response, reduce mitochondrial DNA or viral genome copy numbers, or diminish the mitochondrial membrane potential. 119
Figure III.31 Formate supplementation rescues purine synthesis in newly infected cells. 121
Figure III.33 GCS subunit abundances are not strongly enhanced early in infection. 123

Figure III.34 EBV induces glutathione synthesis and 1C blockade increases cellular ROS levels. 124
Figure III.35 One-carbon metabolism contributes strongly to intracellular glycine and glutathione pools. 126
Figure III.36 Serine withdrawal sensitizes newly infected cells to BSO-mediated glutathione depletion. 128
Figure III.37 Summary of key metabolic pathways induced by EBV and investigated in this work. 129

Chapter IV: EBV upregulates mevalonate metabolism to support protein geranylgeranylation and LMP trafficking

Figure IV.1 Cholesterol and lipid biosyntheses are highly upregulated early in infection. 147
Figure IV.2 EBV induces LDLR expression in newly infected cells. 149
Figure IV.3 Schematic diagram showing de novo lipid synthesis pathway conversion of glucose-derived acetyl-CoA into end products. 150
Figure IV.4 Inhibition of de novo lipid synthesis leads to proliferative defects in newly infected cells. 151
Figure IV.5 Newly infected B-cells depend on palmitate for triglyceride and phospholipid synthesis and protein palmitoylation. 152
Figure IV.6 KEGG analysis reveals SNARE function and vesicular transport as key palmitoylation-regulated processes in newly infected cells. 153
Figure IV.7 EBV upregulates SREBP2 expression in newly infected cells. 155
Figure IV.8 LCL growth and survival depends on SREBP2, not SREBP1. 156
Figure IV.9 SREBP inhibition causes proliferative defects in newly infected B-cells. 158
Figure IV.10 EBV-transformed LCL growth and/or survival depends on SREBP activity. 160
Figure IV.11 EBNA2 and MYC co-occupy the ACACA promoter. 161
Figure IV.12 EBNA2 and/or EBNA-LP activate MYC and ACC1 protein expression. 162
Figure IV.13 EBNA2 and MYC co-regulate ACC1 and HMGCR expression. 164
Figure IV.14 Statin treatment of newly infected cells induces proliferative defects, including increased cell death. 166
Figure IV.15 Statin-induced proliferative defects are significantly ameliorated by geranylgeranyl pyrophosphate (GGPP). 168
Figure IV.16 Flow cytometric analysis of CFSE dye dilution proliferation and 7-AAD cell death assays in newly infected primary B-cells or GM12878 LCL. 169
Figure IV.17 Simvastatin treatment induces apoptosis of newly infected cells, which can be reversed by GGPP supplementation. 170
Figure IV.18 EBV enhances the subunit expression of GGT-II, not GGT-I. 171
Figure IV.19 Chemical epistasis shows that newly infected cells are more reliant on GGT-II. .172
Figure IV.20 Newly infected cells are more sensitive to GGT-II inhibition. 173
Figure IV.21 Ablation of GGT-II, not GGT-I, causes LCL growth inhibition and/or death. 174
Figure IV.22 CRISPR ablation of GGT-II, not GGT-I, leads to consistent diminution of LCL growth and/or survival. 175
Figure IV.23 Rab proteins are dynamically regulated during EBV infection of primary human B-cells. 177
Figure IV.24 EBNA3C activates RAB13 expression. 179
Figure IV.25 RAB13 co-localizes with LMP2A in newly infected cells. 181

Figure IV.26 RAB13 regulates LMP1 and LMP2A signaling. 184
Figure IV.27 RAB13 colocalizes with LMP1 and LMP2A in LCLs. 186
Figure IV.28 Model of EBV-induced cholesterol and lipid biosynthesis pathways remodeling and roles in LMP trafficking. 188

Appendices

Table S1 Full details of enriched terms in Figure II.7. 202
Table S2 Full details of “Mitochondrion” enriched clusters and their components amongst upregulated proteins in Figure II.22. 205
Table S3 GSEA re-analysis of metabolism-related proteins detected in the transformation QTV. 209
Table S4 Full details of enriched terms as shown in Table S3. 210

Acknowledgements

I would like to express my gratitude to my doctoral advisor, Dr. Benjamin Gewurz, for being supportive of my various endeavors throughout graduate school. In day-to-day scientific work, Ben challenges me to think rigorously about my experiments and gives me ample opportunities to attend conferences around the world and the chance to mentor younger members of the group. His breadth of knowledge has also been instrumental in guiding and inspiring me to consider my work in a broader context, and to formulate intellectually meaningful questions that also make a difference to medicine.

I would also like to thank Dr. Frederick Wang, Dr. James DeCaprio, Dr. Nicholas Dyson and Dr. Vamsi Mootha for their service on my dissertation advisory committee. They have been instrumental in providing critical reviews of my work, giving much needed encouragement during the challenging periods of my doctoral career and suggesting new and interesting directions to expand my intellectual horizons as a scientist. I would also like to extend my sincerest thanks to my examiners – Dr. Samuel Rabkin, Dr. Brendan Manning and Dr. Micah Luftig – for taking precious time off their busy schedules to participate in my dissertation defense.

Throughout my time at Harvard, the Ph.D. Program in Virology has been central to my career as a graduate student. I would like to thank Dr. David Knipe, Dr. Sean Whelan and various faculty members whom I have had the fortune of interacting with over the last five years, for their inspiration and mentorship. It has been a fantastic and humbling experience journeying with my class of virologists. My heartfelt thanks go to Joseph Cabral and Max Mertens of the Knipe laboratory for their generous help and advice regarding all things related to herpesviruses. I am also grateful to Matthew Lim from Dr. Steven Gygi's group for useful discussions on proteomic analysis and beyond, as well as being a great friend and critical reader of my work.

I would also like to extend my gratitude to members of the Channing Laboratory and the Division of Infectious Diseases at Brigham and Women's Hospital, particularly Dr. Elliott Kieff, Dr. Bo Zhao, and past and present members of the Gewurz group, especially Dr. Yijie Ma, Dr. Chang Jiang, Dr. Rui Guo and Dr. Nicholas Smith, for their support, encouragement, advice and guidance in the last five years. Special thanks go to the students whom I have had the privilege of mentoring – Jason Nomburg and Zhonghao Wang – for being excellent help at the bench, as well as our unsung technician heroes – Michael Walsh, Stephen Trudeau, Molly Schineller and Emma Wolinsky – who have been instrumental in making sure everything in the laboratory goes like clockwork. I would also like to thank Dr. Agnieszka Szymula from Dr. Kenneth Kaye's group for providing critical feedback on my work.

I am immensely grateful for the productive collaboration I have had with Dr. Vamsi Mootha, Dr. Hongying Shen and Bryn Reinstadler. I came into metabolic research with nothing more than college-level biochemistry, and both Dr. Mootha and Dr. Shen have been the most patient, knowledgeable and inspiring teachers I could ever hope for. I would also like to specially mention Dr. Melissa Walker and Dr. Eran Mick for their technical expertise with the Seahorse XF24 instrument.

I am sincerely thankful for the Agency for Science, Technology and Research (A*STAR) in Singapore for generously funding my undergraduate and doctoral studies, as well as childcare support from the Graduate School of Arts and Sciences (GSAS) at Harvard University. Because of their financial support, I was able to focus on my doctoral studies with no worries.

Last but not least, my heart goes out to all my family and friends who have been supportive in my research career since day one and made extraordinary effort organizing to meet up over the last nine years whenever I was home. I am especially thankful for my wife, Esther, and my daughter, Emily, for being patient with me on the days, weeks and even months when I had to be away from them to finish up my projects. They have been the epitome of forbearance,

strength and love, which I can only hope to measure up to. More importantly, they remind me to have perspective and balance, to work hard and also play hard. I would like to thank my parents, my brother, my parents- and siblings-in-law for being ceaselessly supportive and helpful with caring for Esther and Emily when I had to be away. I am also grateful to my friends and leaders from church – Rev. Andrew Kerhoulas, Rev. Daniel Paik, Michael and Charlene Saji – who have prayed for me on multiple occasions and walked alongside me during the tough times and created a community which I now call home. Gloria in excelsis deo!

Chapter I: Introduction

Epstein-Barr Virus (EBV): Genome Structure and Gene Expression

EBV is a double-stranded DNA (dsDNA) virus that displays tropism predominantly towards B lymphocytes and epithelial cells. Notably, EBV has attained evolutionary success; the vast majority (~95%) of adults worldwide are persistently infected by the virus, many of whom are not symptomatic. The virus was discovered and characterized by Anthony Epstein, Bert Achong and Yvonne Barr, using samples of African lymphomas obtained from Denis Burkitt (Epstein, Achong and Barr, 1964; Epstein *et al.*, 1965; Epstein, Barr and Achong, 1965). During initial infection of B-cells, virions engage host cell complement receptor 2 (CR2, also known as CD21) via gp350 (Fingeroth *et al.*, 1984), leading to attachment. Virion endocytosis and membrane fusion in a low-pH compartment mediate penetration of the limiting endosomal membrane (Tanner *et al.*, 1987; Nemerow and Cooper, 1984). Transport of the capsid and subsequent release of the viral genome into the nucleus leads to the onset of viral gene transcription. However, steps between membrane fusion and nuclear deposition of the viral genome in B-cells remain poorly defined (Valencia and Hutt-Fletcher, 2012).

The prototypical B95-8 laboratory strain of EBV was isolated from a patient with infectious mononucleosis (IM), a condition marked by febrile illness, sore throats, enlargement of lymph nodes and fatigue. The genome is approximately 172 kilobase pairs in length (Baer *et al.*, 1984) with coding potential for about 80 proteins (Young, Arrand and Murray, 2007), which agrees with a recent report where lytic induction of EBV-positive Akata and P3HR-1 Burkitt's lymphoma (BL) cells resulted in detectable increases in approximately 70 EBV-encoded proteins (Ersing *et al.*, 2017). During initial infection of B-cells, the linear viral DNA genome circularizes to form covalently closed circular DNA in the nucleus and is rapidly chromatinized.

Promoter usage varies over the course of transformation from resting B-cells into lymphoblastoid cell lines (LCLs) (Price and Luftig, 2014). The first wave of viral gene transcription occurs within the first two days post-infection and entails the induction of EBV-

encoded nuclear antigen 2 (EBNA2), EBNA-leader protein (EBNA-LP) and potent BCL-2 mimics BALF1 and BHRF1 (Altmann and Hammerschmidt, 2005) through the activation of the W promoter (Wp). The infected cell then uses the C promoter (Cp), leading to a strong decline in Wp activity, producing EBNA1, EBNA2, EBNA-LP, EBNA3A, EBNA3B and EBNA3C; this switch from Wp to Cp is regulated by Wp methylation (Woisetschlaeger *et al.*, 1990; Alfieri, Birkenbach and Kieff, 1991). While Wp activity wanes, it is not completely silenced in the LCL phase; Cp-initiated EBNA2, as well as known EBNA2 target genes, such as CD23 and c-MYC (herein referred to simply as MYC), are still expressed at levels higher than that in resting, uninfected cells. At this time, viral latent membrane proteins are not yet expressed at LCL levels, and the collective expression of EBNAs, viral BCL-2 mimics and non-coding RNAs constitute the latency IIb program (Price and Luftig, 2015; Klein, Nagy and Rasul, 2013). Later in infection, transcripts encoding LMP1, LMP2A and LMP2B are expressed from the bidirectional LMP promoter (LMPp), which is itself responsive to EBNA2 (Höfelmayr *et al.*, 1999). Circularization of the genome is required for production of full-length, functional LMP2 as the coding sequence traverses the terminal repeat regions. LMP transcripts and low-level expression of LMPs can be detected very early on in de novo infection but translation into protein occurs with delayed kinetics and reaches at LCL-level abundance approximately two weeks post-infection (Price *et al.*, 2012). The expression of the full complement of latency-associated genes – EBNA1, EBNA2, EBNA-LP, EBNA3s and LMPs, along with EBV-encoded non-coding RNAs – constitutes the latency III program (also known as the growth program) seen in EBV-positive LCLs.

In other EBV-carrying cell lines, promoter usage differs. BL cells typically use the latency I expression program where the Q promoter (Qp) is activated to express EBNA1 (Schaefer *et al.*, 1991), which functions to maintain episome tethering to the host's chromosomes; Wp, Cp and LMPp activities are low and usually do not lead to detectable expression of EBNA2, EBNA3s

and LMPs (Nonkwelo *et al.*, 1996; Sample, Henson and Sample, 1992). EBV-positive nasopharyngeal carcinomas, T/NK lymphomas and Hodgkin's lymphomas generally exhibit a classical latency II (also known as latency IIa) expression pattern where EBNA1 and LMPs are expressed; *EBNA1* transcription is driven from Qp while *LMP1* transcription is activated by the EBNA2-independent L1-TR promoter within the terminal repeats (Chen *et al.*, 2001).

EBNA2 is a Viral Regulator of MYC Expression

As mentioned earlier, one of the earliest viral proteins expressed during B-cell infection is EBNA2, a transcription factor that induces a number of cellular genes, such as cluster of differentiation 23 (CD23) (Wang *et al.*, 1987; Wang *et al.*, 1991) and MYC (Kaiser *et al.*, 1999). EBNA2 itself has no intrinsic DNA-binding ability and depends largely on RBP-Jκ to engage its DNA targets (Waltzer *et al.*, 1994; Ling *et al.*, 1994; Ling and Hayward, 1995; Johannsen *et al.*, 1995; Pegman *et al.*, 2006). Over the last 20 years, the role of EBNA2 as a master regulator in the growth program has become elucidated in greater detail. Early studies with P493-6 cells that could conditionally express EBNA2 or a heterologous MYC allele (Schuhmacher *et al.*, 2001b; Schuhmacher *et al.*, 1999) revealed a small number of proteins that were co-regulated by EBNA2 and MYC, and even fewer proteins that were regulated by EBNA2 alone (Schlee *et al.*, 2004). The low resolution of that work was due to the use of 2D-PAGE and emerging mass spectrometric techniques. Subsequently, with the availability of newer high-throughput methods, studies with lymphoblastoid cells that conditionally express EBNA2 showed a relatively small subset of host genes to be regulated directly by EBNA2, and even fewer genes that are co-regulated by EBNA2 and MYC (Zhao *et al.*, 2006). During normal B-cell development, RBP-Jκ interacts with Notch intracellular domain (NICD), a protein fragment released subsequent to Notch receptor activation and proteolytic processing. EBNA2 mimics NICD (Höfelmayr *et al.*, 1999; Hsieh *et al.*, 1996; Hofelmayr *et al.*, 2001; Strobl *et al.*, 2000; Gordadze *et al.*, 2001) and activates transcription of RBP-Jκ bound genes by masking RBP-Jκ's transcription repression

domain, thereby displacing co-repressor complexes that normally inhibit transcription (Hsieh and Hayward, 1995). Next-generation sequencing and more sophisticated methods of capturing spatiotemporal details at the chromatin level have further revealed that EBNA2 actually participate in super-enhancer formation and the resultant EBV super-enhancers highly transactivate target genes (Jiang *et al.*, 2017; Zhou *et al.*, 2015; Gunnell *et al.*, 2016). Notably, optimal transactivation of the *MYC* gene is dependent on long-range looping of upstream super-enhancers bound by EBNAs, including EBNA2 (Jiang *et al.*, 2017). The expression kinetics of EBNA2 and the remodeling phenotype of the newly infected B-cell in the first three days before cell division occurs agree with the reported role of MYC as a controller of cell size (Schuhmacher *et al.*, 1999) and underscore the role of EBNA2 transactivation of MYC in the rewiring of B-cell metabolism to meet the immense energetic and biosynthetic demands of proliferation.

MYC as a Master Regulator of Cellular Metabolism

MYC was first described as a cell-transforming gene found in avian myelocytomatosis virus MC29 and subsequently discovered to have a cellular homolog in humans (Vennstrom *et al.*, 1982). In humans, there are several MYC-related genes with c-MYC being the best known due to its pleiotropic effects and frequent activation in cancer (Beroukhim *et al.*, 2010; Koboldt *et al.*, 2012).

MYC family members share a similar domain architecture – they have a transactivation domain, a linker domain and a basic helix-loop-helix (bHLH) domain. The bHLH domain mediates heterodimerization with MAX to produce a transactivation-competent complex. The MYC-MAX heterodimer is then capable of engaging E-box sequences (canonical: 5'-CACGTG-3') in the target gene promoter to activate gene transcription (Reisman *et al.*, 1993; Berberich *et al.*, 1992; Nair and Burley, 2003). E-boxes occur with relatively high frequencies across the genome, with slight variations to the consensus sequence dictating transcription factor binding affinity

(Allevato *et al.*, 2017). Activating transcription factors (ATFs) and sterol regulatory element binding proteins (SREBPs) also possess bHLH domains that recognize E-boxes. Dysregulated MYC expression in the context of tumors is able to alter its affinity for non-canonical E-boxes that are normally bound by other bHLH transcription factors, to result in ectopic transactivation of those genes (Allevato *et al.*, 2017).

Various biological functions of MYC have been reviewed elsewhere (Dang, 1999; Dang, 2012). A prominent role of MYC is its regulatory function in myriad metabolic pathways (Hsieh *et al.*, 2015). For example, MYC acts in concert with hypoxia-inducible factor 1 (HIF-1) to regulate several glycolytic genes, such as the glucose transporter 1 (GLUT1), hexokinase II (HK2) and lactate dehydrogenase A (LDHA) (Kim *et al.*, 2004; Shim *et al.*, 1997). More detailed discussions of MYC's role in the modulation of cellular metabolism can be found in later sections.

Latent EBV Infection of B-Cells Parallels the Germinal Center Reaction

It is thought that EBV infection of B-cells recapitulates several key aspects of B-cell development and maturation (Thorley-Lawson and Gross, 2004). The germinal center model postulates that naïve B-cells newly infected by EBV undergo phases of development similar to that of B-cells involved in antigen- and T-cell-dependent encounters. Initial infection drives lymphoblastic proliferation via the virus-encoded growth programs (latency IIb and III) that resembles initial B-T conjugation in extrafollicular regions. For normal antigen-activated B-cell blasts to survive selection in the germinal center and enter the memory compartment, continual T-cell help, sustained antigen-dependent interactions with follicular dendritic cells and survival signals must be supplied. To bypass these requirements, EBV-infected B-cells execute the default program [latency II(a)] to provide those signals without need for antigen. Eventually, infected cells exit into the periphery and express the latency 0 program, phenotypically resembling memory B-cells. These cells divide infrequently. However, as the cell expresses

EBNA1, new viral genomes can be passed on daughter cells, thereby ensuring long-term latent carriage. How each transition occurs is not fully understood. However, emerging evidence lend some support to the proposed model e.g. interleukin-10 (IL-10) and interleukin-21 (IL-21) being able to induce LMP1 expression independent of EBNA2 (Kis *et al.*, 2010; Kis *et al.*, 2006), CTCF's role in restricting Cp activity to skew oncoprotein expression towards latency I (Hughes *et al.*, 2012). There are notable limitations to the model e.g. primary infection of adults leading to IM does not lead to a detectable presence of circulating EBV-harboring memory B-cells arising from naïve B-cell infection (Kurth *et al.*, 2000; Kurth *et al.*, 2003), naïve and memory B-cells being equally susceptible to virus infection which may allow bypass of the germinal center reaction/intermediate latency programs (Ehlin-Henriksson, Gordon and Klein, 2003). These observations are largely compatible with the prevailing model if one assumes that tonsillar naïve B-cells and memory B-cells alike can be infected but only the latter can form the virus reservoir.

Virus-encoded oncoproteins provide surrogate signals in place of normal physiological stimuli, such as CD40 ligand (CD40L, also known as CD154) and cytokines provided by cognate T-cells in the presence of specific antigens. These proteins behave like their cellular counterparts to activate survival- and growth-promoting pathways. LMP1, first described for its transforming activity in Rat-1 fibroblasts (Wang, Liebowitz and Kieff, 1985), is a CD40 mimic (Uchida *et al.*, 1999) and is capable of binding tumor necrosis factor receptor-associated factor (TRAF) proteins to induce constitutive, ligand-independent signaling (Wang, Jiang and Gewurz, 2017; Luftig *et al.*, 2003). Expression of chimeric CD40-LMP1 (a fusion of LMP1's cytoplasmic signaling domain with CD40's extracellular ligand-binding domain, which renders LMP1 dependent on CD40L for activation) in murine B-cells is sufficient for the chimeric protein to signal, indicating that LMP1 is able to substitute normal CD40 in vivo and allows the EBV-infected B-cell to bypass the requirement for T-cell help (Rastelli *et al.*, 2008). LMP1 activates a number of pathways, most prominently nuclear factor kappa light-chain enhancer of activated B-

cells (NF-κB), extracellular signal-regulated kinase (ERK)/p38 mitogen-activated protein kinase (MAPK) and c-Jun N-terminal kinase (JNK) signaling (Wang, Jiang and Gewurz, 2017).

On the other hand, LMP2A functions as a B-cell receptor (BCR) mimic (Anderson and Longnecker, 2008; Fruehling and Longnecker, 1997; Mancao and Hammerschmidt, 2007; Merchant, Caldwell and Longnecker, 2000). Unlike cellular BCRs, LMP2A does not require CD79 to recruit protein tyrosine kinases (PTKs) for signal transduction; it carries immunoreceptor tyrosine-based activation motifs (ITAMs) that can regulate B-cell development in vivo (Merchant, Caldwell and Longnecker, 2000) through interaction with Fyn, Lyn and Syk protein tyrosine kinases (Fukuda and Kawaguchi, 2014; Fruehling and Longnecker, 1997). LMP2A signals through the phosphatidylinositol 4,5-bisphosphate 3-kinase (PI3K)/AKT pathway to stimulate mammalian target of rapamycin (mTOR) activity as well as ERK/MAPK (Anderson and Longnecker, 2008), driving myriad pro-growth processes such as protein translation, ribosome biogenesis, lipid synthesis and mitochondrial replication. Although LMP2A is dispensable for newly infected cell outgrowth and long-term LCL growth (Longnecker *et al.*, 1992) and lymphomagenesis in vivo (Ma *et al.*, 2017b), LMP2A expression has been described to be important for rescuing germinal center B-cells that lack functional BCRs (Mancao *et al.*, 2005; Mancao and Hammerschmidt, 2007; Caldwell *et al.*, 1998). We and others have also shown that LCLs do require functional activation of BCR/LMP2A pathways e.g. intact Syk, PI3K and AKT activities (Hatton *et al.*, 2011; Ma *et al.*, 2017c; Cen *et al.*, 2018; Swart *et al.*, 2000). Activation of mTOR was observed during de novo EBV infection of primary human B-cells in vitro. In particularly, two populations of early infected cells, namely proliferated-arrested (PA) and proliferated-proliferated (PP) cells (McFadden *et al.*, 2016), exhibited differential mTOR activities, with PP cells displaying greater signaling flux than PA cells. Efficient outgrowth necessitated mTOR signaling competence, even at time points where LMP2A was not expected to be at LCL-level abundance or signaling strength.

Epidemiological Associations of EBV with Lymphoproliferative Disorders and Cancers

Notwithstanding the fact that EBV has evolved largely to establish and maintain long-term asymptomatic carriage in human hosts, it has been associated with a number of lymphoproliferative diseases and malignancies. Indeed, the discovery of EBV was borne out of Anthony Epstein's astute observation that there might be an underlying pathogenic cause of the African lymphomas described by Denis Burkitt, now known as Burkitt's lymphoma (BL). Almost all BL cells have characteristic translocations between the *MYC* gene locus and an immunoglobulin heavy or light chain enhancer, thereby driving high MYC expression. BL cells typically execute the latency I expression program i.e. EBNA1 and viral non-coding RNAs. Endemic Burkitt's lymphoma (eBL) is strongly associated with co-infections with EBV and malaria in a restricted part of Africa termed the "lymphoma belt" (Rochford and Moormann, 2015). Sporadic Burkitt's lymphoma (sBL) that arises elsewhere in the world exhibit limited involvement of EBV in the range of <20% of cases (Giulino-Roth and Goldman, 2016). Nonetheless, analysis of EBV genomic termini across virus-positive eBL and sBL cases revealed clonal expansion of infected cells, indicating that EBV infection is most likely antecedent to malignant transformation (Neri *et al.*, 1991). EBV-associated cancers with type II latency expression profiles include undifferentiated nasopharyngeal carcinoma (NPC) (Tsao, Tsang and Lo, 2017) and classic Hodgkin's lymphoma (HL) (Shannon-Lowe, Rickinson and Bell, 2017; Murray and Bell, 2015). For these cancers, clonality could also be established in addition to active transcription of latency-associated genes, such as LMP1 (Anagnostopoulos *et al.*, 1989; Gulley *et al.*, 1994; Kwok *et al.*, 2012; Liu *et al.*, 2011), suggesting that EBV may act as a driver of malignant transformation in these cell types.

In vitro transformation of B-cells with EBV is a useful model for understanding immunosuppression-related lymphoproliferative conditions such as post-transplant lymphoproliferative disorder (PTLD) and acquired immunodeficiency syndrome (AIDS)-related

lymphomas as the EBV latency program in both situations is identical i.e. latency III (Dharnidharka *et al.*, 2016; Martinez and Krams, 2017; Moosmann *et al.*, 2010; Carbone, 2003; Fassone *et al.*, 2002). Although carriage of latent EBV in healthy individuals typically does not manifest in clinical symptoms, immunosuppression as happens in co-infection with other viruses e.g. human immunodeficiency virus (HIV) or, treatment with immunosuppressants such as cyclosporine, FK506 and rapamycin, often reduces the effectiveness of host immune surveillance against EBV-infected cells, and permits unchecked growth of those cells (Green and Michaels, 2013; Montone *et al.*, 1996; Nalesnik *et al.*, 1988; Newell *et al.*, 1996). This can also be recapitulated in murine models of LMP1/2A-driven lymphoproliferative disorders under conditions of T- and natural killer (NK)-cell depletion (Wirtz *et al.*, 2016; Minamitani *et al.*, 2017).

Metabolic Reprogramming in Cancers and DNA Virus Infections

Induction of Aerobic Glycolysis (the Warburg Effect)

Aerobic Glycolysis Supplies Key Intermediates for the Anabolic Program

To sustain transformed cell growth and survival, extensive rewiring of the cell's metabolic program has to be achieved (Hanahan and Weinberg, 2011). In the early to mid-20th century, Otto Warburg observed that cancer cells used glycolysis as a means of energy transduction even in the presence of sufficient oxygen (Warburg, 1928; Warburg, 1925). It was perplexing why aerobic glycolysis would be used as the preferred mode of ATP production, when complete oxidation via oxidative phosphorylation (OXPHOS) would yield more ATP per glucose molecule imported into the cell. It has become apparent that the upregulation of glycolysis allows for the cell to acquire key metabolic intermediates that can be used for various anabolic processes e.g. nucleotide and amino acid biosyntheses (Vander Heiden, Cantley and Thompson, 2009), and may even modulate intracellular signaling and/or make the tumor microenvironment more conducive for growth and proliferation (Liberti and Locasale, 2016).

Growth and proliferation require the accumulation of biomass, which necessitates cellular acquisition of carbon from external sources. Of the components in standard cell culture media, glucose and glutamine are key molecules used to derive carbon for anabolism. Glucose is taken up via glucose transporters (GLUT1-5, also designated as SLC2A1-5) and phosphorylated by hexokinase to initiate degradation in the cytosol. While glucose can be completely oxidized to yield pyruvate and subsequently acetyl-CoA that can enter the tricarboxylic acid (TCA) cycle, a significant amount of pyruvate is dedicated to lactate production, possibly to regenerate NAD cofactors that are necessary to drive forward flux through glycolysis (Cracan *et al.*, 2017). Lactate is removed from the cell via monocarboxylate transporters (MCTs; exists as four isoforms) and causes acidification of the culture media. In vivo, lactate can be utilized as a substrate for the TCA cycle in both normal tissues and tumors (Hui *et al.*, 2017). Besides the production of energy, glucose uptake and phosphorylation provide important substrates for the pentose phosphate pathway to fuel ribonucleotide synthesis and NADPH production (Patra and Hay, 2014).

Regulation of Aerobic Glycolysis at the Transcriptional Level

Many glycolytic enzymes and transporters are expressed in a MYC-responsive manner (Zeller *et al.*, 2003; Zeller *et al.*, 2006). Chromatin immunoprecipitation and bioinformatic analyses show MYC binding to the promoters of *SLC2A4* (GLUT4), glyceraldehyde 3-phosphate dehydrogenase (*GAPDH*) and enolase 1 (*ENO1*) (Fernandez *et al.*, 2003). Lactate dehydrogenase A-chain (LDHA) is directly regulated by MYC (Shim *et al.*, 1997) and in the Eμ-MYC murine model of BL, transformed B-cells express MCT1 in a MYC-dependent fashion (Doherty *et al.*, 2014). Notably, MYC binds well to canonical E-boxes with the 5'-CACGTG-3' motif as found in the promoters of glycolytic genes hexokinase II (*HK2)*, *ENO1* and *LDHA* but not as efficiently to non-conserved E-boxes found in the remaining glycolytic genes (Kim *et al.*, 2004).

Hypoxia is also a key inducer of glycolysis in cancers (Robey *et al.*, 2005; Semenza, 2013), which can be reversed by activated mTOR (Hudson *et al.*, 2002; Majumder *et al.*, 2004). Hypoxia can also inhibit mTOR signaling via REDD1 induction; loss of REDD1 restores mTOR activity under hypoxic conditions, while REDD1 overexpression reduces phosphorylation of the mTORC1 target S6 kinase (Brugarolas *et al.*, 2004). Intriguingly, in renal carcinoma cells deficient for von Hippel-Lindau (VHL), hypoxia-inducible factor 1 alpha (HIF-1α) upregulation promotes glycolysis while inhibiting oxidative phosphorylation (Zhang *et al.*, 2007). This is achieved by antagonism of MYC via MXI1 and promotion of MYC degradation to prevent PGC-1β (an mTOR target) upregulation for mitochondrial biogenesis.

Oncogenic DNA Virus Manipulation of Aerobic Glycolysis

EBV has been known to induce and/or maintain aerobic glycolysis in host cells. Activation of glycolysis occurs early in infection at a time when the Wp-driven program is expressed (McFadden *et al.*, 2016). EBNA2 is the primary virus-encoded protein that targets MYC for transcriptional upregulation. Recently, it has also been established that EBNA2 reorganizes *MYC* promoter-enhancer interactions to drive high-level *MYC* transcription (Wood *et al.*, 2016; Jiang *et al.*, 2017), thereby augmenting transcription of glycolytic targets, amongst other genes (Zhao *et al.*, 2006). In addition, LMP1 and LMP2A coordinately stimulate MYC targets, glycolysis and oxidative phosphorylation in a murine model of germinal center B-cell lymphoproliferative disorder (Minamitani *et al.*, 2017). Notably, LMP1 alone is also able to induce many of the metabolic changes associated with aerobic glycolysis induction and maintenance e.g. promoting GLUT1 trafficking to the cell membrane to import glucose for glycolytic processing in both LCLs and nasopharyngeal carcinomas (Sommermann *et al.*, 2011; Zhang *et al.*, 2017b), increasing autocrine signaling via fibroblast growth factor receptor (FGFR) activation to drive glycolytic gene expression (Lo *et al.*, 2015), and stimulating poly(ADP-ribose)

polymerase (PARP) expression to co-activate glycolytic gene transcription in tandem with HIF-1α (Hulse *et al.*, 2018).

Other tumor-associated viruses similarly activate glycolysis to support their life cycles. The related gammaherpesvirus, Kaposi's sarcoma-associated herpesvirus (KSHV), induces aerobic glycolysis to support endothelial cell transformation (Delgado *et al.*, 2010; Yogev *et al.*, 2014) as well as lytic replication (Sanchez *et al.*, 2017). Another oncogenic virus, Merkel cell polyomavirus (MCPyV), encodes a small tumor antigen (sT) which promotes glycolytic gene expression (Berrios *et al.*, 2016) while human papillomavirus oncoproteins E6 and E7 upregulate HK2 via MYC in HeLa cervical cancer cells (Hoppe-Seyler *et al.*, 2017).

Mitochondrial One-Carbon (1C) Metabolism

Widespread Expression of Mitochondrial 1C Enzymes in Diverse Cancer Cell Lines

Mitochondrial 1C metabolism is normally induced in a restricted set of physiological contexts, such as embryogenesis and fetal development (Bryant *et al.*, 2018a; Di Pietro *et al.*, 2002) and lymphocyte expansion (Ron-Harel *et al.*, 2016; Ma *et al.*, 2017a). However, it has not been specifically characterized in the contexts of viral infection and B-cell development.

Mitochondrial 1C metabolism utilizes serine as its substrate and converts it into formate, the so-called 1C unit, glycine and reducing power in the form of either NADH or NADPH (Newman and Maddocks, 2017; Ducker and Rabinowitz, 2017; Locasale, 2013; Tedeschi *et al.*, 2013) (Figure I.1). Serine is imported across the inner mitochondrial membrane by sideroflexin 1 (SFXN1), a recently characterized serine transporter (Kory *et al.*, 2018). Serine hydroxymethyltransferase 2 (SHMT2) then catalyzes the breakdown of serine to produce 5,10-methylene tetrahydrofolate (5,10-meTHF) and glycine as a byproduct. Depending on cell type, glycine can undergo different fates, including detoxification by the glycine cleavage system (GCS) (Kim *et al.*, 2015), export to the cytoplasm to be used in the syntheses of proteins, glutathione and/or nucleotides (Jain *et al.*, 2012), or actively excreted by the cell. The next step in the pathway consists of the

conversion of 5,10-meTHF into 10-formyl-THF by 5,10-methylene tetrahydrofolate (THF) dehydrogenase 2 (MTHFD2); this involves the reduction of NAD(P) to NAD(P)H (Patel *et al.*, 2005; Shin, Momb and Appling, 2017). Finally, 10-formyl-THF bifurcates into two distinct fates, either being processed by 5,10-methylene THF dehydrogenase 1-like (MTHFD1L) to produce formate and drive substrate-level phosphorylation of ADP, or undergoing the aldehyde dehydrogenase family 1 member L2 (ALDH1L2)-mediated oxidation reaction to regenerate THF cofactors while producing NADPH and carbon dioxide (Krupenko *et al.*, 2010).

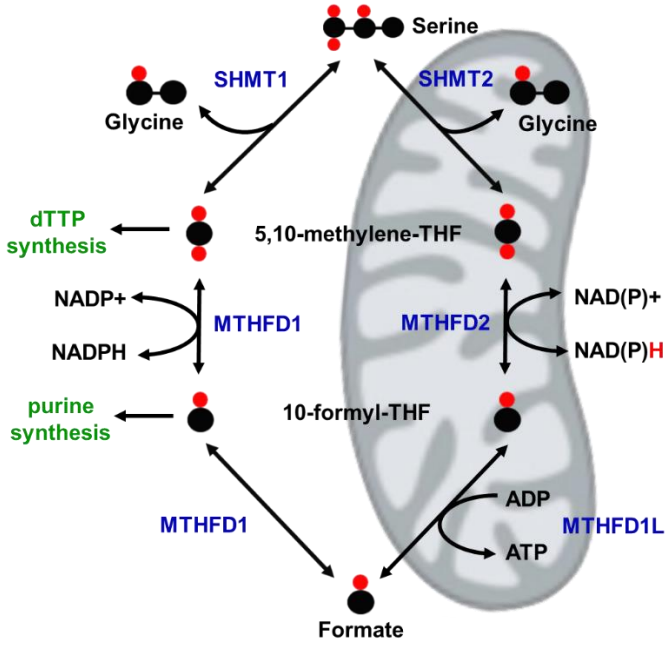

Figure I.1 Schematic of one-carbon metabolism. The cytosolic branch of the pathway is initiated by SHMT1 while the mitochondrial branch begins with SHMT2-mediated serine catabolism to produce formate, glycine and reducing potential. One-carbon flux can, in theory, proceed through either branch. However, due to the cytosol being reducing in nature, the reverse MTHFD1 reaction, namely $NADP^+$ reduction, does not typically occur. Enzymes are shown in blue. Black filled circles represent carbon atoms while red filled circles represent hydrogen atoms.

MTHFD2 is the central enzyme in mitochondrial 1C metabolism. Homozygous null deletion of MTHFD2 in mouse embryos leads to death in utero (Di Pietro *et al.*, 2002; Di Pietro, Wang and MacKenzie, 2004), as do knockouts of SHMT2 (Tani *et al.*, 2018) and MTHFD1L (Bryant *et al.*, 2018b; Momb *et al.*, 2013). Loss of MTHFD2 did not affect mitochondrial protein translation in embryonic tissue (Di Pietro *et al.*, 2002) and, mitochondrial abundance and membrane potential in SV40 large T antigen-transformed embryonic fibroblasts (Patel, Pietro and MacKenzie, 2003). In the latter cells, glycine auxotrophy was observed and supplementation with either formate or hypoxanthine had little to no effect on rescuing MTHFD2-null embryonic growth. However, MTHFD2-null fibroblasts could be rescued with a mitochondrial-localized methylene tetrahydrofolate dehydrogenase-cyclohydrolase using either NAD or NADP as the cofactor (Patel *et al.*, 2005), suggesting that, in murine fibroblasts, the crucial function of MTHFD2 is to permit 1C flux through the mitochondria, rather than specific generation of reduced cofactors.

Intriguingly, diverse cancer cell lines overexpress MTHFD2 (Nilsson *et al.*, 2014), suggesting that this pathway is crucial for supporting transformed cell growth and/or survival. Notably, cells that activate mitochondrial 1C metabolism often have a fully functional cytosolic 1C metabolic pathway with enzymes that perform essentially the same functions; ablation of mitochondrial 1C enzyme expression leads to the reversal of flux into the cytosolic 1C metabolic pathway in human cancer cell lines (Ducker *et al.*, 2016). Curiously, flux reversal is not apparent in MTHFD2-null mouse embryos (Patel, Pietro and MacKenzie, 2003). These observations hint at the possibility that the transformed cell maintains both pathways to maintain metabolic plasticity.

Transcription Regulation of Mitochondrial 1C Enzymes

Expression of mitochondrial 1C enzymes has been variously reported to rely on ATF4 and MYC. In mouse embryonic fibroblasts and the HEK293E human embryonic kidney cell line, MTHFD2 expression relies on mTOR-mediated activation of ATF4 (Ben-Sahra *et al.*, 2016). Short interfering RNA (siRNA) experiments performed by Ben-Sahra and colleagues showed

that MTHFD2 expression was independent of MYC and SREBPs in those cellular contexts. ATF4-mediated 1C metabolism was also upregulated in models of mitochondrial respiratory chain dysfunction using ethidium bromide treatment and heterologous expression of a dominant negative DNA polymerase gamma (POLGdn) (Jazayeri *et al.*, 2003) in 293T cells (Bao *et al.*, 2016). In contrast, Pikman and colleagues (2016) showed via bioinformatic analyses and MYC depletion experiments that MTHFD2 (and other mitochondrial one-carbon metabolic enzymes such as SHMT2) depended on MYC for its expression in K562 acute myeloid leukemia (AML) cells. In several non-small cell lung cancer (NSCLC) cell lines, SHMT2 is regulated by ATF4 in a nuclear erythroid factor 2-related factor 2 (NRF2)-dependent manner (DeNicola *et al.*, 2015). From these published reports, regulation seems to be cell type-dependent; adherent cells generally use ATF4 to activate mitochondrial 1C metabolism while suspension cells largely utilize MYC. Both ATF4 and MYC are E-box binding transcription factors often overexpressed in cancers, and it comes as no surprise that these proteins can regulate mitochondrial 1C metabolism.

Mitochondrial 1C Metabolism Generates Substrates that Support Transformed Cell Growth and Proliferation

As mentioned earlier, mitochondrial 1C metabolism has been described to generate a variety of metabolites that support the anabolic program. In the context of actively proliferating cells, the most important serine-derived metabolite for growth and survival is the 1C unit, formate (Bao *et al.*, 2016; Ma *et al.*, 2017a; Bryant *et al.*, 2018a; Labuschagne *et al.*, 2014). In de novo purine synthesis, two steps require the input of formate in the form of 10-formyl-THF (Pedley and Benkovic, 2017; Baggott and Tamura, 2015), namely (1) conversion of glycineamide ribonucleotide (GAR) into formyl-glycineamide (FGAR) by GAR transformylase (GART) and (2) transformylation of 5-aminoimidazole-4-carboxamide ribonucleotide (AICAR) by AICAR formyltransferase/inosine monophosphate cyclohydrolase (ATIC) to produce formyl-5-

aminoimidazole-4-carboxamide ribonucleotide (FAICAR). It is worth noting that EBV also carries a gene, BNRF1, that encodes the viral homolog of FGAR amidotransferase (FGARAT), another enzyme in the de novo purine synthesis pathway. However, this protein lacks enzymatic activity and instead has been described to perform other roles such as promoting intracellular virus transport during de novo B-cell infection (Feederle *et al.*, 2006), disrupting DAXX-ATRX function to facilitate viral gene expression (Tsai *et al.*, 2011; Tsai *et al.*, 2014) and instigating centrosome amplification that results in genomic instability (Shumilov *et al.*, 2017).

Serine catabolism via 1C metabolism generates glycine as a byproduct. While glycine is detoxified in some types of cells e.g. glioma and breast cancer cells, via the GCS into aminoacetone and methylglyoxal (Adamus *et al.*, 2018; Kim *et al.*, 2015), it may yet serve specific functions in other cell types. Glycine fuels glutathione synthesis in LPS-stimulated, non-proliferating macrophages to enable interleukin 1 beta (IL-1β) production (Rodriguez *et al.*, 2019) and presumably in activated, proliferating T cells as well, since the antioxidant N-acetylcysteine (NAC) is required to rescue SHMT2 suppression (Ron-Harel *et al.*, 2016). Diffuse large B-cell lymphoma (DLBCL) cell lines are also dependent on serine-derived glycine as they are deficient for glycine import from the extracellular environment (Ducker *et al.*, 2017). Ablation of MTHFD2 leads to glycine auxotrophy in murine fibroblasts (Patel *et al.*, 2005). Rapidly proliferating cancer cells e.g. breast cancer cell lines, also draw heavily on glycine for de novo purine synthesis (Jain *et al.*, 2012).

The oxidation of 5,10-meTHF into 10-formyl-THF is coupled to the reduction of nicotinamide adenine dinucleotide cofactors. Human MTHFD2 can catalyze this reaction using either NAD or NADP; conditions dictating the choice of substrate remain ill-defined (Shin, Momb and Appling, 2017). Inhibition of colorectal cancer cell 1C metabolism with the small molecule inhibitor LY345899 (Gustafsson *et al.*, 2017) or small hairpin RNAs (shRNAs) results in redox imbalance (Ju *et al.*, 2018). In some cell lines e.g. HCT116 and HEK293T, oxidation of 5,10-meTHF can be

uncoupled from NAD(P) reduction; instead of producing 10-formyl-THF, 5,10-meTHF can be used as a source of methyl groups for taurinomethylation of mitochondrial transfer RNA (tRNA) uridine bases (Morscher *et al.*, 2018). Consequently, the cell is not able to translate mitochondrial DNA (mtDNA)-encoded respiratory chain subunit transcripts, leading to the collapse of OXPHOS and enhanced glycolysis. Ablation of SHMT2, the enzyme upstream of MTHFD2, also reduces 10-formyl-THF production, leading to decreased mitochondrial formylmethionyl-tRNA (fMet-tRNA^{Met}) levels and diminished mitochondrial translation (Minton *et al.*, 2018).

Aside from its enzymatic function at the mitochondria, MTHFD2 has also been demonstrated to localize to the nucleus at DNA replication sites; the protein moonlights as a growth-promoting factor and does not require its catalytic activity to function in that capacity (Gustafsson Sheppard *et al.*, 2015). Recently, the same group has also shown that nuclear MTHFD2 regulates RNA metabolism and translation (Koufaris and Nilsson, 2018). Several open questions remain: (1) How is the mitochondrial targeting sequence of MTHFD2 masked? (2) Is there a cryptic nuclear localization sequence on MTHFD2? If not, what mediates its nuclear import and/or localization? (3) MTHFD2 normally exists as a homodimer (Gustafsson *et al.*, 2017). Is its localization dependent on monomer identity and/or stoichiometry? It is also worth noting that SHMT2, another mitochondrial 1C enzyme, has a cytosolic/nuclear isoform called SHMT2α, which has been described to function in nuclear thymidylate synthesis (Anderson and Stover, 2009; Anderson *et al.*, 2012) and may interact with nuclear MTHFD2 to drive cancer cell proliferation. Taken altogether, mitochondrial 1C metabolism involving MTHFD2 may perform additional roles in promoting transformed cell growth and/or survival in terms of generating reduced redox cofactors for anabolic processes and possibly regulating cell cycle progression.

De Novo Serine Synthesis (DNSS)

DNSS Enzymes are Upregulated in Transformed Cells Despite Serine Sufficiency

DNSS utilizes the glycolytic intermediate 3-phosphoglycerate (3-PG) to produce serine, a non-essential amino acid that is the primary fuel for mitochondrial 1C metabolism. Enzymes that catalyze this conversion are phosphoglycerate dehydrogenase (PHGDH), phosphoserine aminotransferase (PSAT1) and phosphoserine phosphatase (PSPH). PHGDH oxidizes 3-PG to form 3-phosphooxypyruvate (3-PHP), using NAD as a cofactor. In some instances, PHGDH may also reduce α-ketoglutarate into the oncometabolite D-2-hydroxyglutarate, a potent inhibitor of ten-eleven-translocation (TET) dioxygenase enzymes (Fan *et al.*, 2015), which are key epigenetic regulators often implicated in leukemias and lymphomas (Ko *et al.*, 2015), including latency III-expressing LCLs (Wille *et al.*, 2017; Kataoka *et al.*, 2019; Lu *et al.*, 2017). PSAT1 catalyzes the transamination reaction between 3-PHP and glutamine, generating phosphoserine and α-ketoglutarate. PSPH catalyzes the final step where phosphoserine is dephosphorylated to form serine. Naturally occurring inactivating mutations in genes of the DNSS pathway result in microcephaly, developmental delay and early mortality (Acuna-Hidalgo *et al.*, 2014; Mattos *et al.*, 2015; Shaheen *et al.*, 2014). Of particular interest is the overexpression of PHGDH in breast and lung cancers as well as melanoma (DeNicola *et al.*, 2015; Locasale *et al.*, 2011; Possemato *et al.*, 2011), an observation that has sparked accelerated development of a number of small-molecule inhibitors (Mullarky *et al.*, 2016b; Pacold *et al.*, 2016b; Reid *et al.*, 2018; Wang *et al.*, 2017). Till date, DNSS has not been described to act in B-cells or have functional consequences for EBV-mediated transformation.

Mechanisms of Controlling DNSS Enzyme Activity

PHGDH is amplified at the genetic level in a subset of melanomas and breast cancers, up to 16% of surveyed cancer samples (Locasale *et al.*, 2011; Possemato *et al.*, 2011; Beroukhim *et al.*, 2010), leading to increased PHGDH protein expression. Nonetheless, in the absence of

gene amplification, there are a number of ways to upregulate and maintain DNSS in transformed cells, which may vary depending on cell type. Like many other tumor-associated metabolic pathways, DNSS enzyme expression generally relies on MYC activity (Dang, 2012). The histone H3 lysine 9 (H3K9) methyltransferase G9A can also activate DNSS by monomethylation of H3K9 (H3K9me1) at the promoters of *PHGDH* and *PSAT1* to promote transcription (Ding *et al.*, 2013). H1299 lung carcinoma cell lines upregulate DNSS protein expression during serine starvation in a general control non-derepressible protein 2 (GCN2)-ATF4 dependent manner (Ye *et al.*, 2012). In non-small cell lung cancers (NSCLCs), DNSS enzyme expression is reliant on nuclear factor erythroid 2-related factor 2 (NRF2) (DeNicola *et al.*, 2015). Hypoxia-induced HIF-1α upregulation also drives PHGDH expression in breast cancer cell lines (Samanta *et al.*, 2016). Intriguingly, PHGDH was upregulated in HIF-2α-deficient renal carcinoma cell lines (Yoshino *et al.*, 2017), suggesting complex regulation of PHGDH and/or some degree of tumor type-dependent differences in hypoxia-mediated DNSS activation. Ewing sarcoma cells also upregulate DNSS enzyme expression via the EWS/FLI chimeric transcription factor (Tanner *et al.*, 2017). Ubiquitous transcription factors SP1 and NF-Y have also been found to bind the *PHGDH* promoter to enhance transcription (Jun *et al.*, 2008) and may function to augment existing transcriptional programs that regulate DNSS activity.

DNSS is also regulated at the post-translational level by allosteric binding of serine to pyruvate kinase M2 (PKM2) (Chaneton *et al.*, 2012). Under serine-sufficient conditions, serine binds to and activates PKM2, stimulating high glycolytic flux and allowing for the generation of acetyl-CoA in the TCA cycle. However, with serine deprivation, there are few serine molecules available to allosterically bind to PKM2, resulting in decreased PKM2 activity and backflow of glycolytic intermediates into the DNSS pathway. In several lung adenocarcinoma cell lines, PHGDH protein levels are also regulated by the ubiquitin-proteasome system; specifically, Josephin domain-containing protein 2 (JOSD2) deubiquitinase decreases the turnover of

PHGDH, which could be prevented by proteasome inhibitor treatment or siRNA knockdown (Zhang *et al.*, 2017a). Under conditions of nutrient stress, protein kinase C isoform zeta (PKCζ) phosphorylates PHGDH at threonine 57 and threonine 58 to repress DNSS flux, thereby behaving as a tumor suppressor; low PKCζ activity in patients with colorectal cancers correlated with higher PHGDH levels and poorer prognoses (Ma *et al.*, 2013).

Functions of DNSS in the Transformed Cell

Several groups have proposed that DNSS functions to maintain TCA cycle anaplerosis (Possemato *et al.*, 2011), promote the incorporation of serine-derived 1C units into nucleotides (Pacold *et al.*, 2016b; Pacold *et al.*, 2016a) or to enable flux through the TCA cycle and the pentose phosphate pathway (Reid *et al.*, 2018). It is worth noting that these studies were largely performed with RNA interference (RNAi) technology and small-molecule inhibitors on well-established cancer cell lines; DNSS in transforming and newly transformed cells has not been investigated. There has also not been any cross-comparative study of all presently developed PHGDH inhibitors to determine what the common PHGDH-independent effects are, arising as a consequence of PHGDH inhibition, which could be of interest to polypharmacological investigations (Anighoro, Bajorath and Rastelli, 2014). Recently, it was shown that DNSS confers a growth advantage to tumors in mouse models of *PHGDH*-amplified melanoma and breast cancer by enabling tumor cell synthesis of serine in serine-limited environments (Sullivan *et al.*, 2019). Taking all these studies together, one major open question is, whether serine availability affects the role of DNSS within the transformed cell. Serum serine levels in healthy humans are about 120 μM (Dudman, Tyrrell and Wilcken, 1987), far less than that of standard culture media such as RPMI-1640 (286 μM) and DMEM (400 μM). It is plausible that avid consumption of serine and subsequent sensing of serine deficiency may augment transformed cell DNSS in vivo. It is worth nothing that, apart from PKM2, there has been no other bona fide serine sensor described to date. It may therefore be the case that DNSS enzyme expression in

transformed cells is a fail-safe mechanism to guard against the potential lack of extracellular serine.

Mevalonate Metabolism and De Novo Lipid Biosynthesis

Transformed Cell Lines Increase Cholesterol and Lipid Production

Cancer cell proliferation necessitates the synthesis of new membranes (Rohrig and Schulze, 2016). Apart from the requirement for de novo lipid synthesis, more cholesterol molecules are also needed to maintain membrane integrity and fluidity, which in turn contribute to metastatic potential (Zhao *et al.*, 2016; Sherbet, 1989). Furthermore, cholesterol is enriched in lipid rafts and may be important in maintaining oncogenic signaling (Higuchi, Izumi and Kieff, 2001; Meckes, Menaker and Raab-Traub, 2013; Mollinedo and Gajate, 2015).

Meta-analysis of The Cancer Genome Atlas (TCGA) datasets showed that an increase in expression of cholesterogenic genes was correlated with poorer prognostic outcomes (Kuzu, Noory and Robertson, 2016). Consistent with that, a number of reports link cholesterol pathway-related metabolites with tumor progression e.g. 27-hydroxycholesterol as an agonist of estrogen receptor in estrogen receptor-positive breast cancers (Nelson *et al.*, 2013; Wu *et al.*, 2013). However, there are also instances where pathway intermediates and their adducts may have anti-tumor properties e.g. dendrogenin A as an inhibitor of cholesterol epoxide hydrolase and an activator of autophagy leading to cell death (Dalenc, Poirot and Silvente-Poirot, 2015; de Medina *et al.*, 2013; Segala *et al.*, 2017).

Likewise, enhanced lipogenesis is associated with cancer progression (Rohrig and Schulze, 2016). In a murine model of hepatocellular carcinoma (HCC), mTOR complex 2 (mTORC2) stimulates de novo lipid synthesis to produce glucosylceramide and cardiolipin, contributing to hepatic steatosis that progresses to HCC (Guri *et al.*, 2017). Aberrant synthesis of lysophosphatidic acid (LPA) in ovarian cancer promotes LPA_2 receptor signaling to drive

SREBP activation and AMP-activated protein kinase (AMPK) inhibition, culminating in enhanced lipid biosynthesis to promote transformed cell growth (Mukherjee *et al.*, 2012).

While it is clear that EBV-transformed cell growth and survival depend on cholesterol and lipid sufficiency, it has often been assumed that those dependencies are largely due to the demands of membrane biogenesis and the construction of lipid rafts for oncoprotein signaling (Higuchi, Izumi and Kieff, 2001; Meckes, Menaker and Raab-Traub, 2013; Katano, Pesnicak and Cohen, 2004). Biological functions have not been ascribed to sterol- and lipid-derived metabolites in the context of EBV infection, especially in the early phases prior to establishment of the latency III program.

Bifurcation of Acetyl-CoA Metabolism into Cholesterol or Lipid Production

Citrate and acetate can be converted to acetyl-CoA by ATP-citrate lyase (ACLY) and acetyl-CoA synthetases 1 (ACSS1) and 2 (ACSS2), respectively. Acetyl-CoA is the common substrate of both cholesterol biosynthesis (also known as mevalonate metabolism) and lipogenesis (Figure I.2). Acetyl-CoA carboxylase (ACC1) and fatty acid synthase (FASN) catalyze the conversion of acetyl-CoA into palmitate, which can undergo a number of fates. Palmitate can be further elongated to form longer fatty acids, used directly for protein palmitoylation at target cysteine residues, oxidized to produce NADH and $FADH_2$ or, be further processed to yield triglycerides and phospholipids for energy storage and membrane biogenesis, respectively. For mevalonate metabolism, acetyl-CoA is converted to farnesyl pyrophosphate (FPP), a 15-carbon intermediate, via mevalonate by a number of enzymes, including 3-hydroxy-3-methylglutaryl-CoA reductase (HMGCR). FPP can then have one of two fates, to either continue being reduced in an NADPH-dependent manner to produce squalene and ultimately, cholesterol, or be diverted to isoprenoid synthesis to generate intermediates for protein modification e.g. geranylgeranyl pyrophosphate (GGPP), a 20-carbon molecule.

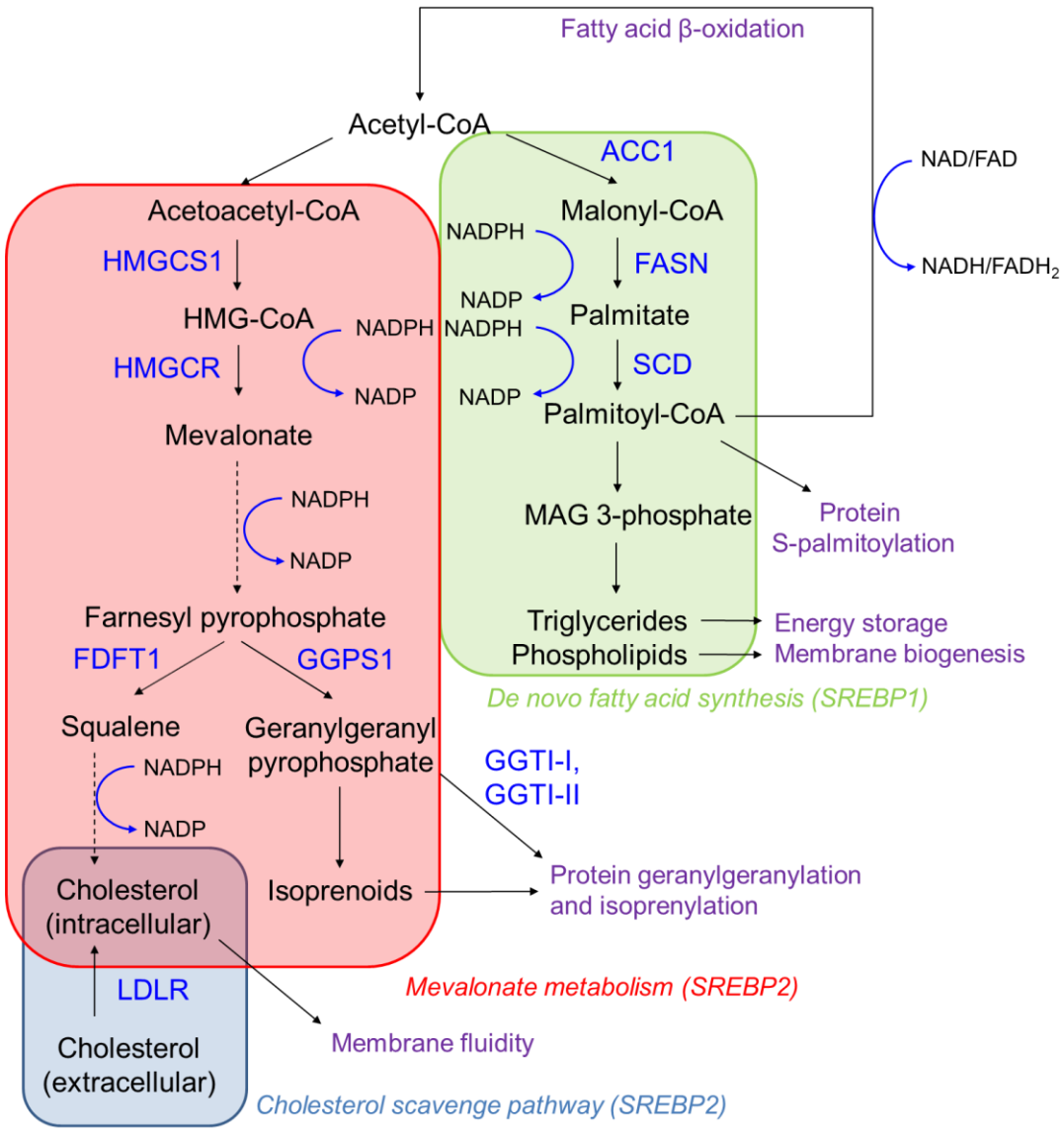

Figure I.2 Schematic of cholesterogenic and lipogenic pathways. Words in deep blue, black and purple indicate enzymes, metabolites/cofactors and functional outcomes, respectively. The pathway utilizes NADPH for the reductive steps while fatty acid β-oxidation yields either NADH or $FADH_2$. Dotted lines indicate multi-step processes where enzymes and intermediates have been omitted for clarity. Green, red and light blue boxes demarcate de novo lipid synthesis, mevalonate metabolism and the cholesterol scavenge pathway. See main text for details.

Regulatory Mechanisms Governing Cholesterogenesis and Lipogenesis

Sterol response element binding proteins (SREBPs) are the classic master regulators of cholesterol and lipid biosyntheses. When the cell senses a lack of lipids and/or sterols, SCAP dissociates from its endoplasmic reticulum retention factor insulin-induced gene 1 (INSIG1) and is activated to escort inactive, full-length SREBPs to the Golgi apparatus in a coat protein complex II (COPII)-dependent manner. SREBPs are then cleaved by resident proteases known as site-1 and site-2 proteases. This liberates the transcriptionally active N-terminal transcription activation domain (N-TAD) of SREBPs that can localize to the nucleus and regulate cognate genes (Figure I.3). Classically, SREBP binding to sites on DNA is dependent on sterol response elements, although relatively weak E-box engagement may also occur in some instances with SREBP1 (Amemiya-Kudo *et al.*, 2002). While SREBPs are functionally redundant, SREBP1 and SREBP2 are known to preferentially activate lipogenic and cholesterogenic programs, respectively (Horton *et al.*, 2003).

SREBP activity is strongly regulated by the PI3K/AKT/mTOR pathway (Porstmann *et al.*, 2008). AKT activation induces the production of SREBPs and enzymes involved in cholesterogenesis and lipogenesis (Porstmann *et al.*, 2005); mutation of the upstream kinase PI3K at histidine 1047 sufficiently induces de novo lipid synthesis in breast cancer cell lines and primary tumors (Ricoult *et al.*, 2016). Mechanistically, mTOR complex 1 (mTORC1) phosphorylates lipin-1 to prevent it from sequestering SREBP N-TADs, thereby allowing SREBP N-TADs to bind their cognate promoters. Another mechanism also exists (Peterson *et al.*, 2011), where mTORC1 phosphorylates CREB-regulated transcription co-activator 2 (CRTC2), a protein that usually inhibits COPII subunit SEC31A (Han *et al.*, 2015). This phosphorylation event relieves the repression of SEC31A and allows COPII-mediated transport of SREBPs to proceed unimpeded. Post-transcriptional regulation of lipid biosynthesis is also exerted by mTORC1; mTORC1 activates S6K1, which in turn phosphorylates serine/arginine-rich (SR) protein kinase 2

(SRPK2), a regulator of RNA splicing. Intriguingly, SRPK2 promotes intron splicing of transcripts encoding lipogenic proteins, thereby enhancing mRNA stability and subsequent translation to culminate in higher lipid production (Lee *et al.*, 2017).

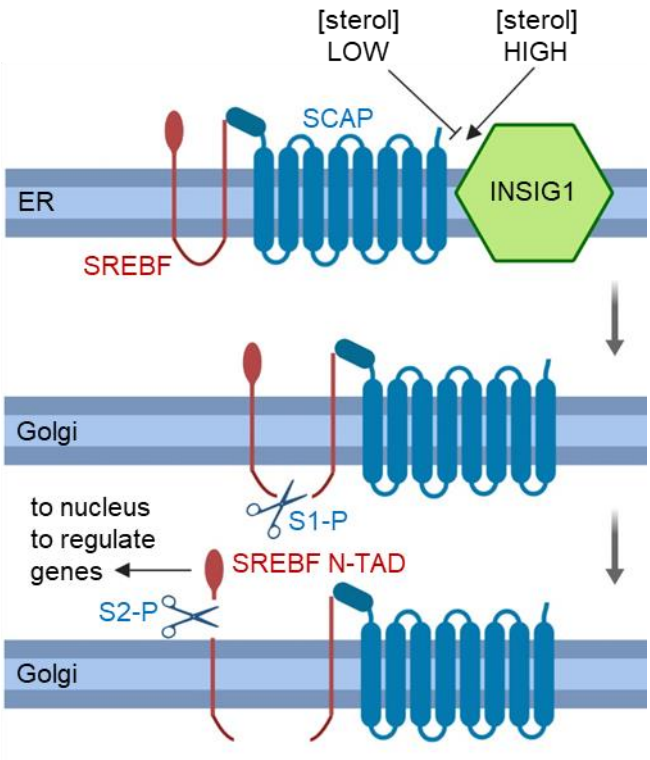

Figure I.3 Schematic of SREBP regulation and activation. ER, endoplasmic reticulum; SREBP, sterol response element binding protein; SCAP, SREBP cleavage activating protein; INSIG1, insulin-induced gene 1; S1-P, site-1 protease; S2-P, site-2 protease; N-TAD, N-terminal transcription activation domain. See main text for an explanation of the process.

Despite MYC having prominent roles in the general remodeling of cellular metabolism, there is actually little evidence for direct activation of lipogenesis and cholesterol biosynthesis by MYC (Dang, 2012; Dang, 2013; Hsieh *et al.*, 2015). *HMGCR* and *ACACA* promoters do not possess

E-box and E2F1 motifs that would normally engage MYC (Zeller *et al.*, 2006). In that same dataset, SREBPs apparently do not display strict MYC-dependent upregulation as well. Curiously, the promoter of *SCAP* has E-box and E2F1 motifs that are MYC-responsive. Thus, while MYC might not bind directly and/or efficiently to the promoters of lipogenic and cholesterogenic genes to transactivate their expression, it may activate de novo lipid and cholesterol biosynthesis indirectly via SCAP overexpression.

Both cholesterogenesis and lipogenesis can also be epigenetically regulated. Acetyltransferases p300 and CREB-binding protein (CBP) target SREBPs to promote their longevity and capacity to transactivate cognate genes (Giandomenico *et al.*, 2003). At the same sites on SREBP1 i.e. lysines 324 and 333, sirtuin 1 (SIRT1) directly deacetylates SREBP1 to promote polyubiquitination and subsequent degradation (Walker *et al.*, 2010). Acetyl transfer to histone H3 at lysines 9, 27 and 56 at the promoters of lipogenic genes e.g. *ACACA* and *FASN*, can also increase gene transcription (Gao *et al.*, 2016). These histone modifications may be opposed by histone deacetylase 3 (HDAC3), a modifier protein that negatively regulates cholesterol synthesis in cell lines as well as in mouse liver (Knutson *et al.*, 2008; Villagra *et al.*, 2007). Taken together, acetyl-CoA levels may be an important link between nutrient availability and epigenetic regulation of the cholesterogenic and lipogenic metabolic programs.

DNA Viral Subversion of Cholesterol and Lipid Biosyntheses

A number of other DNA viruses also make use of cholesterol and lipid biosyntheses to support their infectious life cycles. Lytic infection of fibroblasts by human cytomegalovirus (HCMV), a betaherpesvirus, leads to enhanced acetyl-CoA carboxylase 1 (ACC1) expression (Spencer *et al.*, 2011) and requires acetyl-CoA synthetase 2 (ACSS2) activity to generate acetyl-CoA for lipid synthesis (Vysochan *et al.*, 2017). Surprisingly, CRISPR deletion of ACLY had no effect on lipid production (Vysochan *et al.*, 2017). Underlying those activities is HCMV activating SREBP1 cleavage to drive transcription of lipogenic genes; impressively, the virus is able to do so even in

the presence of excess sterols that should theoretically reinforce SCAP-INSIG1 interactions to prevent SREBP1 translocation to the Golgi (Yu, Maguire and Alwine, 2012). Ultimately, the high levels of lipids allow for efficient virion production. In the related gammaherpesvirus KSHV, de novo lipid synthesis is induced to enable virion maturation during lytic replication as well as for peroxisomal long-chain fatty acid metabolism in latently infected cells (Delgado *et al.*, 2012; Sanchez *et al.*, 2017; Sychev *et al.*, 2017). Vaccinia virus (VACV) also upregulates lipid synthesis to produce fatty acids for β-oxidation, even in the presence of sufficient glucose (Greseth and Traktman, 2014). ATP produced from fatty acid β-oxidation is crucial for virion assembly. Strikingly, glucose is dispensable for vaccinia virus replication; glutamine provides the substrates needed for TCA cycle maintenance and supports VACV protein synthesis (Fontaine, Camarda and Lagunoff, 2014; Findlay and Ulaeto, 2015). VACV likely uses glutamine for acetyl-CoA production as well.

Chapter II: Quantitative temporal viromics reveal dynamic, global changes to the host and viral proteomes during primary B-cell infection with EBV

Contributions

Dr. Hongying Shen in the laboratory of Dr. Vamsi Mootha assisted in the design of metabolomics experiments, running of samples on the LC-MS and data analysis. Ina Ersing in the laboratory of Dr. Benjamin E. Gewurz optimized the multiplexed proteomics workflow and performed all proteomics experiments described in this chapter, including primary B-cell isolation, B95-8 virus preparation and titration, experimental infections, cell labeling and sorting and subsequent sample processing and normalization, in collaboration with the Weekes laboratory. Luis Nobre and Dr. Michael P. Weekes, as well as Dr. Joao A. Paulo in the laboratory of Dr. Steven P. Gygi, performed the mass spectrometry experiments. Analysis of the proteomic dataset to identify enriched pathways and processes were jointly performed by Luis Nobre and Dr. Michael P. Weekes, as well as Liang Wei Wang and Dr. Benjamin E. Gewurz. Stephen Trudeau and Jason Nomburg in the laboratory of Dr. Benjamin E. Gewurz assisted with the running of immunoblot samples. Zhonghao Wang in the laboratory of Dr. Benjamin E. Gewurz assisted in the microscopy work pertaining to cell diameter measurements. Dr. Yijie Ma in the laboratory of Dr. Benjamin E. Gewurz assisted in data visualization. Bryn Reinstadler in the laboratory of Dr. Vamsi Mootha performed natural isotope correction on raw LC-MS data pertaining to experiments that utilized heavy tracers. Dr. Melissa Walker and Dr. Eran Mick in the laboratory of Dr. Vamsi Mootha provided useful technical support for the use of the Seahorse XF24 Extracellular Flux Analyzer. We also thank the Flow Cytometry and Confocal Microscopy core facilities at Brigham and Women's Hospital for services rendered and use of the Zeiss LSM 800 instrument, and Dr. Bo Zhao for helpful discussions.

This work was supported by R01 AI137337, a Burroughs Wellcome Career Award in Medical Sciences and an American Cancer Society Research Scholar award to Dr. Benjamin E. Gewurz, a Wellcome Senior Clinical Research Fellowship (108070/Z/15/Z) to Dr. Michael P. Weekes, NIH R01 GM67945 to Dr. Steven P. Gygi, R35GM122455 to Dr. Vamsi K. Mootha,

NIH/NIDDK grant K01 DK098285 to Dr. Joao A. Paulo, K99GM124296 to Dr. Hongying Shen, and a Singapore Agency for Science, Technology and Research (A*STAR) pre-doctoral fellowship to Liang Wei Wang.

This work has been submitted for publication with the following citation:

Liang Wei Wang*, Hongying Shen*, Luis Nobre*, Ina Ersing*, Joao A. Paulo, Stephen Trudeau, Zhonghao Wang, Nicholas A. Smith, Yijie Ma, Bryn Reinstadler, Jason Nomburg, Thomas Sommermann, Ellen Cahir-McFarland, Steven P. Gygi, Vamsi K. Mootha, Michael P. Weekes and Benjamin E. Gewurz. 2019. Epstein-Barr Virus Induced One-Carbon Metabolism Drives B-Cell Transformation. *Cell Metabolism* (under 2nd round review). (* denotes co-first author)

Abstract

EBV infection of B-cells drives a shift from quiescence to continual growth, proliferation and survival, underpinned by widespread changes to cellular metabolism to support anabolic processes. How and when these processes are activated, especially at the proteomic level, are largely unknown. Here, we utilized multiplexed proteomics to uncover virus-upregulated pathways during de novo EBV infection. Newly infected cells induced aerobic glycolysis by coordinately upregulating cell surface expression of glucose transporters, glycolytic enzyme abundances and lactate export. EBV also remodeled the B-cell mitochondrial proteome, culminating in enhanced oxidative capacity and the induction of growth-promoting pathways such as one-carbon metabolism.

Introduction

EBV infection of primary human B-cells results in a dramatic physiological shift from quiescence to hyperproliferation and sustained long-term cellular growth and survival. Most of our knowledge regarding viral transformation of B-cells have been gleaned from studies on stably transformed B-cells known as lymphoblastoid cell lines (LCLs). Recently, a number of groups

have intensively investigated the early pre-latent phases of infection and incipient transformation in the contexts of epigenetic and RNA regulation (Mrozek-Gorska *et al.*, 2018; Saha *et al.*, 2015) and the induction of DNA damage responses (Hafez *et al.*, 2017; McFadden *et al.*, 2016; Price *et al.*, 2012). However, little is known about proteome-wide remodeling during EBV infection. In this study, we adopt a previously published approach (Weekes *et al.*, 2014) to quantitate the relative abundances of host and viral proteins in resting and newly infected cells out to 35 days post-infection, to uncover upregulated pathways that may have growth- and/or survival-promoting functions in newly established latent EBV infection.

Materials and Methods

Culture of established cell lines

HEK293T were cultured in DMEM with 10% fetal bovine serum (FBS). GM12878 lymphoblastoid cells were derived from a Caucasian female and were obtained from Coriell. GM12878 Cas9+ cell lines were previously described (Ma *et al.*, 2017c). The 2-2-3 EBNA2-HT conditional EBNA2 allele cell line was a kind gift from Dr. Bo Zhao and Dr. Elliott Kieff (Harvard Medical School) and maintained continuously in the presence of 4-hydroxytamoxifen (4HT). EBNA2-HT cells contain a conditional EBNA2 allele, where EBNA2 is fused to the ligand binding domain of a modified estrogen receptor that binds to 4HT but is not activated by calf estrogens. In the presence of 4HT, EBNA2HT localizes to the nucleus, but upon 4HT withdrawal, it re-localizes to the cytosol and is destabilized. To remove 4HT, cells were washed five times with 4HT-free media with the last two washes 30 minutes each before re-seeding at 300,000 cells per mL. Cells were then grown for a further 48 hours before harvesting for RNA extraction and cell lysate preparation. The P493-6 cell line (Schuhmacher *et al.*, 1999; Schuhmacher *et al.*, 2001b) was a kind gift from Dr. Micah Luftig (Duke University). P493-6 cells are LCLs that also contain a conditional EBNA2-HT allele. In addition, they have an exogenous Tet-OFF *MYC* allele, where withdrawal of tetracyclines induces high-level MYC expression.

P493-6 cells were maintained continuously in a BL-like state with high exogenous MYC expression by culturing cells in the absence of doxycycline and in the absence of 4HT. To grow P493-6 cells in the lymphoblastoid cell state (which has intermediate MYC level), P493-6 cells were grown in the presence of both 1 μM 4HT to induce EBNA2-HT nuclear translocation and 1μg/mL doxycycline to suppress exogenous *MYC* allele expression. In this state, EBNA2 induces endogenous MYC expression. To shift P493-6 cells to a low EBNA2 and low MYC state, cells were washed five times and returned to media with 1μg/mL doxycycline but without 4HT. After 48 hours of growth in any of these conditions, whole cell lysates were prepared. For selection following lentiviral transduction, hygromycin (Calbiochem) at 200 μg/mL or puromycin (Invitrogen) at 3 μg/mL was used. All cells were cultured in RPMI-1640 (Invitrogen) supplemented with 10% standard FBS and penicillin-streptomycin in a humidified incubator at 37˚C and at 5% CO_2. All cells were routinely confirmed to be mycoplasma-negative.

Primary human B-cell isolation and culture

Platelet-depleted venous blood obtained from the Dana-Farber Cancer Institute blood bank were used for primary human B-cell isolation, following our Institutional Review Board-approved protocol for discarded and de-identified samples. RosetteSep and EasySep negative isolation kits (STEMCELL Technologies) were used sequentially to isolate CD19+ B-cells with the following modifications made to the manufacturer's protocols. For RosetteSep, 40 μL of antibody cocktail was added per mL of blood and then layered onto Lymphoprep density medium for centrifugation. For EasySep, 10 μL of antibody cocktail was added per mL of B-cells, followed by 15 μL of magnetic bead suspension per mL of B-cells. After negative selection, the cells obtained were ≥95% positive for CD19, a nearly pan-B-cell surface marker (CD19 is weakly expressed on plasma cells). For most experiments, cells were cultured in RPMI-1640 (Invitrogen) supplemented with 10% standard FBS and penicillin-streptomycin. For metabolite withdrawal and labeling experiments, RPMI-1640 without glucose, serine and glycine

(Teknova) was used, and supplemented with 10% dialyzed FBS (Gemini Biosciences) and penicillin-streptomycin and, if applicable, the appropriate chemical supplement. Cells were cultured in a humidified incubator at 37˚C and at 5% CO_2.

EBV infection of primary B-cells

EBV B95-8 virus was produced from B95-8 cells with conditional ZTA expression. 4HT was used at a concentration of 1 μM to induce EBV lytic replication, removed 24 hours later, and cells were resuspended in 4HT-free RPMI/10% FBS for 96 hours. Virus-containing supernatants were collected and subject to filtration through a 0.45 μm filter to remove producer cells. Titer was determined experimentally by transformation assay. The P3HR-1 EBV strain was produced by using a P3HR-1 cell line with conditional 4HT-responsive ZTA-HT and RTA-HT alleles, a kind gift from Dr. Eric Johannsen and Dr. Elliott Kieff (Ersing *et al.*, 2017; Calderwood, Holthaus and Johannsen, 2008). P3HR1 ZHT/RHT cells were induced with 1 μM of 4HT for 24 hours. RPMI/FBS media was then exchanged for fresh media, and viral supernatants were collected from induced cultures 96 hours thereafter. Viral supernatants were purified by filtration through a 0.45 μM filter. Genomic DNA content of preparations of this non-transforming virus were quantitated by PCR for *BALF5* on total DNA extracted, and cross-compared with levels from B95-8 preparation, which were also measured by this approach in a parallel assay at the same time, in order to normalize input virus amounts for subsequent cell infection studies. The plasmid pHAGE-BALF5 was used for standard curves. Calculated genome copy numbers were used to normalize B95-8 and P3HR-1 amounts used for de novo infection cross-comparison studies. UV irradiation of B95-8 virus supernatants was performed at a cumulative intensity of 3J per square centimeter on ice, to prevent heat-induced virus degradation. To validate equal B95-8 and P3HR-1 uptake 24 hours post-infection, cells were extensively washed in PBS and then total DNA was extracted from newly infected cells and used for the *BALF5* qPCR assay

described above. Immunofluorescence analysis was done for EBNA1 at 48 hours post-infection to further validate equal infection.

Antibodies, reagents and kits

The following antibodies were used: mouse anti-EBV EBNA1 (OT1x) (a kind gift from Jaap Middledorp), mouse anti-EBV EBNA2 (PE2) (a kind gift from Jeffrey Cohen), sheep anti-EBV EBNA3A (Exalpha, Cat#F115P), sheep anti-EBV EBNA3C (a kind gift from Michelle West and Martin Rowe), mouse-anti LMP1 (S12) hybridoma, rat anti-EBV LMP2A antibody (14B7) (a kind gift from Richard Longnecker), mouse anti-EBV gp350 (72A1) (BioXCell), rabbit ant-DDX1 (Bethyl Laboratories, Cat#A300-521A), PE mouse IgG1, κ isotype control (Clone MOPC-21) (BD Biosciences, Cat#555749), mouse anti-human CD23 PE (Clone M-L233) (BD Biosciences, Cat#555711), mouse anti-CD19 APC (BD Biosciences, Cat#555415), mouse IgG2b, κ isotype control (Clone 27-35) (BD Biosciences, Cat#565378), mouse anti-human GLUT1 Alexa Fluor 647 (Clone 202915) (BD Biosciences, Cat#566580).

The following chemicals and reagents were used: tandem mass tag (TMT) 10-plex isobaric reagents (Thermo Fisher, Cat# 90110), HPLC water (VWR, Cat# 23595.328), LC-MS grade acetonitrile (Merck, Cat# 1.00029.2500), acetonitrile (LC/MS) (Fisher Scientific, Cat#A955-1), methanol (LC/MS) (Fisher Scientific, Cat#A456-1), water (LC/MS) (Fisher Scientific, Cat#W6-4), ammonium acetate (LC/MS) (Sigma-Aldrich, Cat#14267), ammonium Hydroxide (LC/MS) (Fisher Scientific, Cat#A470-250), ammonium carbonate (HPLC) (Fluka, Cat#74415-250G-F), sodium L-lactate ($13C_3$) (Cambridge Isotope Laboratories, Cat#CLM-1579-0.5), formic acid (LC/MS) (Fisher Scientific, Cat#A117-50), cOmplete Protease Inhibitor Cocktail (Roche, Cat#11836153001), piericidin A (Cayman Chemicals, Cat#15379), tunicamycin, Streptomyces lysosuperficus (Sigma-Aldrich, Cat#654380), antimycin A from Streptomyces sp. (Sigma-Aldrich, Cat#A8674), 8M guanidine hydrochloride solution (ThermoFisher Scientific, Cat#24115), D-(+)-galactose (Sigma-Aldrich, Cat#G5388), (Z)-4-hydroxytamoxifen (Sigma-

Aldrich, Cat#H7904), doxycycline hyclate (Sigma-Aldrich, Cat#D98910, 2-NBDG (2-(N-(7-nitrobenz-2-oxa-1,3-diazol-4-yl)amino)-2-deoxyglucose) (ThermoFisher Scientific, Cat#N13195), carbonyl cyanide m-chlorophenylhydrazone (CCCP) (Sigma-Aldrich, Cat#C2759), carbonyl cyanide 4-(trifluoromethoxy)phenylhydrazone (FCCP) (Sigma-Aldrich, Cat#C2920), oligomycin A (Sigma-Aldrich, Cat#75351), Cell-Tak Cell and Tissue Adhesive (Corning, Cat#C354240), , Standard Fetal Bovine Serum, Qualified, USDA-Approved Regions (ThermoFisher Scientific, Cat#10437028), RPMI 1640 Medium (ThermoFisher Scientific, Cat#11875085), RosetteSep™ Human B-cell Enrichment Cocktail (STEMCELL Technologies, Cat#15064) and EasySep™ Human B-cell Enrichment Kit (STEMCELL Technologies, Cat#19054).

The following kits and parts were used: BCA Protein Assay Kit (Thermo Fisher Scientific, Cat#23227), Micro BCA Protein Assay Kit (Thermo Fisher Scientific, Cat#23235), Lactate-Glo™ Assay (Promega, Cat#J5021), Seahorse XF24 FluxPak (Agilent Technologies, Cat#100850-001), Seahorse XF24 V7 PET Culture Microplates (Agilent Technologies, Cat#101037-004), Magic C4 resin (5 mm, 100 A°) (Michrom Bioresources, Cat#PM5/64100/00), GP118 resin (1.8 mm, 120 A°) (Sepax Technologies), XBridge BEH Amide VanGuard Pre-column, 130Å, 2.5 µm, 2.1 mm X 5 mm, 3/pkg (Waters, Cat#186007763), Xbridge BEH amide 2.5 µm, 2.1 mm X 100 mm (Waters, Cat#186006091), SeQuant® ZIC®-pHILIC (5 µm polymer) PEEK 150 x 2.1 mm (EMD Millipore, Cat#150460), Proxeon EASY-nLC 1000 LC pump (ThermoFisher Scientific, Cat#LC120), Orbitrap Fusion Lumos Mass Spectrometer (ThermoFisher Scientific, Cat# IQLAAEGAAP FADBMBHQ), Q Exactive Plus orbitrap mass spectrometer equipped with an Ion Max source and a HESI II probe (ThermoFisher Scientific), Dionex UltiMate 3000 UPLC system (ThermoFisher Scientific) and LSM 800 with Airyscan (Zeiss).

Cell preparation for three biological replicates of TMT proteomic analysis

Three biological replicates were performed. For each biological replicate, B-cells were isolated from four anonymous human donors. Although we routinely achieved CD19+ B-cell

purity >95%, we cultured B-cell preparations from each donor separately, to eliminate the chance of allogenic responses from rare co-purifying T-cells between donor cells. With respect to the transformation time course, uninfected B-cells (for the 0 DPI timepoint) were stained with propidium iodide and anti-CD19 antibody, and FACSort was performed for live (based on forward and side scatter parameters) CD19+ B-cells on a BD FACSAria cytometer at the Brigham & Women's Hospital Flow Cytometry core facility, to control for effects of FACSsort at subsequent timepoints. EBV was added to the remaining purified B-cells at an MOI of 0.1 (approximately 250 µL of supernatant from ZHT cells 5 days after ZHT stimulation, with washout of 4HT after 24 hours, per million purified B-cells). Cells were cultured in a humidified chamber at 37˚C in complete growth media, again maintaining cultures from each B-cell donor in separate flasks. At each indicated time point, cells from each donor were stained with antibody against CD23, a surrogate marker of EBV-infected cells upregulated by EBNA2 early after EBV infection. Live (based on forward and side scatter gates) CD23+ cells were sorted on the same BD FACSAria cytometer. Whole cell lysates (WCL) and plasma membrane (PM) samples were prepared as described in "*Protein preparation for TMT-based proteomics*". Samples from each donor were sorted sequentially. Immediately following the sort, cells were lysed as described below for WCL analysis or subjected to plasma membrane profiling. Samples were combined at constant ratios at the cell lysis step. The three proteomic time course biological replicates were performed at least one month apart.

Protein preparation for TMT-based proteomics

Plasma membrane profiling was performed as described previously (Weekes *et al.*, 2014; Weekes *et al.*, 2012). Briefly, FACS sorted B-cells were washed twice with ice-cold PBS. Sialic acid residues were oxidized with sodium meta-periodate (Thermo Fisher) then biotinylated with aminooxy-biotin (Biotium). The reaction was quenched, cell numbers for each condition were normalized to 2 x 10^6 using a BioRad TC20 automated cell counter and the biotinylated cells

were lysed in 1.6% Triton X-100 lysis buffer. Biotinylated glycoproteins were enriched with high affinity streptavidin agarose beads (Pierce) and washed extensively. Captured protein was denatured with DTT, alkylated with iodoacetamide (IAA, Sigma) and digested on-bead with trypsin (Promega) in 200 mM HEPES pH 8.5 for 3h. Tryptic peptides were collected.

For whole proteome samples, cells were washed twice with PBS, and 150 ul of 6M guanidine/50 mM HEPES pH 8.5 lysis buffer added. Samples were vortexed extensively then sonicated. Cell debris was removed by centrifuging at 13,000 g for 10 min twice. Dithiothreitol (DTT) was added to a final concentration of 5mM and samples were incubated for 20 min. Cysteines were alkylated with 15mM iodoacetamide and incubated 20 min at room temperature in the dark. Excess iodoacetamide was quenched with DTT for 15 min. Samples were diluted with 200 mM HEPES pH 8.5 to 1.5 M guanidine, followed by digestion at room temperature for 3 hr with LysC protease at a 1:100 protease-to protein ratio. Trypsin was then added at a 1:100 protease-to-protein ratio followed by overnight incubation at 37oC. The reaction was quenched with 1% formic acid, samples were spun at 21,000g for 10 min to remove debris and undigested protein, then subjected to C18 solid-phase extraction (Sep-Pak, Waters) and vacuum centrifuged to near-dryness

In preparation for TMT labelling, desalted peptides were dissolved in 200 mM HEPES pH 8.5. For whole proteome samples, peptide concentration was measured by micro BCA (Pierce), and 50 mg of peptide labelled with TMT reagent. For plasma membrane samples, 100% of each peptide sample was labelled. TMT reagents (0.8 mg) were dissolved in 43 μl anhydrous acetonitrile and 5 μl added to peptide sample at a final acetonitrile concentration of 30% (v/v). Samples were labelled as follows: Experiment WCL1: CD19+ uninfected (TMT 126); CD23+ infected d1 (TMT 127N); CD23+ infected d2 (TMT 127C); CD23+ infected d4 (TMT 128N); CD23+ infected d7 (TMT 128C); CD23+ infected d10 (TMT 129N); CD23+ infected d14 (TMT 129C); CD23+ infected d18 (TMT 130N); CD23+ infected d21 (TMT 130C); CD23+ infected d28

(TMT 131). For Experiment WCL2: CD19+ uninfected (TMT 126); CD23+ infected d2 (TMT 127N); CD23+ infected d4 (TMT 127C); CD23+ infected d7 (TMT 128N); CD23+ infected d10 (TMT 128C); CD23+ infected d14 (TMT 129N); CD23+ infected d18 (TMT 129C); CD23+ infected d21 (TMT 130N); CD23+ infected d28 (TMT 130C); CD23+ infected d35 (TMT 131). Experiment WCL3: CD19+ uninfected (TMT 126); CD23+ infected d2 (TMT 127N); CD23+ infected d4 (TMT 127C); CD23+ infected d7 (TMT 128N); CD23+ infected d10 (TMT 128C); CD23+ infected d14 (TMT 129N); CD23+ infected d18 (TMT 129C); CD23+ infected d21 (TMT 130N); CD23+ infected d24 (TMT 130C); CD23+ infected d28 (TMT 131). Experiment PM1: CD19+ uninfected (TMT 126); CD23+ infected d2 (TMT 127N); CD23+ infected d4 (TMT 127C); CD23+ infected d7 (TMT 128N); CD23+ infected d10 (TMT 128C); CD23+ infected d14 (TMT 129N).

Following incubation at room temperature for 1 hr, the reaction was quenched with hydroxylamine to a final concentration of 0.5% (v/v). TMT-labeled samples were combined at a 1:1:1:1:1:1:1:1:1:1 ratio. The sample was vacuum-centrifuged to near dryness and subjected to C18 solid-phase extraction (SPE) (Sep-Pak, Waters).

Offline high pH reversed-phase fractionation of peptides from experiments WCL1-3, and offline tip-based strong cation exchange fractionation of the PM sample were performed, and WCL peptide fractions combined as described previously (Weekes *et al.*, 2014).

Peptide fragmentation and detection by LC-MS3

Mass spectrometry data were acquired using an Orbitrap Lumos coupled with a Proxeon EASY-nLC 1000 LC pump (ThermoFisher Scientific, San Jose, CA). Peptides were separated on a 75 mm inner diameter microcapillary column packed with 0.5 cm of Magic C4 resin (5 mm, 100 A°, Michrom Bioresources) followed by approximately 20 cm of GP118 resin (1.8 mm, 120 A°, Sepax Technologies). Peptides were separated using a 3 hr gradient of 6 to 30% acetonitrile in 0.125% formic acid at a flow rate of 300 nL/min. Each analysis used an MS3-based TMT

method (McAlister *et al.*, 2012; Ting *et al.*, 2011). The scan sequence began with an MS1 spectrum (Orbitrap analysis, resolution 120,000, 350-1400 Th, AGC target 5×10^5, maximum injection time 100 ms). 'Rapid' was selected for MS2 analysis, which consisted of CID (quadrupole ion trap analysis, AGC 1.8×10^4, NCE 35, maximum injection time 120 ms). For MS3 analysis, precursors were fragmented by HCD prior to Orbitrap analysis (NCE 55, max AGC 2×10^5, maximum injection time 150 ms, isolation specificity 0.7 Th, resolution 50,000).

Analysis of LC-MS3 data

Mass spectra were processed using a Sequest-based in-house software pipeline called "MassPike" as described previously (Weekes *et al.*, 2014). Briefly, MS spectra were converted to mzXML using a modified version of ReAdW.exe. A combined database was constructed from (a) the human Uniprot database (February 4th, 2014), (b) B95-8 strain EBV, (c) all open reading frames from a six-frame translation of B95-8 strain EBV and (d) common contaminants such as porcine trypsin and endoproteinase LysC. The combined database was concatenated with a reverse database composed of all protein sequences in reversed order. Searches were performed using a 20 ppm precursor ion tolerance. Product ion tolerance was set to 0.03 Th. TMT tags on lysine residues and peptide N termini (229.162932 Da) and carbamidomethylation of cysteine residues (57.02146 Da) were set as static modifications, while oxidation of methionine residues (15.99492 Da) was set as a variable modification. To control the fraction of erroneous protein identifications, we used a target-decoy strategy (Elias and Gygi, 2007; Elias and Gygi, 2010). Peptide spectral matches (PSMs) were filtered to an initial peptide-level false discovery rate (FDR) of 1% with subsequent filtering to attain a final protein-level FDR of 1%. PSM filtering was performed using a linear discriminant analysis, as described previously (Huttlin *et al.*, 2010), considering the following parameters: Xcorr, DCn, missed cleavages, peptide length, charge state, and precursor mass accuracy. Protein assembly was guided by principles of parsimony to produce the smallest set of proteins necessary to account for all

observed peptides. Data for all three biological WCL replicates and the PM analysis were initially filtered and assembled together to produce a single list of quantified proteins.

Proteins were quantified by summing TMT reporter ion counts across all matching peptide-spectral matches using in-house software, as described previously (Pease *et al.*, 2013). Briefly, a 0.003 Th window around the theoretical m/z of each reporter ion (126, 127N, 127C, 128N, 128C, 129N, 129C, 130N, 130C, 131) was scanned for ions, and the maximum intensity nearest to the theoretical m/z was used. We required every individual peptide used for quantitation to contribute sufficient TMT reporter ions (minimum of 1,250 per spectrum) so that each on its own provided a representative picture of relative protein abundance (McAlister *et al.*, 2012). We additionally employed an isolation specificity filter to minimize peptide coisolation (Ting *et al.*, 2011). Peptide-spectral matches with poor quality MS3 spectra (more than 9 TMT channels missing and/or a combined signal to noise ratio of less than 250 across all TMT reporter ions) or no MS3 spectra at all were excluded from quantitation. Protein quantitation values were exported for further analysis in Excel. For protein quantitation, reverse and contaminant proteins were removed, then each reporter ion channel was summed across all quantified proteins and normalized assuming equal protein loading across all 10 samples. To calculate relative abundance, the maximal reporter ion counts for any channel for a given protein were set to 1. All other channels and their associated reporter ion counts were normalized to the aforementioned maxima and presented as relative abundance. Gene Ontology terms were downloaded from www.uniprot.org. XLStat (Addinsoft, https://www.xlstat.com/en/) was used to determine the number of distinct k-means clusters. Hierarchical centroid clustering was based on Euclidian Distance. Hierarchical and k-means clustering were performed using Cluster 3.0 (Stanford University and University of Tokyo, http://bonsai.hgc.jp/~mdehoon/software/cluster/software.htm) and visualized using Java Treeview (SourceForge.net, http://jtreeview.sourceforge.net).

Pathway Analysis was performed using the Database for Annotation, Visualization and Integrated Discovery (DAVID) (Huang da, Sherman and Lempicki, 2009) version 6.8 with default settings. A given cluster was always searched against a background of all proteins quantified within the relevant experiment. To generate lists of proteins for DAVID enrichment analysis, for WCL data, proteins were included if they were quantified in all three experiments WCL1-3. Parent terms were either derived from a hierarchical structure in Uniprot, or Gene Ontology (http://supfam.org/SUPERFAMILY/cgi-bin/go.cgi).

Gene Set Enrichment Analysis (GSEA)

The calculated differences in the proteomics data between uninfected cells and 4 DPI cells were used to generate a ranked list for GSEA Preranked analysis using the Molecular Signatures Database v5.2 (C7:immunologic signatures) (Subramanian *et al.*, 2005). Gene sets with nominal p value < 0.05 and false discovery rate (FDR) <0.25 were defined as significantly enriched gene sets, which were selected for visualization.

Nuclear imaging and cell diameter measurements

Cells were seeded on glass slide and fixed with 4% PFA solution for 10 minutes. Fixed cells were permeabilized with 0.5% Triton X-100/PBS solution and blocked with 20% newborn goat serum (NGS). Cells were incubated with a solution of Hoechst 33258 (10 µg/mL) for 10 minutes to stain nuclear DNA and dehydrated sequentially from 70% to 90% to 100% ethanol. ProLong anti-fade was applied to the slide and sealed with a No. 1.5 coverslip. Image acquisition was performed at the Brigham and Women's Hospital core facility with the Zeiss LSM 800 instrument. Image analysis was performed with the Zeiss ZEN Lite (Blue) software. For measurements of cell diameter, differential interference contrast (DIC) microscopy was performed and cells were manually picked out from the micrographs. Circular ROIs were drawn around the cells and diameters were automatically computed by the ZEN Lite (Blue) software.

Immunofluorescence microscopy

Approximately 1 million cells were pelleted and resuspended in 1-2 µL PBS and streaked onto glass slides to dry. Cells were fixed with 4% paraformaldehyde/PBS solution for 10 minutes and permeabilized with 0.5% (v/v) Triton X-100/PBS solution for 5 minutes, with PBS washing in between and after each of those steps. Cells were incubated with 20% normal goat serum (NGS) blocking reagent for 1 hour. EBNA1-specific OT1x antibody was diluted 1:100 in the blocking reagent and added to cells for 1 hour. Cells were washed and incubated with Alexa Fluor 488-conjugated goat anti-mouse secondary antibody (diluted 1:1000 in blocking reagent) for 30 minutes. Cells were washed and incubated with a 10 µg/mL Hoechst 33258/PBS solution for 3-5 minutes. Cells were washed and successively dehydrated in 70% (1 minute), 90% (1 minute) and 100% ethanol (1 minute). ProLong Gold antifade reagent was added to each well and a No. 1.5 coverslip was attached. Data acquisition was performed using a Zeiss LSM 800 instrument. Processing and analysis were performed using ZEN Blue software (Zeiss). All steps were performed at room temperature.

Immunoblotting

Crude cell lysates were generated by resuspending cell pellets in 1X Laemmli loading buffer (containing SDS) and sonicating on ice for 10 seconds. Lysates were then boiled for 10 minutes. Samples were loaded onto and electrophoretically resolved on 10% polyacrylamide gels and transferred onto nitrocellulose membranes for 1 hour at 100 V at 4˚C. Membranes were probed with primary antibodies, typically at a 1:1000 dilution overnight at 4˚C, washed three times with PBS-T for 10 minutes per wash, incubated with HRP-conjugated secondary antibodies in 5% skim milk/PBS-T for 30 minutes to 1 hour, and finally washed three times with PBS-T for 10 minutes per wash. Blots were imaged on Carestream or Li-Cor workstations.

Flow cytometry analysis

Flow cytometry was performed on a BD FACSCalibur instrument. Cells were washed once with ice-cold PBS supplemented with 0.5% bovine serum albumin (BSA). Cells were then incubated with a 1:100 dilution of fluorophore-conjugated primary antibody (and, if applicable, a 1:500 dilution of fluorophore-conjugated secondary antibody) in PBS with 0.5% BSA for 1 hour. Cells were pelleted and resuspended in 400 µL of PBS, strained into flow cytometry-compatible tubes and processed immediately with a flow cytometer. Sample processing was performed either immediately or within 24 hours after staining. For 2-NBDG staining, cells were incubated with 10 µg/mL 2-NBDG in complete media for 1 hour at 37˚C.

LC-MS metabolite analysis

Cells were seeded at 1 million cells/mL with fresh media (containing labeled amino acids, if required) 24 hours prior to harvesting. To prepare cellular metabolite extracts, cells were washed once with ice-cold PBS and once with ice-cold 100 mM ammonium acetate before lysis with acetonitrile-methanol-water (27:9:1). To prepare media metabolite extracts, 50 µL of media was extracted with acetonitrile-methanol (3:1). All extraction steps were performed at 4^{o}C. Crude extracts were centrifuged at maximum speed at 4^{o}C for 20 minutes to remove cellular debris, and supernatants were either used immediately or frozen at -80^{o}C for short-term storage.

LC-MS-based analyses were performed on a Q Exactive Plus orbitrap mass spectrometer equipped with an Ion Max source and a HESI II probe, which was coupled to a Dionex UltiMate 3000 UPLC system (Thermo Fisher Scientific).

Polar metabolites in the spent media and cellular extracts were analyzed using Xbridge BEH Amide XP HILIC 2.5 µm, 2.1 mm x 100 mm column (Waters) with the guard column and SeQuant ZIC-pHILIC Polymeric 5 µm, 150 x 2.1 mm column (EMD-Millipore).

For the amide method, the mobile phase A was 5% acetonitrile, 20mM ammonium acetate/ammonium hydroxide, pH 9. The mobile phase B was 100% acetonitrile. The flow rate was 220 µl/min from 0 – 15 min, and 420 µl/min from 15 – 25 min. The gradient was as follows: 0 min: 85% B; 0.5 min: 85% B; 9 min: 35% B; 11 min: 2% B; 13.5 min: 85% B; 15 min: 85% B; 22 min: 85% B. The MS data was collected in the polarity switching mode with full scan mode in a range of 70–1000 m/z, with the resolution at 70,000, the AGC target at 1E6, and the maximum injection time at 80 ms, the sheath gas flow at 50 units, the auxiliary gas flow at 10 units, the sweep gas flow at 2 units, the spray voltage at 2.5 kV, the capillary temperature at 310 °C, and the auxiliary gas heater temperature at 370°C.

Progenesis QI software (Waters, NC) and Xcalibur (Thermo Fisher Scientific) were used to analyze the data. Absolute quantification of glucose, serine and lactate in the spent media was measured by comparing to the ^{13}C-labeled internal standards at different spiked concentrations.

Natural isotope correction

Mass isotopomer distributions were corrected for the natural abundance of heavy isotopes of hydrogen, carbon, oxygen, and nitrogen. Phosphorus is considered monoisotopic. Natural abundances were found in the Table of Isotopic Compositions of the Elements (TICE) maintained by the International Union of Pure and Applied Chemistry (IUPAC) (Meija *et al.*, 2016).

Element	**M+0**	**M+1**	**M+2**
H	0.999885	0.000115	
C	0.9893	0.0107	
O	0.99757	0.00038	0.00205
N	0.99632	0.00368	

P 1

This method takes into account the different isotope abundance distributions in the labelled molecule as compared to the isotope abundance distributions in the unlabeled molecule (the proportionality “skew”). The corrected mass isotopomer distribution MID_{corr} is obtained by multiplying the observed mass isotopomer distribution (MID_{obs}) by a correction matrix (CM); the CM for dTTP is shown below:

$$\begin{bmatrix} M0_{obs} \\ M1_{obs} \\ M2_{obs} \\ \vdots \end{bmatrix} = CM_{dTTP} \begin{bmatrix} M0_{corr} \\ M1_{corr} \\ M2_{corr} \\ \vdots \end{bmatrix}$$

$$= CM_{H_{17}} CM_{C_{10}} CM_{O_{14}} CM_{N_2} CM_{P_3} \begin{bmatrix} M0_{corr} \\ M1_{corr} \\ M2_{corr} \\ \vdots \end{bmatrix}$$

Using the example of the oxygen correction matrix, a correction matrix for any non-labelled atom type takes the form:

$$CM_{O_{14}} = \begin{bmatrix} p(_{16}O_{14}) & 0 & 0 & 0 & \dots \\ p(_{16}O_{13}{}_{\cdot 17}O_1) & p(_{16}O_{14}) & 0 & 0 & \dots \\ p(_{16}O_{12}{}_{\cdot 17}O_2) + p(_{16}O_{12}{}_{\cdot 18}O_1) & p(_{16}O_{13}{}_{\cdot 17}O_1) & p(_{16}O_{14}) & 0 & \dots \\ \vdots & \vdots & \vdots & \vdots & \ddots \end{bmatrix}$$

Defining:

$$p(\text{elemental isotopomer}) = \binom{N}{f(I_i), \dots, f(I_n)} \times \Pi_{i=1}^{n} p(I_i)^{f(I_i)}$$

$$= N! \times \Pi_{i=1}^{n} \left(\frac{p(I_i)^{f(I_i)}}{f(I_i)!} \right)$$

Where N is the number of atoms of the element (in this case, oxygen) in the molecule, n is the number of naturally occurring isotopes, I_1, … I_n, of the element, p(I_i) gives the natural abundance of isotope I_i, and $f(I_i)$ is the frequency of the i-th isotope in the molecule.

The correction matrix for hydrogen takes a special form since hydrogen is the element being labelled:

$$CM_{H_{17}} = \begin{bmatrix} p({}_1H_{17}) & 0 & 0 & 0 & \dots & \dots \\ p({}_1H_{16}{\cdot}{}_2H_1) & p({}_1H_{16}) & 0 & 0 & \dots & \dots \\ p({}_1H_{15}{\cdot}{}_2H_2) & p({}_1H_{16}{\cdot}{}_2H_1) & p({}_1H_{15}) & 0 & \dots & \dots \\ \vdots & \vdots & \vdots & \vdots & \ddots & \\ p({}_2H_{17}) & p({}_2H_{16}) & p({}_2H_{15}) & \dots & \dots & 1 \end{bmatrix}$$

We used a least-squares implementation of the accepted optimal approach for natural abundance correction, the “skewed” method as outlined by Midani et al. in reference to earlier works by Rosenblatt and Fernandez et al. (Midani, Wynn and Schnell, 2017; Fernandez *et al.*, 1996; Rosenblatt *et al.*, 1992). The R package *nnls* was used to find the non-negative least squares solution. Details of algorithmic implementation were adapted from Yang et al. (Yang *et al.*, 2009). Full code is available online at github.com/BrynMarieR/natural_isotope_correction/.

Growth curve analysis

Newly infected B-cells were seeded at 500,000 cells per well in a volume of 1 mL of RPMI/FBS and grown for two days before measurements of cell numbers were made. For GM12878 lymphoblastoid cells, 100,000 cells were seeded per well in a volume of 1mL and grown for two days prior to measurements of live cell number. For live cell measurements, cells were pelleted and resuspended in the same volume of media, trypan blue was added 1:1, and live cell number was quantitated with the TC20 automatic cell counter (Bio-Rad). After measurements were taken, cells were passaged accordingly to give 100,000 cells per mL in RPMI/10% FBS and grown for two more days. The same procedure was repeated to obtain measurements at later

time points. At each time point, cells were treated with the appropriate inhibitor and/or rescue metabolite(s) at the indicated concentrations after passaging.

Mitochondrial stress test

Cell culture plates were layered with Cell-Tak (Corning) to enable adhesion of the B-cells. Cells were seeded at 500,000 per well. For standard measurements, complete bicarbonate-free RPMI-1640 supplemented with 25 mM HEPES, 10% dialyzed FBS and 2 mM L-glutamine was used as the growth media during the period of data acquisition. Detection of changes in oxygen consumption and extracellular acidification rates was achieved with the use of Seahorse XF24 sensor cartridges. The following mitochondrial poisons were used: 3.5 μM oligomycin, 2 μM CCCP and 100 nM piericidin A. Data acquisition was performed with the Seahorse XF24 Extracellular Flux Analyzer (Agilent).

Results

EBV infection of primary B-cells induces a drastic increase in cell size

We established a proteomic approach to study EBV transformation of B-cells, a process where a quiescent B-cell dramatically enlarges by four days post-infection (DPI) (Figure II.1A) and eventually becomes an actively dividing B lymphoblast. Consistent with the fact that cell size is regulated by the mammalian target of rapamycin (mTOR) pathway (Fingar *et al.*, 2002), mTOR protein abundance was increased over the course of infection with concomitant upregulation of the key mTOR complex 1 (mTORC1) positive regulator Ras homolog enriched in brain (RHEB) and downregulation of the programmed cell death 4 (PDCD4) protein, a suppressor of cap-dependent translation downstream of mTORC1-mediated signaling (Figure II.1B) (Dennis, Jefferson and Kimball, 2012; Dorrello *et al.*, 2006; Schmid *et al.*, 2008).

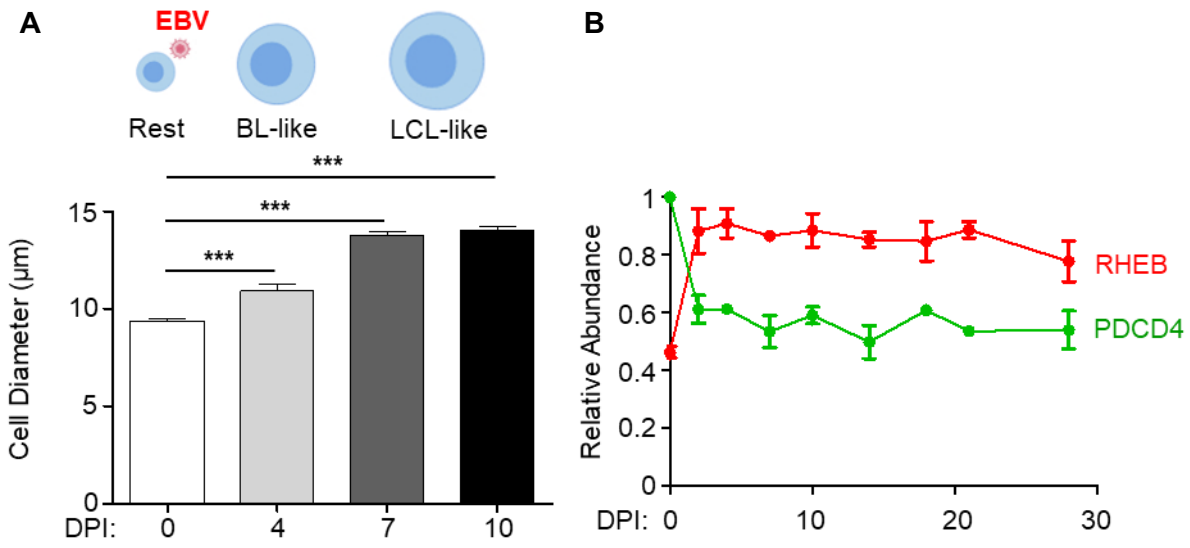

Figure II.1 EBV infection induces an early increase in cell size concomitant with mTOR activation. (A) B-cell diameter measurements at the indicated days post-infection (DPI) by EBV. At least four independent confocal microscopy fields-of-view were quantitated. Data show the mean + SEM, n > 25 cells from three independent experiments. ***, p< 0.005 (two-tailed t-test). (B) Temporal proteomic traces of protein relative abundances for the mammalian target of rapamycin (mTOR) pathway regulator Ras homolog enriched in brain (RHEB) and mTOR target programmed cell death protein 4 (PDCD4). Data show the mean with SEM, n=3.

EBV upregulation of human B-cell metabolic pathways

To identify virus-induced metabolic pathways important for EBV-driven B-cell growth, we used 10-plexed tandem-mass-tag (TMT) and MS3 mass spectrometry to analyze primary human CD19+ B-cells either left uninfected or infected at a low multiplicity with the B95-8 strain of EBV, which was originally isolated from a patient with IM. Successfully infected B-cells were isolated by flow cytometry at nine time points after initial infection using CD23 plasma membrane (PM) expression as a proxy for infection (Wang *et al.*, 1987; Thorley-Lawson and Mann, 1985). Three whole cell lysate (WCL) biological replicates, each comprising cells pooled from four distinct

human donors, were performed (Figure II.2A). We additionally quantified changes in PM protein expression for one replicate. Immunoblots demonstrated the expected pattern of EBV oncoprotein expression (Figure II.2B).

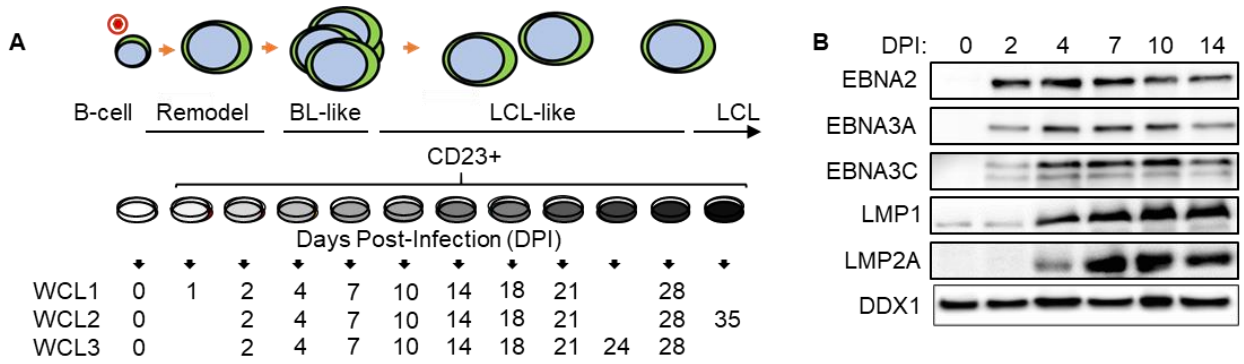

Figure II.2 Outline of the proteomics approach and confirmation of viral gene expression. (A) Schematic of experimental workflow. Primary human B-cells (3 biological replicates, each consisting of 4 independent donors) were analyzed prior to and at 9 time points after EBV infection. CD23+ EBV-infected cells were enriched by FACS. WCL, whole cell lysate. (B). Representative immunoblots (n=3) of EBV nuclear antigens (EBNAs), latent membrane proteins (LMPs) and load-control DDX1 of newly infected primary B-cells at the indicated days post-infection (DPI). I. Ersing generated lysates that were electrophoretically processed by S. Trudeau.

We quantified 8,054 B-cell and 29 EBV-encoded proteins in at least one replicate. Across all three replicates, 6,455 B-cell and 11 EBV-encoded proteins (Figure II.3) were quantified; data exhibited strong concordance across replicates (Figures II.3B-C).

Figure II.3 Strong concordance between biological replicates. (A) Peptides and proteins quantified in all experiments in this manuscript. Of 712 human proteins quantified in experiment PM1, 475 were annotated by Gene Ontology ‘plasma membrane’, ‘cell surface’, ‘extracellular’ or ‘short GO’. (B) Hierarchical cluster analysis of all proteins quantified in all three WCL experiments by 2 or more peptides. (C) Matrix of Pearson correlations for all three WCL experiments. For every sample, fold change was calculated compared to the relevant uninfected control and then correlated to the fold change of every other sample. Bioinformatic analyses were performed by L. Nobre and M.P. Weekes.

Figure II.3 (Continued)

A

	All peptides	Human proteins	EBV proteins
WCL1	73146	7627	21
WCL2	52270	6986	17
WCL3	62810	7255	22
All3 WCL		6445	11
PM1	3988	712	2

B

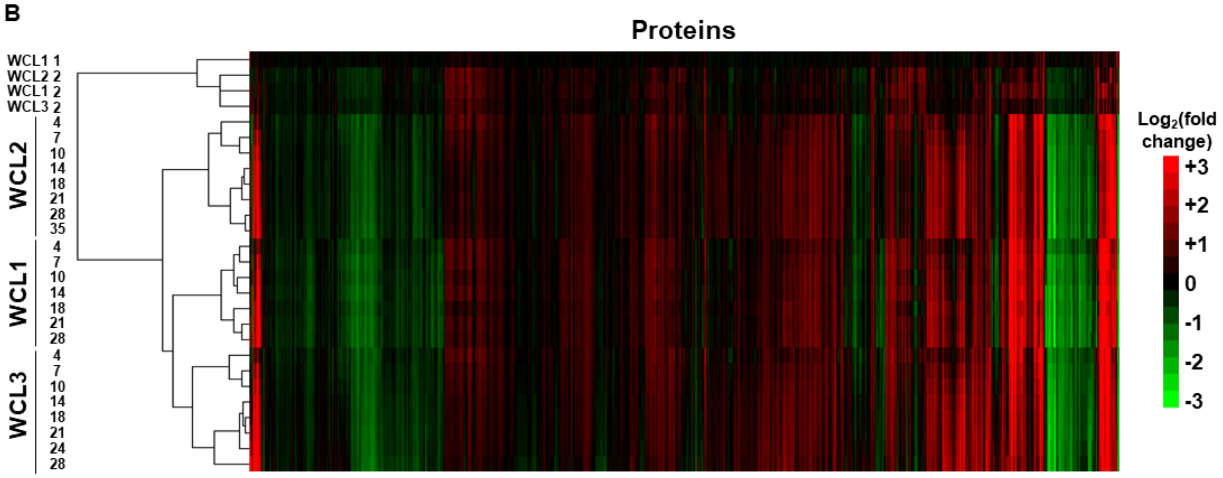

C

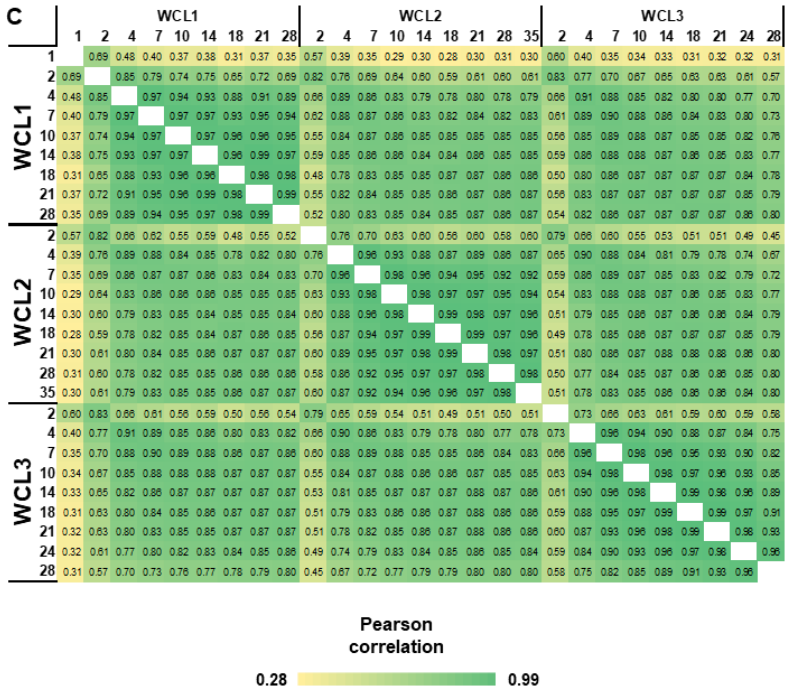

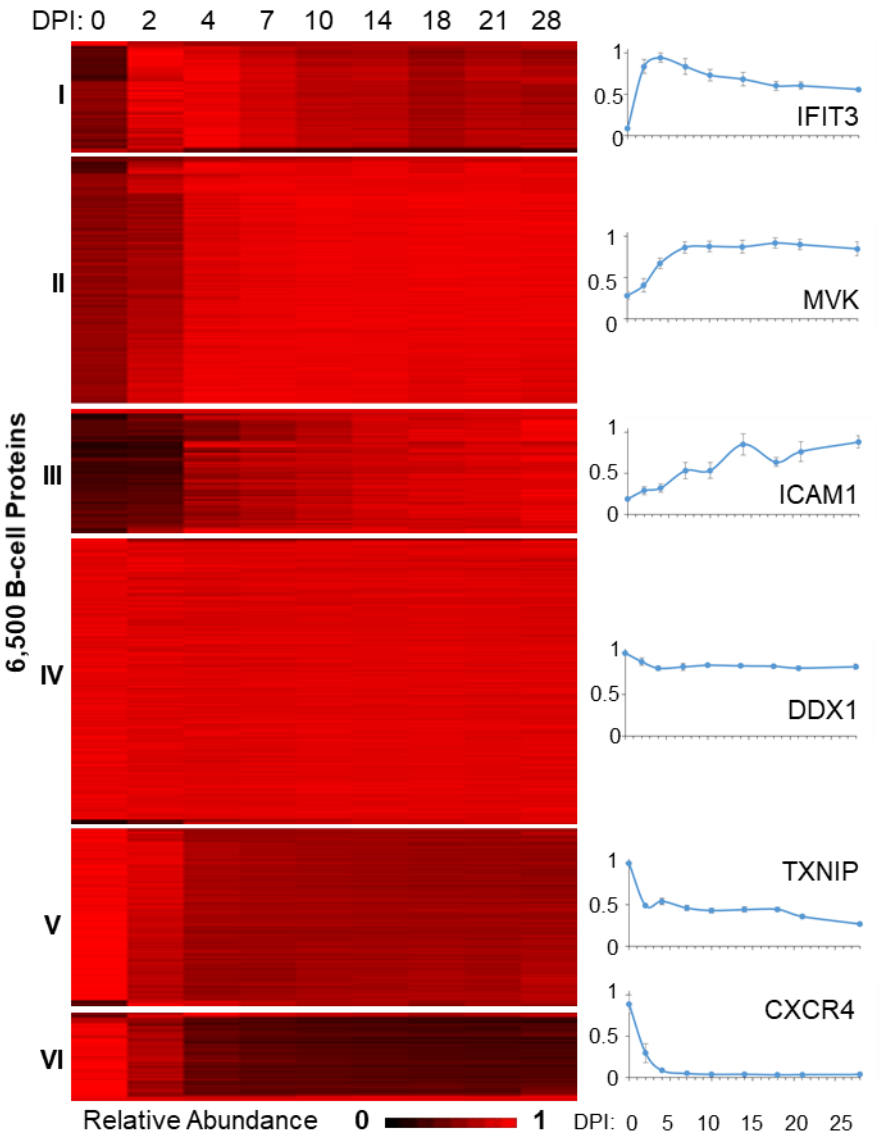

Figure II.4 k-means clustering of quantified B-cell proteins based on averaged relative abundances. Representative expression profiles are shown to the right of each k-means cluster. To determine the actual number of distinct classes of host protein expression, the k-means approach was used with 1-12 classes to cluster viral proteins, and the summed distance of each protein from its cluster centroid was calculated. Bioinformatic analyses were performed by L. Nobre and M.P. Weekes.

Six clusters of B-cell proteins with distinct temporal expression patterns (Figure II.4) over the transformation time course were identified by way of k-means analysis (Figure II.5). Through this approach, we were also able to determine proteins that could serve as good load-controls for protein-based assays e.g. DDX1 and DDX46 (Figure II.6).

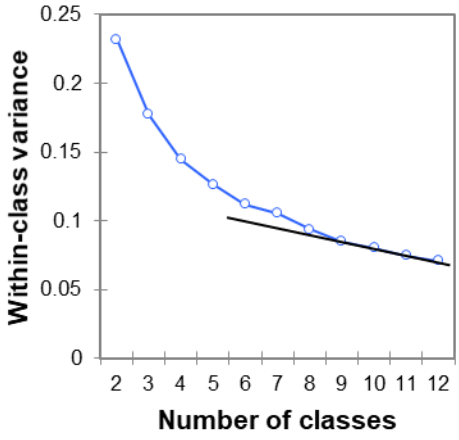

Figure II.5 Plot of within-class variance against number of classes. Bioinformatic analyses were performed by L. Nobre and M.P. Weekes.

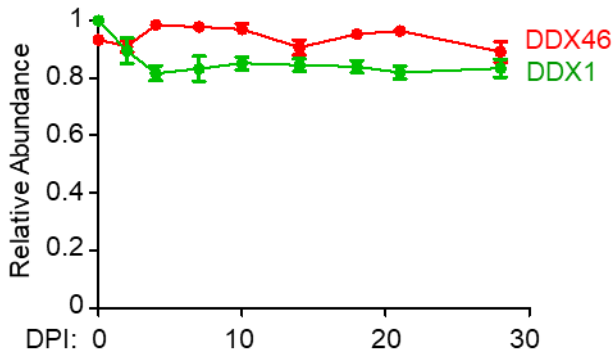

Figure II.6 DDX1 and DDX46 levels remain unchanged over the infection time course. Temporal proteomic traces of the DEAD box DNA helicases DDX1 and DDX46 at the indicated DPI of primary human B-cell EBV infection. Data show the mean + SEM of n=3 biological replicates.

We used DAVID software (Huang, Sherman and Lempicki, 2009b; Huang, Sherman and Lempicki, 2009a) to identify pathways enriched among significantly upregulated proteins (Clusters I-III) at four days post-infection (DPI), and identified multiple metabolic terms including one-carbon metabolism and serine biosynthesis, as well as cholesterol biosynthesis (Figure II.7).

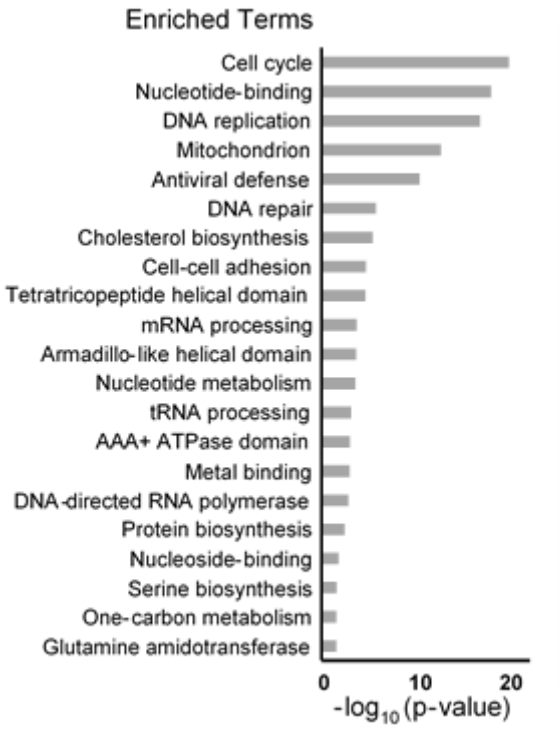

Figure II.7 Term enrichment analysis for proteins significantly upregulated at 4 DPI. Functional enrichment within all proteins upregulated >2-fold with $p<0.075$ four days post EBV infection (Clusters I-III) against a background of all quantified proteins. Overall, 41 clusters were significantly enriched (Table S1). For the purposes of simplified display, these were concatenated into hierarchical parent terms, where available for individual clusters that had been identified using Uniprot or Gene Ontology. For example, ‘Sister chromatid cohesion’, ‘DNA condensation’, ‘Kinesin, motor domain’ were concatenated into ‘Cell cycle’. Bioinformatic analyses were performed by L. Nobre and M.P. Weekes.

Amongst quantified viral proteins, particularly high EBNA2 expression was observed 2 DPI, which correlated with markedly elevated levels of MYC, a well-known master regulator of cellular metabolism (Figures II.8-9).

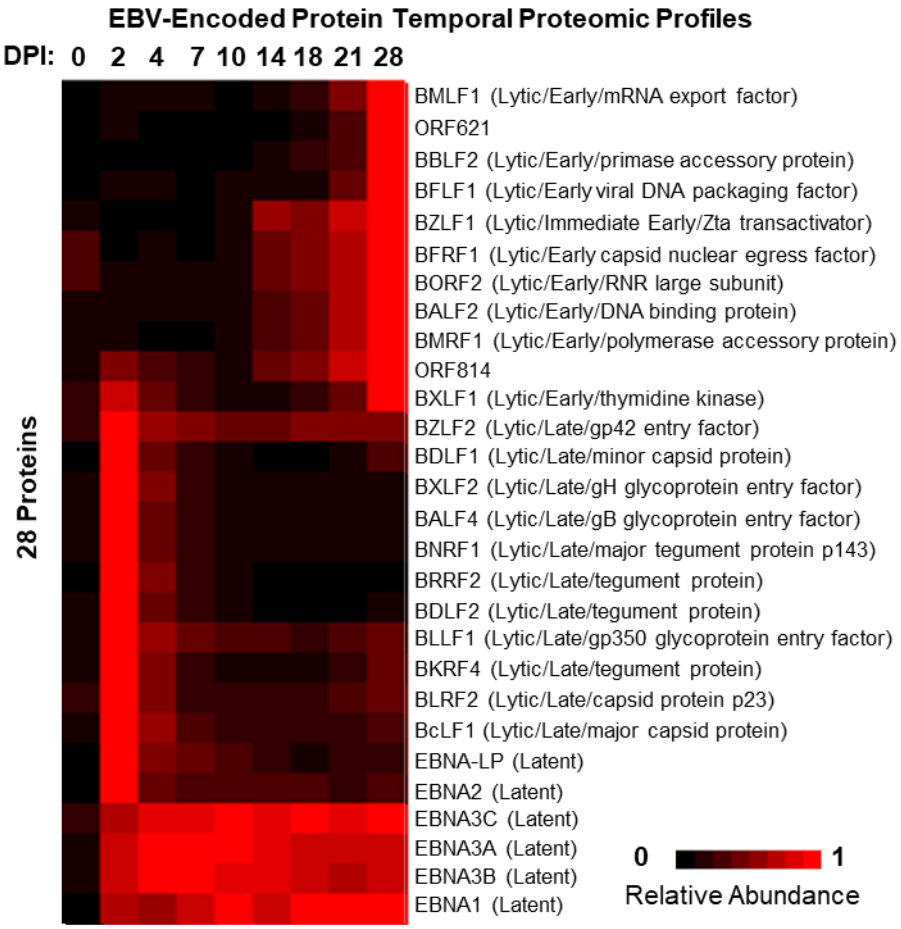

Figure II.8 Heatmap temporal proteomic plots of EBV proteins quantified in any of the three WCL replicates. Three distinct profiles were observed. Proteins have been annotated as latent or lytic cycle, expressed with immediate early, early or late kinetics, and associated function, if known. Bioinformatic analyses were performed by L. Nobre and M.P. Weekes.

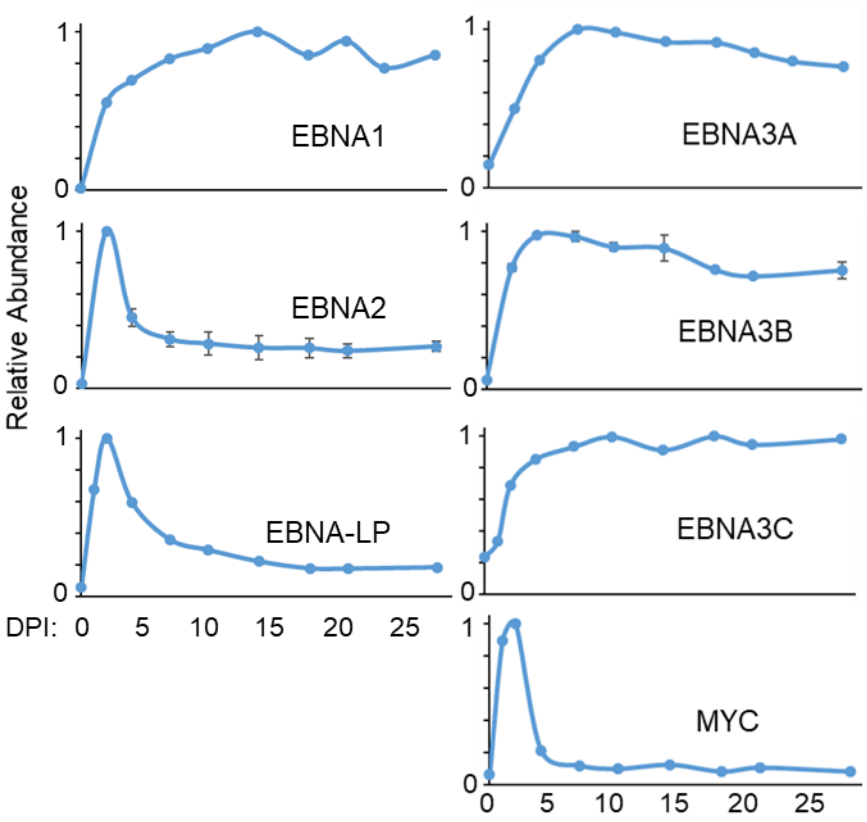

Figure II.9 Temporal proteomic profiles of EBNA and MYC proteins. EBNA2 and EBNA3B were consistently detected (3 out of 3 runs) and therefore have been plotted with SEM error bars. The rest of the transcription factors were not consistently detected by mass spectrometry. Bioinformatic analyses were performed by L. Nobre and M.P. Weekes.

We also discovered two new EBV open reading frames, whose expressed gene products increased late in infection (Figure II.10).

ORF814, Frame 5

IITMEACPHIRYAFQNDKLLLQQASVGRLTLVNKTTILLRPMKTTTVDLGLYARPP
EGHGLMLWGSTSRPVTSHVGIIDPGYTGELRLILQNQRRYNSTLRPSELKIHLAA
FRYATPQMEEDKGPINHPQYPGDVGLDVSLPKDLALFPHQTVSVTLTVPPPSIP
HHRPTIFGRSGLAMQGILVKPCRWRRGGVDVSLTNFSDQTVFLNKYRRFCQLV
YLHKHHLTSFYSPHSDAGVLGPRSLFRWASCTFEEVPSLAMGDSGLSEALEGR
QGRGFGSSGQ

ORF621, Frame 4

SSWRKDFNGRAFPLLLLAMRPKKDGLEDFLRLTPEIKKQLGSLVSDYCNVLNK
EFTAGSVEITLRSYKICKAFINEAKAHGREWGGLMATLNICNFWAILRNNRVRR
RAENAGNDACSIACPIVMRYVLDHLIVVTDRFFIQAPSNRVMIPATIGTAMYKLL
KHSRVRAYTYSKVLGVDRAAIMASGKQVVEHLNRMEKEGLLSSKFKAFCKWV
FTYPVLEEMFQTMVSSKTGHLTDDVKDVRALIKTLPRASYSSHAGQRSYVSGV
LPACLLSTKSKAVETPILVSGADRMDEELMGNDGGASHTEARYSESGQFHAFT
DELESLPSPTMPLKPGAQSADCGDSSSSSSDSGNSDTEQSEREEARAEAPRL
RAPKSRRTSRPNRGQTPCPSNAAEPEQPWIAAVHQESDERPIFPHPSKPTFLP
PVKRKKGLRDSREGMFLPKPEAGSAISDVFEGREVCQPKRIRPFHPPGSPWA
NRPLPASLAPTPTGPVHEPVGSLTPAPVPQPLDPAPAVTPEASHLLEDPDEET
SQAVKALREMADTVIPQKEEAAICGQMDLSHPPPRGHLDELTTTLESMTEDLN
LDSPLTPELNEILDTFLNDECLLHAMHISTGLSIFDTSLF

Figure II.10 Primary sequences of two newly discovered EBV gene products. Amino acid sequences of newly identified EBV ORF814 and ORF621 are shown. Detected peptides are indicated in green. Bioinformatic analyses were performed by L. Nobre and M.P. Weekes.

Approximately 20 EBV lytic cycle proteins were also quantified, including several metabolic enzymes (Figure II.8). Of those lytic proteins, 11 were late gene products and whose apparent protein expression spiked at 2 DPI before falling to very low levels at later time points. These proteins have been previously described to be part of the virus particle (Johannsen *et al.*, 2004). The expression profiles for these 11 proteins are consistent with virus entry into the cell and subsequent degradation of the virion's structural proteins. For the remaining lytic gene products, they likely represent a leaky lytic gene expression program rather than true lytic replication as we were able to detect 72 EBV proteins in our similar TMT analysis of the EBV B-cell lytic cycle (Ersing *et al.*, 2017). Alternatively, it might have been due to full or abortive lytic replication in a small population of cells. However, flow cytometric analysis at 4 DPI identified that most cells

were negative for gp350 (Figure II.11), indicating that lytic reactivation was unlikely and also would not be a dominant contributor to the observed metabolic changes. It is currently not fully understood why lytic protein expression would occur late in latent infection and how this expression program might be activated.

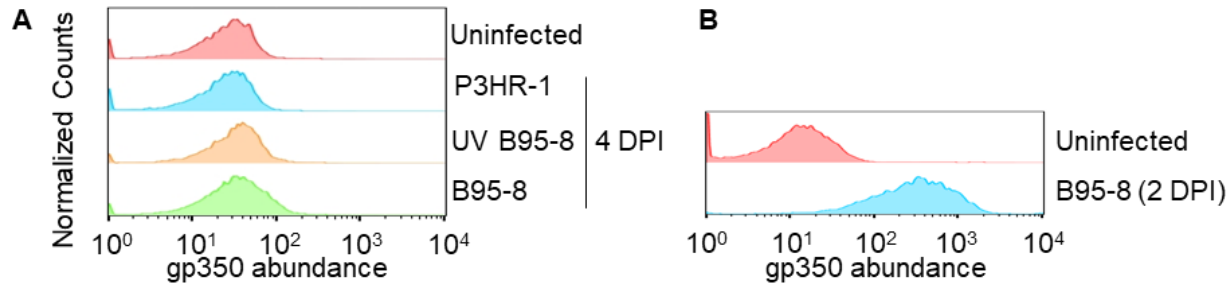

Figure II.11 Flow cytometric analysis of newly infected B-cells for surface gp350 abundance. (A) Flow cytometric analysis of cell surface EBV gp350 expression on primary B-cells infected with the indicated virus strains 4 DPI. Data shown is representative of n=3. (B) Flow cytometric analysis of cell surface EBV gp350 expression on resting primary B-cells and cells infected with B95-8 virus 2 DPI. Data shown is representative of n=3.

Profiling of 712 PM proteins revealed widespread EBV-driven remodeling of the PM proteome, particularly amino acid and ion transporters, coinciding with the onset of B-cell hyperproliferation (Figures II.12A-C).

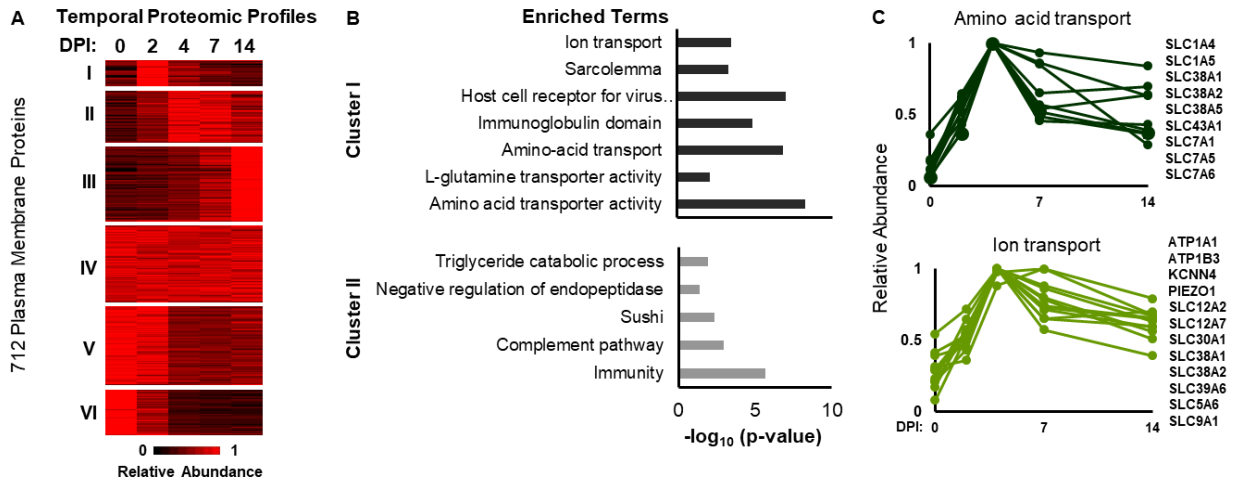

Figure II.12 EBV remodels the plasma membrane proteome. (A) Hierarchical cluster k-means analysis of the 712 B-cell plasma membrane (PM) proteins quantified in experiment PM1, by biotin labeling and streptavidin pulldown. K-means analysis was used to cluster B-cell PM proteins into 6 temporal categories. (B) Functional enrichment analysis of EBV-induced PM proteins upregulated during EBV-induced transformation (clusters I-II). (C) Temporal proteomic relative abundances of PM amino acid or ion transporters induced by EBV infection. Bioinformatic analyses were performed by L. Nobre and M.P. Weekes.

Notably, whole cell and plasma membrane abundances of the heterodimeric transporter for leucine and essential amino acids (EAAs), SLC3A2/SLC7A5, were strongly upregulated (Figure II.13). In particular, both subunits' plasma membrane expression levels tracked with that of MYC. This is particularly intriguing as leucine is a well-known activator of mTOR signaling; in the absence of LMP2A-mediated PI3K/AKT signaling, EBNA2-induced MYC expression may upregulate leucine and EAA uptake to activate mTOR (Nicklin *et al.*, 2009; Wolfson *et al.*, 2016). In an EBNA2-inducible system, conditional loss of EBNA2 led to a significant decrease in *SLC7A5* transcript abundance (Zhao *et al.*, 2006), further supporting the idea that EBNA2 may have an mTOR-activating role in incipient infection prior to sufficient LMP2A expression.

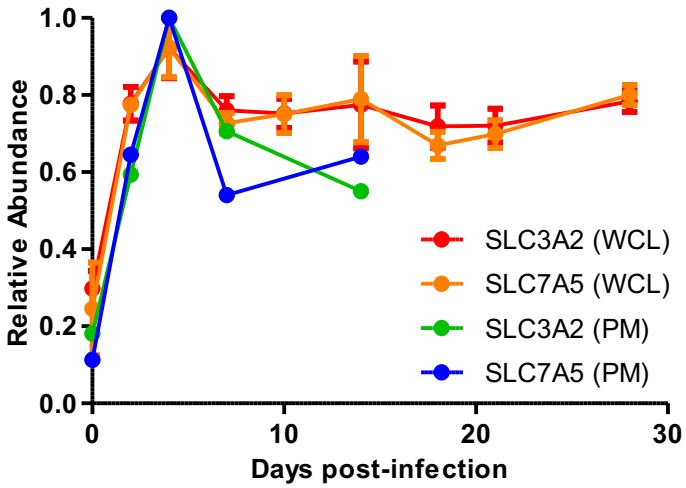

Figure II.13 Early upregulation of large amino acid transporter subunits. Temporal proteomic traces of the SLC3A2 and SLC7A5 at the indicated DPI of primary human B-cell EBV infection. Data show the mean + SEM of n=3 biological replicates for WCL samples and single values for PM samples.

Early induction of aerobic glycolysis in newly infected B-cells

EBV induces aerobic glycolysis in infected B-cells but how early this occurs in B-cell transformation remains undefined (McFadden *et al.*, 2016; Darekar *et al.*, 2012; Sommermann *et al.*, 2011). Early upregulation of all glycolytic enzymes was detected, with the rate limiting enzyme hexokinase 2 (HK2) highly induced by 2 DPI (Figure II.14). Thioredoxin-interacting protein (TXNIP), a potent negative regulator of glucose metabolism (Parikh *et al.*, 2007), was concomitantly and strongly downregulated by EBV (Figure II.14).

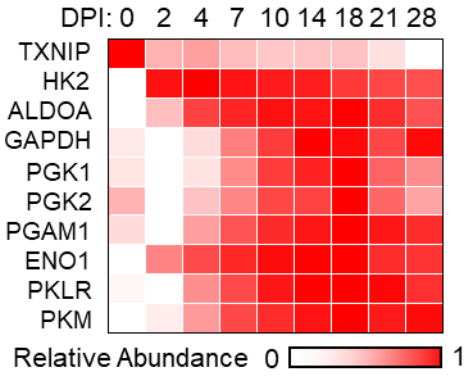

Figure II.14 Heatmap of averaged relative abundances of glycolytic enzymes. Relative abundances of each enzyme at the indicated time points are plotted.

PM proteomic data and subsequent validation by flow cytometry suggested that EBV infection induced substantial re-localization of GLUT1 to the plasma membrane (Figure II.15). Consistent with GLUT1 trafficking to the PM and subsequent enhanced glycolytic flux, B-cell glucose consumption and lactate release were increased by 2 DPI and maximal at 4 DPI (Figure II.16).

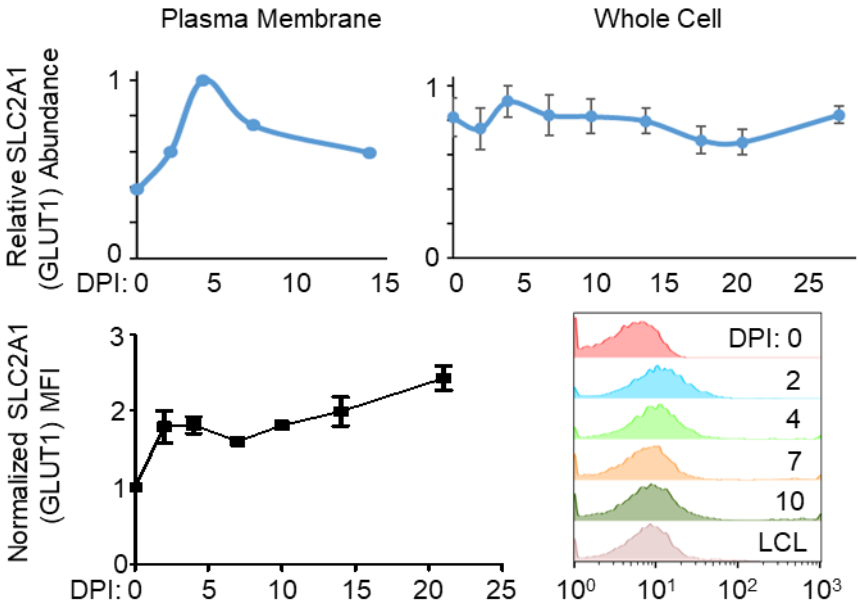

Figure II.15 Glucose transporter SLC2A1 expression is upregulated during EBV infection. Temporal proteomic traces of SLC2A1 (GLUT1) glucose transporter PM and WCL relative abundances. Normalized GLUT1 median fluorescent intensity (MFI) and flow cytometric histograms were also plotted against time for newly infected cells. Data shown are representative of n=3 biological replicates. Data for MFI show the mean ± SEM, n=3.

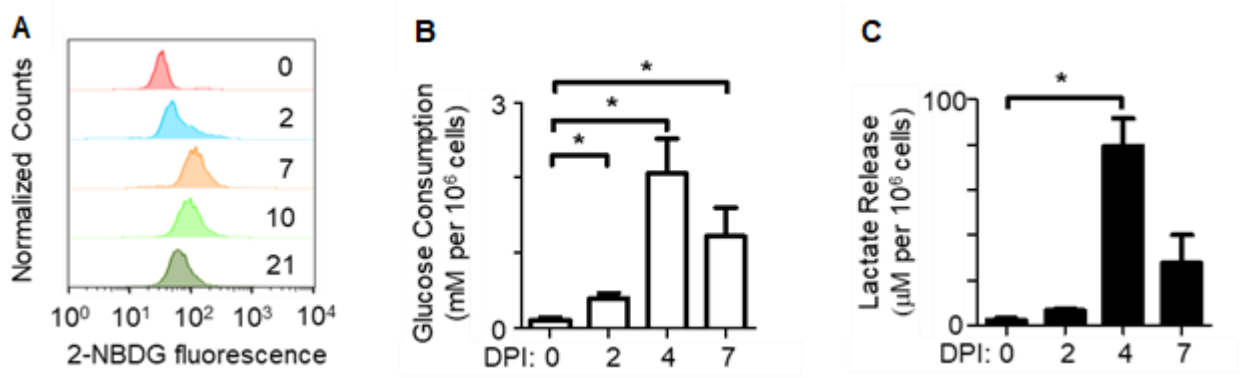

Figure II.16 EBV induces high rates of glucose consumption and glycolytic flux. (A) Flow cytometry analysis of primary human B-cell glucose analogue 2-NBDG uptake at the indicated DPI. Histograms are representative of n=3 biological replicates. LC-MS analysis of media (B) glucose consumption and (C) lactate production from cultures of primary B-cells at the indicated time points post-infection. The 24-hour mean ± SEM decrease in media glucose and 24-hour increase in media lactate are shown at the indicated DPI, n=3. *, $p<0.05$ (paired one-tailed t-test).

As EBNA2 is the major EBV transcription factor expressed at this early timepoint, we determined whether it was necessary for EBV-driven aerobic glycolysis. We made use of the 2-2-3 EBNA2-HT B-cell line (hereafter referred to as EBNA2-HT), where 4-hydroxytamoxifen (4HT) positively regulates nuclear localization and stability of a conditional EBNA2 allele, comprised of EBNA2 fused to a mutant estrogen receptor ligand binding domain (Zhao *et al.*, 2006; Schuhmacher *et al.*, 2001a). Conditional inactivation of EBNA2-HT by 4HT withdrawal strongly impaired LCL lactate release (Figure II.17), further suggesting an important EBNA2 role in stimulating glycolysis.

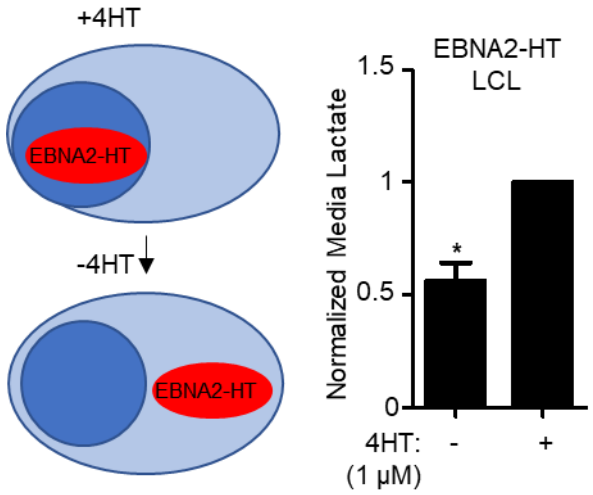

Figure II.17 EBNA2 upregulates glycolysis. Normalized lactate secretion values from LCLs with conditional EBNA2-HT alleles, in the absence or presence of 4HT for 48 hours, as indicated. Mean + SEM are shown from n=3 biological replicates. *, $p<0.05$ (one-sample t-test).

EBV remodels the B-cell mitochondrial proteome, dynamically altering respiratory chain complex subunit abundances

EBV-driven outgrowth was strongly impaired when cells were cultured in media containing galactose instead of glucose (Figure II.18), highlighting glucose as a key carbon source in viral B-cell transformation.

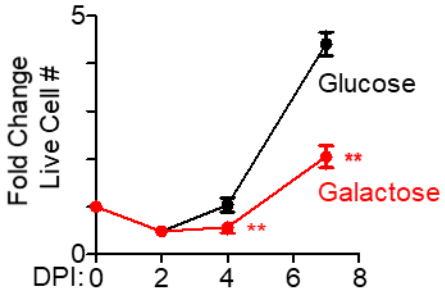

Figure II.18 Substitution of glucose with galactose inhibits newly infected cell growth. Growth curves of newly infected primary human B-cells grown in complete media containing either glucose or galactose. Data show the mean ± SEM, n=3. **, $p<0.01$ (paired one-tailed t-test).

Bioinformatic analysis enriched mitochondrial proteins as being significantly upregulated (Figure II.7). Yet, relatively little is known about EBV-mediated reprogramming of the mitochondrion. Using the MitoCarta 2.0 database (Calvo, Clauser and Mootha, 2016), we identified 799 B-cell mitochondrial proteins in our temporal proteomic profiling (Figure II.19). Mitochondrial proteome remodeling commenced shortly after infection and even prior to mitosis, which is suggestive of an important role in viral B-cell growth transformation. Notably, since most mitochondrial proteins are encoded by the host cell nuclear genome, EBV nuclear antigens can regulate their expression.

EBV upregulated 35 of the 98 quantified nuclear genome-encoded electron transport chain (ETC) components (Figure II.20) by ≥ 1.5-fold at ≥ one time point. Three ETC components encoded by the mitochondrial genome, MT-ND5 (1 out of 3 runs), MT-ATP6 (2 out of 3 runs) and MT-ATP8 (3 out of 3 runs), were also detected but did not show appreciable increases in abundance.

Figure II.19 Heatmap of detected mitochondrial proteins over the infection time course. Hierarchical k-means cluster analysis of EBV-mediated remodeling of 799 MitoCarta-annotated proteins quantified by temporal proteomic analysis of viral primary B-cell growth transformation. Representative expression profiles of averaged relative abundances are shown to the right of each k-means cluster. Bioinformatic analyses were performed by L. Nobre and M.P. Weekes.

Figure II.19 (Continued)

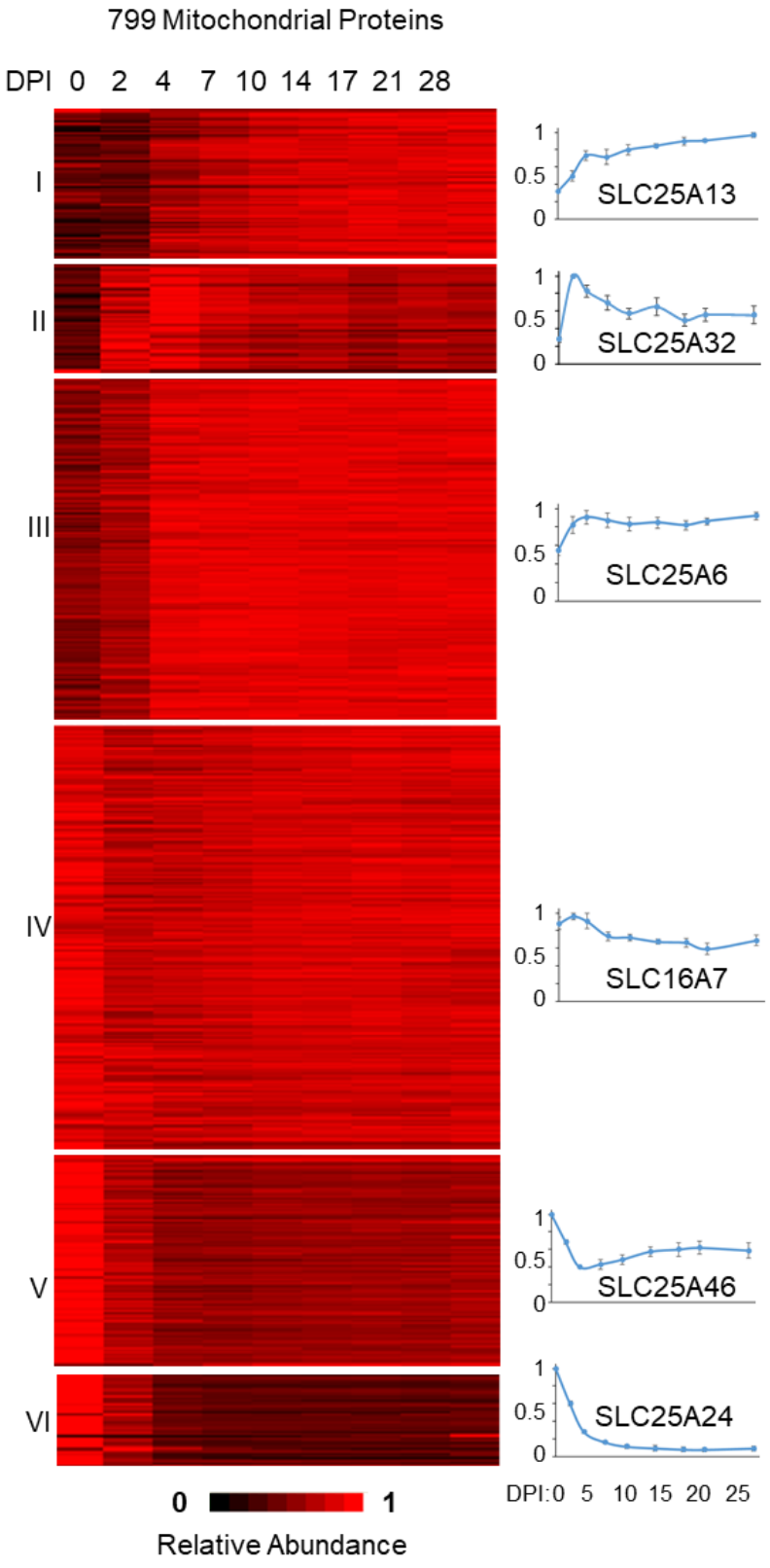

Figure II.20 Heat map of averaged relative abundances of mitochondrial electron transport chain components. Relative abundances for each of the 98 quantified nuclear-encoded proteins at the indicated time points are plotted. Only proteins that were consistently detected are shown here.

Figure II.20 (Continued)

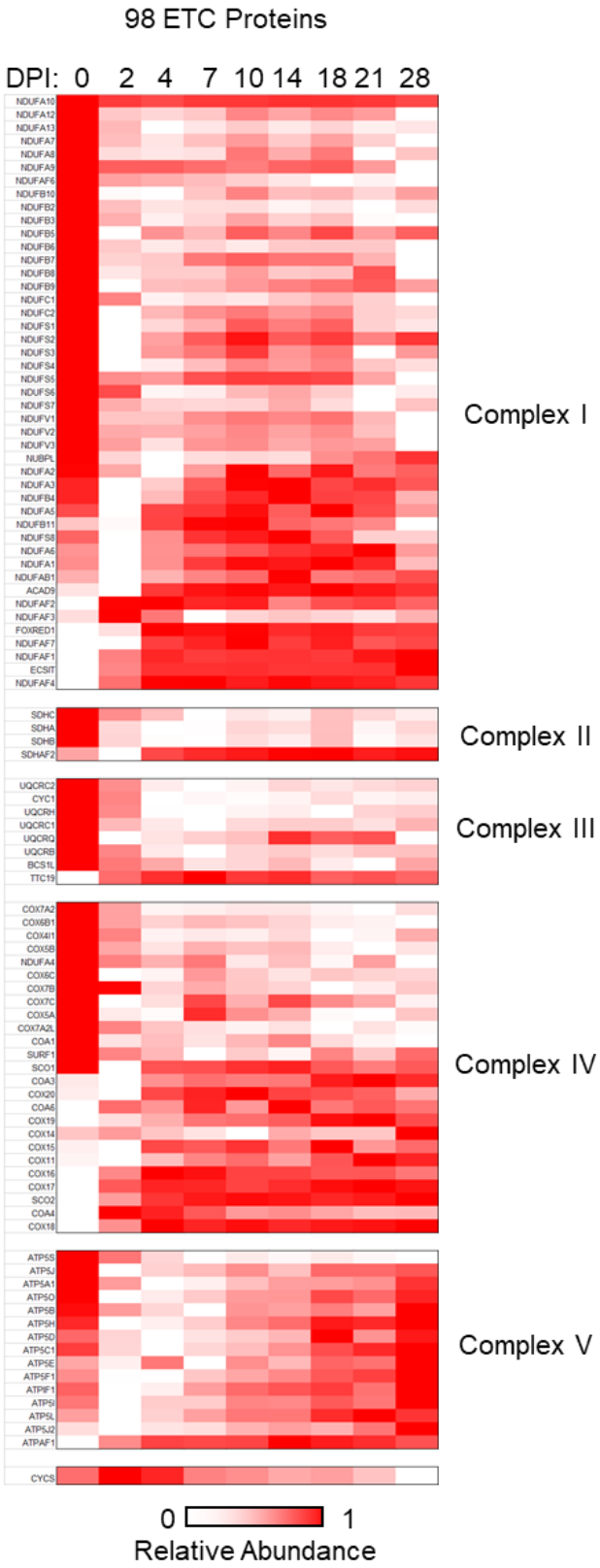

We observed enhanced basal and maximal oxygen consumption rates (OCRs) in newly infected cells (Figure II.21A), suggesting that increased oxidative capacity might be important for successful outgrowth. Newly infected cells were treated with either piericidin A, a complex I inhibitor, or antimycin, a complex III inhibitor. Each significantly diminished EBV-driven B-cell outgrowth (Figure II.21B). Thus, the concurrent induction of the Warburg effect and the upregulation of oxidative phosphorylation (OXPHOS) are each important for supporting outgrowth of B-cells undergoing viral transformation.

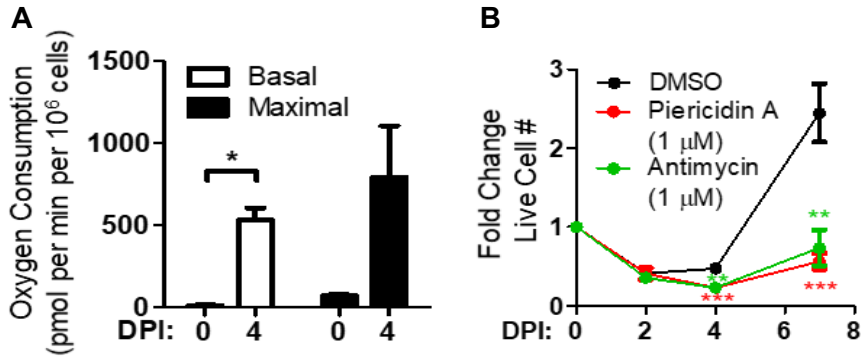

Figure II.21 EBV-induced OXPHOS upregulation is crucial for outgrowth of newly infected cells. (A) Seahorse flux analysis of basal and maximal oxygen consumption rate in primary B-cells uninfected or at 4 DPI. Data show the mean + SEM, n=3. *, $p<0.05$ (paired one-tailed t-test). (B) Growth curves of primary B-cells at the indicated DPI treated with DMSO vehicle, the complex I antagonist, piericidin A (1 μM), or the complex III antagonist, antimycin (1 μM). n=3 replicates. Data show the mean ± SEM, n=3. **, $p<0.01$; ***, $p<0.005$ (paired one-tailed t-test).

DAVID analysis identified ribosome biogenesis and 1C metabolism as the most strongly upregulated mitochondrial pathways in newly infected B-cells (Figure II.22A). Mitochondrial 1C metabolism uses serine as a precursor for 1C unit, NAD(P)H, ATP and glycine generation. EBV robustly upregulated mitochondrial 1C enzymes by 2 DPI whereas relative abundances of

cytoplasmic 1C, mitochondrial fatty acid oxidation and TCA cycle proteins showed little change (Figure II.22B).

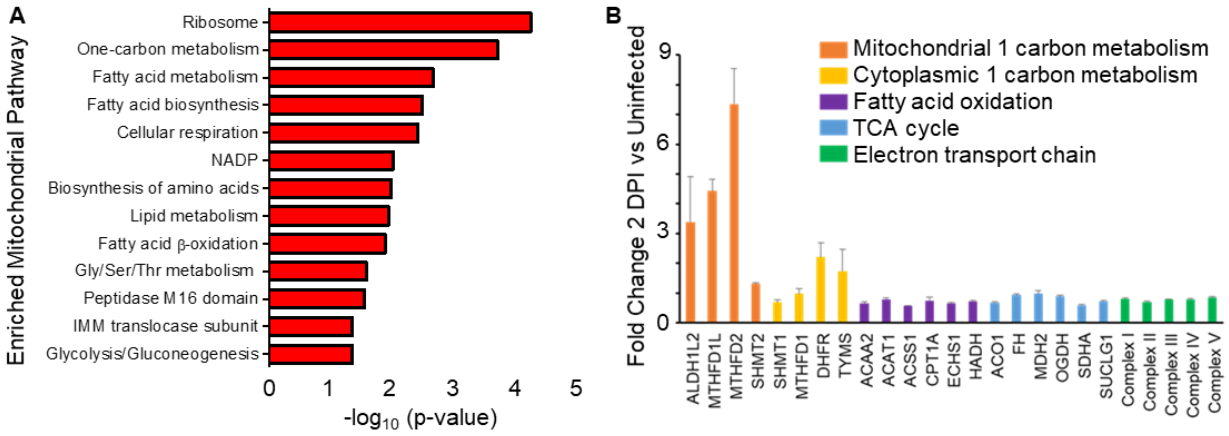

Figure II.22 Analysis of changes to the mitochondrial proteome highlights ribosome biogenesis and one-carbon metabolism. (A) Functional enrichment of mitochondrial pathways most highly induced by primary human B-cell upon EBV infection. Enrichment was examined in the subset of proteins upregulated by at least >2-fold, at ≥1 time point, in comparison to all quantified mitochondrial proteins. Representative terms are shown, and full details of enriched terms are shown in Table S2. (B) Fold change in expression of select metabolic enzymes at 2 DPI relative to resting B-cells. Data shows the mean + SD, n=3. Bioinformatic analyses were performed by L. Nobre, M.P. Weekes and Y. Ma.

EBV also upregulated the mitochondrial folate transporter SLC25A32, dihydrofolate reductase (DHFR), which is responsible for generating the 1C carrier tetrahydrofolate (THF) and is a target of the antifolate drug methotrexate, and the recently identified mitochondrial serine transporter, sideroflexin 1 (SFXN1) (Kory *et al.*, 2018) (Figure II.23).

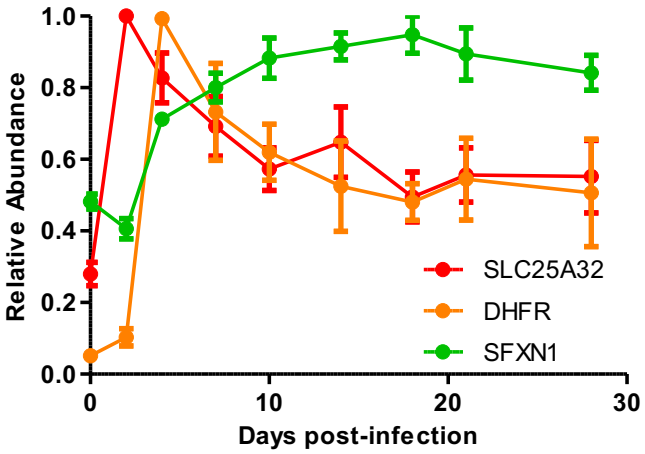

Figure II.23 Early upregulation of folate-dependent one-carbon metabolism in newly infected cells. Temporal proteomic traces of SLC25A32, DHFR and SFXN1 at the indicated DPI of primary human B-cell EBV infection. Data show the mean + SEM of n=3 biological replicates.

Notably, EBV upregulated MTHFD2, a mitochondrial enzyme not expressed by resting B-cells or by most adult cells but is amongst the most highly-induced metabolic enzyme in human cancer (Nilsson *et al.*, 2014) (Figure II.22B). Collectively, these data suggest that EBV remodels B-cell mitochondria to support the substantial physiological shift from quiescence to rapid lymphoblastic proliferation.

Discussion

Humoral immune responses require B-cells to rapidly upregulate metabolic activity, in order to support lymphoblast transformation, growth and survival. This plasticity is necessary for adaptive immune responses where B-cell clones that successfully recognize foreign antigens are selected and expanded in lymph node germinal center reactions. Through expression of a

small number of viral oncoproteins, EBV takes advantage of this plasticity by mimicking germinal center B-cell activation signals. Viral subversion of host metabolic pathways underlies EBV's ability to maintain lifelong carriage and its association with multiple B-cell cancers, particularly in immunosuppressed hosts. Yet, a systematic analysis of EBV-mediated metabolic reprograming necessary for B-cell activation and transformation has not been performed.

We therefore undertook a near-global scale proteomic analysis of resting primary human B-cells and their transition through stages of EBV growth transformation. Our proteomic approach revealed that EBV targets the mitochondrial 1C pathway, beginning shortly after infection and prior to the first mitosis, a time point where little information has been available. Our results provide insights into early events in EBV-mediated metabolic reprograming in B-cell growth transformation and have general implications for understanding primary B-cell activation.

EBV induced aerobic glycolysis within the first four days post-infection. The Warburg effect has been widely documented in latency III-expressing LCLs and latency II-expressing NPCs in an LMP1-dependent manner (Hulse *et al.*, 2018; Darekar *et al.*, 2012; Lo *et al.*, 2015; Zhang *et al.*, 2017b; Sung *et al.*, 2017), as well as in a number of reports on newly infected B-cells (McFadden *et al.*, 2016; Price *et al.*, 2012). However, it remains mechanistically unclear how aerobic glycolysis is activated early in infection, since LMP1 is not highly expressed during that period (Price *et al.*, 2012; Price, Messinger and Luftig, 2018). Through our experiments with EBNA2 and MYC conditional systems as well as our present dataset, we show that the early induction of aerobic glycolysis is dependent on EBNA2, likely by way of MYC activation. We also speculate that aerobic glycolysis in newly infected cells is driven in part by mTOR stimulation of hypoxia-inducible factor-1 alpha (HIF-1α) signaling (Cheng *et al.*, 2014; Düvel *et al.*, 2010; Sun *et al.*, 2011; Mushtaq *et al.*, 2015). Consistent with that is the fact that we could consistently detect an early increase (within 4 DPI) in abundance of HIF-1α's binding partner, aryl hydrocarbon receptor nuclear translocator (ARNT) in our proteomic dataset. As MYC levels

taper later in infection, LMP1 and LMP2A may act to sustain glycolysis by maintaining the expression of glucose transporters (Zha *et al.*, 2015; Sommermann *et al.*, 2011; McFadden *et al.*, 2016) and glycolytic enzymes (Hulse *et al.*, 2018; Anderson and Longnecker, 2008; Dawson *et al.*, 2001; DeKroon *et al.*, 2018; Mancao and Hammerschmidt, 2007; Minamitani *et al.*, 2017; Moody *et al.*, 2005; Wakisaka *et al.*, 2004).

In addition, EBV infection of primary B-cells also resulted in enhanced OXPHOS activity. Apart from the generation of ATP via OXPHOS, another key function of the ETC is to produce aspartate for protein and nucleotide syntheses (Birsoy *et al.*, 2015; Sullivan *et al.*, 2015). Recently, it has been shown that cell cycle arrest and provocation of the DNA damage response in a sub-population of cells newly infected with EBV could be attributed to nucleotide deficiencies, particularly that of purines (Hafez *et al.*, 2017; McFadden *et al.*, 2016). Interestingly, those defects were not apparent later in infection with stably transformed lymphoblastoid cells (Hafez *et al.*, 2017), suggesting that virus-induced hyperproliferation leads to a limited period of intense replicative stress. We speculate that EBV augments B-cell oxidative capacity early in infection to produce aspartate in support of hyperactive synthesis of nucleotides during the hyperproliferative phase. Furthermore, the chemical reduction of oxygen in OXPHOS generates reactive oxygen species, which are important for the activation of pro-growth and survival signaling e.g. NF-κB, HIF-1α and signal transducer and activator of transcription 3 (STAT3) pathways (Wakisaka *et al.*, 2004; Chen, Kamranvar and Masucci, 2016). The virus may have evolved to upregulate ROS production to stimulate those growth and survival promoting pathways.

Chapter III: EBV upregulates mitochondrial 1C metabolism and DNSS in B-cells to support metabolic demands of transformed cell growth and proliferation

Contributions

Dr. Hongying Shen in the laboratory of Dr. Vamsi Mootha assisted in the design of metabolomics experiments, running of samples on the LC-MS and data analysis. Stephen Trudeau and Jason Nomburg in the laboratory of Dr. Benjamin E. Gewurz assisted in the running of immunoblot samples. Zhonghao Wang in the laboratory of Dr. Benjamin E. Gewurz assisted in the running of immunoblot samples and the microscopy work pertaining to cell diameter measurements and EBNA1 immunofluorescence detection. Dr. Nicholas A. Smith in the laboratory of Dr. Benjamin E. Gewurz assisted in the production of EBV viruses and performed primary B-cell agonist experiments. Dr. Yijie Ma in the laboratory of Dr. Benjamin E. Gewurz performed the CD40L stimulation RNA-seq experiments. Bryn Reinstadler in the laboratory of Dr. Vamsi Mootha performed natural isotope correction on raw LC-MS data pertaining to experiments that utilized heavy tracers. Dr. Melissa Walker and Dr. Eran Mick in the laboratory of Dr. Vamsi Mootha provided useful technical support for the use of the Seahorse XF24 Extracellular Flux Analyzer. Dr. Zhaoyue Zhang, Dr. Wenyun Lu in the laboratory of Dr. Joshua Rabinowitz provided helpful pointers on the NADPH labeling experiment. Dr. Adam Friedman, Dr. Mark Manfredi and Dr. Nello Mainolfi of Raze Therapeutics generously provided chemical inhibitors. Dr. Chao Hui Yang in the laboratory of Dr. Rachael Clark assisted in the use of the BD FACSCanto I flow cytometer. We also thank the Flow Cytometry and Confocal Microscopy core facilities at Brigham and Women's Hospital for services rendered and use of the Zeiss LSM 800 instrument, and Dr. Bo Zhao for helpful discussions.

This work was supported by R01 AI137337, a Burroughs Wellcome Career Award in Medical Sciences and an American Cancer Society Research Scholar award to Dr. Benjamin E. Gewurz, R35GM122455 to Dr. Vamsi K. Mootha, K99GM124296 to Dr. Hongying Shen, and a

Singapore Agency for Science, Technology and Research (A*STAR) pre-doctoral fellowship to Liang Wei Wang.

This work has been submitted for publication with the following citation:

Liang Wei Wang*, Hongying Shen*, Luis Nobre*, Ina Ersing*, Joao A. Paulo, Stephen Trudeau, Zhonghao Wang, Nicholas A. Smith, Yijie Ma, Bryn Reinstadler, Jason Nomburg, Thomas Sommermann, Ellen Cahir-McFarland, Steven P. Gygi, Vamsi K. Mootha, Michael P. Weekes and Benjamin E. Gewurz. 2019. Epstein-Barr Virus Induced One-Carbon Metabolism Drives B-Cell Transformation. *Cell Metabolism* (under 3rd round review). (* denotes co-first author)

Abstract

Epstein-Barr virus (EBV) causes Burkitt's, Hodgkin's, and post-transplant B-cell lymphomas. How EBV remodels metabolic pathways to support rapid B-cell outgrowth remains largely unknown. To gain insights, primary human B-cells were profiled by tandem-mass-tag based proteomics at rest and at nine time points after infection. >8000 host and 29 viral proteins were quantified, revealing mitochondrial remodeling and induction of one-carbon (1C) metabolism. EBV-encoded EBNA2 and its target MYC were required for upregulation of the central mitochondrial 1C enzyme MTHFD2, which played key roles in EBV-driven B-cell growth and survival. MTHFD2 was critical for maintaining elevated NADPH levels in infected cells, and oxidation of mitochondrial NADPH diminished B-cell proliferation. Tracing studies underscored contributions of 1C to nucleotide synthesis, NADPH production and redox defense. EBV upregulated import and synthesis of serine to augment 1C flux. Our results highlight EBV-induced 1C as a potential therapeutic target and provide a new paradigm for viral onco-metabolism.

Introduction

Epstein-Barr virus (EBV) is a gamma-herpes virus that successfully colonizes the B-cell compartment of ~95% of adults worldwide and was the first identified human tumor virus. EBV is the etiological agent of infectious mononucleosis (IM) and is associated with ~1% of all human cancers worldwide, including multiple B-cell malignancies (Longnecker, 2013) such as endemic Burkitt's lymphoma (BL), Hodgkin's lymphoma (HL), diffuse large B-cell lymphoma (DLBCL) of the elderly and primary central nervous system lymphoma (Shannon-Lowe, Rickinson and Bell, 2017). EBV is also the major cause of post-transplant lymphoproliferative disorder (PTLD), where viral oncoproteins drive uncontrolled B-cell growth in 1-20% of solid organ and stem-cell transplants (LaCasce, 2006; Green and Michaels, 2013).

A hallmark of EBV is its ability to transform primary human B-cells into hyperproliferating blasts followed ultimately by establishment of latency, in which viral oncoproteins are expressed, but infectious virus is not produced. Through a genetically-encoded viral program comprised of at least three phases *in vitro* (Nikitin *et al.*, 2010), EBV subverts major B-cell activation pathways normally operative in lymph node germinal center reactions (Thorley-Lawson, 2015). First, EBV dramatically remodels B-cell architecture over 72 hours post-infection, where Epstein Barr virus nuclear antigen 2 (EBNA2) and its coactivator EBNA-leader protein (EBNA-LP) act in concert to convert small quiescent cells into large activated blasts. Next, EBNA2 drives MYC expression and hyperproliferation reminiscent of BL, the fastest-growing human tumor (Molyneux *et al.*, 2012), with mitosis every 8-12 hours (Nikitin *et al.*, 2010). Finally, EBNA2 induces expression of oncogenic EBNA3s and latent membrane proteins (LMPs). LMP1 mimics CD40 signaling to constitutively activate NF-κB (Wang, Jiang and Gewurz, 2017; Kieser and Sterz, 2015), whereas LMP2A subverts the B-cell receptor pathway to activate the PI3K/AKT/mTOR pathway (Cen and Longnecker, 2015). Growth transformation in vitro culminates in the generation of

immortalized lymphoblastoid cell lines (LCLs), which serve as a major model of EBV-driven lymphoblastic lymphomas.

Each B-cell transformation phase necessitates widespread remodeling of host metabolic pathways. Metabolic stress is a major barrier to EBV-induced B-cell transformation; newly infected cells that fail to transform undergo growth arrest characterized by mitochondrial dysfunction and attenuated mammalian target of rapamycin (mTOR) signaling (McFadden *et al.*, 2016). Metabolic remodeling has not been systematically investigated during EBV-driven B-cell transformation or in primary human B-cell activation more generally. While viral genes essential for B-cell transformation have been identified, their global effects on B-cell metabolism are poorly understood. There is little knowledge regarding the mechanisms by which EBV induces or activates key metabolic pathways to transform a quiescent B-lymphocyte into a lymphoblast. Likewise, the roles of metabolic pathways in establishing and/or maintaining continual lymphoblastoid B-cell growth are not well-characterized.

A systematic quantitative analysis of temporal changes in host and viral proteins over the course of transformation in primary human B-cells could provide a comprehensive understanding of EBV-driven metabolic reprogramming and give insights into pathways important in EBV-driven malignancies. Here, we used multiplexed tandem-mass tag (TMT)-based proteomics to measure >8,000 host proteins and 29 viral proteins over nine time points of infection of primary human B-cells and in uninfected cells (Weekes *et al.*, 2014). We found that EBV remodels B-cell mitochondria, and that mitochondrial one-carbon (1C) metabolism was one of the most highly induced pathways. 1C plays key roles in supporting rapid cell growth in embryonic development (Christensen and Mackenzie, 2008; Patel *et al.*, 2005; Di Pietro *et al.*, 2002; Patel, Pietro and MacKenzie, 2003), cancer (Nilsson *et al.*, 2014) and T-cell activation (Ron-Harel *et al.*, 2016) but has not previously been studied in the context of viral oncogenesis or in primary human B-cell activation.

Materials and Methods

Antibodies, reagents and kits

The following antibodies were used: mouse anti-EBV EBNA1 (OT1x) (a kind gift from Jaap Middledorp), mouse anti-EBV EBNA2 (PE2) (a kind gift from Jeffrey Cohen), mouse anti-γH2AX (Ser139) (JBW301) (EMD Millipore, Cat#05-636), rabbit anti-H2AX (Bethyl Laboratories, Cat#A300-083A), rabbit anti-PHGDH (Bethyl Laboratories, Cat#A304-732A), mouse anti-PSAT1 (Novus Biologicals, Cat#H00029968-A01), rabbit anti-PSPH (Proteintech, Cat#14513-1-AP), rabbit anti-SHMT2 (Cell Signaling, Cat#12762), rabbit anti-MTHFD2 (Proteintech, Cat#12270-1-AP), rabbit anti-MTHFD1L (Cell Signaling, Cat#14998), rabbit ant-DDX1 (Bethyl Laboratories, Cat#A300-521A), rabbit anti-c-MYC (N-262) (Santa Cruz, Cat#sc-764), rabbit anti-FLAG (DYKDDDDK) (Cell Signaling, Cat#2368S), mouse anti-α-tubulin (DM1A) (Abcam, Cat#ab7291), mouse anti-GAPDH (6C5) (Abcam, Cat#ab8245), rabbit anti-ASCT2 (D7C12) (Cell Signaling, Cat#8057), rabbit anti-phospho-AMPKα (Thr172) (40H9) (Cell Signaling, Cat#2535), rat anti-ATF4 (W16016A) (Biolegend, Cat#693901), goat anti-rabbit IgG (H+L) Alexa Fluor 488 (Invitrogen, Cat#A-11034), goat anti-mouse IgG (H+L) Cross-Adsorbed Secondary Antibody, Alexa Fluor 488 (Invitrogen, Cat#A-11001), goat F(ab')2 Anti-Human IgM (Southern Biotech, Cat#2022-01), PE mouse IgG1, κ isotype control (Clone MOPC-21) (BD Biosciences, Cat#555749) and mouse anti-human CD23 PE (BD Biosciences, Cat#555711).

The following chemicals and reagents were used: acetonitrile (LC/MS) (Fisher Scientific, Cat#A955-1), methanol (LC/MS) (Fisher Scientific, Cat#A456-1), water (LC/MS) (Fisher Scientific, Cat#W6-4), ammonium acetate (LC/MS) (Sigma-Aldrich, Cat#14267), ammonium Hydroxide (LC/MS) (Fisher Scientific, Cat#A470-250), ammonium carbonate (HPLC) (Fluka, Cat#74415-250G-F), D-glucose (U-$^{13}C_6$) (Cambridge Isotope Laboratories, Cat#CLM-1396-1), L-serine (2,3,3-D_3) (Cambridge Isotope Laboratories, Cat#DLM-582-0.1), L-serine ($13C_3$) (Cambridge Isotope Laboratories, Cat#CLM-1574-H-0.1), formic acid (LC/MS) (Fisher Scientific,

Cat#A117-50), piericidin A (Cayman Chemicals, Cat#15379), tunicamycin, Streptomyces lysosuperficus (Sigma-Aldrich, Cat#654380), antimycin A from Streptomyces sp. (Sigma-Aldrich, Cat#A8674), (Z)-4-hydroxytamoxifen (Sigma-Aldrich, Cat#H7904), doxycycline hyclate (Sigma-Aldrich, Cat#D9891), sodium formate (Fisher Scientific, Cat#S648-500), glycine (American Bioanalytical, Cat#AB00730-05000), L-buthionine-sulfoximine (Sigma-Aldrich, Cat#B2515), H2DCFDA (H2-DCF, DCF) (ThermoFisher Scientific, Cat#D399), propidium iodide - 1.0 mg/mL solution in water (ThermoFisher Scientific, Cat#P3566), PureLink™RNase A (20 mg/mL) (ThermoFisher Scientific, Cat#12091021), Hoechst 33258, Pentahydrate (bis-Benzimide) - FluoroPure™ Grade (ThermoFisher Scientific, Cat#H21491), Prolong™ Gold Antifade Mountant (ThermoFisher Scientific, Cat#P36930), JC-1 Dye (Mitochondrial Membrane Potential Probe) (ThermoFisher Scientific, Cat#T3168), CellTrace™ CFSE Cell Proliferation Kit (ThermoFisher Scientific, Cat#C34554), 7-AAD (7-Aminoactinomycin D) (ThermoFisher Scientific, Cat#A1310), Luperox® TBH70X, tert-Butyl hydroperoxide solution (Sigma-Aldrich, Cat#458139), carbonyl cyanide m-chlorophenylhydrazone (CCCP) (Sigma-Aldrich, Cat#C2759), carbonyl cyanide 4-(trifluoromethoxy)phenylhydrazone (FCCP) (Sigma-Aldrich, Cat#C2920), oligomycin A (Sigma-Aldrich, Cat#75351), Cell-Tak Cell and Tissue Adhesive (Corning, Cat#C354240), CBR-5884 (Cayman Chemicals, Cat#19236), NCT-503 (Cayman Chemicals, Cat#19718), SHIN1 (Raze Therapeutics), MTH-1479 (Raze Therapeutics), MEGACD40L® Protein (soluble) (human), (recombinant) (Enzo Life Sciences, Cat#ALX-522-110-C010), CpG ODN 2006 [Integrated DNA Technologies, synthesized as follows: T*C*G*T*C*G*T*T*T*T*G*T*C*G*T*T*T*T*G*T*C*G*T*T (*=phosphorothioate modification)], recombinant human IL-4 (carrier-free) (Biolegend, Cat#574004), Standard Fetal Bovine Serum, Qualified, USDA-Approved Regions (ThermoFisher Scientific, Cat#10437028), RPMI 1640 Medium w/o L-Glutamine, L-Serine, HEPES (Powder) - 10L (US Biological, Cat#R8999-15), 1X RPMI-1640 Media without Glucose, Glycine and Serine. 500mL, Sterile. 2 Pack (Teknova, Cat#R9660-02), RPMI 1640 Medium (ThermoFisher Scientific, Cat#11875085), HEPES (1M)

(ThermoFisher Scientific, Cat#15630080), RosetteSep™ Human B-cell Enrichment Cocktail (STEMCELL Technologies, Cat#15064) and EasySep™ Human B-cell Enrichment Kit (STEMCELL Technologies, Cat#19054).

The following kits and parts were used: NAD/NADH-Glo™ Assay (Promega, Cat#G9071), NADP/NADPH-Glo™ Assay (Promega, Cat#G9081), Lactate-Glo™ Assay (Promega, Cat#J5021), Seahorse XF24 FluxPak (Agilent Technologies, Cat#100850-001), Seahorse XF24 V7 PET Culture Microplates (Agilent Technologies, Cat#101037-004), XBridge BEH Amide VanGuard Pre-column, 130Å, 2.5 µm, 2.1 mm X 5 mm, 3/pkg (Waters, Cat#186007763), Xbridge BEH amide 2.5 µm, 2.1 mm X 100 mm (Waters, Cat#186006091), SeQuant® ZIC®-pHILIC (5µm polymer) PEEK 150 x 2.1 mm (EMD Millipore, Cat#150460), High Precision Glass Cover Slip, box of 100, No 1.5, 24x50mm (Bioscience Tools, Cat#CSHP-No1.5-24x50), LSM 800 with Airyscan (Zeiss), Q Exactive Plus orbitrap mass spectrometer equipped with an Ion Max source and a HESI II probe (ThermoFisher Scientific) and Dionex UltiMate 3000 UPLC system (ThermoFisher Scientific).

Agonist stimulation of primary B-cells

Freshly isolated primary B-cells were seeded in complete RPMI media and 10% standard FBS at 1 million cells per mL. The following agonists were used at these indicated concentrations: MEGACD40L (50 ng/mL), goat $F(ab')_2$ anti-human IgM (αIgM) (1 µg/mL), CpG ODN 2006 (1 µM) and interleukin 4 (IL-4) (20 ng/mL). Cells were harvested at 24 hours and 96 hours for whole cell lysate preparation. For the latter timepoint, agonist replenishment was performed without removal of the spent media at 48 hours.

LC-MS metabolite analysis

Cells were seeded at 1 million cells/mL with fresh media (containing labeled amino acids, if required) 24 hours prior to harvesting. To prepare cellular metabolite extracts, cells were washed once with ice-cold PBS and once with ice-cold 100 mM ammonium acetate before lysis

with acetonitrile-methanol-water (27:9:1). For detection of cellular M+3 serine with $U^{13}C$-glucose, the same procedure was used with the labeling period shortened to 4 hours to minimize exchange between cellular serine and media serine. For the detection of nicotinamide dinucleotides, several modifications were made, namely a shorter labeling period (4 hours), the omission of wash steps to avoid hydride exchange, and the use of a modified lysis buffer [acetonitrile-methanol-water (27:9:1) mixture with 0.1 M formic acid] followed by immediate neutralization with 15% (w/v) ammonium bicarbonate solution (within 15 seconds of lysis buffer addition). To prepare media metabolite extracts, 50 µL of media was extracted with acetonitrile-methanol (3:1). All extraction steps were performed at 4˚C. Crude extracts were centrifuged at maximum speed at 4˚C for 20 minutes to remove cellular debris, and supernatants were either used immediately or frozen at -80˚C for short-term storage.

LC/MS-based analyses were performed on a Q Exactive Plus orbitrap mass spectrometer equipped with an Ion Max source and a HESI II probe, which was coupled to a Dionex UltiMate 3000 UPLC system (Thermo Fisher Scientific).

Polar metabolites in the spent media and cellular extracts were analyzed using Xbridge BEH Amide XP HILIC 2.5 µm, 2.1 mm x 100 mm column (Waters) with the guard column and SeQuant ZIC-pHILIC Polymeric 5 µm, 150 x 2.1 mm column (EMD-Millipore).

For the amide method, the mobile phase A was 5% acetonitrile, 20mM ammonium acetate/ammonium hydroxide, pH 9. The mobile phase B was 100% acetonitrile. The flow rate was 220 µl/min from 0 – 15 min, and 420 µl/min from 15 – 25 min. The gradient was as follows: 0 min: 85% B; 0.5 min: 85% B; 9 min: 35% B; 11 min: 2% B; 13.5 min: 85% B; 15 min: 85% B; 22 min: 85% B. The MS data was collected in the polarity switching mode with full scan mode in a range of 70–1000 m/z, with the resolution at 70,000, the AGC target at 1E6, and the maximum injection time at 80 ms, the sheath gas flow at 50 units, the auxiliary gas flow at 10 units, the

sweep gas flow at 2 units, the spray voltage at 2.5 kV, the capillary temperature at 310 °C, and the auxiliary gas heater temperature at 370°C.

For dTTP, AMP, GSH and GSSG using the ZIC-pHILIC method, the mobile phase A was 20mM ammonium carbonate/ammonium hydroxide, pH 9.6. The mobile phase B was 100% acetonitrile. The flow rate was 150 µl/min. The gradient was as follows: 0 min: 80% B; 0.5 min: 80% B; 20.5 min: 20% B; 21.5 min: 80% B; 29 min: 80% B. The MS data acquisition was collected in the polarity switching mode with full scan mode in a range of 70–1000 m/z, with the resolution at 70,000, the AGC target at 1E6, and the maximum injection time at 80 ms with the same parameters mentioned above.

For NAD(P) and NAD(P)H using the ZIC-pHILIC method, the mobile phase A was 20mM ammonium carbonate/ammonium hydroxide, pH 9.6. The mobile phase B was 100% acetonitrile. The flow rate was 110 µl/min. The gradient was as follows: 0 min: 80% B; 2 min: 80% B; 18 min: 62% B; 25 min: 20% B; 26 min: 80% B; 37 min: 80% B. The MS data was collected in the negative polarity mode with full scan mode in a range of 300–1000 m/z, with the resolution at 70,000, the AGC target at 3E6, and the maximum injection time at 400 ms, and the same parameters mentioned above.

Progenesis QI software (Waters, NC) and Xcalibur (Thermo Fisher Scientific) were used to analyze the data. Absolute quantification of glucose, serine and lactate in the spent media was measured by comparing to the ^{13}C-labeled internal standards at different spiked concentrations.

Natural isotope correction

See the Materials and Methods section of the previous chapter.

Flow cytometry analysis

Flow cytometry studies (FACS) were performed on a BD FACSCalibur instrument. Cells were washed once with cold PBS supplemented with 0.5% bovine serum albumin (BSA). Cells were

then incubated with a 1:100 dilution of fluorophore-conjugated primary antibody (and, if applicable, a 1:500 dilution of fluorophore-conjugated secondary antibody) in PBS with 0.5% BSA for 1 hour. Cells were pelleted and resuspended in 400 µL of PBS, strained into flow cytometry-compatible tubes and processed immediately with a flow cytometer. Sample processing was performed either immediately or within 24 hours after staining.

For DCFDA staining, cells were treated with 10 µM DCFDA in complete media for 20 minutes before processing with the flow cytometer. As a positive control, pre-treatment of cells with 100 µM tert-butyl hydrogen peroxide (TBHP) for 3 hours was performed. For JC-1 staining, cells were treated with 10 µM JC-1 in complete media for 15 minutes before processing with the flow cytometer. As a positive control, concurrent treatment of cells with 100 µM CCCP was performed. For 2-NBDG staining, cells were incubated with 10 µg/mL 2-NBDG in complete media for one hour at 37˚C. For CFSE staining, 4 DPI cells and GM12878 LCLs were stained with 10 µM CFSE for 15 minutes at 37˚C, washed and resuspended at 100 000 cells/mL. For 7-AAD staining, cells were stained with 1 µM 7-AAD at room temperature for 5 minutes before being placed at ice until further processing with the flow cytometer. For propidium iodide staining, 7DPI cells and GM12878 LCL fixed in ice-cold 90% ethanol/PBS for at least two days were re-hydrated in PBS and stained with a solution of 20 µg/mL propidium iodide, 40 µg/mL RNase A and 1:1000 (v/v) Triton X-100 for 30 minutes before immediate processing by the flow cytometer.

Flow cytometric data was acquired with a BD FACSCalibur instrument in most instances (with the exception of the CFSE and 7-AAD experiments, whose data were acquired with a BD FACSCanto I flow cytometer) and analysis was performed with FlowJo.

Immunofluorescence microscopy

Approximately 1 million cells were pelleted and resuspended in 1-2 µL PBS and streaked onto glass slides to dry. Cells were fixed with 4% paraformaldehyde/PBS solution for 10 minutes and

permeabilized with 0.5% (v/v) Triton X-100/PBS solution for 5 minutes, with PBS washing in between and after each of those steps. Cells were incubated with 20% normal goat serum (NGS) blocking reagent for 1 hour. EBNA1-specific OT1x antibody was diluted 1:100 in the blocking reagent and added to cells for 1 hour. Cells were washed and incubated with Alexa Fluor 488-conjugated goat anti-mouse secondary antibody (diluted 1:1000 in blocking reagent) for 30 minutes. Cells were washed and incubated with a 10 µg/mL Hoechst 33258/PBS solution for 3-5 minutes. Cells were washed and successively dehydrated in 70% (1 minute), 90% (1 minute) and 100% ethanol (1 minute). ProLong Gold antifade reagent was added to each well and a No. 1.5 coverslip was attached. Data acquisition was performed using a Zeiss LSM 800 instrument. Processing and analysis were performed using ZEN Blue software (Zeiss). All steps were performed at room temperature.

In vitro transformation assays

Freshly isolated primary human B-cells, purified as outlined above by negative selection, were seeded into 96-well plates at a density of 500,000 cells/mL in 100 µL per well of RPMI/10% FBS. B95-8 virus supernatant (see section entitled, "*EBV infection of primary B-cells*", for details) was diluted ten-fold to give a five-point dilution series. To each well, 100 µL of virus supernatant was added. DMSO vehicle, MTH-1479 or SHIN1 were added at the indicated concentrations (5 or 10 µM). Vehicle or drug were refreshed every 3 to 4 days by carefully aspirating 100 µL of spent media and replenishing with fresh drug-containing media. At four weeks post-infection, the proportion of wells with B-cell outgrowth was plotted against the dilution of virus supernatant used per well, as previously described (Henderson *et al.*, 1977). One transforming unit per well was defined as the amount of virus required to attain B-cell outgrowth in 62.5% of wells.

Growth curve analysis

Newly infected B-cells were seeded at 500,000 cells per well in a volume of 1 mL of RPMI/FBS and grown for two days before measurements of cell numbers were made. For GM12878 lymphoblastoid cells, 100,000 cells were seeded per well in a volume of 1mL and grown for two days prior to measurements of live cell number. For live cell measurements, cells were pelleted and resuspended in the same volume of media, trypan blue was added, and live cell number was quantitated with the TC20 automatic cell counter (Bio-Rad). After measurements were taken, cells were passaged accordingly to give 100,000 cells per mL in RPMI/10% FBS and grown for two more days. The same procedure was repeated to obtain measurements at later time points. At each time point, cells were treated with the appropriate inhibitor and/or rescue metabolite(s) at the indicated concentrations after passaging.

CRISPR editing in GM12878 LCL

Single guide RNA (sgRNA) constructs were generated as previously described (Jiang *et al.*, 2018) using sgRNA sequences from the Broad Institute Avana Library. The MTHFD2^{R} cDNA rescue construct utilizes the pLX_TRC313 (Hyg^{R}) vector backbone and was synthesized and sequence-validated by GenScript. C166T and G349A silent point mutations were introduced into the MTHFD2 cDNA sequence to produce synonymous mutations that conferred resistance to sgRNA #1 and sgRNA #2, respectively.

Gene & sgRNA Identifier	**sgRNA Sequence**
MTHFD2 #1	CCTCTTACCGAACTGCCGCG
MTHFD2 #2	CCTTCGCCCTTTCCACCTCG

LCL CRISPR editing was performed as previously described (Jiang *et al.*, 2018). Briefly, lentiviruses encoding sgRNAs were generated by transient transfection of 293T cells with packaging plasmids and pLentiGuide-Puro plasmids. GM12878 cells stably expressing Cas9 were transduced with the lentiviruses and selected with 3 μg/mL puromycin for three days

before replacement with antibiotic-free media. For rescue experiments or cDNA overexpression, 293T cells were transiently transfected to produce lentiviruses that carry the rescue or control GFP cDNA and a hygromycin resistance marker. GM12878 cells were transduced with 293T rescue lentivirus supernatants at 48 and 72 hours post-293T cell transfection and selected with RPMI/10% FBS supplemented with 200 μg/mL hygromycin 48 hours later. Cells were hygromycin selected for at least one week before transduction with sgRNA-encoding lentiviruses. CRISPR editing and rescue cDNA expression were confirmed by immunoblot.

Kit-based quantitation of ATP, NAD(P)H and extracellular lactate

Cells were assayed using commercially available kits (Promega), namely CellTiter-Glo (ATP measurements), NADH-Glo (NADH and NAD measurements), NADPH-Glo (NADPH and NADP measurements) and Lactate-Glo, accordingly to manufacturer's instructions.

Quantitative PCR

RT-qPCR analysis of mRNA abundance was performed on a BioRad CFX Connect Real-time PCR detection system, using Power SYBR Green RNA-to-CT 1-Step Kit (Applied Biosystems) for 40 cycles. Expression values relative to 18S rRNA expression were calculated using CFX Manager Software. Quantitative PCR of viral genome copies utilized host cell *GAPDH* gene copy number as control. To quantitate mitochondrial DNA copy number, total cellular DNA was extracted using the DNAeasy kit (Qiagen). Quantitative PCR was then performed on 10 ng input DNA using *MT-ND2* (mtDNA)-specific and *AluYb8* (nuclear DNA)-specific primers. C_t values obtained from *AluYb8* amplification were used for normalization. Primer sequences can be found as follows.

Gene and Primer Orientation	**Primer Sequence (5' to 3')**
PHGDH Forward	GCAAAGAGGAGCTGATAGCG
PHGDH Reverse	TTCTCAGCTGCGTTGATGAC
MTHFD2 Forward	TGGCTGCGACTTCTCTAATGT

MTHFD2 Reverse	CCTTCCAGAAATGACAACAGC
18S rRNA Forward	CGGCTACCACATCCAAGGAA
18S rRNA Reverse	GCTGGAATTACCGCGGCT
BALF5 vDNA Forward	GAGCGATCTTGGCAATCTCT
BALF5 vDNA Reverse	TGGTCATGGATCTGCTAAACC
GAPDH gDNA Forward	ACTTCAACAGCGACACCCACTC
GAPDH gDNA Reverse	TCTCTTCCTCTTGTGCTCTTGCT
AluYb8 gDNA Forward	CTTGCAGTGAGCCGAGATT
AluYb8 gDNA Reverse	GAGACGGAGTCTCGCTCTGTC
MT-ND2 mtDNA Forward	TGTTGGTTATACCCTTCCCGTACTA
MT-ND2 mtDNA Reverse	CCTGCAAAGATGGTAGAGTAGATGA

Mitochondrial stress test

Cell culture plates were layered with Cell-Tak (Corning) to enable adhesion of the B-cells. Cells were seeded at 500,000 per well. For standard measurements, complete bicarbonate-free RPMI-1640 supplemented with 25 mM HEPES, 10% dialyzed FBS and 2 mM L-glutamine was used as the growth media during the period of data acquisition. For serine withdrawal and subsequent rescue experiments, complete bicarbonate- and serine-free RPMI-1640 supplemented with 25 mM HEPES, 10% dialyzed FBS and 2 mM L-glutamine was used, with serine and formate added accordingly to the appropriate wells. Detection of changes in oxygen consumption and extracellular acidification rates was achieved with the use of Seahorse XF24 sensor cartridges. The following mitochondrial poisons were used: 3.5 μM oligomycin, 2 μM CCCP and 100 nM piericidin A. Data acquisition was performed with the Seahorse XF24 Extracellular Flux Analyzer (Agilent).

Results

EBV upregulates mitochondrial one-carbon metabolism via EBNA2 and MYC

ATF4 is the major mitochondrial 1C gene transcription activator (Ben-Sahra *et al.*, 2016; Bao *et al.*, 2016). Although *ATF4* is transcribed in LCLs (Arvey *et al.*, 2012), ATF4 protein was not detected by proteomics or by immunoblot. In support of this result, we validated the ATF4 antibody by showing that LCL ATF4 immunoblot signal could be induced by tunicamycin treatment, and that this signal could be suppressed by CRISPR ATF4 targeting. Notably, neither tunicamycin-mediated ATF4 induction nor CRISPR-mediated ATF4 depletion altered LCL MTHFD2 levels (Figure III.1).

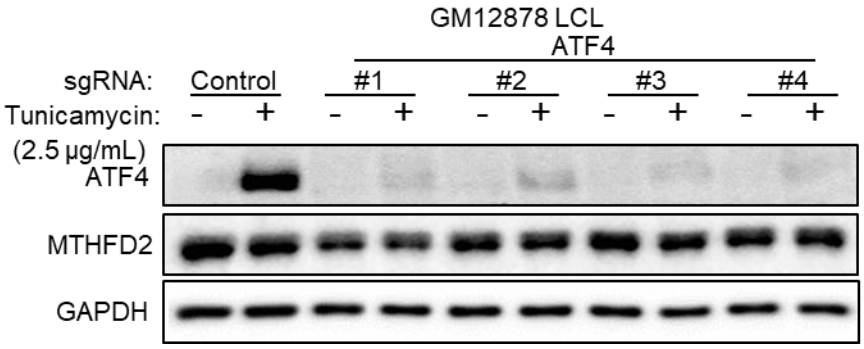

Figure III.1 ATF4 is dispensable for MTHFD2 expression. Immunoblot analysis of ATF4, MTHFD2 and load-control GAPDH expression in the Cas9+ EBV-transformed GM12878 lymphoblastoid cell line expressing non-targeting control or independent *ATF4*-targeting sgRNAs and treated with DMSO vehicle or tunicamycin (2.5 µg/mL) as indicated. Representative of n=3.

Likewise, leaky EBV lytic gene expression was unlikely to drive 1C induction, since our prior proteomic analysis of B-cell EBV lytic reactivation (Ersing *et al.*, 2017) did not demonstrate 1C enzyme induction (Figure III.2).

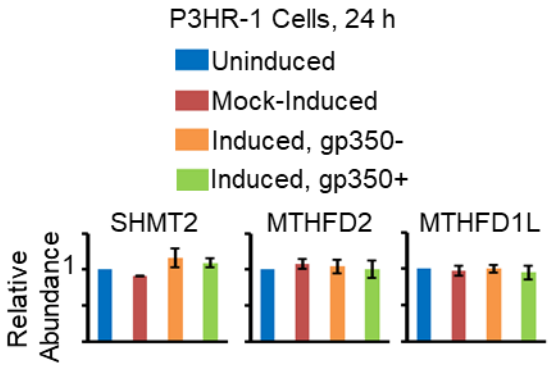

Figure III.2 Lytic reactivation does not contribute to enhanced mitochondrial 1C enzyme expression. Relative abundances of the mitochondrial 1C enzymes SHMT2, MTHFD2 and MTHFD1L in parental P3HR-1 cells that do not have the ZHT/RHT conditional alleles but that were mock-induced by 4HT treatment for 24 hours (red), or in P3HR-1 cells that stably express conditional alleles of the EBV immediate early factors ZTA and RTA fused to modified estrogen receptor binding domain that were either uninduced (blue), or induced by 400 nM 4HT treatment for 24 hours and sorted into gp350- (orange) or lytic gp350+ (green) populations. Proteomic data is extracted from Ersing *et al.* (2017) and show the mean ± SEM of n=3 biological replicates.

Given the key EBNA2 role in aerobic glycolysis induction, we hypothesized that EBNA2 might be a viral master regulator of B-cell metabolism and tested its role in mitochondrial 1C induction. Primary human B-cells were equally infected with B95-8 or the non-transforming P3HR-1 EBV strains (Miller *et al.*, 1974; Miller, Robinson and Heston, 1975), using viral genome copy number and EBNA1 confocal immunofluorescence (Figure III.3) to normalize level of infection. P3HR-1 lacks EBNA2 and most of the EBNA-LP open reading frames (Rowe *et al.*, 1985; Rymo, Klein and Ricksten, 1985; Tsang *et al.*, 1991; Wang *et al.*, 1990).

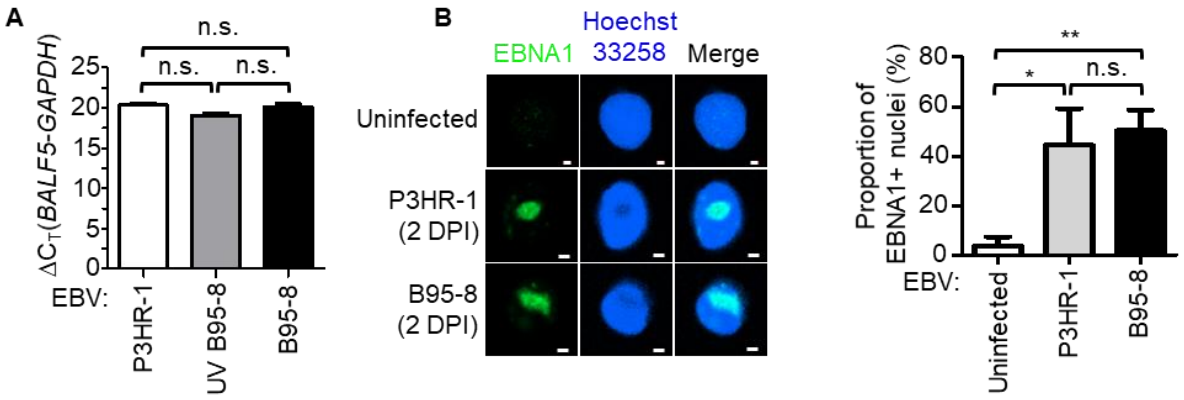

Figure III.3 Equal infection of primary human B-cells with various EBV strains. (A) Quantitative PCR-based EBV genome copy number assays on primary B-cells newly infected with the indicated virus strains 24 hours post-infection. The difference in C_T values for *BALF5* and *GAPDH* was plotted for each condition. Data show the mean with SEM, n=3. (B) Left: Representative EBNA1 immunofluorescence micrographs of primary B-cells newly infected with the indicated virus strains. White scale bars indicate a distance of 1 μm. Right: quantitation of EBNA1+ nuclei 2 DPI in ≥3 independent field of views for each condition. *, $p<0.05$; **, $p<0.01$ (unpaired two-tailed t-test).

B95-8, but not P3HR-1 or UV-irradiated B95-8, could induce the expression of mitochondrial 1C enzymes at 4 DPI (Figure III.4). These data suggest that expression of EBV-encoded EBNA2 and/or EBNA-LP, rather than an innate immune response to the viral particle, is required for the induction of mitochondrial 1C metabolism.

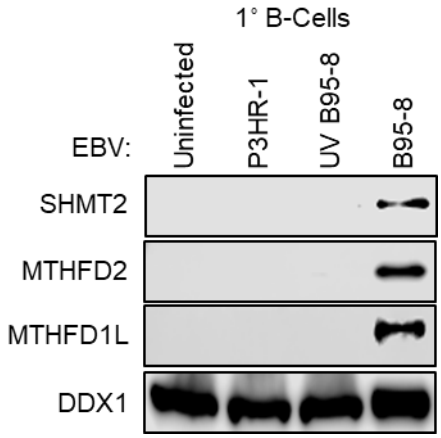

Figure III.4 B95-8 induces the expression of mitochondrial 1C enzymes. Immunoblot analysis of SHMT2, MTHFD2, MTHFD1L or DDX1 expression in uninfected cells, or cells equally infected with either P3HR-1, UV-inactivated B95-8 or B95-8 virus 4 DPI. n=2.

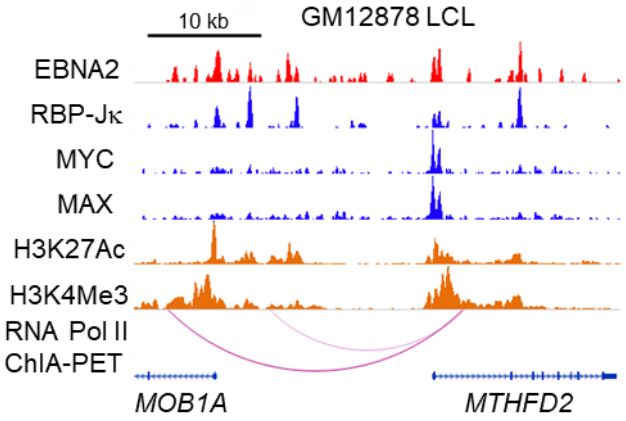

Figure III.5 EBNA2, MYC and their binding partners co-localize at the MTHFD2 promoter. ChIP-seq tracks of the indicated transcription factors or the activating histone epigenetic marks H3K27Ac or H3K4Me3 at the GM12878 LCL *MTHFD2* locus. Shown also are GM12878 ChIA-PET-defined long-range DNA linkages between an upstream *MOB1A* locus enhancer and *MTHFD2.* ChIP-sequencing data was obtained from the ENCODE database.

To further investigate possible EBNA2 roles in MTHFD2 induction, we used publicly available LCL chromatin immunoprecipitation with deep sequencing (ChIP-seq) (Consortium, 2012; Wood *et al.*, 2016; Zhao *et al.*, 2011b) and chromatin interaction analysis by paired-end tag (ChIA-PET) data (Jiang *et al.*, 2017) to identify transcription factor occupancy. EBNA2 and its cofactor RBP-Jκ were found to co-occupy the *MTHFD2* promoter, as well as upstream intragenic and intergenic enhancers that loop to the *MTHFD2* promoter (Figure III.5). Inactivation of the conditional EBNA2 allele resulted in rapid loss of MTHFD2 transcript and protein (Figure III.6).

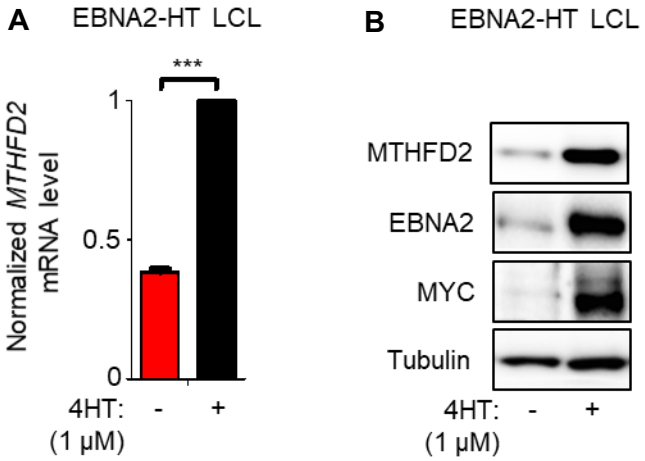

Figure III.6 EBNA2 regulates MTHFD2 expression in LCLs. (A) Quantitative PCR analysis of *MTHFD2* transcript expression in EBNA2-HT cells cultured in the presence (permissive for growth) or absence (non-permissive for growth) of 4HT (1 μM) for 48 hours. Data show the mean + SEM, n=3. ***, $p<0.005$ (one-sample t-test). (B) Immunoblot analysis of MTHFD2, MYC and tubulin expression in EBNA2-HT cells cultured in the presence or absence of 4HT (1 μM). Representative of n=3.

EBNA2 highly upregulates MYC (Kaiser *et al.*, 1999; Zhou *et al.*, 2015) and both proteins can act synergistically to induce EBV targets. As expected, conditional EBNA2 inactivation caused rapid downregulation of MYC levels (Figure III.6). Since MYC and MAX co-occupy the LCL

MTHFD2 promoter (Figure III.5) and given MYC's role in MTHFD2 regulation in acute myelogenous leukemia (Pikman *et al.*, 2016), we investigated a potential role for MYC in EBV induction of MTHFD2 expression. With the P493-6 B-cell line, an LCL that conditionally expresses a conditional 4HT-responsive EBNA2 allele and also carries a heterologous MYC allele controlled by a Tet-OFF promoter (Schuhmacher *et al.*, 2001a), we found that re-expression of MYC was sufficient to restore MTHFD2 expression upon EBNA2 inactivation by 4HT withdrawal (Figure III.7A) and observed that MTHFD2 and MYC levels were closely correlated. Cas9 editing of *MYC* directed by either of two distinct sgRNAs caused loss of MYC protein and a concomitant decrease in MTHFD2 protein abundance prior to LCL cell death (Figure III.7B). Taken together, these results identify EBNA2 as the first viral oncoprotein important for mitochondrial 1C metabolism induction, by a mechanism that involves MYC instead of ATF4.

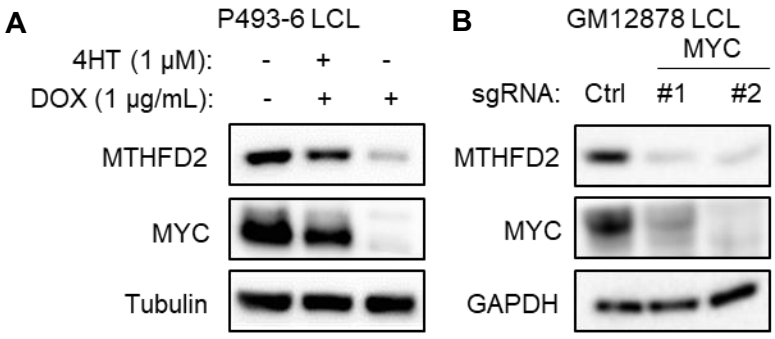

Figure III.7 The EBNA2 target gene MYC controls MTHFD2 expression in LCLs. (A) Immunoblot analysis of MTHFD2, MYC and tubulin expression in P493-6 cells cultured with the indicated supplement. Representative of n=3. (B) Immunoblot analysis of MYC, MTHFD2 and GAPDH expression in Cas9+ GM12878 LCLs following expression of non-targeting control or independent *MYC*-targeting sgRNAs. n=2. MYC CRISPR knockouts were generated and analyzed by S. Trudeau.

EBNA2 and MYC upregulate B-cell import and mitochondrial 1C catabolism of serine

Serine and glycine fuel mitochondrial 1C metabolism (Ducker and Rabinowitz, 2017; Yang and Vousden, 2016). We hypothesized that newly infected cells might therefore increase uptake and/or de novo synthesis of serine or glycine. Media LC-MS analysis revealed avid consumption of serine, but not of glycine over the first week after EBV infection, which peaked at 4 DPI, coinciding with the onset of BL-like hyperproliferation and maximal MYC abundance (Figure III.8).

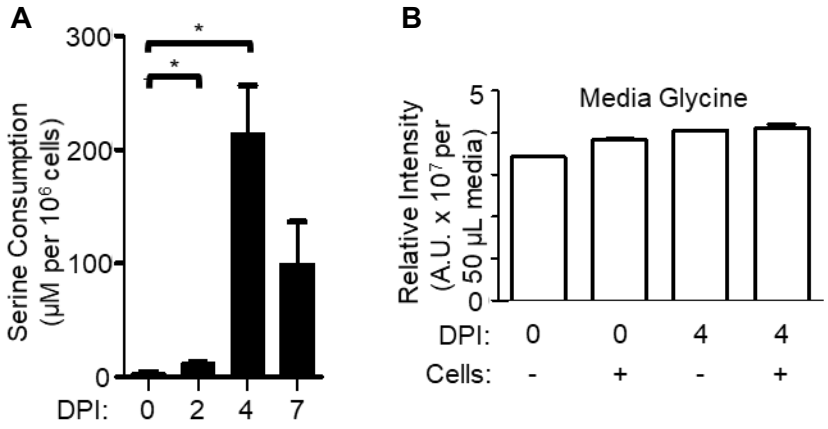

Figure III.8 Net consumption of serine and glycine by newly infected B-cells. (A) LC-MS measurements of media serine concentrations of primary B-cells cultured at the indicated DPI. Values indicate mean + SEM serine consumption over a 24-hour period at the indicated time point, n=3. *, $p<0.05$ (paired two-tailed t-test). (B) LC-MS measurement of media glycine levels in the absence or presence of primary human B-cells (seeded at 1 x 10^6 cells per mL) for 24 hours at the indicated DPI. Data shows the mean + SEM, n=3. LC-MS data acquisition and analysis was jointly performed by L.W. Wang and H. Shen.

Consistent with this observation, EBV markedly upregulated whole cell and PM levels of the major serine transporters SLC1A4 (ASCT1) and SLC1A5 (ASCT2) by four days post-infection

(Figure III.9A-C). In contrast, neither EBNA2-deficient P3HR-1 nor UV-irradiated B95-8 EBV robustly upregulated ASCT2 (Figure III.9D).

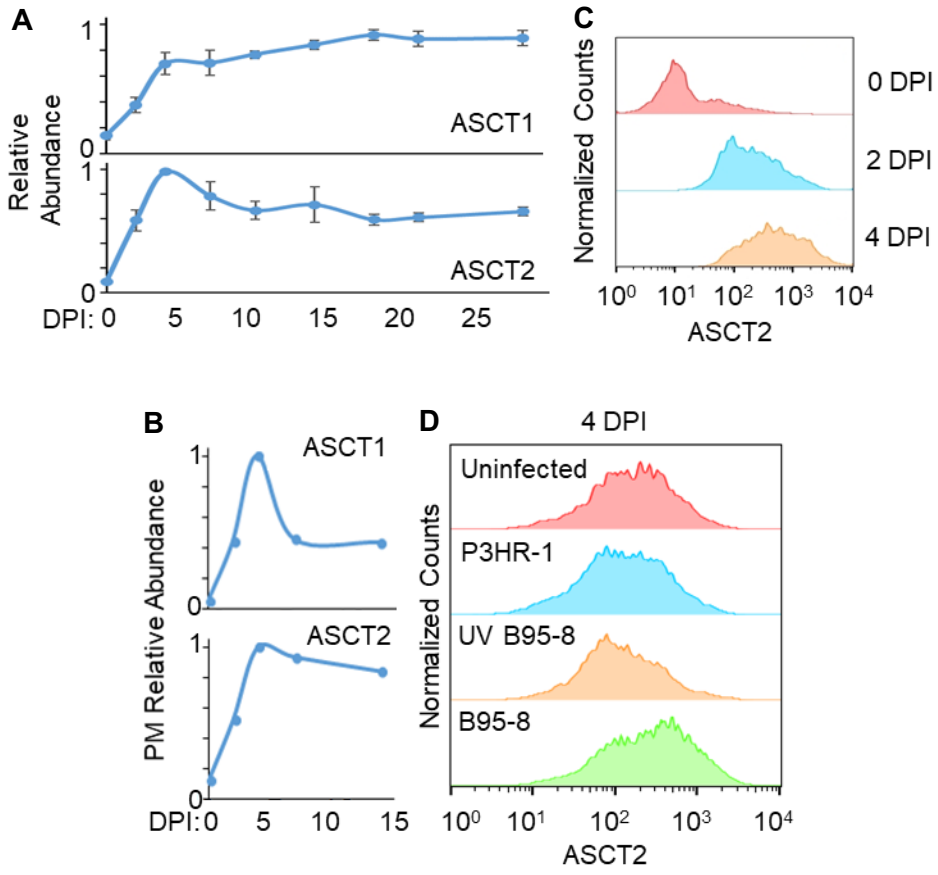

Figure III.9 EBV EBNA2 induces ASCT1 and ASCT2 expression and trafficking to the cell surface. (A) Temporal WCL proteomic profiles of ASCT1 and ASCT2 relative abundances at the indicated timepoints DPI. Data show the mean ± SEM, n=3. (B) Temporal proteomic plots of PM relative abundances of the neutral amino acid transporters ASCT1 and ASCT2. (C) Flow cytometry analysis of CD23+ primary B-cell ASCT2 PM levels at the indicated DPI. Representative of n=3. (D) Flow cytometry of ASCT2 in uninfected B-cells maintained in culture for 4 days or at 4 DPI with the indicated EBV strain at equal levels of infection. Representative of n=3.

Serine and glycine are non-essential amino acids but are often important for transformed cell growth (Locasale *et al.*, 2011; Possemato *et al.*, 2011). To test whether EBV infection renders primary B-cells auxotrophic for serine and/or glycine, we performed growth transformation assays in either replete media or media deficient for serine and/or glycine. Interestingly, while glycine withdrawal had little effect, exogenous serine depletion significantly impaired EBV-driven primary B-cell outgrowth (Figure III.10). The lack of effect with glycine withdrawal was consistent with the notion that serine catabolism generates sufficient intracellular glycine (Ducker *et al.*, 2017). These results support a model where EBNA2 upregulates import of exogenous serine to enable B-cell metabolic remodeling and hyperproliferation.

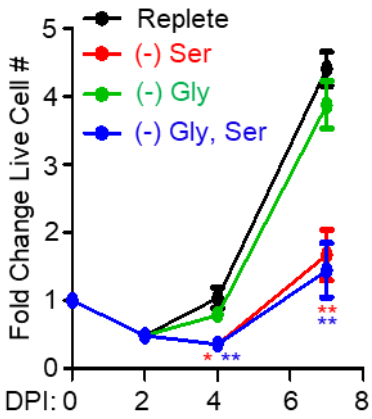

Figure III.10 Serine deprivation leads to a proliferative defect in newly infected B-cells. Growth curves of newly infected primary B-cells cultured in either replete media or media lacking serine, glycine or both serine and glycine. Data show the mean ± SEM, n=3. *, $p<0.05$; **, $p<0.01$ (paired one-tailed t-test with means compared against the replete condition).

Imported serine can be catabolized by either the cytosolic or mitochondrial 1C pathways. To identify the 1C compartment activated by EBV infection, we performed isotope tracing experiments on newly infected primary human B-cells grown in the presence of [2,3,3-^{2}H]-serine. The cytosolic pathway results in the stable incorporation of two deuterons into deoxythymidylate triphosphate (M+2 labeling of dTTP), whereas mitochondrial 1C results in the production of M+1 labeled dTTP (Figure III.11A). Isotope tracing identified M+1 dTTP as the predominant species (Figure III.11B), indicating that EBV activates mitochondrial 1C metabolism in newly infected cells, and that a major reason that EBV upregulates the import of exogenous serine is to support mitochondrial 1C metabolism.

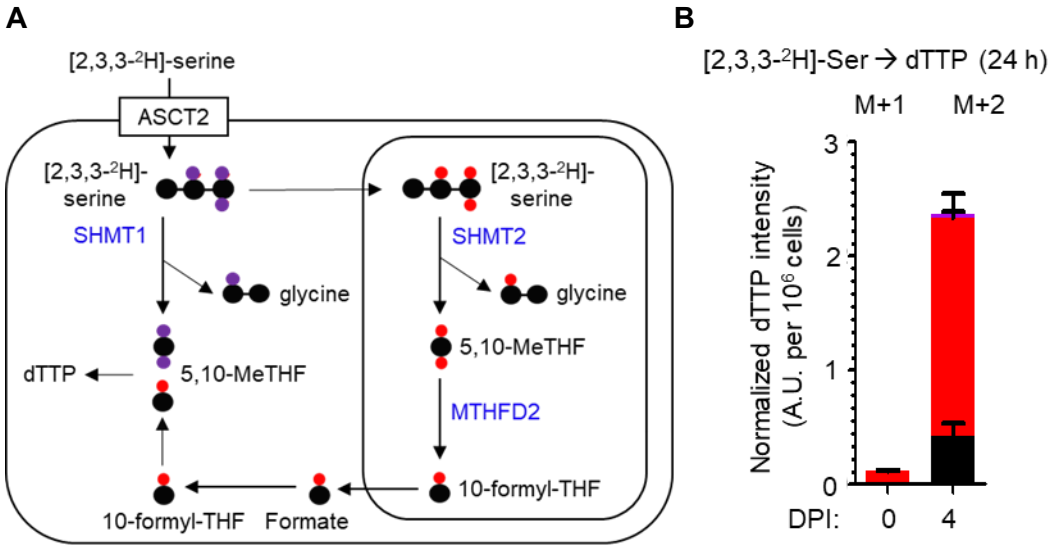

Figure III.11 Serine is preferentially consumed by the mitochondrial branch of one-carbon metabolism. (A) Schematic illustrating the fate of [2,3,3-^{2}H]-serine in either the cytosolic (purple) or mitochondrial (red) one-carbon metabolic pathway. Enzymes involved in catabolizing serine are indicated in blue bold font. (B) LC-MS measurements of dTTP isotopomers from 0 and 4 DPI cells grown in the presence of [2,3,3-^{2}H]-serine. Data show the mean with SEM, n=3. LC-MS data acquisition and analysis was jointly performed by L.W. Wang and H. Shen while LC-MS natural isotope correction was performed by B. Reinstadler.

EBNA2 and MYC upregulate de novo synthesis of the 1C fuel serine

In addition to EBV's effects on serine import, temporal proteomic analysis also highlighted EBV upregulation of the de novo serine synthesis (DNSS) pathway, which converts the glycolytic intermediate 3-phosphoglycerate (3-PG) into serine. All DNSS enzymes were strongly induced by EBV by 4 DPI (Figure III.12).

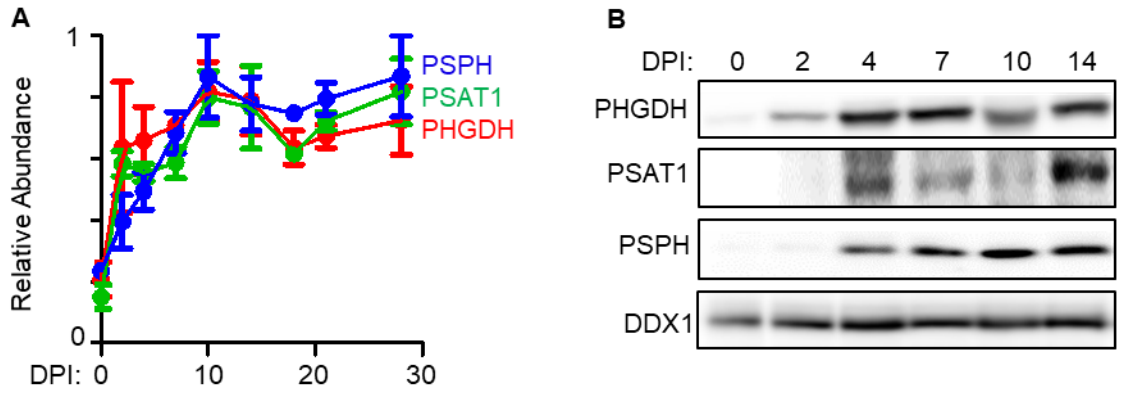

Figure III.12 EBV induces DNSS enzyme expression in newly infected cells. (A) Temporal proteomic profiles of the indicated DNSS enzymes at the indicated DPI. Data show the mean ± SEM, n=3. (B) Immunoblot analysis of DNSS enzyme expression from whole cell lysates of primary B-cells at the indicated time points of EBV infection. Blots are representative of n=3 biological replicates. Lysates were generated by I. Ersing and electrophoretically processed by S. Trudeau.

Given the finding that EBV infection induces serine auxotrophy, we next tested whether DNSS was also important for infected cell growth. Newly infected cells and GM12878 LCLs were treated with either DMSO or with one of two structurally distinct PHGDH inhibitors, CBR-5884 (Mullarky *et al.*, 2016a; Mullarky *et al.*, 2016b) or NCT-503 (Pacold *et al.*, 2016b; Pacold *et al.*, 2016a). PHGDH inhibition by either antagonist significantly diminished B-cell proliferation (Figure III.13).

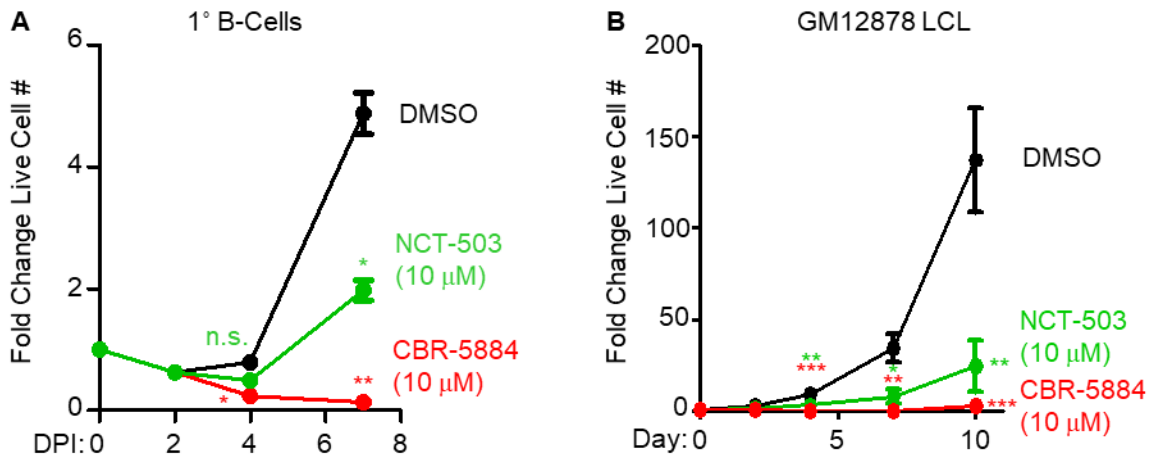

Figure III.13 PHGDH inhibition leads to proliferative defects in EBV-infected B-cells. (A) Growth curves of newly infected primary B-cells treated with either DMSO, PHGDH-selective antagonists CBR-5884 (10 μM) or NCT-503 (10 μM). Data show the mean with SEM, n=3. *, $p<0.05$; **, $p<0.01$ (paired two-tailed t-test). (B) Growth curves of GM12878 LCLs treated with either DMSO, PHGDH-selective antagonists CBR-5884 (10 μM) or NCT-503 (10 μM). Data show the mean with SEM, n=3. *, $p<0.05$; **, $p<0.01$; ***, $p<0.005$ (unpaired two-tailed t-test). Z. Wang performed the LCL growth curve analysis.

To investigate EBV's effects on serine flux, isotope tracing with $U^{13}C$-glucose was performed with resting and newly infected B-cells (Figure III.14A). M+3 labeled serine was detected in newly infected cells while resting cells showed no detectable signal, suggesting increased DNSS from $U^{13}C$-glucose-derived 3-PG and consistent with the notion that EBV activates DNSS flux (Figure III.14B). Treatment of newly infected cells with either CBR-5884 or NCT-503 resulted in significant decreases in cellular and media M+3 serine levels, indicative of the inhibitors' on-target effects (Figure III.14B). Cellular M+3 serine abundance was relatively low (~1%) in newly infected cells grown under replete conditions, perhaps because DNSS-derived serine may be rapidly consumed. However, when serine was excluded from the media and

formate was supplemented at millimolar levels, the proportion of M+3 serine increased to nearly 15% (Figure III.14C). This finding is consistent with the hypothesis that DNSS may serve to augment intracellular serine pools under conditions of limiting extracellular serine, as might happen in vivo and has been reported in a recent paper (Sullivan *et al.*, 2019).

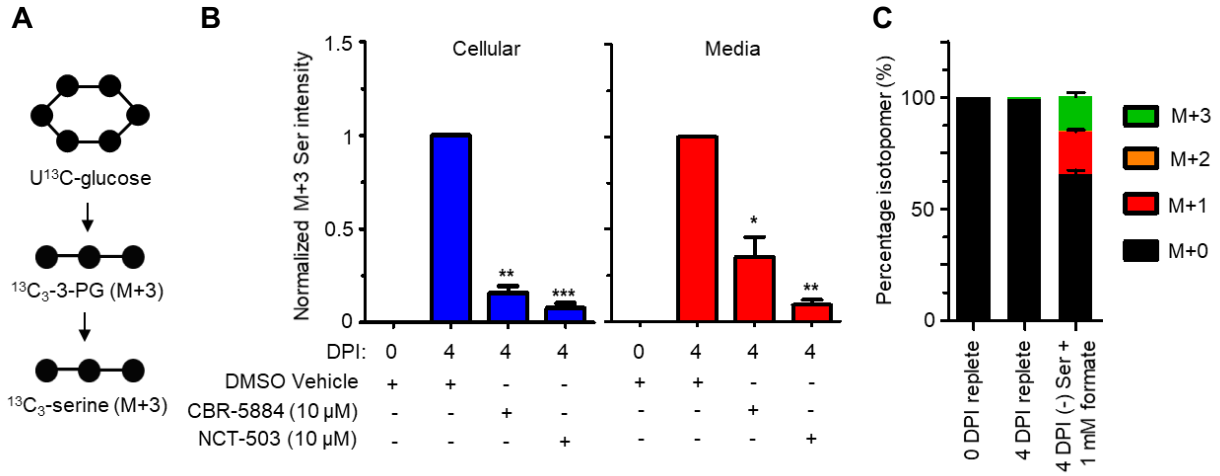

Figure III.14 EBV induces DNSS flux which is augmented by serine depletion from media. (A) Schematic illustrating metabolic tracing of U^{13}C-glucose in its conversion to ^{13}C-labeled serine. (B) LC-MS detection of M+3 labeled serine in primary B-cell cellular and media extracts at the indicated time points and under the indicated conditions. DMSO treatment was used for normalization i.e. set as 1. Data show the mean with SEM, n=3. *, $p<0.05$; **, $p<0.01$; ***, $p<0.005$ (one-sample t-test). (C) LC-MS detection of M+3 labeled serine in primary B-cell cellular extracts at the indicated time points post-infection and under replete or serine-deprived, formate-supplemented conditions. LC-MS data acquisition and analysis was jointly performed by L.W. Wang and H. Shen while natural isotope correction was performed by B. Reinstadler.

Further supporting the role of EBNA2 as a viral master regulator of B-cell metabolism, its conditional inactivation of EBNA2 in the EBNA2-HT cell line impaired *PHGDH* mRNA expression (Figure III.15A). In addition, conditional MYC expression in P493-6 B-cells grown

under EBNA2-non-permissive conditions was sufficient to upregulate mRNAs encoding 1C and DNSS enzymes (Figure III.15B) (Lin *et al.*, 2012). Collectively, our data suggest that EBNA2- and MYC-induced serine uptake and synthesis are important determinants of EBV-infected B-cell proliferation.

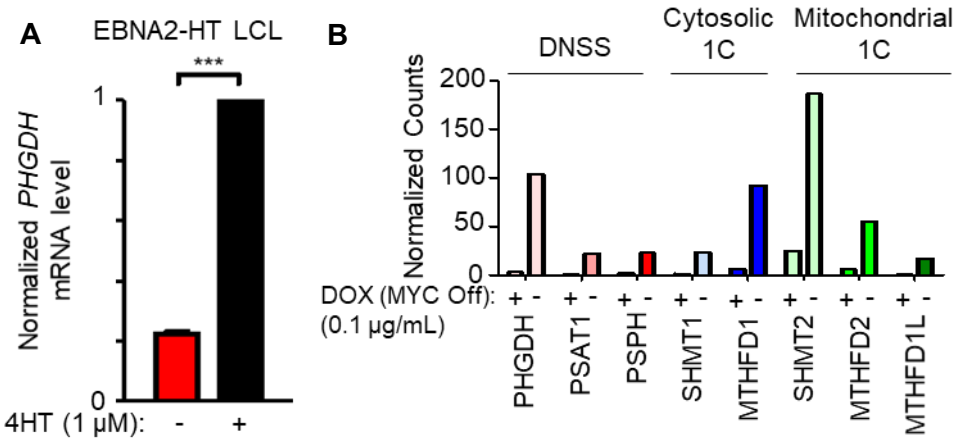

Figure III.15 EBNA2 and its target MYC regulate DNSS gene expression in LCLs. (A) Quantitative PCR analysis of normalized *PHGDH* mRNA levels in 2-2-3 EBNA2-HT LCLs grown in the presence (permissive for growth) or absence (not permissive for growth) of 4HT (1 μM) conditions for 48 hours. Data shows the mean with SEM, n=3. ***, $p<0.005$ (one-sample t-test). (B) Normalized mRNA read abundances in P493-6 LCLs grown under EBNA2 non-permissive conditions in the absence (exogenous *MYC* on) or presence of doxycycline (exogenous *MYC* off) (0.1 μg/mL). RNA-sequencing data was extracted from Lin *et al.* (2012) and plotted.

Serine catabolism and mitochondrial 1C are critical for EBV-infected B-cell growth

To test whether EBV-induced 1C metabolism was important for transforming B-cell outgrowth, newly infected primary B-cells were treated with one of two chemically distinct 1C pathway inhibitors. SHIN1 selectively blocks cytosolic SHMT1 and mitochondrial SHMT2 (Ducker *et al.*, 2017), while MTH-1479 is a specific MTHFD2 antagonist (Chandrasekaran *et al.*, 2017).

Inhibition of either SHMT1/2 or MTHFD2 significantly diminished EBV-driven primary B-cell proliferation (Figure III.16).

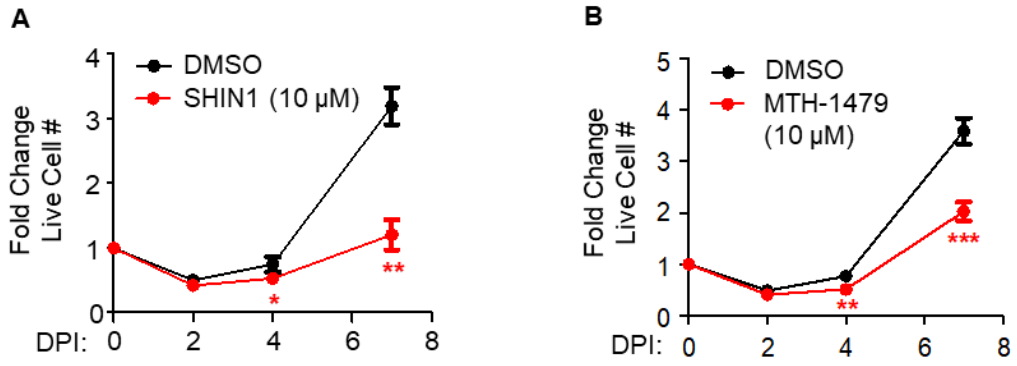

Figure III.16 Inhibition of mitochondrial 1C metabolism impairs newly infected cell outgrowth. (A) Growth curves of newly infected primary B-cells treated with DMSO or SHIN1 (10 μM). Data show the mean ± SEM, n=4. **, $p<0.01$ (paired one-tailed t-test). (B) Growth curves of newly infected B-primary cells treated with DMSO or MTH-1479 (10 μM). Data show the mean ± SEM, n=7. ***, $p<0.005$ (paired one-tailed t-test).

We confirmed the on-target effects of SHIN1 and MTH-1479 by LC-MS analysis of dTTP from cells fed [2,3,3-^{2}H]-serine and treated with either inhibitor. As expected for on-target effects, SHIN1 treatment resulted in loss of M+1 labeled dTTP and an increase in the unlabeled M+0 population, while MTH-1479 treatment caused a decrease in M+1 dTTP with a concomitant, large increase in the M+2 isotopomer, consistent with reversal of 1C flux (Figure III.17).

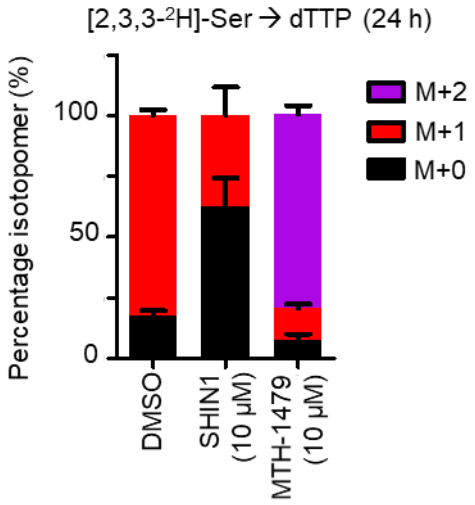

Figure III.17 SHIN1 and MTH-1479 exert on-target effects on mitochondrial 1C metabolism. LC-MS measurements of dTTP isotopomers from 4 DPI cells treated for 24 hours with either DMSO, SHIN1 (10 μM) or MTH-1479 (10 μM), and grown in the presence of [2,3,3-^{2}H]-serine. Data show the mean with SEM, n=3. LC-MS data acquisition and analysis was jointly performed by L.W. Wang and H. Shen. Natural isotope correction was performed by B. Reinstadler.

To further assess 1C roles in EBV-driven proliferation and survival, we treated newly infected primary B-cells and GM12878 LCL with SHIN1 and performed carboxyfluorescein diacetate succinimidyl ester (CFSE) dye dilution and 7-aminoactinomycin D (7-AAD) viability assays. SHIN1 decreased proliferation and increased cell death of both newly infected B-cells and fully transformed GM12878 LCLs (Figure III.18).

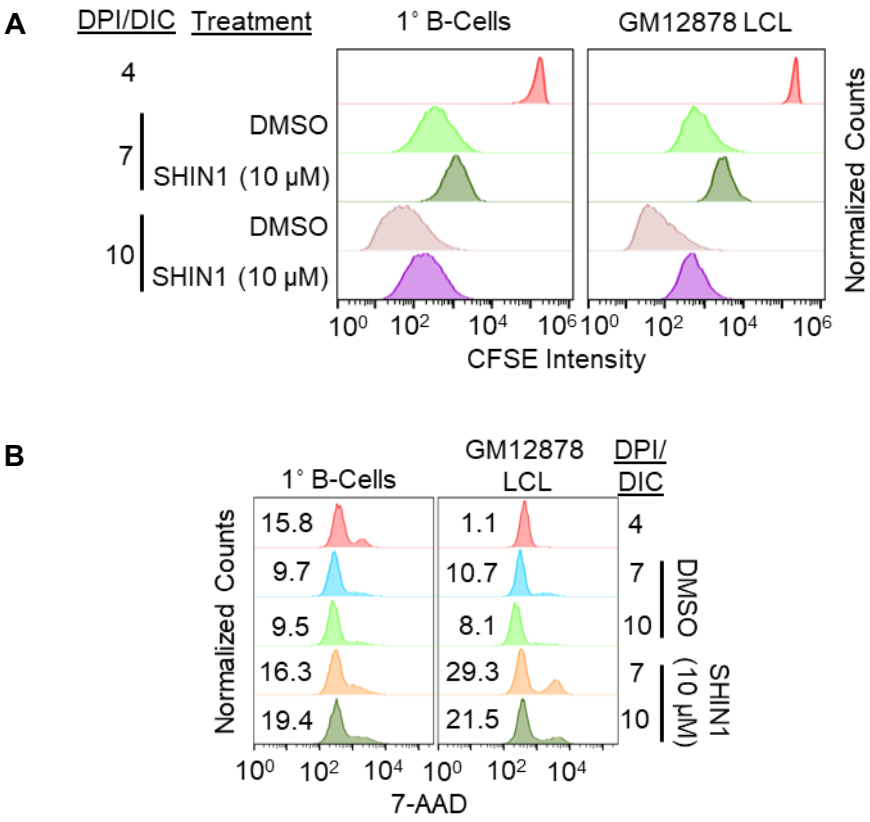

Figure III.18 Inhibition of one-carbon metabolism reduces proliferation and increases death of EBV-infected B-cells. (A) CFSE dye dilution assays of newly infected primary B-cells and LCLs treated with either DMSO or SHIN1 (10 μM). Cells were stained with CFSE at 4 DPI or DIC (days in culture) and immediately treated with either DMSO or SHIN1. Data shown is representative of n=3. (B) Apoptosis assays by 7-AAD staining of newly infected primary B-cells and LCLs treated with either DMSO or SHIN1 (10 μM). Data was collected at 4, 7 and 10 DPI/DIC. In-panel numbers indicate the average percentage of cells that were 7-AAD+. Data shown is representative of n=3.

To exclude the possibility that these proliferative defects were due to off-target effects of SHIN1, we attempted to rescue SHIN1-treated cells with formate supplementation. Addition of millimolar levels of formate to the culture media rescued the growth of newly infected cells; addition of excess glycine did not promote further growth (Figure III.19).

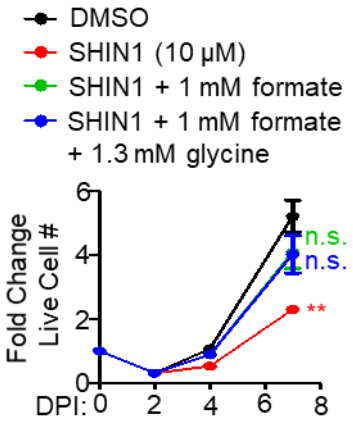

Figure III.19 Formate supplementation rescues the SHIN1-induced proliferative defects. Growth curve analysis of newly infected cells treated with either DMSO, SHIN1 (10 μM) or SHIN1 with the indicated supplements. Data show the mean ± SEM, n=4. **, $p<0.01$ (paired two-tailed t-test with means compared against the DMSO condition).

Furthermore, SHIN1 negatively impacted outgrowth of primary human B-cells in an in vitro transformation assay (Figure III.20).

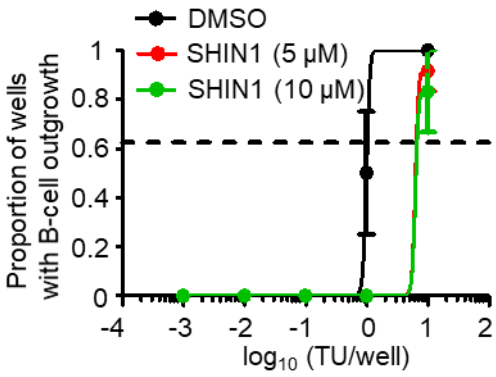

Figure III.20 SHIN1 decreases transformation efficiency of EBV infection. In vitro transformation assays of isolated primary human B-cells treated continuously for 4 weeks with either DMSO or the indicated dose of SHIN1. Data show fitted non-linear regression curves with means ± SEM, n=3.

To further investigate EBV-induced mitochondrial 1C roles in lymphoblastoid B-cell growth and survival, Cas9-expressing GM12878 LCLs were transduced with lentivirus expressing non-targeting control or an *MTHFD2* targeting sgRNA. MTHFD2 knockout (KO) by either of two independent sgRNAs significantly diminished LCL proliferation (Figure III.21A) and caused accumulation of cells at the G1/S phase (Figure III.21B).

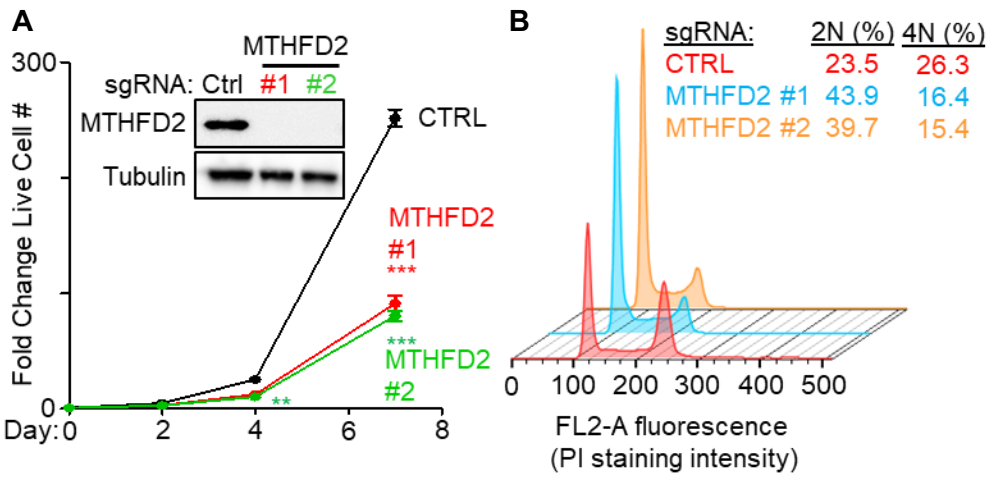

Figure III.21 MTHFD2 KO in LCLs leads to G1/S arrest. (A) Growth curve analysis of Cas9+ GM12878 LCLs following expression of non-targeting control versus independent *MTHFD2*-targeting sgRNAs. Data show the mean ± SEM, n=3. **, p<0.05; ***, p<0.005 (unpaired two-tailed t-test). Inset: immunoblot analysis of MTHFD2 and tubulin load-control in Cas9+ GM12878 LCLs with the indicated sgRNAs. Shown are representative blots, n=3. (B) PI staining of Cas9+ GM12878 LCLs expressing the indicated control or MTHFD2-targeting sgRNAs. Average percentages for 2N and 4N peaks across n=3 biological replicates are shown. Histograms are representative of n=3 biological replicates.

Stable expression of a Cas9-resistant silent point mutant *MTHFD2* cDNA (MTHFD2^{R}) restored cell proliferation in *MTHFD2* KO LCLs (Figure III.22), confirming the role of MTHFD2 in promoting LCL growth and survival.

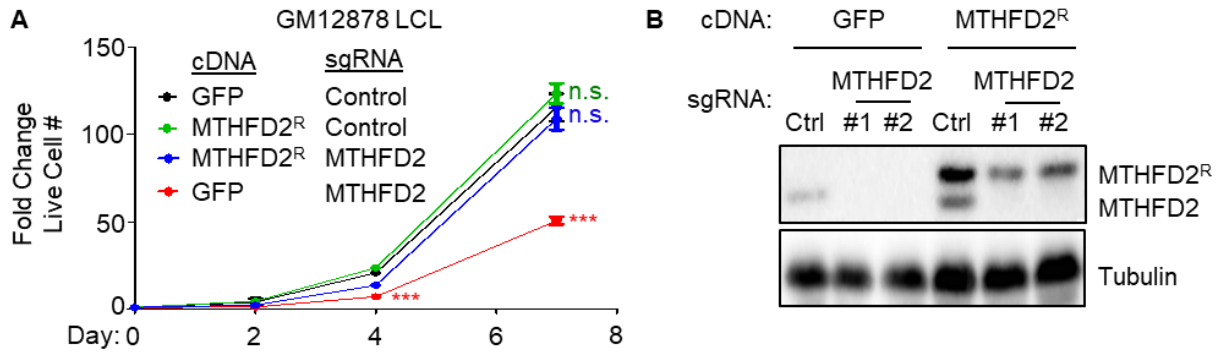

Figure III.22 KO of endogenous MTHFD2 can be rescued with sgRNA-refractory cDNA encoding wild-type MTHFD2. (A) Growth curve analysis of Cas9+ GM12878 LCL following expression of the indicated *GFP* control or *MTHFD2*^{R} rescue cDNAs and the indicated control or *MTHFD2*-targeting sgRNAs. ***, p<0.005 (paired one-tailed t-test with means compared against the GFP cDNA + control sgRNA condition). (B) Immunoblot analysis of WCL from Cas9+ GM12878 LCL following expression of the indicated *GFP* control or *MTHFD2*^{R} rescue cDNAs and the indicated control or *MTHFD2*-targeting sgRNAs. Representative blot of n=3 replicates shown.

EBV mimics physiological signals to drive germinal center B-cell growth and survival. We hypothesized that 1C metabolism was likewise activated by prototypical agonists operative in germinal center reactions. RNA-seq analysis of resting versus recombinant CD40 ligand (CD40L)-stimulated primary human B-cells revealed robust upregulation of mitochondrial 1C enzymes within 24 hours post-stimulation that was sustained at 96 hours post stimulation (Figure III.23A). Similarly, stimulation by either B-cell receptor cross-linking or Toll-like receptor 9 agonist CpG, but not by interleukin-4 (IL4), induced primary B-cell MTHFD2 expression (Figure III.23B).

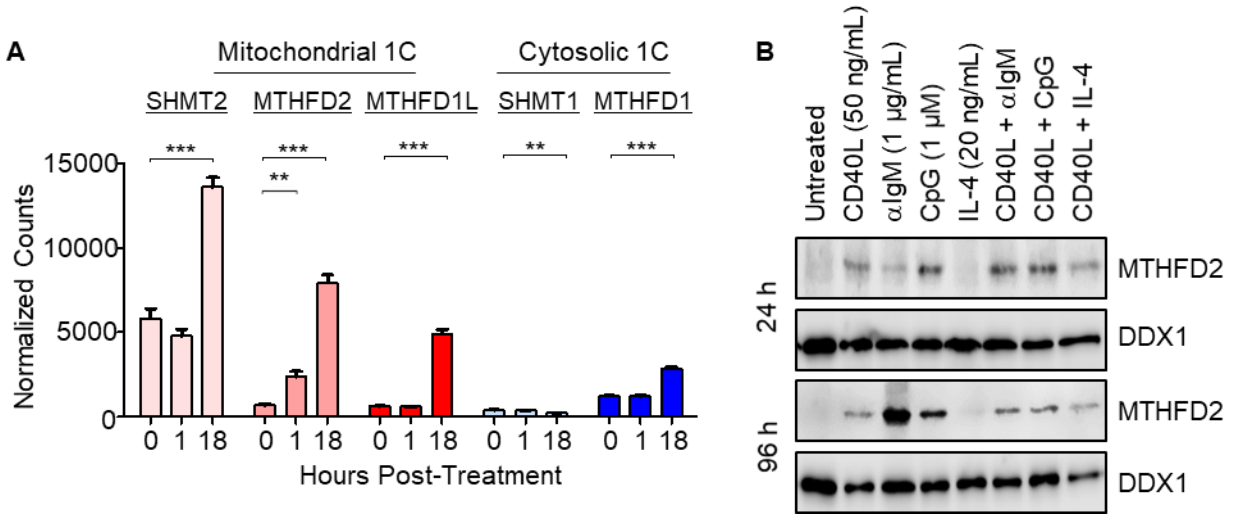

Figure III.23 Primary B-cell stimulation with myriad agonists activates one-carbon metabolism. (A) Normalized RNA-seq counts of the indicated mRNAs encoding 1C enzymes in primary human B-cells stimulated by MEGACD40L (50 ng/mL) for the indicated times. *, $p<0.05$; **, $p<0.01$; ***, $p<0.005$ (unpaired two-tailed t-test). (B) Immunoblot analysis of WCL from primary human B-cells stimulated as indicated. Representative of n=2. RNA-sequencing data as shown in panel A was generated by Y. Ma while N. Smith repeated primary B-cell stimulation experiments whose data are shown here in panel B.

EBV-induced mitochondrial 1C metabolism generates compartment-specific NADPH

Proteomic profiling highlighted viral induction of anabolic pathways that avidly consume NADPH, including fatty acid and cholesterol biosyntheses (Figures II.7, II.22). In addition to key roles in providing carbon units for anabolic reactions, mitochondrial 1C metabolism generates reducing power and substrate-level ATP. While the glucose-derived oxidative pentose phosphate pathway (oxPPP) shunt is traditionally considered the major NADPH source, primary B-cells do not have robust PPP physiology (Xiao *et al.*, 2018), and EBV downregulated several

PPP enzymes, including the rate-limiting enzyme, glucose-6-phosphate dehydrogenase (G6PD) (Figure III.24).

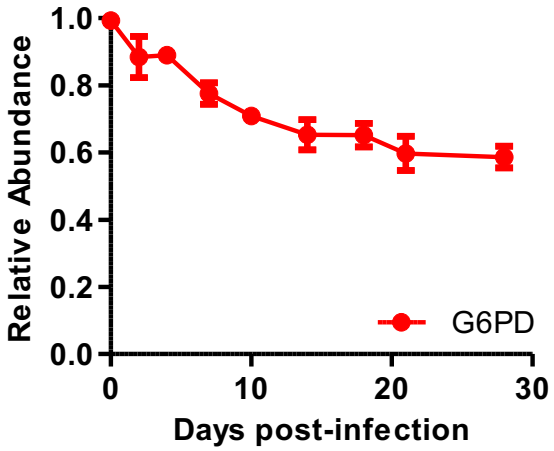

Figure III.24 EBV downmodulates G6PD protein expression. Temporal proteomic profile of G6PD at the indicated DPI. Data show the mean ± SEM, n=3.

Yet, despite EBV induction of NADPH-consuming pathways, we found that EBV infection significantly increased NADPH/NADP ratios in newly infected B-cells, with little effect on NADH/NAD ratios out to 7 DPI (Figure III.25). These results suggest that EBV induces NADPH production, likely through a non-PPP mechanism.

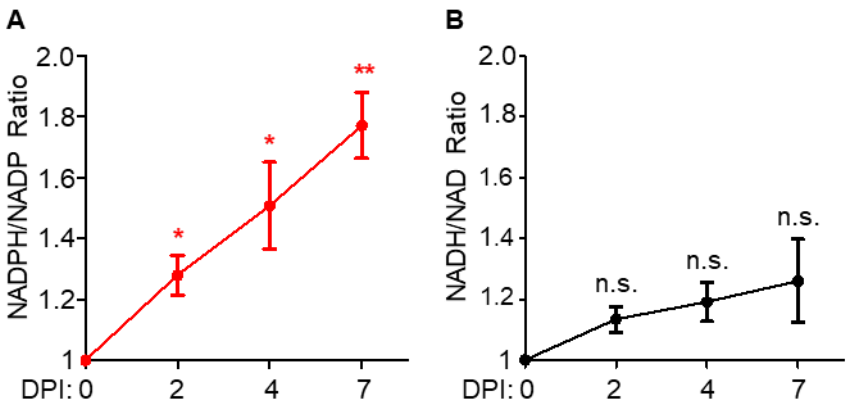

Figure III.25 EBV selectively increases overall NADPH/NADP ratios in newly infected cells. (A) Whole cell NADPH/NADP ratios in primary B-cells at the indicated time points post-EBV infection. Shown are mean ± SEM values from n=4 replicates. *, $p<0.05$; **, $p<0.01$ (one-sample t-test). (B) Whole cell NADH/NAD ratios in primary B-cells at the indicated time points post-EBV infection. Data show the mean ± SEM values from n=4 replicates. n.s., not significant (one-sample t-test).

We hypothesized that EBV may utilize mitochondrial 1C as an important NAPDH source. To experimentally determine whether EBV induces NADPH production through mitochondrial 1C pathways, we performed [2,3,3-^{2}H]-serine labeling experiments with newly infected cells (Figure III.26). [2,3,3-^{2}H]-serine catabolism yields ^{2}H-containing 10-formyl-THF, which contributes to deuterium labeling of the adenine backbone of NADP(H) cofactors, as well as redox-active hydrides. Compared to the $NADP^{+}$ labeling pattern, NADPH displayed a shift towards the heavy M+3 and M+4 isotopologues, suggesting that the redox-active hydrogen atoms are derived from exogenous serine through 1C metabolism over the timescale (four hours) of this labeling experiment. 1C blockade by SHIN1 diminished M+3 and M+4 labeling, supporting the idea that 1C metabolism is a crucial means of generating reducing power in the form of NADPH.

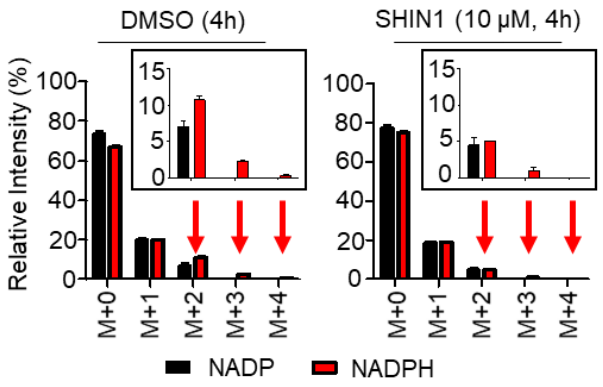

Figure III.26 One-carbon metabolism is a significant source of NADPH in newly infected cells. LC-MS analysis of nicotinamide adenine dinucleotide cofactors in primary B-cells at 4 DPI fed [2,3,3-^{2}H]-serine for 4 hours in the presence of either DMSO or SHIN1 (10 μM). Natural isotope correction was not performed. LC-MS data acquisition and analysis was jointly performed by L.W. Wang and H. Shen.

To gain insights into compartment-specific NADPH roles in the proliferation of fully transformed LCLs, we utilized the genetically-encoded NADPH oxidase triphosphopyridine nucleotide oxidase (TPNOX), which can be expressed as cytosolic or mitochondrial probes (Cracan *et al.*, 2017; Titov *et al.*, 2016). While expression of cytosolic TPNOX had little effect on LCL proliferation, mitochondrial TPNOX significantly diminished LCL growth (Figure III.27), indicating an important intramitochondrial NADPH role. In contrast, expression of either TPNOX isoform had little effect on HeLa cell growth (Cracan *et al.*, 2017).

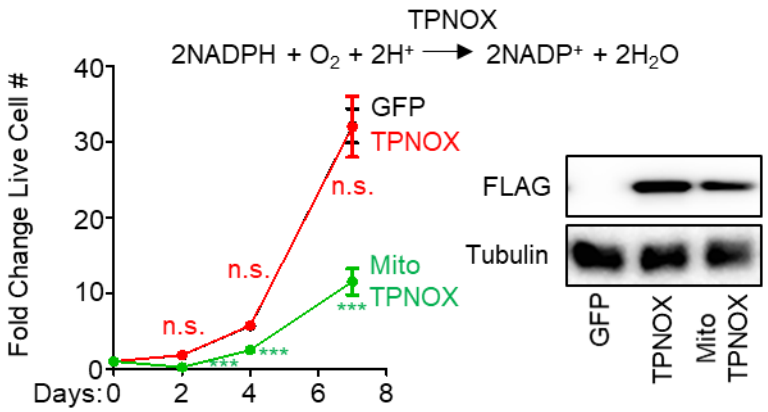

Figure III.27 Expression of a mitochondria-localized NADPH oxidase (TPNOX) impairs LCL growth and/or survival. Growth curves of GM12878 LCLs with stable GFP, TPNOX or MitoTPNOX expression. Data show the mean ± SEM, n=3. n.s., not significant; *** $p<0.005$ (unpaired two-tailed t-test with means compared to the GFP condition). Bottom: a representative immunoblot of whole cell extracts for FLAG-tagged TPNOX or MitoTPNOX and tubulin load-control, n=3.

Furthermore, the LCL NADPH/NADP ratio was significantly diminished by MTHFD2 knockout and restored by MTHFD2^{R} cDNA rescue (Figure III.28A). Conditional EBNA2 inactivation significantly reduced LCL NADPH/NADP ratio while also inducing a small but significant increase in the NADH/NAD ratio (Figure III.28B), indicating that EBV-induced MTHFD2 has a key role in producing intramitochondrial NADPH in support of EBV-transformed B-cell growth.

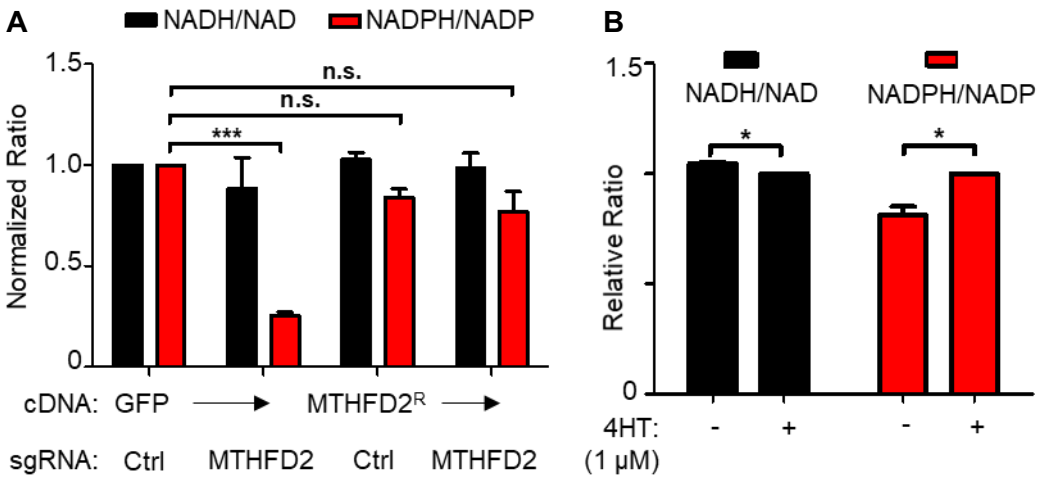

Figure III.28 EBNA2-regulated MTHFD2 expression increases whole cell NADPH/NADP ratios. (F) Quantitation of overall NADH/NAD (black) and NADPH/NADP (red) ratios in Cas9+ GM12878 LCLs expressing the indicated control or MTHFD2-targeting sgRNA as well as the indicated *GFP* or *MTHFD2*^{R} rescue cDNA. Data show the mean + SEM, n=3. n.s., not significant; ***, p<0.005 (one-sample t-test). J. Nomburg performed the NAD(P)H/NAD(P) quantitation experiments shown in panel A.

Serine-derived formate fuels infected B-cell nucleotide synthesis

EBV triggers B-cell transition from quiescence to hyperproliferation, greatly increasing the need for de novo nucleotide synthesis. We hypothesized that a major role for EBV-induced 1C metabolism is to provide 1C units and/or glycine for nucleotide synthesis. We therefore tested the extent to which formate supplementation could rescue outgrowth of EBV-infected cells in serine-deficient media. Exogenous serine withdrawal effects on EBV-driven cell proliferation could be significantly rescued by the 1C donor formate (Figure III.29), suggesting that 1C is a major source of carbon units for nucleotide synthesis in newly infected B-cells. Addition of glycine together with formate did not further enhance proliferation (Figure III.29), perhaps due to intrinsic B-cell deficiencies in glycine uptake (Ducker *et al.*, 2017).

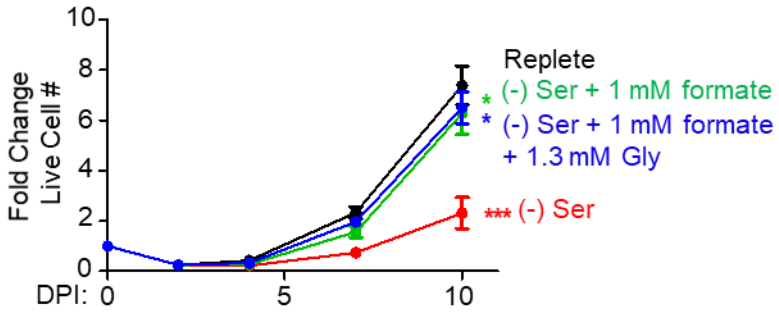

Figure III.29 Serine depletion-induced proliferative defects in newly infected cells can be rescued by formate supplementation. Growth curves of newly infected primary B-cells cultured in either replete media, serine-deficient media, or serine-deficient media with the indicated supplement (formate ± glycine). Data show the mean ± SEM, n=7. *, $p<0.05$; ***, $p<0.005$ (paired two-tailed t-test).

Despite important roles in nucleotide synthesis, serine withdrawal did not provoke an overt DNA damage response in newly infected cells, as judged by immunoblot for γH2AX (Figure III.30A), suggesting that nucleotide imbalance-related genome instability was not a major cause of growth inhibition. Similarly, serine withdrawal or 1C blockade by SHIN1 did not reduce mitochondrial DNA (mtDNA) or EBV genome copy numbers (Figures III.30B-E). MTHFD2 KO also did not diminish the mitochondrial membrane potential (Figure III.30F). These results suggest that EBV-induced 1C was instead necessary for nucleotide synthesis for other roles, possibly including B-cell nuclear genome synthesis and/or RNA transcription.

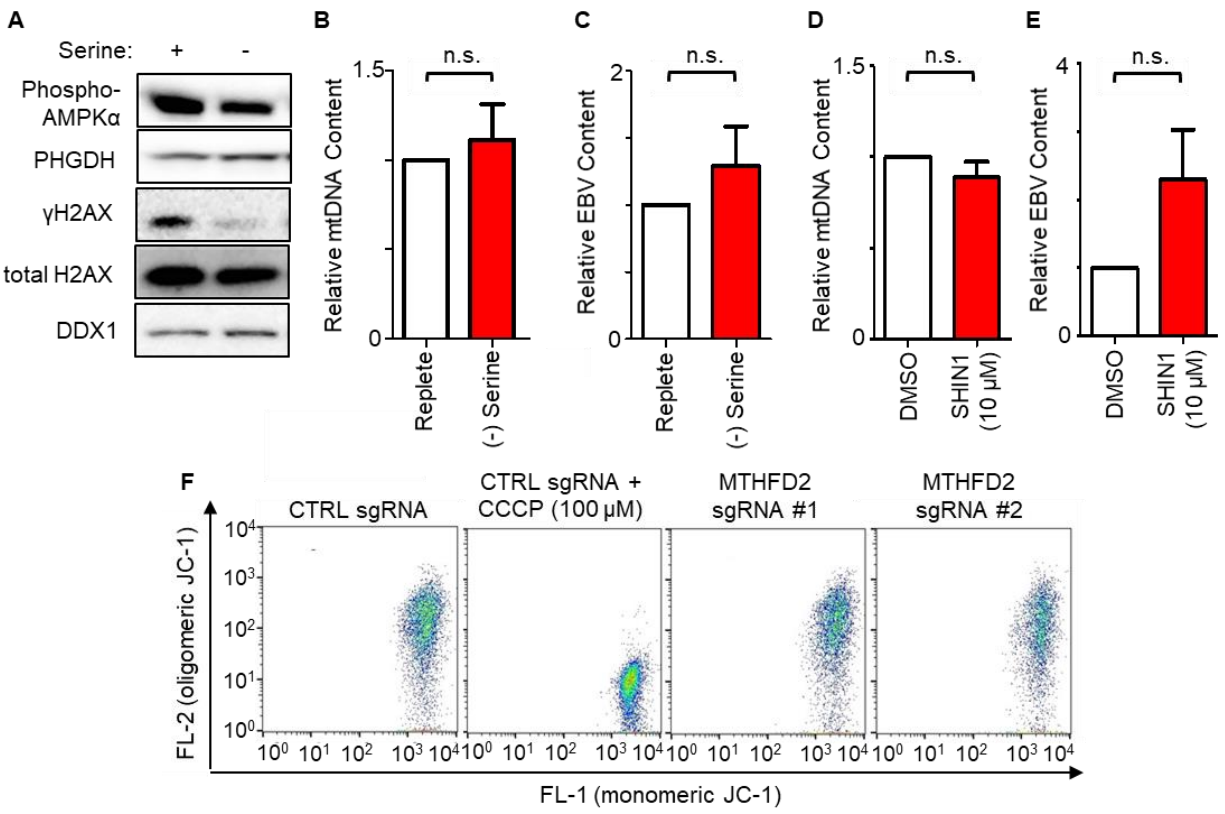

Figure III.30 Inhibition of one-carbon metabolism does not provoke the DNA damage response, reduce mitochondrial DNA or viral genome copy numbers, or diminish the mitochondrial membrane potential. (A) Immunoblot analysis of WCL from primary B-cells at 4 DPI grown in replete or serine-deficient media. Blots are representative of n=3 replicates. (B) Relative mitochondrial DNA (mtDNA) content and (C) relative EBV content in primary B-cells at 4 DPI grown in replete or serine-deficient media. Data show the mean + SEM, n=3. n.s., not significant (one-sample t-test). (D) Relative mtDNA content and (E) relative EBV content in primary B-cells at 4 DPI grown in complete media with DMSO or SHIN1 (10 μM). Mean + SEM from n=3. n.s., not significant (one-sample t-test). (F) JC-1 staining of Cas9+ GM12878 LCLs transduced with either control sgRNA or one of two *MTHFD2*-targeting sgRNAs. CCCP treatment was performed as a positive control. Contour plots shown are representative of n=2 replicates.

We hypothesized that serine was required to meet the bioenergetic requirements of newly infected cell outgrowth. Indeed, exogenous serine withdrawal decreased newly infected B-cell ATP levels, which could be reversed with formate supplementation (Figure III.31A). $U^{13}C$-serine metabolic tracing readily labeled cellular adenosine monophosphate (AMP) pools (Figure III.31B), suggestive of serine-derived formate and glycine incorporation (Jain *et al.*, 2012). Mechanistically, serine deprivation caused the accumulation of de novo purine synthesis intermediates glycinamide ribonucleotide (GAR) and 5-aminoimidazole-4-carboxamide ribonucleotide (AICAR), which were completely consumed once cells were supplemented with formate (Figure III.31C). Taken together, these results strongly suggest important contributions from 1C metabolism and de novo purine biosynthesis in supporting adenine nucleotide levels.

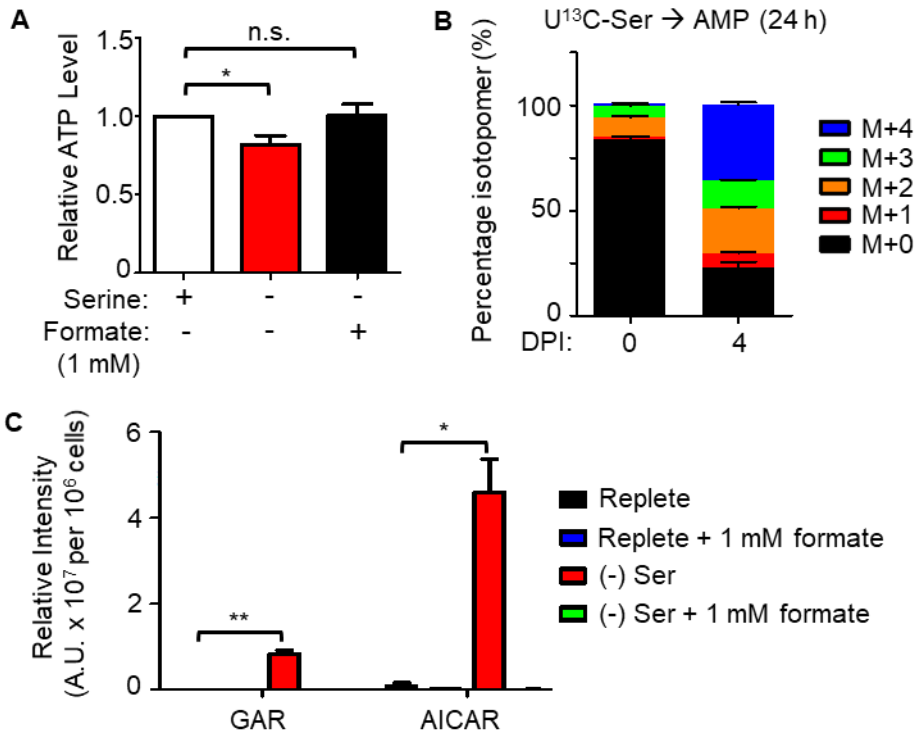

Figure III.31 Formate supplementation rescues purine synthesis in newly infected cells. (A) Relative ATP levels in primary B-cells 7 DPI grown in replete or serine-deficient media, supplemented with formate, as indicated. Data show the mean + SEM, n=4. n.s., not significant; *, $p<0.05$ (one-sample t-test). (B) LC-MS detection of AMP isotopomers extracted from resting B-cells and 4 DPI cells after labeling with $U^{13}C$-serine for 24 hours. Data shows the mean with SEM, n=5. (C) LC-MS detection of de novo purine synthesis intermediates GAR and AICAR in newly infected primary B-cells 4 DPI. Data shows the mean with SEM, n=3. *, $p<0.05$; **, $p<0.01$ (paired two-tailed t-test). LC-MS data acquisition and analysis were jointly performed by L.W. Wang and H. Shen while natural isotope correction was performed by B. Reinstadler.

Serine deprivation also diminished newly infected cell basal and maximal OCRs (Figure III.32). Consistent with an earlier report (Maddocks *et al.*, 2016), serine deprivation did not result in an increase in Thr172 phosphorylation on AMP-activated protein kinase α (AMPKα) (Figure

III.30A), likely because AMP, ADP and ATP are equally affected by serine deprivation and the adenylate charge is not substantially altered.

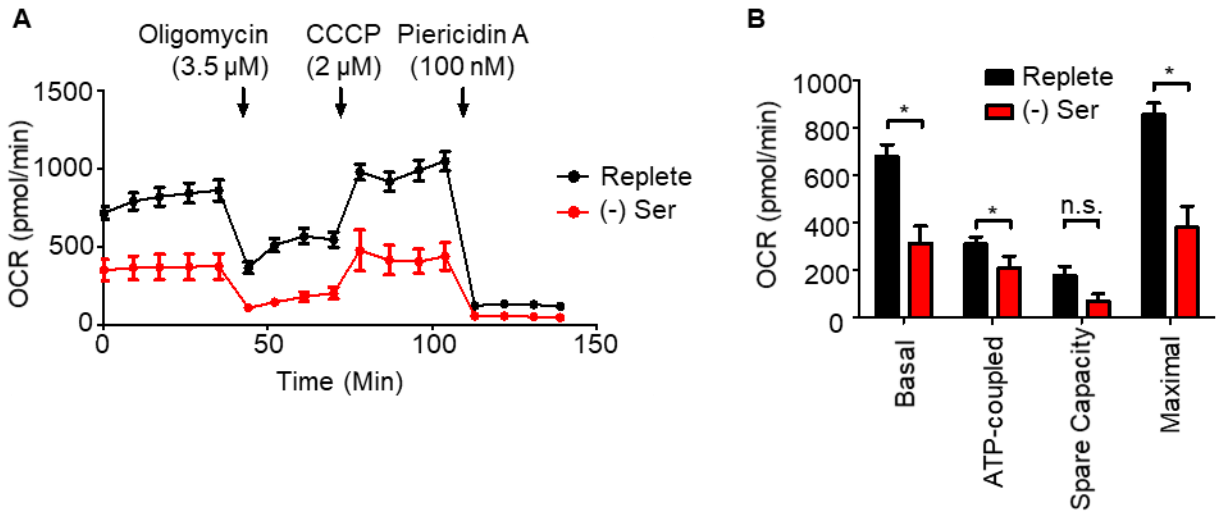

Figure III.32 Serine deprivation reduces the oxidative capacity of newly infected cells. (A) Oxygen consumption rates (OCRs) of primary B-cells 4 DPI grown in replete or serine-deficient media and subject to flux analysis in the presence of the indicated ETC inhibitors. Data shown the mean ± SEM, n=4. (B) Calculated metabolic parameters of primary cells 4 DPI grown in replete or serine-deficient media. Shown are mean + SEM, n=4. n.s., not significant; *, $p<0.05$ (paired two-tailed t-test).

Viral activation of mitochondrial 1C generates glutathione for redox and glycine toxicity defense

Marked upregulation of cholesterol and lipid synthetic pathways during EBV transformation may be necessary for B-cell remodeling but likely generates lipid free radicals that can trigger ferroptosis (Yang and Stockwell, 2016). Furthermore, while mitochondrial 1C was recently found to be a key source of B-cell lymphoma glycine (Ducker *et al.*, 2017), high 1C flux can generate potentially toxic levels of intracellular glycine, which necessitates disposal through the glycine cleavage system (GCS; comprises four different protein subunits – GLDC, DLD, GCSH and AMT) or via efflux systems. However, we did not observe strong or substantial upregulation of

key GCS subunits, GLDC and DLD, over the first few days post-infection at timepoints of maximal mitochondrial 1C enzyme induction (Figure III.33). Yet, glycine release into the media was only modestly increased at 4 DPI (Figure III.8B). These observations prompted us to investigate if there was a major cellular sink for serine-derived glycine during early infection.

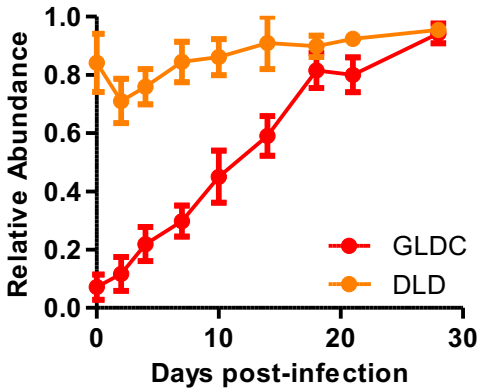

Figure III.33 GCS subunit abundances are not strongly enhanced early in infection. Temporal proteomic traces of protein relative abundances for GLDC and DLD. Data show the mean with SEM, n=3.

De novo glutathione synthesis is central to redox defense and may represent an avenue for glycine disposal without causing overt cytotoxicity. Blockade of the 1C pathway either by SHIN1 (Figure III.34A) or MTH-1479 (Figure III.34B) increased newly infected B-cell intracellular reactive oxygen species (ROS) levels, and EBV infection strongly induced synthesis of glutathione (Figure III.34C).

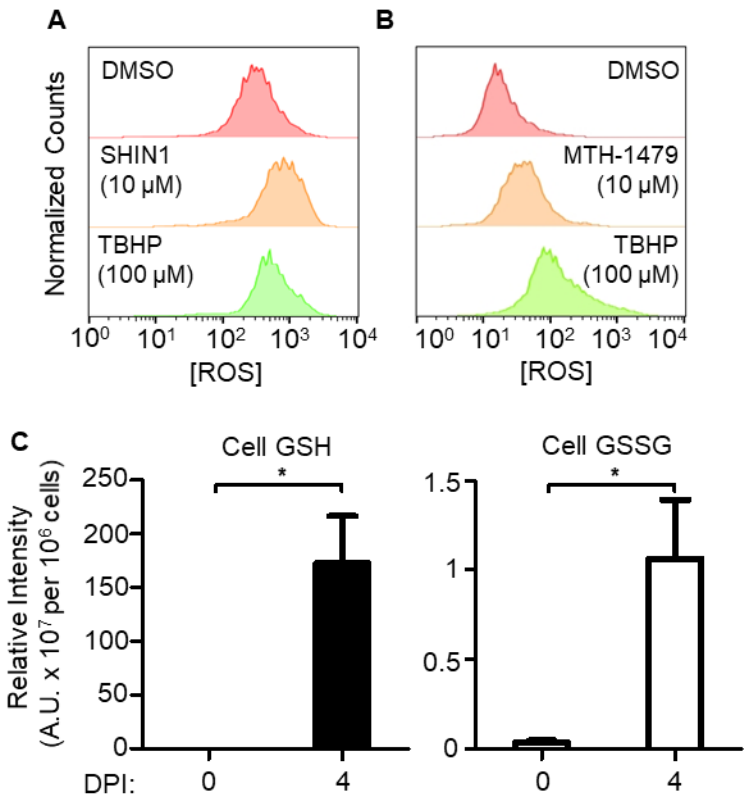

Figure III.34 EBV induces glutathione synthesis and 1C blockade increases cellular ROS levels. (A) Flow cytometry of primary B-cells 7 DPI treated with either DMSO or SHIN1 (10 μM) and stained with DCFDA for intracellular ROS quantitation. TBHP (100 μM) was used as a positive control. n=2. (B) Flow cytometry of primary B-cells 7 DPI treated with either DMSO or MTH-1479 (10 μM) and stained with DCFDA for intracellular ROS quantitation. TBHP (100 μM) was used as a positive control. n=2. (C) LC-MS detection of reduced glutathione (GSH) and oxidized glutathione (GSSG) extracted from primary B-cells at 0 and 4 DPI. Data show the mean + SEM, n=3. *, $p<0.05$ (paired one-tailed t-test). LC-MS data acquisition and analysis were jointly performed by L.W. Wang and H. Shen.

We therefore asked if 1C-derived glycine was being utilized for glutathione synthesis. $U^{13}C$-serine tracing labeled approximately 50% of cellular glycine and significant fractions of the intracellular reduced glutathione (GSH) and oxidized glutathione (GSSG) pools (Figure III.35), indicating that serine catabolism was indeed a major source of glycine in the newly infected cell and that 1C-derived glycine was heavily utilized for glutathione synthesis.

Figure III.35 One-carbon metabolism contributes strongly to intracellular glycine and glutathione pools. (A) Schematic showing metabolic tracing of U^{13}C-serine-derived glycine in de novo synthesis of glutathione. Black circles denote heavy ^{13}C atoms while white circles denote light ^{12}C atoms. The reactive thiol bonds are indicated as SH. GSS, glutathione synthase. (B) LC-MS analysis of glycine abundance in metabolite extracts of resting B-cells and 4 DPI cells fed U^{13}C-serine for 24 hours. Data show the mean + SEM, n=4. (C) LC-MS analysis of GSH and GSSG abundances in metabolite extracts of resting B-cells and 4 DPI cells fed U^{13}C-serine for 24 hours. Data show the mean + SEM, n=4. LC-MS data acquisition and analysis were jointly performed by L.W. Wang and H. Shen while natural isotope correction was performed by B. Reinstadler.

Figure III.35 (Continued)

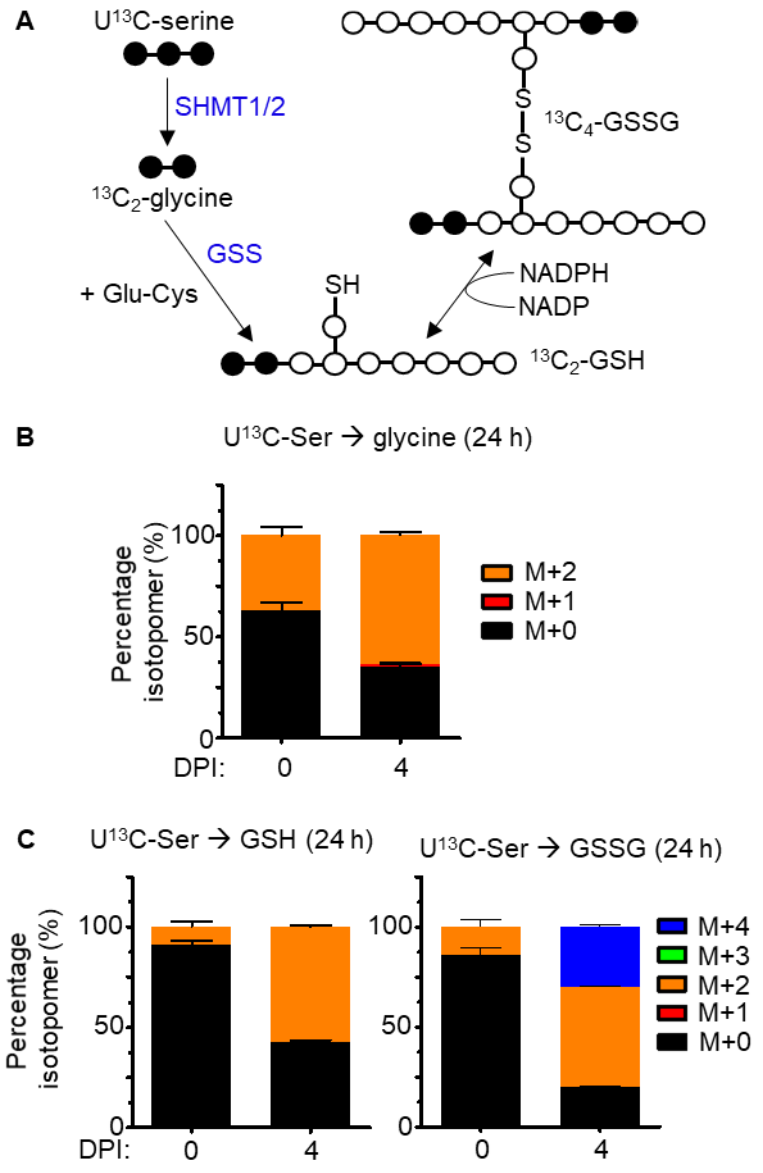

Serine withdrawal also significantly increased newly infected B-cell sensitivity to buthionine sulfoximine (BSO), which inhibits the first step of glutathione synthesis, as evidenced by the 4-fold decrease in IC_{50} levels on cell viability (Figure III.36).

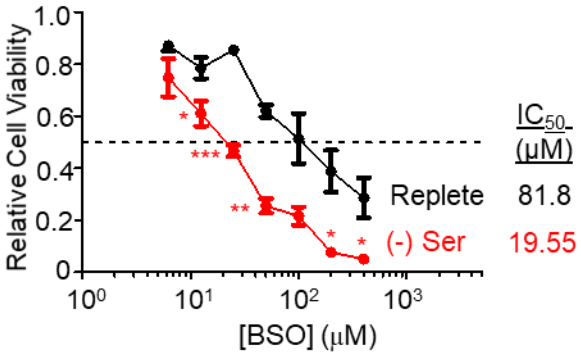

Figure III.36 Serine withdrawal sensitizes newly infected cells to BSO-mediated glutathione depletion. Relative viability of primary B-cells grown either in replete or serine-deficient media and exposed to the indicated doses of buthionine sulfoximine (BSO) for 3 days from 4 DPI to 7 DPI. Data show the mean ± SEM of n=3 experiments. *, $p<0.05$; **, $p<0.01$, ***, $p<0.005$ (paired one-tailed t-test). IC50 values were calculated by non-linear regression analysis.

These observations are consistent with the ideas that SHMT2 and MTHFD2 are key EBV-induced mediators of NADPH and glutathione production and that a significant role exists for mitochondrial 1C in newly infected cell redox defense. Taken together, these results are consistent with the hypothesis that a second major role for EBV-induced serine catabolism is the provision of metabolites and reducing power for glutathione synthesis to mitigate redox stress, and possibly also to serve as a sink for excess glycine produced by 1C metabolism.

Discussion

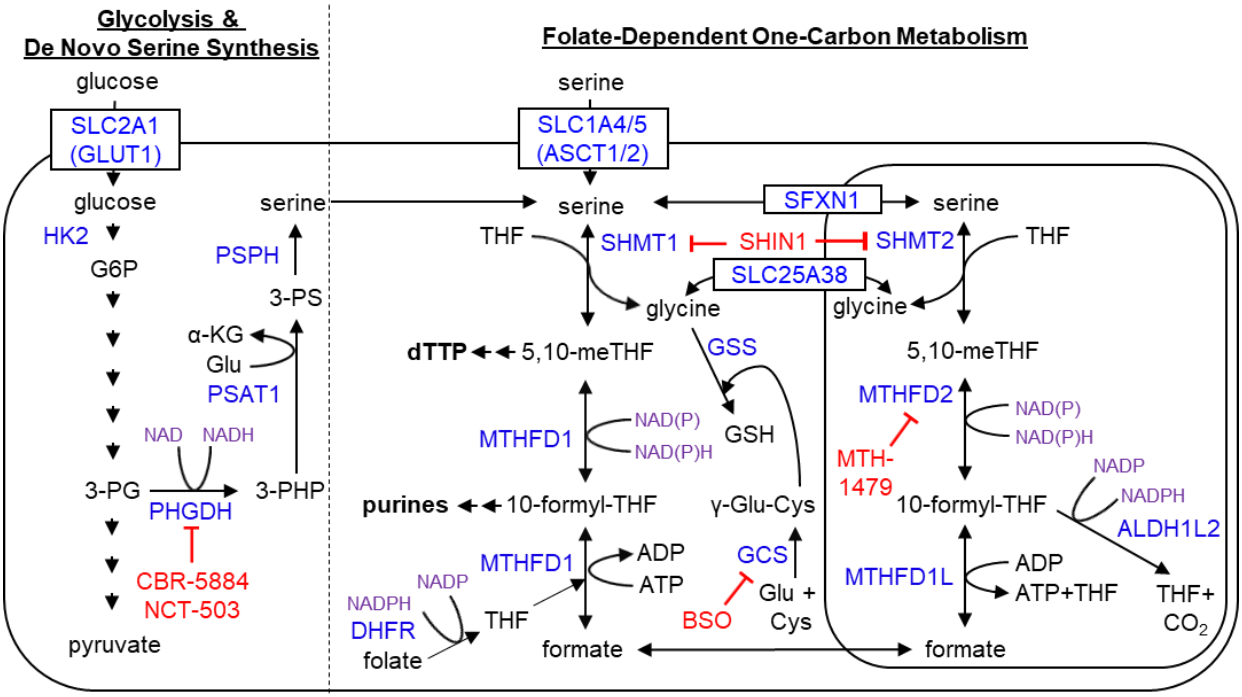

Figure III.37 Summary of key metabolic pathways induced by EBV and investigated in this work. Key metabolites are indicated in black. Cofactors are indicated in purple. Enzymes and transporters are indicated in blue. Small-molecule inhibitors used in this work are indicated in red.

To support 1C induction and other demands of hyperproliferation, EBV coordinately induced the uptake of extracellular serine as well as de novo serine synthesis within the first four days post-infection (Figure III.37) by means of EBNA2 and its host target MYC. Thus, EBNA2 is a key oncoprotein that mediates adaptation of newly infected B-cells into a physiologic state compatible with rapid cell growth. Notably, we also found that BL-like overexpression of MYC was also able to induce mitochondrial 1C. These data suggest that high MYC activity may support germinal center dark zone B-cells expansion in humoral responses. EBNA2 also induces EBV oncoproteins including the CD40 mimic LMP1, which may also serve to support

1C induction in the lymphoblastoid phase timepoints where EBNA2 and MYC abundances have decreased.

EBV-induced mitochondrial 1C was found to be a major supplier of carbon units for purine, thymidylate and glutathione synthesis necessary for rapid B-cell growth, particularly during BL-like hyperproliferation (Figure III.37). Similarly, B-cell activation by physiological ligands, including CD40L and B-cell receptor stimulation, also upregulated MTHFD2 expression, suggesting similarly important roles in physiological B-cell humoral responses.

1C metabolism is highly compartmentalized; MTHFD2 ablation was not rescued by reversal of 1C flux through the cytosolic pathway, highlighting non-redundancy between the cytosolic and mitochondrial 1C pathways. In contrast to SHMT2 inactivation in primary murine T-cells, which could be rescued by formate and the antioxidant N-acetyl-cysteine (NAC) (Ron-Harel *et al.*, 2016), we were unable to fully rescue serine deprivation with this combination (data unpublished). Our TPNOX and CRISPR results suggest that generation of intramitochondrial NADPH is a second major role of 1C metabolism in EBV B-cell growth transformation. In contrast to activated primary T-cells, serine withdrawal also did not produce overtly deleterious effects on mtDNA replication or cause DNA damage checkpoint activation, suggesting that mitochondrial 1C metabolism may have unique functions in B-cell physiology and EBV pathobiology. Additional roles in substrate-level ATP generation remain plausible.

MTHFD2 may boost flux through B-cell mitochondrial 1C pathways, as occurs during early embryogenesis (Shin *et al.*, 2014; Shin, Momb and Appling, 2017). Although the isozyme MTHFD2L has key roles in later embryogenesis and in adult tissues, we did not detect its expression in B-cells. B-cells have been reported to exhibit constitutively low PPP activity, with glucose carbon utilization skewed towards glycolysis (Xiao *et al.*, 2018). Intriguingly, while the phosphatase PP2A was found to redirect glucose carbon units to PPP in DLBCLs, we found PP2A catalytic subunit PPP2CA expression to be unchanged by EBV infection, and EBV

suppressed G6PD expression by nearly two-fold. Furthermore, LCLs can be established from G6PD-deficient human B-cell donors (Maeda *et al.*, 1992). Taken together with the finding that MTHFD2 ablation reduced LCL NADPH/NADP ratios, our results suggest that EBV may induce mitochondrial 1C metabolism in lieu of increasing PPP flux to provide NADPH for B-cell transformation, with possible roles in redox defense and anabolic growth. MTHFD2 has been reported to be a major contributor to cellular NADPH in HEK293 cells (Fan *et al.*, 2014), but not previously implicated in primary cell or B-cell NADPH generation.

Temporal proteomic analysis revealed that EBV significantly upregulates fatty acid and cholesterol synthesis pathways. Lipid peroxides can be a major source of free radicals that may trigger ferroptosis in the absence of sufficient NADPH and glutathione. Our recent CRISPR analysis of EBV-transformed B-cell dependency factors (Ma *et al.*, 2017c) found that LCLs are exquisitely dependent on the key glutathione-dependent ferroptosis regulator glutathione peroxidase 4 (GPX4). While resting B-cells did not appreciably produce glutathione, EBV infection robustly upregulated serine-dependent glutathione production.

Although EBV robustly induces aerobic glycolysis, we found that an intact ETC was crucial for efficient EBV-induced transformation. While ETC integrity is primarily linked to OXPHOS-dependent ATP generation, interaction with mitochondrial 1C metabolism may also underpin its importance in sustaining proliferative cell growth. Consistent with this hypothesis, SHMT2 inhibition causes impaired mitochondrial translation and defective OXPHOS (Morscher *et al.*, 2018), and ETC dysfunction causes alterations in 1C metabolism, with diminished serine-derived formate production (Bao *et al.*, 2016; Meiser *et al.*, 2016).

Epigenetic silencing plays key roles in EBV B-cell growth transformation. Hypermethylation silences host tumor suppressors and viral lytic genes (Saha *et al.*, 2015). Serine-dependent de novo ATP synthesis can have a key role in maintaining nucleic acid methylation marks (Maddocks *et al.*, 2016). It is plausible that newly infected B-cells catabolize serine to generate

ATP to support methylation of tumor suppressor genes and viral genome CpG islands (Kalla *et al.*, 2010; Kalla, Göbel and Hammerschmidt, 2012). However, under conditions used in this study, where the methyl donors methionine, vitamins B6 and 12 were present in culture, serine is likely not required for DNA and histone methylation. Nonetheless, as a secondary methyl donor, serine levels may become significant in vivo, such as in lymphoid germinal center reactions, where localized depletion of primary methyl group donors could occur.

Methotrexate inhibits DHFR and is a cornerstone of antifolate therapies used to target neoplastic and autoimmune B-cell conditions. Denis Burkitt and colleagues reported the use of methotrexate as a chemotherapeutic agent to treat endemic BL (Oettgen, Burkitt and Burchenal, 1963). Yet, methotrexate and other antifolates in clinical use are limited by toxicities, including effects on rapidly growing gastrointestinal tract epithelia. Folate-dependent mitochondrial 1C metabolism pathway components, specifically MTHFD2, may therefore be attractive targets in therapeutic treatment of EBV-driven B-cell malignancies, given the narrower range of cells that constitutively express this enzyme.

In summary, temporal proteomic profiling provided new insights into metabolic reprograming in EBV-mediated B-cell growth transformation and highlighted mitochondrial 1C induction as a key oncogenic event. Our findings underscore mitochondrial 1C metabolism as a critical source of 1C units for purine and thymidylate syntheses, as a means of producing reducing power in the form of NADPH and as a pathway for generating glycine for glutathione synthesis.

Chapter IV: EBV upregulates mevalonate metabolism to support protein geranylgeranylation and LMP trafficking

Contributions

Analysis of the proteomic dataset to identify enriched pathways and processes were jointly performed by Luis Nobre and Dr. Michael P. Weekes, as well as Liang Wei Wang and Dr. Benjamin E. Gewurz. The dataset used in this chapter was originally generated by Ina Ersing, Dr. Benjamin Gewurz, Luis Nobre and Dr. Michael P. Weekes. Zhonghao Wang in the laboratory of Dr. Benjamin E. Gewurz assisted in the acquisition of images from cells stained for LMPs and RAB13 and immunoblot experiments. Stephen Trudeau in the laboratory of Dr. Benjamin E. Gewurz assisted in the running of immunoblot samples. Dr. Bo Zhao provided the ChIP-seq datasets for the EBNA2HT cell line.

This work was supported by R01 AI137337, a Burroughs Wellcome Career Award in Medical Sciences and an American Cancer Society Research Scholar award to Dr. Benjamin E. Gewurz, a Wellcome Senior Clinical Research Fellowship (108070/Z/15/Z) to Dr. Michael P. Weekes and a Singapore Agency for Science, Technology and Research (A*STAR) pre-doctoral fellowship to Liang Wei Wang.

This work has been submitted for publication with the following citation:

Liang Wei Wang*, Zhonghao Wang*, Ina Ersing, Luis Nobre, Stephen Trudeau, Bo Zhao, Michael P. Weekes and Benjamin E. Gewurz. Epstein-Barr Virus Subverts Mevalonate and Fatty Acid Pathways to Promote Infected B-Cell Proliferation and Survival. *PLoS Pathogens* (under 1st round review). (* denotes co-first author)

Abstract

Epstein-Barr virus (EBV) causes infectious mononucleosis and is associated with multiple human malignancies. EBV drives newly infected B-cell proliferation, which contributes to B-cell compartment colonization and to the pathogenesis of multiple B-cell cancers. Yet, knowledge of how EBV subverts host biosynthetic pathways to remodel newly infected B-cells remains

incomplete. Using a recently constructed proteomic dataset of EBV-driven primary human B-cell transformation, we identified the cholesterol and fatty acid biosynthetic pathways to be highly enriched amongst EBV-induced metabolic enzymes. Epstein-Barr nuclear antigen 2, sterol response element binding factors and MYC were found to be key inducers of expression of cholesterol and fatty acid pathway rate-limiting enzymes. Unexpectedly, chemical epistasis experiments revealed a key mevalonate pathway role in the production of geranylgeranyl pyrophosphate (GGPP) rather than cholesterol in support of B-cell outgrowth. Chemical and CRISPR genetic analysis identified key GGPP roles in Rab protein activation. RAB13, a small G protein frequently upregulated in cancer, was found to be highly EBV induced in an EBNA3C-dependent manner. RAB13 colocalized with EBV latent membrane proteins 1 (LMP1) and 2A (LMP2A) and had key roles in LMP1/2A trafficking and target gene activation. Collectively, these studies identify EBV subversion of key metabolic pathways in support of transforming B-cell outgrowth and highlight multiple potential therapeutic targets.

Introduction

The gammaherpesvirus Epstein-Barr virus (EBV) causes infectious mononucleosis (IM) and is associated with multiple B-cell and epithelial malignancies (Longnecker, 2013). EBV is a major source of B-cell lymphoproliferative disease in immunosuppressed hosts, including following organ transplantation, with human immunodeficiency virus co-infection, with immunosenescence of aging or in the setting of primary immunodeficiency (Shannon-Lowe, Rickinson and Bell, 2017; LaCasce, 2006; Green and Michaels, 2013). EBV causes endemic Burkitt's lymphoma (BL), the most common pediatric lymphoma in sub-Saharan Africa (Makata *et al.*, 1996; Daniel, 1990) and is strongly associated with a subset of Hodgkin's lymphoma (Longnecker, 2013; Hammerschmidt and Sugden, 2004). While much has been learned about viral factors necessary for oncogenic transformation, knowledge of how EBV manipulates host metabolic pathways, a hallmark of cancer (Hanahan and Weinberg, 2011), remains incomplete.

In primary infection, EBV translocates across the tonsillar epithelial barrier to reach the B-cell compartment, which is the reservoir for lifelong infection. Whereas epithelial cell infection typically results in production of infectious virions by the viral lytic cycle, EBV frequently establishes latency in newly infected B-cells. Early in the course of IM, considerable numbers of latently infected B-cells can be detected in peripheral blood (Robinson, Smith and Niederman, 1981), although innate and adaptive immune responses subsequently limit the outgrowth of cells that express viral transforming proteins (Taylor *et al.*, 2015; Munz, 2016).

EBV uses a series of latency programs to expand the infected cell reservoir and to reach the memory B-cell compartment, the site of long-term latency (Longnecker, 2013; Thorley-Lawson, 2015). In vitro, EBV has the remarkable ability to convert resting primary B-cells into immortalized lymphoblastoid cell lines (LCLs). Reverse genetics have identified Epstein-Barr nuclear antigens (EBNAs) and latent membrane protein (LMPs) necessary for B-cell transformation in vitro (Kang and Kieff, 2015), but much remains to be learned about how these factors achieve B-cell growth transformation. Importantly, the transition from B-cell quiescence to rapid proliferation requires major metabolic pathway remodeling, only some of which are presently understood.

EBV B-cell growth transformation takes place over at least three phases in vitro (Nikitin *et al.*, 2010). Over the first 72 hours of infection, the EBV-encoded transcription factors EBNA2 and EBNA-leader protein (EBNA-LP) are highly expressed as EBV converts quiescent B-lymphocytes into activated blasts. EBNA2 uses RBP-Jκ and other B-cell transcription factors to reach host and viral genome sites. EBNA2 highly upregulates the proto-oncogene MYC (Kaiser *et al.*, 1999; Zhao *et al.*, 2006; Zhao *et al.*, 2011b), which together with its binding partner MAX can strongly influence metabolic remodeling (Stine *et al.*, 2015). However, key EBNA2, EBNA-LP and MYC target genes important for primary B-cell remodeling and activation remain to be defined in this early period post-infection.

Over days 3 to 7 post-infection, viral oncogenes together with their host targets drive rapid BL-like cell proliferation, with mitoses occurring as frequently as every 8-12 hours (Nikitin *et al.*, 2010). EBNA2 upregulates EBNA3A, EBNA3B and EBNA3C, all of which use host transcription factors to target key host and viral genome sites (Marshall and Sample, 1995; Robertson *et al.*, 1995; Wang *et al.*, 2015; Schmidt *et al.*, 2015; Jiang *et al.*, 2017; Jiang *et al.*, 2014). EBV upregulates glycolysis, oxidative phosphorylation and the mitochondrial one-carbon pathway (McFadden *et al.*, 2016; Wang *et al.*, 2019), though knowledge of EBV-mediated metabolic pathway remodeling in support of hyperproliferation remains incomplete. EBV-driven increases in uptake of amino acids over this time period may likely also activate the nutrient sensing mammalian target of rapamycin (mTOR) pathway (Sabatini, 2017; Wang *et al.*, 2019). By day 7 post-infection, mitosis slows to once daily as transforming cells increase latent membrane oncoproteins (LMP) 1 and 2A expression and remodel to lymphoblastoid-like physiology (Nikitin *et al.*, 2010; McFadden *et al.*, 2016; Price *et al.*, 2012; Price, Messinger and Luftig, 2018). LMP1 and LMP2A mimic CD40 and B-cell receptor signaling, respectively, to activate NF-κB and PI3K/AKT/mTOR pathways, respectively (Wang, Jiang and Gewurz, 2017; Kieser and Sterz, 2015; Cen and Longnecker, 2015; Mancao and Hammerschmidt, 2007).

Recently, we used multiplexed tandem mass tag mass spectrometry to gain insights into EBV-driven metabolic pathway remodeling. We constructed a temporal proteomic map of EBV-driven primary human B-cell outgrowth by performing whole cell and plasma membrane proteomic profiling on primary human B-cells at rest and at nine timepoints following infection by the B95-8 EBV strain (Wang *et al.*, 2019). Our analysis was performed in biological triplicate using primary B-cells from four human donors. We and others (McFadden *et al.*, 2016; Price *et al.*, 2012; Wang *et al.*, 2019) identified that EBV highly induces glucose uptake and aerobic glycolysis in newly infected B-cells. Although glycolysis generates less ATP per metabolized glucose, it together with downstream pathways such as the TCA cycle produce intermediates

for anabolic biosynthetic reactions needed to remodel quiescent B-lymphocytes into activated lymphoblasts. Remodeling and rapid cell growth place huge demands on cholesterol and lipid syntheses, which are crucial for membrane biogenesis.

Here, we identify that EBV highly induces the mevalonate pathway, which uses glucose-derived acetyl-CoA and NADPH to produce sterols, isoprenoids, cholesterol and fatty acids in newly infected B-cells. We investigate how EBV and host transcription factors activate these key anabolic pathways and identify key downstream roles in EBV-driven B-cell proliferation and survival.

Materials and Methods

Culture of established cell lines

293T were purchased from American Type Culture Collection (ATCC) and cultured in DMEM with 10% fetal calf serum (FCS, Gibco). GM12878 lymphoblastoid cells were obtained from Coriell. GM12878 Cas9+ cell lines were previously described (Ma *et al.*, 2017c). The 2-2-3 EBNA2HT LCL with conditional EBNA2 allele was a kind gift from Bo Zhao and Elliott Kieff (Brigham & Women's Hospital, Harvard Medical School). 2-2-3 LCLs express EBNA2 fused to a modified estrogen receptor 4HT-binding domain. In the presence of 4HT, the EBNA2HT allele localizes to the nucleus and is active, but upon 4HT withdrawal is redistributed to the cytosol where it is destabilized. 2-2-3 LCLs were maintained in the presence of 1 μM 4-hydroxytamoxifen (4HT). To remove 4HT, cells were washed five times with 4HT-free media, including two incubations for 30 minutes, and then re-seeded at 100,000 cells per mL in media with or without 4HT, as indicated. Cells were then grown for 48 hours and harvested for RNA extraction and cell lysate preparation. The C19 EBNA3CHT (Maruo *et al.*, 2006) was a kind gift from Bo Zhao and Elliott Kieff. It was maintained in the presence of 4HT. To remove 4HT, cells were grown in 4HT-free media for three days, washed five times as described above, and re-seeded at 100,000 cells per mL. Cells were then expanded for 14 days before harvesting for

RNA extraction and cell lysate preparation. The conditional P493-6 LCL was a kind gift from Micah Luftig (Duke University). P493-6 cells have a conditional EBNA2HT allele similar to 2-2-3 LCLs, and also have a TET-Off exogenous *MYC* allele. In the absence of tetracyclines, high level exogenous *MYC* is induced. P493-6 cells were maintained continuously in the absence of 4HT or doxycycline to induce a BL-like state of high MYC expression. To grow in the lymphoblastoid cell state (intermediate MYC), P493-6 cells were grown in the presence of both 4HT and doxycycline. To induce a low MYC state and consequently G1 growth arrest, cells were grown in the absence of 4HT and presence of 1 μM doxycycline. After 48 hours of growth in any of these conditions, cells were collected for lysate preparation. For selection, 200 μg/mL hygromycin (Calbiochem) or 3 μg/ml puromycin (Invitrogen) was used. B95-8 cells and P3HR1 cells with conditional ZTA-HT alleles responsive to 4HT were kind gifts from Eric Johannsen and Elliott Kieff. All cells were cultured in RPMI-1640 (Invitrogen) supplemented with 10% standard FBS and penicillin-streptomycin in a humidified incubator at 37˚C and at 5% CO_2. All cells were routinely confirmed to be mycoplasma-negative by MycoAlert assay (Lonza).

Primary human B-cell isolation and culture

Platelet-depleted venous blood obtained from the Dana-Farber Cancer Institute blood bank were used for primary human B-cell isolation, following our Institutional Review Board-approved protocol for discarded and de-identified samples. RosetteSep and EasySep negative isolation kits (STEMCELL Technologies) were used sequentially to isolate CD19+ B-cells with the following modifications made to the manufacturer's protocols. For RosetteSep, 40 μL of antibody cocktail was added per mL of blood and then layered onto Lymphoprep density medium for centrifugation. For EasySep, 10 μL of antibody cocktail was added per mL of B-cells, followed by 15 μL of magnetic bead suspension per mL of B-cells. After negative selection, the cells obtained were routinely ≥95% positive for CD19, a nearly pan-B-cell surface marker (though not strongly expressed on plasma cells). For most experiments, cells were

cultured in RPMI-1640 (Invitrogen) supplemented with 10% standard FBS and penicillin-streptomycin. Cells were cultured in a humidified incubator at 37˚C and at 5% CO_2.

EBV infection of primary B-cells

EBV B95-8 virus was produced from B95-8 cells with conditional ZTA expression and purified by filtration through a 0.45 µm filter (Calderwood, Holthaus and Johannsen, 2008; Johannsen *et al.*, 2004). EBV titer was determined experimentally by transformation assay. The P3HR-1 EBV strain was produced from P3HR-1 cells with conditional ZHT expression (Ersing *et al.*, 2017; Calderwood, Holthaus and Johannsen, 2008). Genomic DNA content of preparations of this non-transforming virus were quantitated by PCR for *BALF5* on total DNA extracted, and cross-compared with levels from B95-8 virus preparations. The plasmid pHAGE-BALF5 was used for generation of standard curves of EBV genome copy number. Calculated genome copy numbers were used to normalize B95-8 and P3HR-1 input DNA amounts. UV irradiation of B95-8 virus supernatants was performed at a cumulative intensity of 3J per square centimeter on ice, to prevent heat-induced virus degradation. EBV was added to purified B-cells at an MOI of 0.1 (250 µL of supernatant from ZHT cells 5 days after ZHT stimulation, with washout of 4HT after 24 hours, per million purified B-cells). We also ensured equal infection by performing quantitative PCR on intracellular DNA extracted from cells and by anti-EBNA1 (OT1x) immunofluorescence microscopy at 24 hours post-infection following at least five washes. Cells were cultured in a humidified chamber at 37˚C in RPMI/10% FCS. For most experiments, virus-containing media was replaced with virus-free media for subsequent experimentation two days post-infection.

Antibodies and reagents

Antibodies against the following proteins were used in this study: ACC1 (Proteintech, Cat#21923-1-AP), HMGCR (Proteintech, Cat#13533-1-AP), SCAP (Proteintech, Cat#12266-1-AP), DDX1 (Bethyl, Cat#A300-521A), DDX46 (Proteintech, Cat#16927-1-AP), MYC (Santa

Cruz, Cat#764), EBNA2 (mouse monoclonal antibody clone PE2, kindly provided by Dr Jeffrey Cohen) , EBNA3C (Abcam, Cat#16128), RABGGTA (Proteintech, Cat#14448-1-AP), RABGGTB (Bethyl, A304-323A), RAB13 (Santa Cruz, Cat#517224), phospho-mTOR (Ser2448) (Cell Signaling, Cat#2971), TRAF1 (Cell Signaling, Cat#4715), GAPDH (Abcam, Cat#8245), α-tubulin (Abcam, Cat#7291), horse anti-mouse IgG HRP-linked antibody (Cell Signaling, Cat#7076), goat anti-rabbit IgG HRP-linked antibody (Cell Signaling, Cat#7074), goat anti-rat IgG HRP-linked antibody (Cell Signaling, Cat#7077), Alexa Fluor 488 goat anti-mouse (ThermoFisher, Cat#A-11029), Alexa Fluor 594 goat anti-rabbit (ThermoFisher, Cat#NC0414256), Alexa Fluor 647 goat anti-rat (ThermoFisher, Cat#A-21247), LMP1 (Abcam, Cat#136633), LMP2A (rat monoclonal antibody clone 4E11, kindly provided by Prof Richard Longnecker).

The following chemicals were obtained from Sigma-Aldrich: fatostatin hydrobromide (Cat#F8932), simvastatin (Cat#S6196), atorvastatin calcium salt trihydrate (Cat#PZ0001), geranylgeranyl pyrophosphate (GGPP) (Cat#G6025), squalene (Cat#S3626), GGTI-2133 (Cat#G5294), BMS-214662 hydrochloride (Cat#BM0008), doxycycline hyclate (Cat#D9891), (Z)-4-hydroxytamoxifen (Cat#H7904) and 2-bromopalmitate (Cat#238422). Etomoxir (Cat#4539), G28UCM (Cat#5446) were obtained from Tocris. Triacsin C (Cat#200574) was purchased from Santa Cruz. TOFA (Cat#BML-EI321-0010) was obtained from Enzo Life Sciences. Hoechst 33258 (Cat#H21491) and propidium iodide (Cat#P3566) were obtained from ThermoFisher Scientific.

Immunoblot analysis for RAB13

Cells were lysed in a modified TNE buffer (50 mM Tris-HCl pH 7.5, 150 mM NaCl, 1 mM EDTA, 0.5% NP-40, 0.5% sodium deoxycholate, 0.1% SDS) supplemented with protease inhibitor cocktail (Roche cOmplete Mini EDTA-free Protease Inhibitor Cocktail, Cat# 4693159001), 2 mM sodium pyrophosphate, 10 mM β-glycerophosphate and 1 mM PMSF on ice for 15 minutes. The crude cell lysate was then sonicated on ice for 5 minutes using a probe sonicator at the

maximum setting and centrifuged at 17,000 x g for 15 minutes. The supernatant was mixed with 5X Laemmli loading buffer and boiled for 10 minutes. Samples were loaded onto and electrophoretically resolved on 12% or 4-20% gradient gels and transferred onto nitrocellulose membranes for 45 minutes at 100 V at 4˚C. Membranes were probed with primary antibodies, typically at a 1:1000 dilution overnight at 4˚C and with HRP-conjugated secondary antibodies in 5% skim milk/PBST for 1 hour. Blots were imaged on Carestream or Li-Cor workstations.

Flow cytometry

Cells were washed once with cold PBS supplemented with 0.5% bovine serum albumin (BSA). Cells were then incubated with a 1:100 dilution of fluorophore-conjugated primary antibody (and, if applicable, a 1:500 dilution of fluorophore-conjugated secondary antibody) in PBS with 0.5% BSA for 1 hour. Cells were pelleted and resuspended in 400 µL of PBS, strained into flow cytometry-compatible tubes and processed immediately. Sample processing was performed either immediately or within 24 hours after staining. Flow cytometric data was acquired with a BD FACSCalibur instrument and analysis was performed with FlowJo.

Immunofluorescence

Cells were seeded on glass slide and fixed with 4% PFA solution for 10 minutes. Fixed cells were permeabilized with 0.5% Triton X-100/PBS solution and blocked with 20% newborn goat serum (NGS). Subsequently, cells were incubated with a cocktail of primary antibodies against LMPs and RAB13 for an hour and then a cocktail of secondary antibodies for an additional half hour. Finally, cells were incubated with a solution of Hoechst 33258 (10 µg/mL) for 10 minutes to stain nuclear DNA and dehydrated sequentially from 70% to 90% to 100% ethanol. ProLong anti-fade was applied to the slide and sealed with a No. 1.5 coverslip. Image acquisition was performed at the Brigham and Women's Hospital core facility with the Zeiss LSM 800 instrument. Image analysis was performed with the Zeiss ZEN Lite (Blue) software. For measurements of cell diameter, differential interference contrast (DIC) microscopy was

performed and cells were picked out by eye from the micrographs. Circular ROIs were drawn around the cells and diameters were automatically computed by the ZEN Lite (Blue) software.

Growth curve analysis

Newly infected primary human B-cells were seeded at 500,000 per well in a volume of 1 mL and grown for two days before measurements of cell densities were made. For GM12878 lymphoblastoid cells, 100,000 cells were seeded per well in a volume of 1mL and grown for two days prior to measurements of cell densities. For cell density measurements, cells were pelleted and resuspended in the same volume of media and counted with the TC20 automatic cell counter (Bio-Rad). After measurements had been taken, cells were passaged accordingly to give 100,000 cells per mL and grown for two more days. The same procedure was repeated to obtain measurements at subsequent timepoints. At each time point, after passaging, cells were treated with the appropriate inhibitor and/or rescue metabolite(s) at the indicated concentrations. Growth was then calculated using the initial seeding density for normalization.

CRISPR editing in GM12878 LCL

Single guide RNA (sgRNA) constructs were generated as previously described (Jiang *et al.*, 2018) using sgRNA sequences from the Broad Institute Avana or Brunello sgRNA libraries (Doench *et al.*, 2016; Shalem *et al.*, 2014). Sequences used to construct the sgRNA-encoding plasmids are as follows:

Gene & sgRNA Identifier	**sgRNA Sequence (5' to 3')**
SCAP #1	GGGCGAGTAATCCTTCACAG
SCAP #2	CTGCTGGACATAAGCCACCG
MYC #1	GGTAGGGGAAGACCACCGAG
MYC #2	GTATTTCTACTGCGACGAGG
PGGT1B #1	CCTCCCATCTTCCAGCTGAA
PGGT1B #2	CTAAATCGCTGTGGTTTCCG
RABGGTA #1	GCTGCAGGACTCACTAAGAG
RABGGTA #2	GCTGCTGGAGCACCTCTCGT
RABGGTB #1	CTAAGAGTGTATAAAAGATG
RABGGTB #2	CTGACAGTAATGGATCTCAT

RAB13 #1	TCCGCACTGTGGATATAGAG
RAB13 #2	CTGGATGAAAAGCATCAAGG

Note that Avana sgRNA designations are specific to the library used by Ma et al. (2017c) and are not the same as the sgRNA designations used elsewhere in this chapter. LCL CRISPR editing was performed as previously described (Jiang *et al.*, 2018). Briefly, lentiviruses encoding sgRNAs were generated by transient transfection of 293T cells with packaging plasmids and pLentiGuide-Puro plasmids. GM12878 cells stably expressing Cas9 were transduced with the lentiviruses and selected with 3 μg/mL puromycin for three days before replacement with antibiotic-free media. For rescue experiments or cDNA overexpression, 293T cells were transiently transfected to produce lentiviruses that carry the rescue/overexpression cDNA and a hygromycin resistance marker. GM12878 cells were transduced with rescue lentiviruses and selected with 200 μg/mL hygromycin for at least one week before transduction with sgRNA-encoding lentiviruses. CRISPR editing and rescue cDNA expression were confirmed by immunoblotting. To construct the rescue RAB13 ($RAB13^R$) vector, we made use of the Genscript GenParts synthesis service to synthesize a cDNA fragment containing wild-type RAB13 with cytosine 141 mutated to thymidine (C141T) and guanosine 162 mutated to thymidine (G162T) and incorporating flanking attB1 and attB2 sites. Engineering the C141T and G162T mutations at the PAM sites confers resistance to Cas9-mediated cutting by sgRNA #1 and sgRNA #2, respectively. We also introduced a stop codon at the end of the coding sequence. We performed BP cloning of the gene fragment into a donor vector, pDONR223. The resultant entry vector, pDONR223-$RAB13^R$, was used for LR cloning with pLX_TRC313, a destination vector which carries a hygromycin resistance marker. Because pLX_TRC313 normally has a C-terminal V5 epitope tag sequence which could interfere with RAB13 function, the engineered cDNA fragment used for BP cloning contained a stop codon at the end of the coding sequence but upstream of the 3' attB sequence.

Quantitative PCR

Reverse transcription-quantitative PCR analysis of mRNA abundance was performed on a BioRad CFX Connect Real-time PCR detection system, using Power SYBR Green RNA-to-CT 1-Step Kit (Applied Biosystems) for 40 cycles. Expression values relative to 18S rRNA or GAPDH expression were calculated using CFX Manager Software. Quantitative PCR of viral genome copies utilized host cell GAPDH gene copy number as control. Primer sequences can be found as follows:

Gene & Primer Orientation	**Primer Sequence (5' to 3')**
SCD Forward	GTTCTACACCTGGCTTTGGG
SCD Reverse	GCAGCCGAGCTTTGTAAGAG
ACLY Forward	GGTGCTCCGGATTTTGC
ACLY Reverse	ACATGGCTGCAGAGAGACCT
HMGCR Forward	TCGGTGGCCTCTAGTGAGAT
HMGCR Reverse	TGTCCCCACTATGACTTCCC
TRAF1 Forward	CTATAAGCCCAGGAAGCCG
TRAF1 Reverse	CTTCCCTTGAAGGAGCAGC
18S rRNA Forward	CGGCTACCACATCCAAGGAA
18S rRNA Reverse	GCTGGAATTACCGCGGCT
BALF5 Forward	GAGCGATCTTGGCAATCTCT
BALF5 Reverse	TGGTCATGGATCTGCTAAACC
GAPDH Forward	ACTTCAACAGCGACACCCACTC
GAPDH Reverse	TCTCTTCCTCTTGTGCTCTTGCT

Bioinformatic analysis

Pathway Analysis was performed using the Database for Annotation, Visualization and Integrated Discovery (DAVID) (Huang da, Sherman and Lempicki, 2009) version 6.8 with default settings. A given cluster was always searched against a background of all proteins quantified within the relevant experiment. Proteins were included in this analysis if they were (1) contained in the metabolism gene list published by Birsoy and colleagues (Birsoy *et al.*, 2015) and (2) quantified in all three experiments. The cluster that demonstrated >2-fold upregulation at 4 days post-infection with a p-value cut-off of 0.075 was searched against the full list to determine enriched terms. The mass spectrometry proteomics data used for this paper have been deposited to the

ProteomeXchange Consortium (http://www.proteomexchange.org/) via the PRIDE partner repository and can be retrieved with the dataset identifier PXD013034.

Results

EBV strongly induces cholesterol and fatty acid syntheses in newly infected B-cells

EBV infection causes dramatic B-cell remodeling that begins early after infection and converts resting B-cells into activated lymphoblasts. To gain insights into metabolic pathways highly upregulated upon EBV infection, metabolic pathway enrichment analysis was performed on our recently generated multiplexed tandem mass tag proteomic analysis of newly EBV infected primary human B-cells (Wang *et al.*, 2019). Using a curated list of human metabolism-associated proteins (Birsoy *et al.*, 2015) (Tables S3, S4), the cholesterol biosynthesis pathway was found to be the most highly upregulated host biosynthetic pathway at four days post infection (4 DPI) versus resting B-cell baseline levels (Figure IV.1A). Notably, the enzyme 3-hydroxy-3-methylglutaryl-CoA (HMG-CoA) synthetase 1 (HMGCS1), which condenses acetoacetyl-CoA and acetyl-CoA to produce HMG-CoA, and the rate-limiting pathway enzyme HMG-CoA reductase (HMGCR) (Goldstein and Brown, 1990) were strongly upregulated by 2 DPI (Figure IV.1B). EBV infection similarly induced eight enzymes that convert mevalonate and into cholesterol (Figure IV.1B). EBV induction of HMGCR was validated by immunoblotting of whole cell extracts from resting versus EBV-infected primary B-cells, where again a spike in its expression was evident at 2 to 4 DPI, as EBV induces B-cell remodeling and the onset of BL-like hyperproliferation (Figure IV.1C). Upregulation at this timepoint, prior to the onset of newly infected cell proliferation, is consistent with an important role in EBV-induced B-cell remodeling.

Figure IV.1 Cholesterol and lipid biosyntheses are highly upregulated early in infection. (A) Pathway enrichment analysis of proteins whose abundance was at least 2-fold upregulated by EBV infection at 4 DPI versus resting B-cell levels and with $p<0.075$ across three biological replicates in our proteomic analysis (Wang *et al.*, 2019). Only proteins with annotated metabolic function identified in a recent curated dataset (Birsoy *et al.*, 2015) were used for bioinformatic analysis. (B) Heatmap representation of cholesterol and de novo lipid biosynthesis pathway enzyme relative abundance at the indicated DPI of primary human B-cell infection by EBV. (C) Immunoblot analysis of HMGCR, ACC1, FASN and load-control DDX1 levels in whole cell lysate (WCL) prepared from primary B-cells infected by EBV for the indicated days. Representative blots (n=3) are shown. L. Nobre and M.P. Weekes performed the bioinformatic analysis. S. Trudeau electrophoretically processed lysates generated by I. Ersing.

Figure IV.1 (Continued)

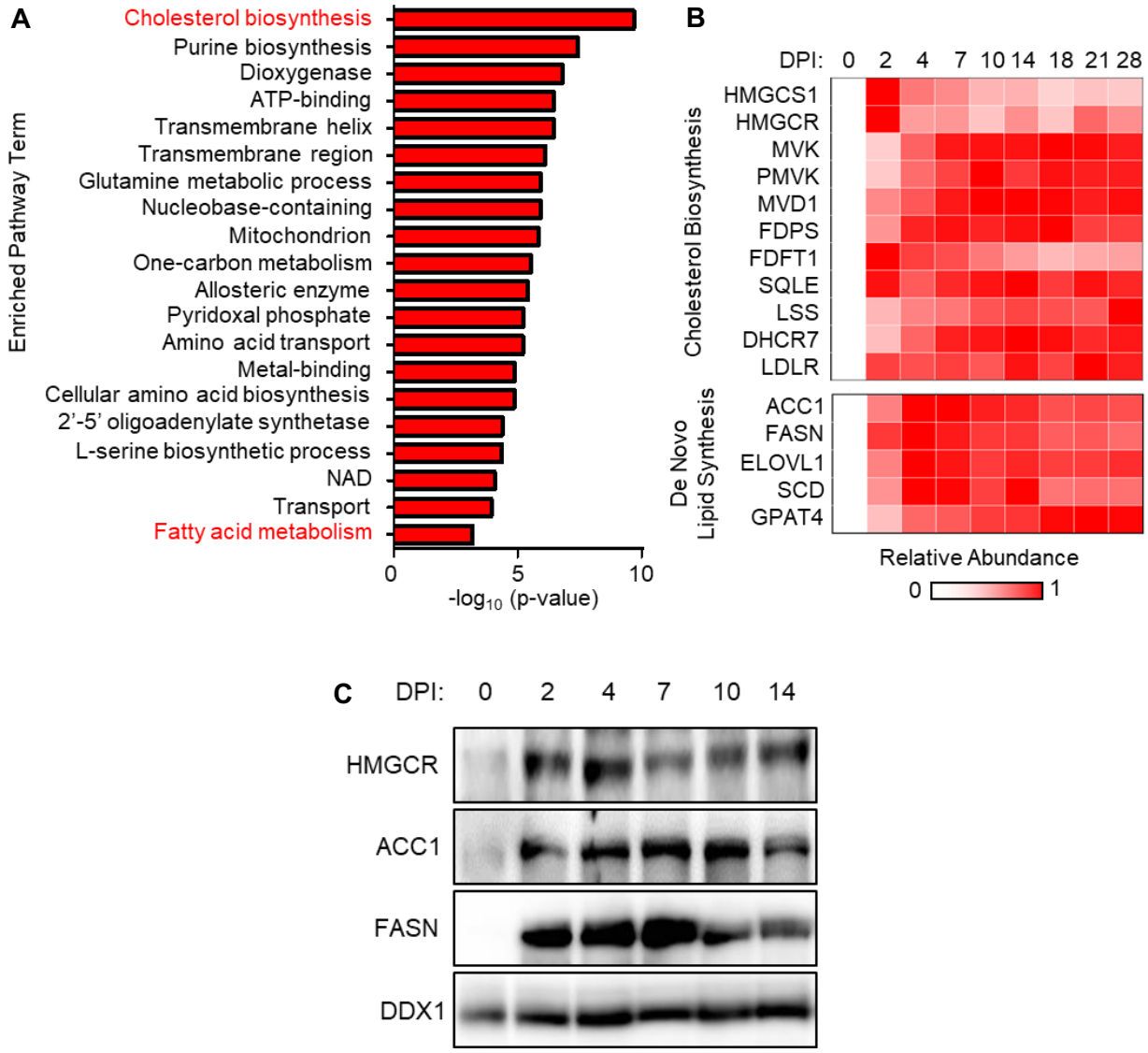

In further support of an important cholesterol role in newly infected cell remodeling, LCLs abundantly express the plasma membrane low-density lipoprotein receptor (LDLR) (Valente, Morris and Walton, 1980; Crumpton *et al.*, 1983; Arvey *et al.*, 2012), which mediates endocytosis of cholesterol-rich LDL. We found that EBV rapidly upregulated whole cell and plasma membrane LDLR levels in newly infected primary B-cell infection (Figures IV.1B, IV.2). Sustained expression of cholesterol biosynthetic enzymes and LDLR is suggestive of an ongoing role in the lymphoblastoid phase.

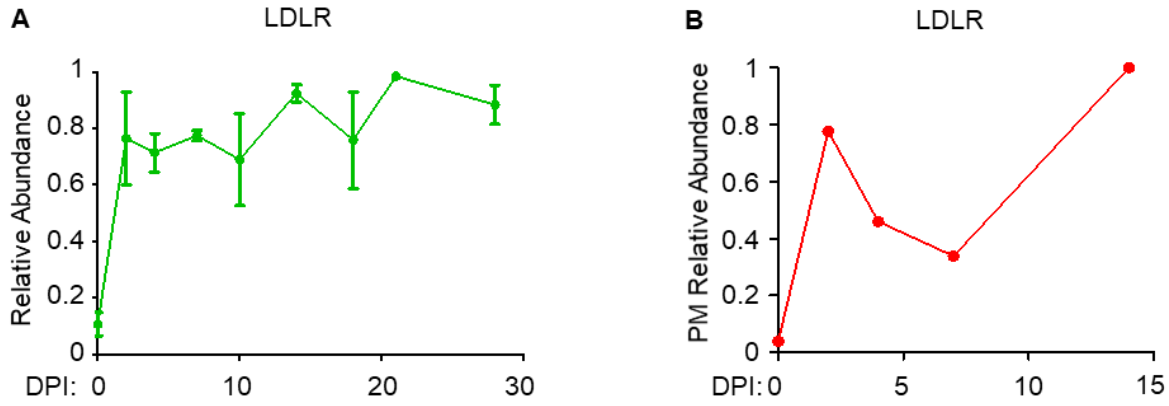

Figure IV.2 EBV induces LDLR expression in newly infected cells. (A) Temporal proteomic traces of LDL receptor (LDLR) relative abundances at the indicated DPI of primary human B-cell EBV infection. Data show the mean + SEM of n=3 biological replicates. (B) Temporal proteomic traces of plasma membrane (PM) LDLR relative abundances at the indicated DPI of primary human B-cell EBV infection.

Further underscoring key host lipid metabolism roles in early EBV-driven B-cell growth transformation, enrichment analysis also highlighted fatty acid metabolism as highly EBV-induced (Figures IV.1B-C). EBV upregulated the rate-limiting fatty acid biosynthesis pathway enzyme acetyl-CoA carboxylase 1 (ACC1), which converts acetyl-CoA into malonyl-CoA. EBV similarly induced the subsequent pathway enzyme fatty acid synthase (FASN), which converts

malonyl-CoA to palmitate, an important substrate for palmitoylation, mitochondrial β-oxidation triglyceride and long-chain fatty acid production (Carta *et al.*, 2017) (Figure IV.3). ACC1 and FASN upregulation were validated by whole cell lysate immunoblot analysis in uninfected and at multiple timepoints of EBV infection (Figure IV.1C).

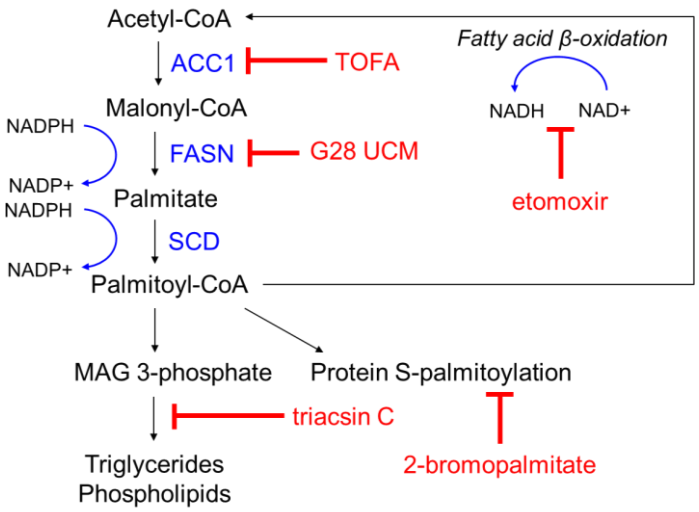

Figure IV.3 Schematic diagram showing de novo lipid synthesis pathway conversion of glucose-derived acetyl-CoA into end products. NADPH-dependent acetyl-CoA reduction produces palmitate, which can be directed to one of three routes: (a) oxidation via the fatty acid β-oxidation pathway to produce reducing power in the form of NADH and possibly be used to generate ATP via OXPHOS, (b) be used for post-translational palmitoylation of target protein cysteine residues; (c) be condensed with other molecules to produce triglycerides for energy storage and/or phospholipids for membrane biogenesis. Enzymes are indicated in blue, and chemical inhibitors used elsewhere in this figure are shown in red.

We next investigated fatty acid synthesis pathway functional roles in transforming B-cell outgrowth. Chemical blockade of ACC1 or FASN by the well-characterized antagonists TOFA

and G28UCM (Puig *et al.*, 2009; Puig *et al.*, 2011), respectively, diminished EBV-mediated B-cell outgrowth (Figure IV.4), suggesting an important palmitate role in newly infected B-cells.

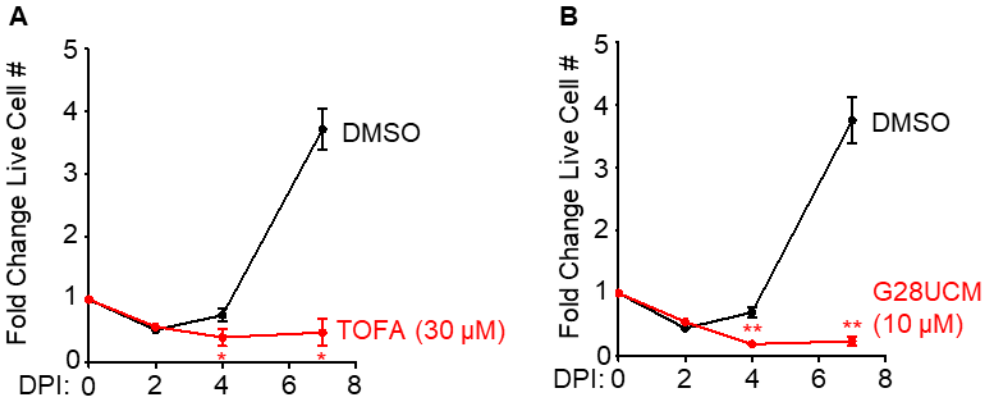

Figure IV.4 Inhibition of de novo lipid synthesis leads to proliferative defects in newly infected cells. (A) Growth curve analysis of newly infected primary human cells cultured in the presence of DMSO or the ACC1 chemical antagonist TOFA (30 μM). Shown are the mean + SEM relative fold change live cell numbers from n=5 biological replicates. *, $p<0.05$ (paired two-tailed t-test). (B) Growth curve analysis of newly infected primary human cells cultured in the presence of DMSO or the FASN chemical antagonist G28UCM (10 μM). Shown are the mean + SEM relative fold change live cell numbers from n=4 biological replicates. **, $p<0.01$ (paired two-tailed t-test).

Palmitate is a substrate for NADH production by β-oxidation, phospholipid and triglyceride syntheses and protein palmitoylation (Liu *et al.*, 2010). While inhibition of β-oxidation by the chemical antagonist etomoxir (Lopaschuk *et al.*, 1988) did not affect EBV-driven B-cell outgrowth, triacsin C blockade of phospholipid and triglyceride syntheses, and 2-bromopalmitate (2-BP) inhibition of protein palmitoylation (Pedro *et al.*, 2013; Davda *et al.*, 2013) did significantly diminish newly infected cell outgrowth (Figure IV.5).

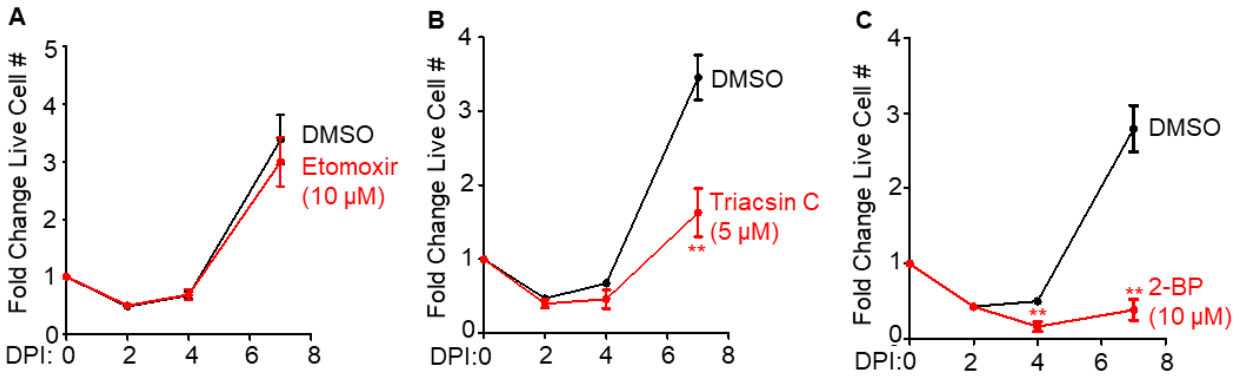

Figure IV.5 Newly infected B-cells depend on palmitate for triglyceride and phospholipid synthesis and protein palmitoylation. (A) Growth curve analysis of newly infected primary human cells cultured in the presence of DMSO or the antagonist etomoxir (10 μM), which blocks fatty acyl chain transport to the mitochondria for β-oxidation. Shown are the mean + SEM relative fold change live cell numbers from n=n biological replicates. No significant relationships were detected by paired two-tailed t-test. (B) Growth curve analysis of newly infected primary human cells cultured in the presence of DMSO or triacsin C (5 μM), which blocks the conversion of palmitate into triglycerides and phospholipids. Shown are the mean + SEM relative fold change live cell numbers from n=7 biological replicates. **, $p<0.01$ (paired two-tailed t-test). (C) Growth curve analysis of newly infected primary human cells cultured in the presence of DMSO or the protein palmitoylation inhibitor 2-bromopalmitate (2-BP) (10 μM). Shown are the mean + SEM relative fold change live cell numbers from n=4 biological replicates. **, $p<0.01$ (paired two-tailed t-test).

KEGG gene ontology analysis of predicted palmitoylation targets expressed in newly infected B-cells identified SNARE function and vesicular transport as the most enriched pathways (Figure IV.6).

Figure IV.6 KEGG analysis reveals SNARE function and vesicular transport as key palmitoylation-regulated processes in newly infected cells. (A) Heatmap representation of candidate palmitoylated target protein relative abundances in primary human B-cells infected by EBV for the indicated DPI. Palmitoylation candidates were previously identified in 293T cell proteomic analyses (Davda *et al.*, 2013). (B) KEGG pathway enrichment analysis of candidate palmitoylated target proteins that were induced by at least 2-fold by primary human B-cell infection.

Figure IV.6 (Continued)

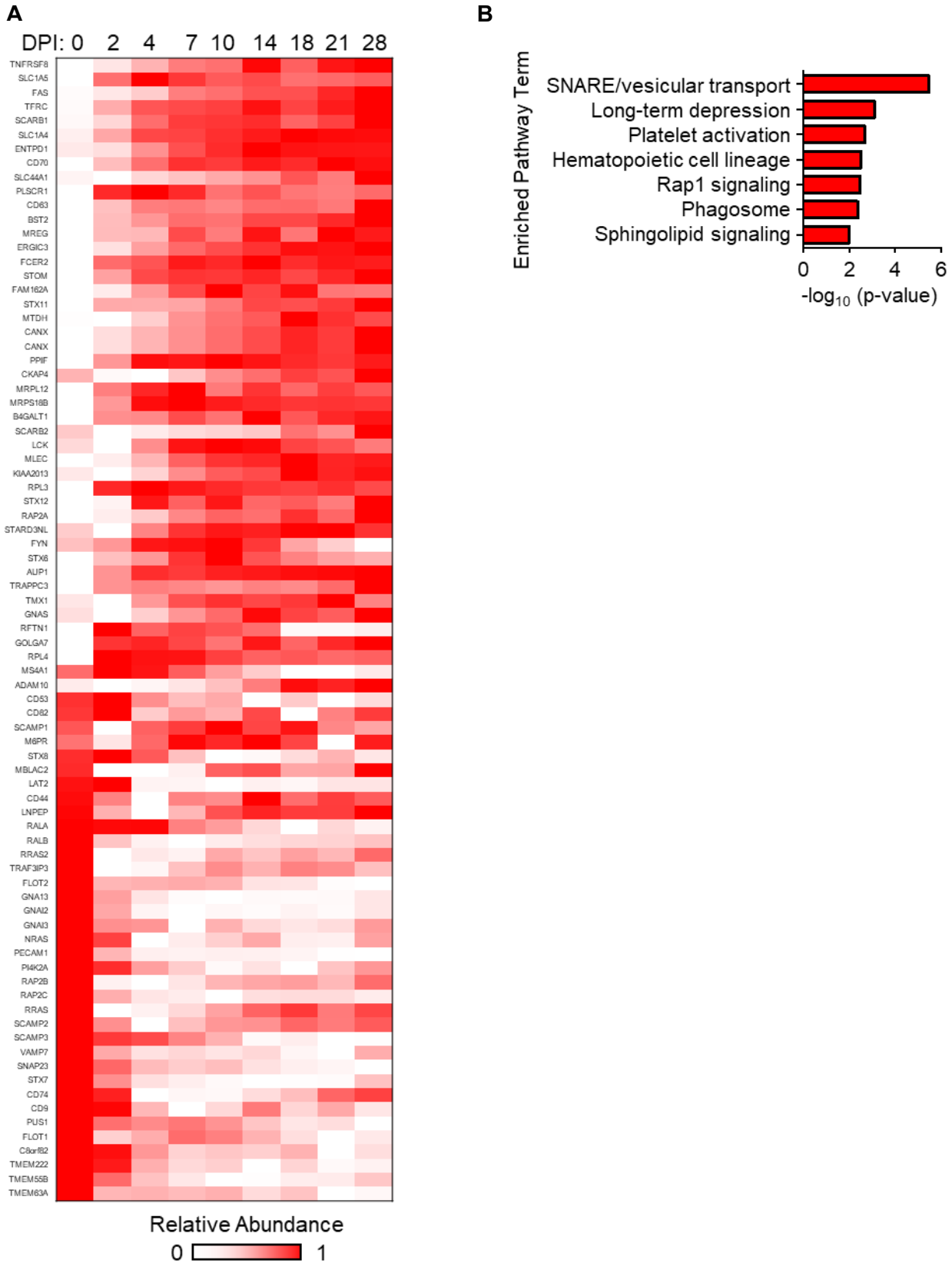

SREBPs, EBNA2 and MYC induce cholesterol and fatty acid biosynthesis enzymes

Sterol response element binding proteins (SREBPs) are basic-helix-loop-helix leucine zipper transcription factors that bind to SREs on DNA to induce expression of mevalonate and fatty acid pathway components (Foretz *et al.*, 1999; Amemiya-Kudo *et al.*, 2002; Shimano *et al.*, 1999). Since SREBPs are major inducers of cholesterol and lipid metabolism programs in many contexts (Zeller *et al.*, 2003; Lin *et al.*, 2012; Dang, 2013), we hypothesized that EBV may subvert SREBPs to transactivate cholesterol and lipid synthesis genes in newly infected B-cells. In support, SREBP2 abundance was upregulated by 2 DPI (Figure IV.7A), though curiously, SREBP1 was not detected by our proteomic analysis. LCL ChIP-seq identified EBNA2 occupancy of the *SREBP2* promoter (Figure IV.7B) (Davis *et al.*, 2018; Consortium, 2012).

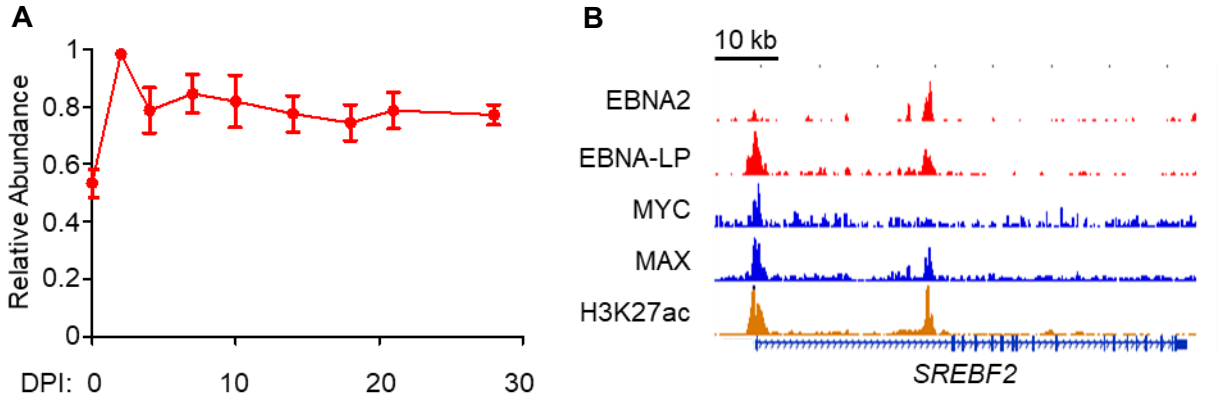

Figure IV.7 EBV upregulates SREBP2 expression in newly infected cells. (A) Temporal proteomic profile of SREBP2 abundance over the indicated DPI of primary human B-cells. Data show the mean + SEM from three biological replicates, n=3. (B) ChIP-seq tracks for the indicated transcription factors or H3K27Ac at the LCL *SREBF2* locus.

Notably, all four CRISPR single guide RNAs (sgRNAs) against *SREBF2* were strongly depleted in our recent 21-day Cas9+ GM12878 LCL Achilles' heel screen (Zhao *et al.*, 2011b) (Figure

IV.8A), suggesting an important SREBP2 role in LCL growth and/or survival. By contrast, sgRNAs targeting *SREBF1* were virtually unchanged over the 21-day screen (Figure IV.8B).

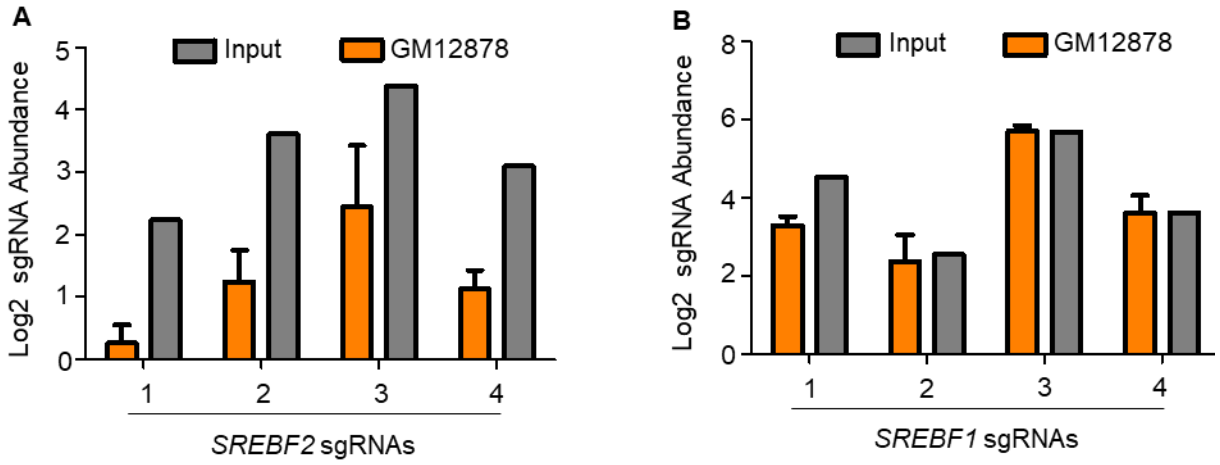

Figure IV.8 LCL growth and survival depends on SREBP2, not SREBP1. (A) Mean + SEM of input versus day 21 *SREBF2*-targeting sgRNA abundances from genome-scale CRISPR/Cas9 screen performed in quadruplicate in Cas9+ GM12878 LCLs (Ma *et al.*, 2017c). Each sgRNA targets an independent *SREBF2* exon regions. The y-axis value refers to the log2-transformed number of reads for each sgRNA normalized to the total number of reads. (B) Mean + SEM of input versus day 21 *SREBF1*-targeting sgRNA abundances from genome-scale CRISPR/Cas9 screen performed in quadruplicate in Cas9+ GM12878 LCLs (Ma *et al.*, 2017c). Each sgRNA targets an independent *SREBF1* exon regions. The y-axis value refers to the log2-transformed number of reads for each sgRNA normalized to the total number of reads.

SREBPs are also subject to tight post-translational regulation, though specific mechanisms operative in EBV-infected B-cells have not been studied. When cholesterol and lipid pools are sufficient, SREBP cleavage activating protein (SCAP) retains SREBPs at the endoplasmic reticulum (ER) by binding to the ER retention factor insulin-induced gene 1 (INSIG1) (Engelking *et al.*, 2004; Yang *et al.*, 2002). Upon depletion of cholesterol or lipid pools, SREBPs traffic to

the Golgi, where resident site-1 and site-2 proteases target SREBPs to liberate an N-terminal transcription factor fragment that traffics to the nucleus to regulate cognate genes (Kamisuki *et al.*, 2009) (Figure IV.9A).

To investigate potential SCAP roles in EBV-mediated SREBP activation, newly infected cells were treated with the small molecule antagonist fatostatin, which blocks SCAP ER to Golgi transport (Kamisuki *et al.*, 2009). Fatostatin treatment significantly impaired EBV-mediated primary B-cell outgrowth (Figure IV.9B) and downmodulated expression of two prototypic SREBP target genes, *ACLY and SCD* (Figure IV.9C).

To next test SCAP LCL roles and address potential concerns over potential off-target effects of fatostatin (Gholkar *et al.*, 2016; Shao, Machamer and Espenshade, 2016), control versus independent *SCAP*-targeting sgRNAs were expressed in Cas9+ GM12878 LCLs. SCAP depletion strongly downregulated LCL HMGCR and ACC1 expression and LCL proliferation (Figures IV.10A-B), suggesting shared SCAP roles in LCL SREBP-mediated target gene regulation. In further support of a role in LCL mevalonate pathway activation, GM12878 ChIP-seq also identified SREBP2 occupancy at the *HMGCR* promoter (Davis *et al.*, 2018; Consortium, 2012) (Figure IV.10C)

Figure IV.9 SREBP inhibition causes proliferative defects in newly infected B-cells. (A) Schematic showing SREBP regulation by sterol levels. Under sterol-sufficient conditions, SCAP binds to INSIG to promote SREBP ER retention. When sterol levels are insufficient, SCAP dissociates from INSIG and chaperones SREBPs to the Golgi apparatus, where site-1 and site-2 proteases (S1-P and S2-P, respectively) cleave SREBPs. Transcriptionally active N-terminal SREBP domains re-localize to the nucleus to transactivate cholesterogenic and lipogenic target genes. (B) Growth curve analysis of newly infected primary B-cells cultured in the presence of DMSO or the SREBP/SCAP inhibitor fatostatin (5 μM). Data show the mean + SEM fold change values relative to day 0, n=3. **, $p<0.01$; ***, $p<0.005$ (two-tailed t-test). (C) Quantitative RT-PCR analysis of SREBP target gene *SCD* and *ACLY* mRNA levels in 7 DPI newly infected B-cells which were cultured in the presence of DMSO versus fatostatin (5 μM) for 5 days. Data show the mean + SEM, n=3. *, $p<0.05$ (one-sample t-test).

Figure IV.9 (Continued)

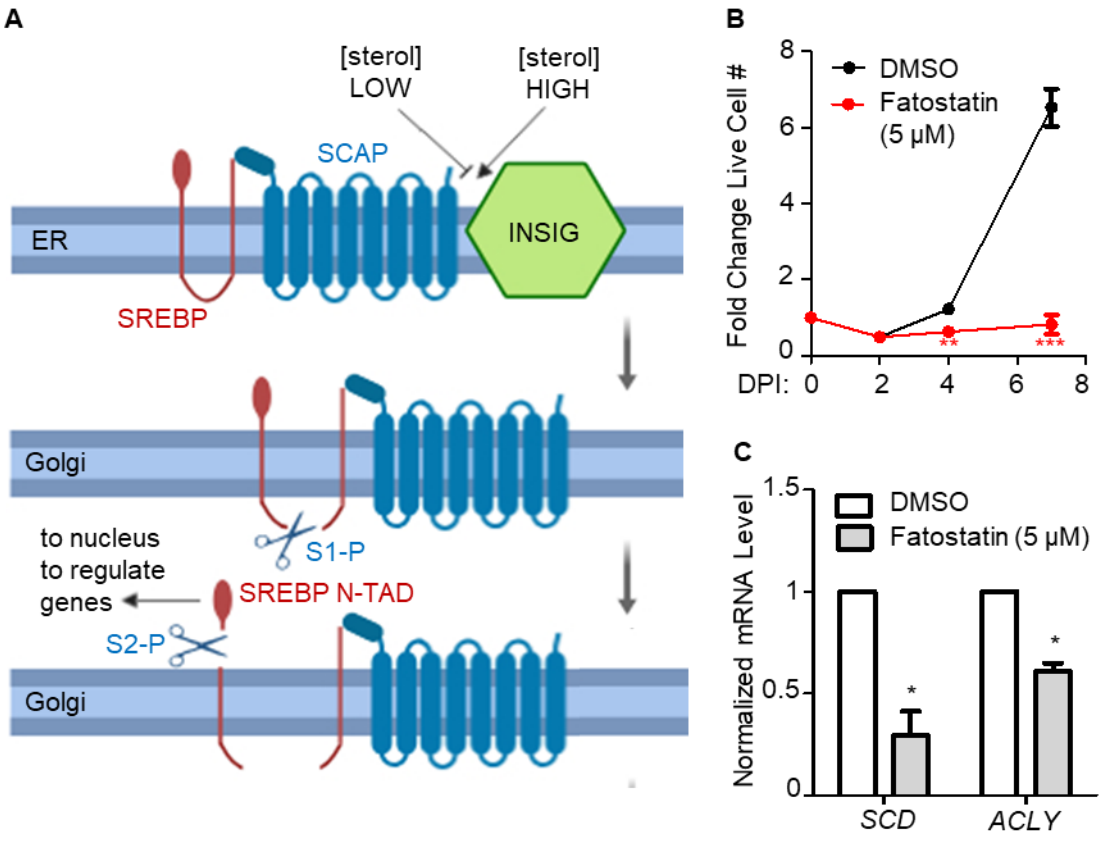

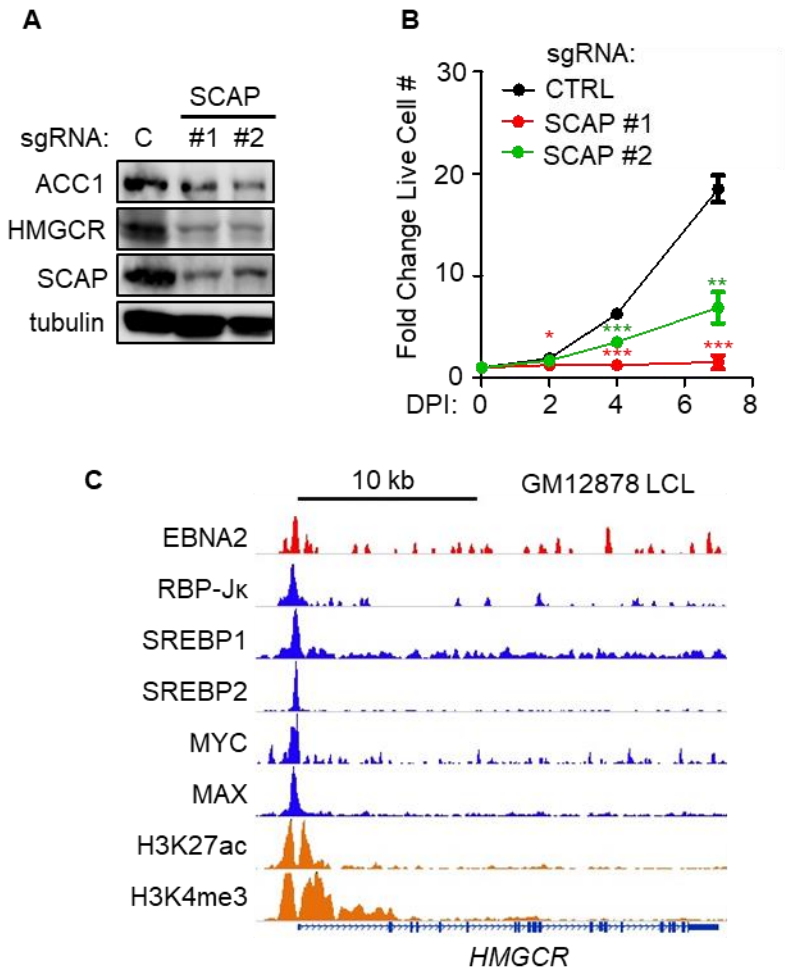

Figure IV.10 EBV-transformed LCL growth and/or survival depends on SREBP activity.

(A) Immunoblot analysis of ACC1, HMGCR, SCAP and tubulin levels in WCL prepared from Cas9+ GM12878 LCL expressing the indicated non-targeting control (denoted as 'C') or independent *SCAP* targeting sgRNAs. Representative blots of n=3 replicates are shown. (B) Growth curve analysis of Cas9+ GM12878 LCL that express either control or independent *SCAP*-targeting sgRNAs. Mean + SEM fold change values relative to day 0 levels are shown for n=3 replicates. *, $p<0.05$; **, $p<0.01$; ***, $p<0.005$ (two-tailed t-test). (C) Chromatin immunoprecipitation (ChIP)-sequencing (ChIP-seq) tracks for the indicated transcription factors or histone epigenetic marks histone epigenetic marks histone 3 lysine 27 acetyl (H3K27Ac) or histone 3 lysine 4 trimethyl (H3K4Me3) at the LCL *HMGCR* locus.

LCL ChIP-seq datasets (Zhao *et al.*, 2011b; Davis *et al.*, 2018; Consortium, 2012) were used to identify additional transcription factors present at the *HMGCR* and *ACACA* promoters. Interestingly, EBNA2, RBP-Jk, MYC and MAX were found to co-occupy *HMGCR* and *ACACA* promoter sites together with SREBP2 (Figures IV.10C, IV.11), indicating possible shared roles in mevalonate and fatty acid pathway induction.

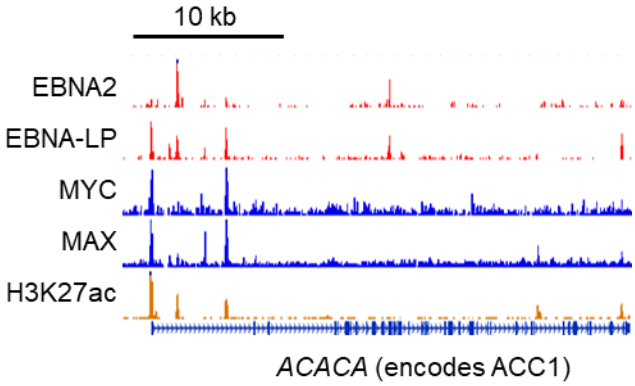

Figure IV.11 EBNA2 and MYC co-occupy the ACACA promoter. Chromatin immunoprecipitation (ChIP)-sequencing (ChIP-seq) tracks for the indicated transcription factors or histone H3 lysine 27 acetylation (H3K27Ac) at the LCL *ACACA* locus.

To investigate whether EBNA2 and EBNA-LP are required for EBV-driven ACC1 induction, primary cells were infected with equal amounts of the non-transforming EBV strain P3HR-1, which is deficient for EBNA2 and most of the EBNA-LP open reading frames (Rowe *et al.*, 1985; Rymo, Klein and Ricksten, 1985; Tsang *et al.*, 1991; Wang *et al.*, 1990) or transforming B95-8 virus. P3HR-1 infection failed to upregulate ACC1 or EBNA2 target MYC, as did infection with UV-irradiated B95-8, which can infect cells but is highly impaired for EBV gene expression (Miller *et al.*, 1974; Miller, Robinson and Heston, 1975) (Figure IV.12). These data suggest that EBNA2 and/or EBNA-LP, rather than an innate immune response to the incoming viral particle, are required for the induction of de novo lipid synthesis in newly infected B-cells.

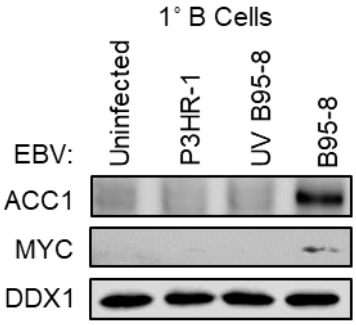

Figure IV.12 EBNA2 and/or EBNA-LP activate MYC and ACC1 protein expression. Immunoblot analysis for the indicated proteins using WCL obtained from primary cells that were either mock-infected or infected with equal amounts of the non-transforming P3HR-1, UV-irradiated B95-8 or B95-8 EBV strains for four days. Representative blots (n=2) are shown. Z. Wang assisted in performing experimental infections and subsequent electrophoretic analysis of the samples.

To next investigate EBNA2 roles in sustained cholesterol and lipid biogenesis in transformed cells, we used LCLs with conditional EBNA2 alleles. 2-2-3 and P493-6 LCLs each express EBNA2 fusion proteins (EBNA2-HT) under the control of a mutant estrogen receptor ligand binding domain that is controlled by 4-hydroxytamoxifen (4HT). In the absence of 4HT, EBNA2-HT re-localizes to the cytoplasm and is destabilized (Zhao *et al.*, 2006). Conditional EBNA2 inactivation by 4HT withdrawal for 48 hours diminished HMGCR and ACC1 abundances (Figures IV.13A-B), in support of an LCL EBNA2 role in upregulation of these rate limiting enzymes.

LCL ChIP-seq identified that the oncoproteins MYC and MAX, which form a heterodimeric complex that binds to E-box DNA sites to amplify target gene transcription (Lin *et al.*, 2012) also co-occupied the *HMGCR* promoter (Figure IV.10C, IV.11). To investigate MYC roles in upregulating key LCL lipid synthesis genes, we first asked whether MYC could rescue the loss of ACC1 expression in LCLs upon conditional EBNA2 inactivation. P493-6 LCLs stably express a conditional TET-off *MYC* allele, allowing for rescue of *MYC* expression in LCLs with conditional EBNA2 inactivation (Schuhmacher *et al.*, 1999; Schuhmacher *et al.*, 2001b). High level MYC expression induced by doxycycline withdrawal was sufficient to drive ACC1 expression, even with EBNA2 inactivation by 4HT withdrawal, suggesting that elevated MYC expression can compensate for the absence of EBNA2 (Figure IV.13B). Further underscoring a MYC role in fatty acid metabolism induction in LCLs, MYC depletion by two independent sgRNAs strongly decreased Cas9+ GM12878 ACC1 and HMGCR expression (Figure IV.13C). Intriguingly, MYC loss also strongly downmodulated SCAP abundance (Figure IV.13C), suggesting a further level of cross-regulation between MYC and the SCAP/SREBP axis in LCLs.

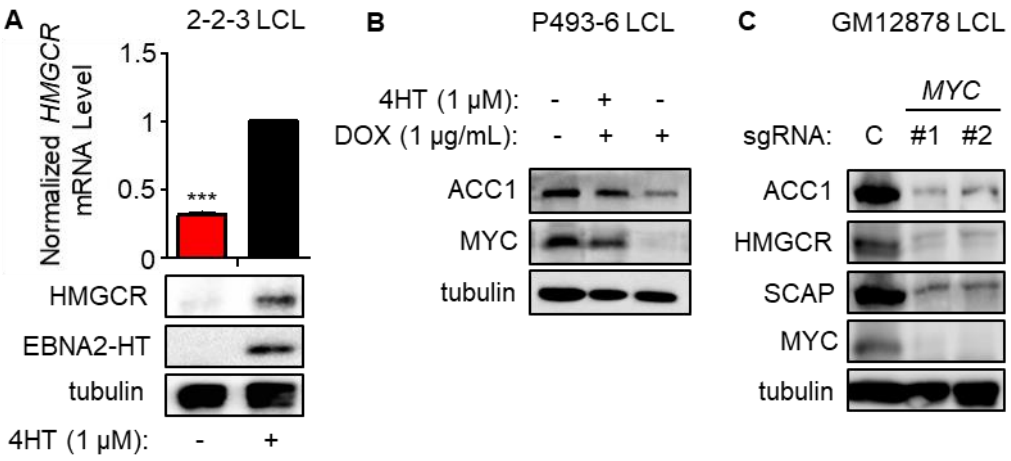

Figure IV.13 EBNA2 and MYC co-regulate ACC1 and HMGCR expression. (A) Quantitative PCR and immunoblot analyses of samples prepared from EBNA2-HT LCLs grown in the absence (EBNA2 non-permissive) or presence (EBNA2 permissive) of 4HT (1 μM) for 48 hours. Quantitative PCR data show the mean + SEM from n=3 replicates. ***, $p<0.005$ (one-sample t-test). Representative blots (n=3) are shown. (B) Immunoblot analysis of WCL prepared from conditional P493-6 LCLs treated with doxycycline (DOX) to suppress exogenous *MYC* allele expression and/or with 4HT for 48 hours, as indicated. Representative blots (n=3) are shown. (C) Immunoblot analysis of WCL prepared from Cas9+ GM12878 LCL expressing control (denoted as 'C') or independent *MYC*-targeting sgRNAs, as indicated. Representative blots from n=3 experiments are shown.

The mevalonate pathway product geranylgeranyl pyrophosphate is important for EBV-infected B-cell outgrowth

We next investigated the biological significance of EBV-mediated cholesterol biosynthesis pathway in newly infected cells. Notably, it was previously reported that treatment with simvastatin, but not with the related HMG-CoA reductase inhibitor pravastatin, causes LCL death (Katano, Pesnicak and Cohen, 2004). This phenotype was attributed to off-target simvastatin effects on leukocyte function antigen 1 (LFA-1), an LMP1-induced integrin, and simvastatin-mediated dissociation of LMP1 from lipid rafts (Katano, Pesnicak and Cohen, 2004). Since newly infected primary human B-cells do not express LCL-levels of LMP1 until 1 to 2 weeks post-infection (Price *et al.*, 2012), we first sought to determine whether early EBV-driven B-cell outgrowth was sensitive to simvastatin, or to another HMG-CoA reductase inhibitor atorvastatin, which has not been shown to share the LFA-1 off-target effect. Simvastatin and atorvastatin each significantly inhibited outgrowth of newly EBV-infected B-cells over the first week of infection (Figures IV.14A-B). Propidium iodide cell cycle analysis demonstrated that treatment with either simvastatin or atorvastatin increased the sub-2N population and decreased the 2N population, indicative of cell death (Figure IV.14C). We performed subsequent experiments with simvastatin due to the vast literature pertaining to its use in preclinical studies and clinical trials.

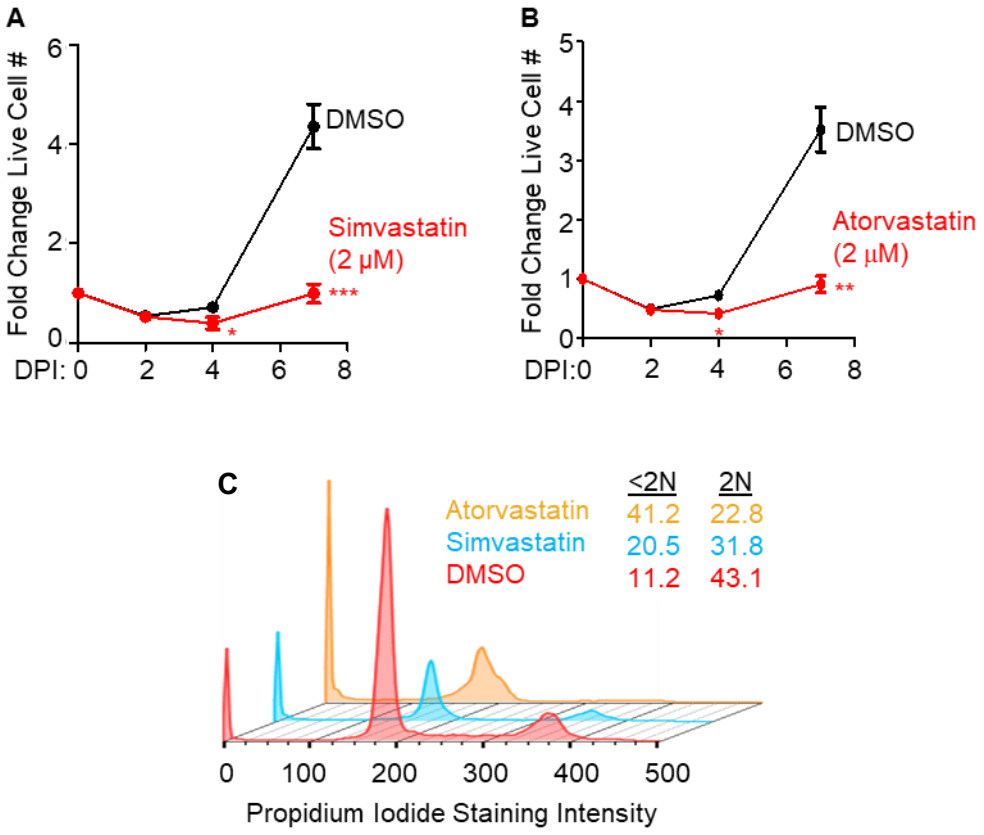

Figure IV.14 Statin treatment of newly infected cells induces proliferative defects, including increased cell death. (A) Fold change in live cell number of primary human B-cells infected by EBV for the indicated DPI, cultured in the presence of DMSO or simvastatin (2 μM) from 2 DPI to 7 DPI. Data show the mean + SEM from n=3 replicates. *, $p<0.05$; ***, $p<0.005$ (two-tailed t-test). (B) Growth curve analysis of newly infected primary B-cells cultured in the presence of DMSO or the HMG-CoA inhibitor atorvastatin (2 μM). Shown are the mean + SEM of n=6 replicates. *, $p<0.05$; **, $p<0.01$ (paired two-tailed t-test). (C) Flow cytometry (FACS) analysis of propidium iodide levels in fixed primary B-cells that had been treated with DMSO or the HMG-CoA reductase inhibitors simvastatin (2 μM) or atorvastatin (2 μM) from 2 DPI to 7 DPI. Representative cell cycle analysis FACS plots from n=2 experiments are shown. The percentages of cells with <2N (sub-G1) and 2N (G1) DNA content are indicated.

HMGCR is the rate-limiting enzyme of the mevalonate pathway (Goldstein and Brown, 1990), which branches to produce either cholesterol or isoprenoids (Figure IV.15A). To determine if either branch was crucial, we tested whether add-back of squalene (SQL) or geranylgeranyl pyrophosphate (GGPP) could rescue simvastatin-treated cells. Interestingly, GGPP nearly completely rescued outgrowth in the presence of simvastatin (Figure IV.15B), suggesting that isoprenoid synthesis and/or protein prenylation was/were critical. Cholesterol scavenging by EBV-upregulated LDLR (Figure IV.2) may have supplied cells with sufficient cholesterol. This result also suggests that simvastatin acts on-target to block B-cell outgrowth rather than by effects on LFA-1 or LMP1, which are not known to be geranylgeranylated.

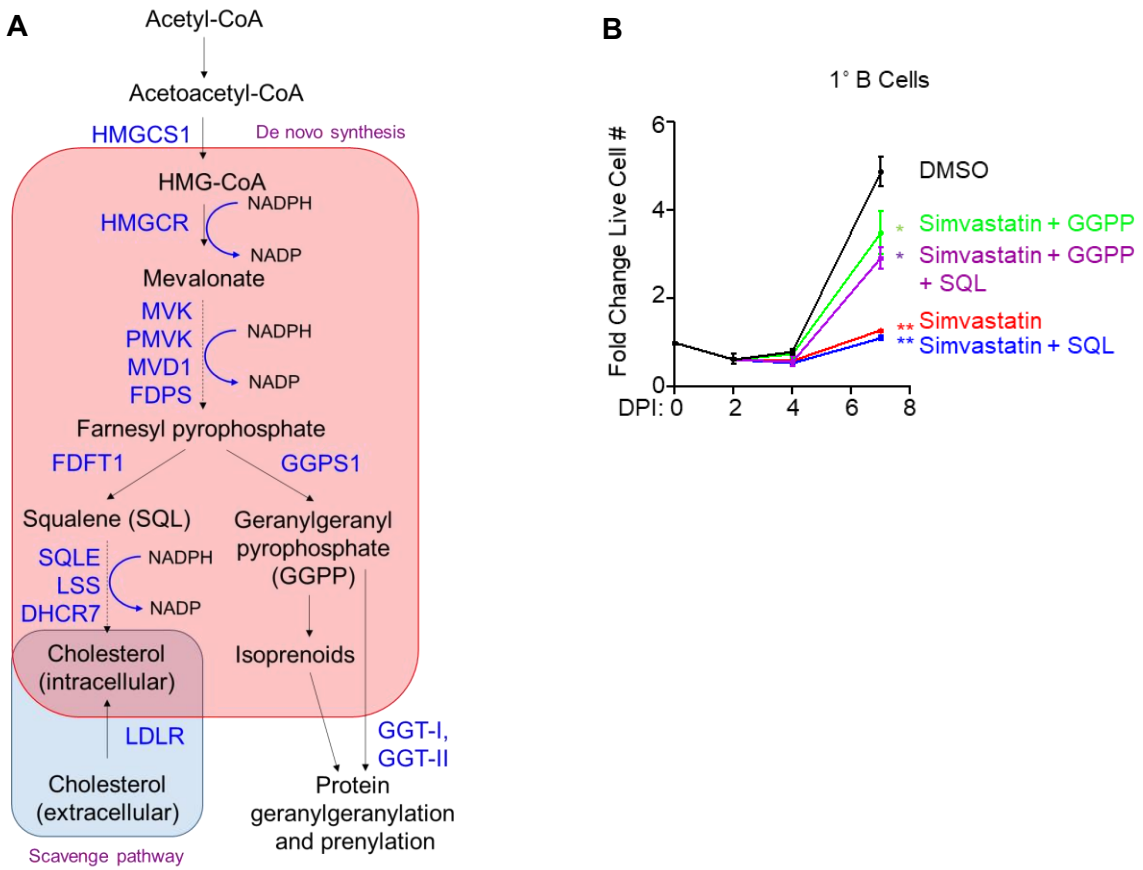

Figure IV.15 Statin-induced proliferative defects are significantly ameliorated by geranylgeranyl pyrophosphate (GGPP). (A) Schematic diagram of the mevalonate pathway branches that produce cholesterol or isoprenoids, with key enzymes indicated in dark blue color. Acetyl-CoA can be reduced in an NADPH-dependent manner by HMGCR to produce mevalonate. Mevalonate is then converted into farnesyl pyrophosphate, which can either be used to synthesize squalene for cholesterol biosynthesis or be diverted toward GGPP syntheses. Cholesterol can also be scavenged from the extracellular environment via the LDL receptor (LDLR). (B) Relative fold-change in live cell numbers of newly infected primary B-cells cultured in the presence of DMSO or simvastatin (2 μM) and supplemented with squalene (SQL, 100 μM), GGPP (1 μg/mL) or both, from 2 to 7 DPI. Data show the mean + SEM from n=3 replicates. *, $p<0.05$; **, $p<0.01$ (two-tailed t-test with means compared against DMSO-treated cells).

To next investigate whether GGPP was important for growth or survival, newly infected cells and LCL were treated with simvastatin, in the absence or presence of GGPP. Interestingly, simvastatin more strongly inhibited proliferation in newly infected cells but induced higher frequencies of cell death in LCLs (Figure IV.16). Incomplete GGPP rescue of LCL death may be accounted for by the prior observations that simvastatin off-target effects on LFA1 also cause LCL apoptosis (Katano, Pesnicak and Cohen, 2004).

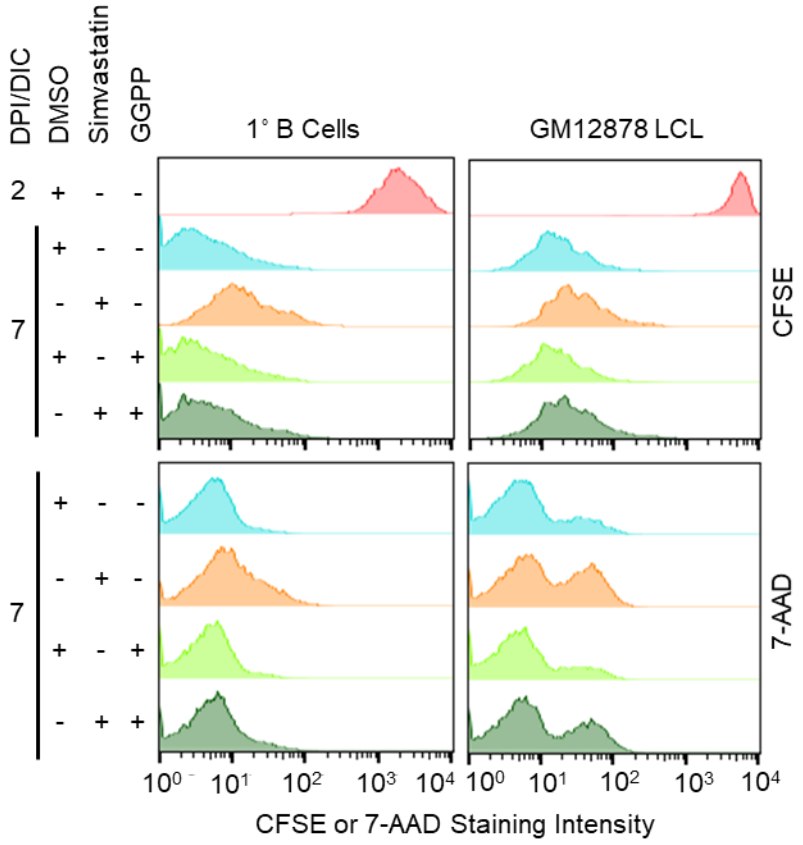

Figure IV.16 Flow cytometric analysis of CFSE dye dilution proliferation and 7-AAD cell death assays in newly infected primary B-cells or GM12878 LCL. Cells were treated with DMSO, simvastatin (2 μM) and/or GGPP (1 μg/mL) as indicated, from days post-infection (DPI) 2-7 for newly infected cells or, from days in culture (DIC) 2-7 for GM12878 LCLs. Representative histograms from n=3 replicates are shown.

Simvastatin induced cleavage of poly (ADP-ribose) polymerase (PARP), an event characteristic of apoptosis induction (Figure IV.17), further supporting the notion of GGPP being a crucial metabolite that supports viral transformation.

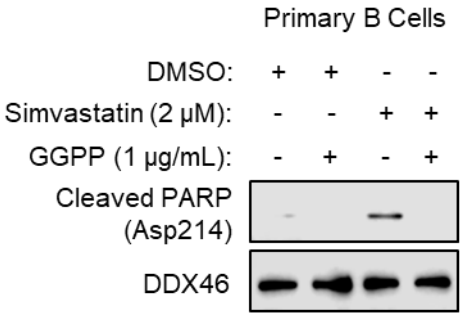

Figure IV.17 Simvastatin treatment induces apoptosis of newly infected cells, which can be reversed by GGPP supplementation. Immunoblot analysis of WCL from newly infected primary B-cells cultured in the presence of DMSO, simvastatin or GGPP from days 2-7 post infection. Cleaved PARP (aspartate-214 specific) was detected, together with DDX46 load-control. Representative blots from n=3 experiments are shown.

The Rab geranylgeranyltransferase GGT-II complex is important for EBV-driven B-cell outgrowth

Geranylgeranyltransferase (GGT) complexes transfer GGPP to small GTP-binding protein targets (Berndt, Hamilton and Sebti, 2011). We asked whether GGT-I or GGT-II activity necessitates the GGPP dependency. GGT-I catalyzes GGPP addition to Ras superfamily proteins including Rac and Rho G proteins (Casey and Seabra, 1996), whereas GGT-II geranylates Rab proteins to enable their membrane association (Hutagalung and Novick, 2011). Notably, EBV infection upregulated GGT-II but downmodulated GGT-I subunits (Figure IV.18).

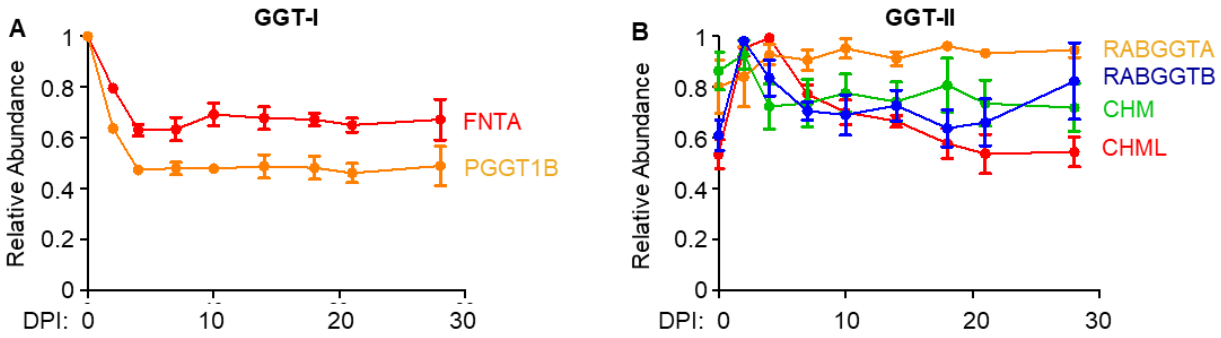

Figure IV.18 EBV enhances the subunit expression of GGT-II, not GGT-I. (A) Temporal proteomic traces of protein relative abundances for the GGT-I subunits FNTA and PGGT1B. Mean + SEM levels for three biological replicates are shown. (B) Temporal proteomic traces of protein relative abundances for GGT-II subunits RABGGTA, RABGGTB, CHM and CHML. Mean + SEM levels for three biological replicates are shown.

To test whether either GGT activity is critical for EBV-driven B-cell outgrowth, we performed chemical epistasis experiments with highly selective chemical antagonists. GGPP failed to rescue EBV-mediated B-cell outgrowth in cells treated with simvastatin and the GGT-II inhibitor BMS-214662, which is 1000-fold selective over GGT-I. By contrast, GGPP partially rescued the outgrowth of cells treated with simvastatin and the GGT-I inhibitor GGTI-2133, which is 140-fold selective over GGT-II (Wagner *et al.*, 2011; Lackner *et al.*, 2005; Nguyen *et al.*, 2009) (Figure IV.19). Additionally, newly infected cell survival was more sensitive to GGT-II than GGT-I inhibition (Figure IV.20).

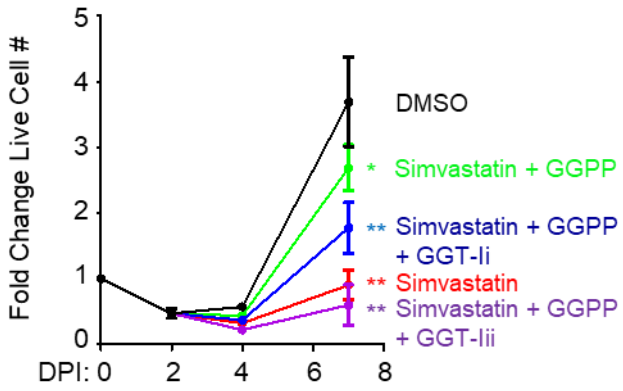

Figure IV.19 Chemical epistasis shows that newly infected cells are more reliant on GGT-II. Newly infected cells were cultured with DMSO, simvastatin (2 μM), GGPP (1 μg/mL), the GGT-I inhibitor GGTI-2133 at 10 μM (GGT-Ii) or the GGT-II inhibitor BMS-214662 at 10 μM (GGT-IIi). Mean + SEM fold change live cell numbers from n=3 replicates are shown. **, $p<0.01$ (two-tailed t-test with means compared against the DMSO condition).

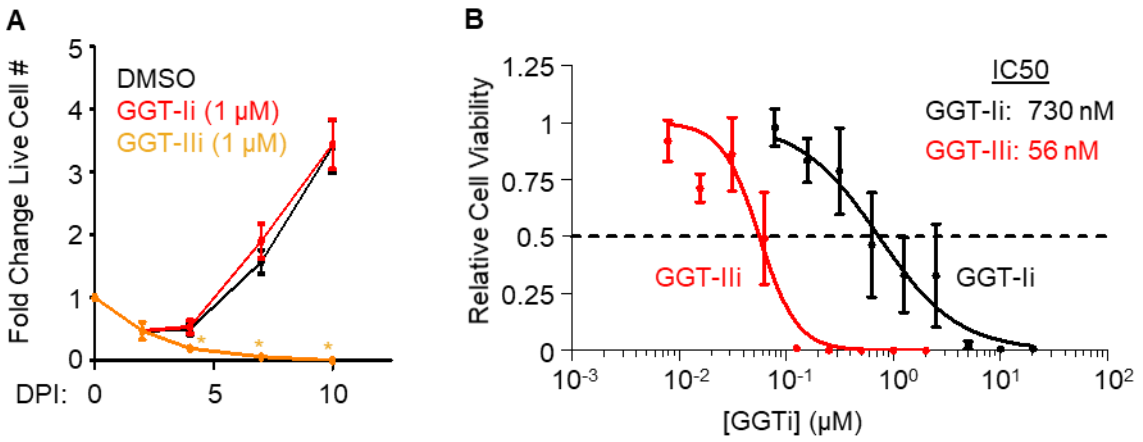

Figure IV.20 Newly infected cells are more sensitive to GGT-II inhibition. (A) Growth curve analysis of newly infected primary B-cells cultured in the presence of DMSO, GGTI-2133 (GGT-Ii, 1 μM) or BMS-214662 (GGT-IIi) (1 μM) from 2 DPI to 7 DPI. Mean + SEM fold change live cell numbers from n=3 replicates are shown. *, $p<0.05$; **, $p<0.01$ (two-tailed t-test). (B) Relative live cell numbers of EBV-infected primary human B-cells treated with either GGT-Ii inhibitor GGTI-2133 (GGT-Ii) or the GGT-IIi inhibitor BMS-214662 (GGT-IIi) from 4 DPI to 7 DPI at the indicated concentrations. Relative live cell numbers were calculated based on comparison with values obtained for DMSO vehicle treated control cells. Non-linear regression analysis was performed to fit a curve to the observed data for IC_{50} calculation. Shown are the mean + SEM from n=3 replicates. Z. Wang performed the growth curve experiment shown in panel A.

Consistent with this conclusion, independent sgRNAs against the genes encoding GGT-II subunits RABGGTA and RABGGTB but not against the GGT-I subunit PGGT1B strongly decreased Cas9+ LCL growth and/or survival (Figure IV.21). Furthermore, sgRNAs targeting genes encoding GGT-II subunits were more strongly depleted from Cas9+ LCL pools after 21 days of growth than those targeting GGT-I subunits in a recent genome-wide CRISPR screen (Ma *et al.*, 2017c) (Figure IV.22). Collectively, these results strongly suggest that EBV upregulates GGPP production for Rab protein activation.

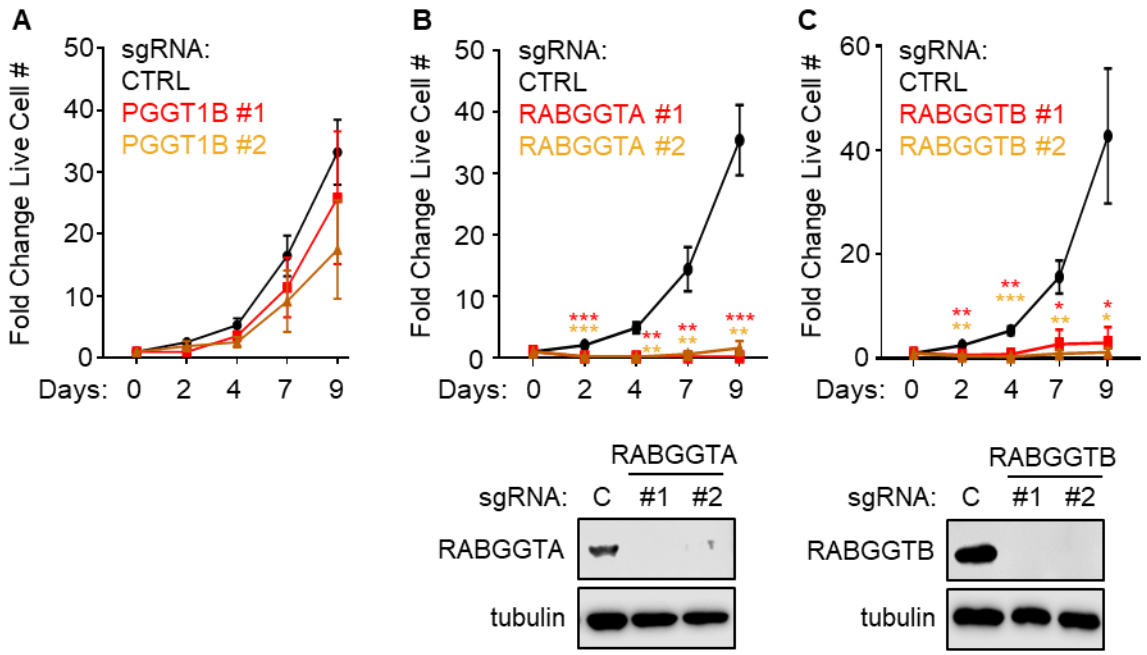

Figure IV.21 Ablation of GGT-II, not GGT-I, causes LCL growth inhibition and/or death. (A) Growth curve analysis of Cas9+ GM12878 LCL that express control (denoted as 'C') or independent *PGGT1B*-targeting sgRNAs are shown. Mean + SEM fold change live cell numbers from n=4 replicates are shown. (B) Growth curve analysis of Cas9+ GM12878 LCL that express control (denoted as 'C') or independent *RABGGTA*-targeting sgRNAs, as indicated. Mean + SEM fold change live cell numbers from n=4 replicates are shown. **, p<0.01; ***, p<0.005 (two-tailed t-test). Below, representative immunoblots (n=2) of RABGGTA and tubulin levels in WCL from LCLs expressing the indicated sgRNA are shown. (C) Growth curve analysis of Cas9+ GM12878 LCL that express control (denoted as 'C') or independent *RABGGTB*-targeting sgRNAs, as indicated. Mean + SEM fold change live cell numbers from n=4 replicates are shown. *, p<0.05; **, p<0.01; ***, p<0.005 (two-tailed t-test). Below, representative immunoblot analysis (n=2) of RABGGTB and tubulin levels in WCL from LCLs expressing the indicated sgRNA are shown. Nomenclature of sgRNAs here is not related to that in Figure IV.22. Z. Wang performed growth curve and immunoblot analyses presented in this figure.

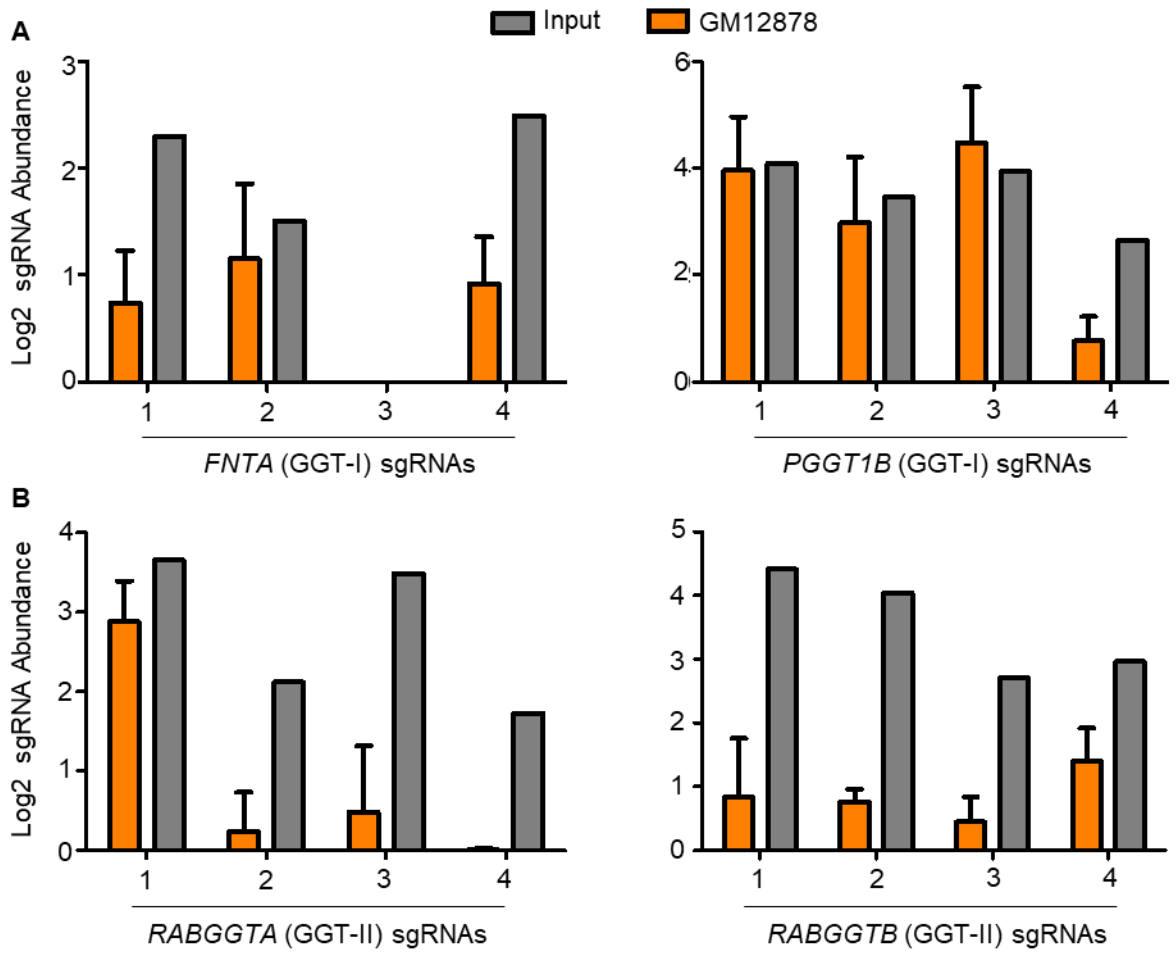

Figure IV.22 CRISPR ablation of GGT-II, not GGT-I, leads to consistent diminution of LCL growth and/or survival. (A) Mean + SEM of input versus day 21 *FNTA*-targeting (left) or *PGGT1B*-targeting (right) sgRNA abundances from genome-scale CRISPR/Cas9 screening done in quadruplicate in GM12878 LCLs (Ma *et al.*, 2017c). *FNTA* and *PGGT1B* encode GGT-I subunits. (B) Mean + SEM of input versus day 21 *RABGGTA*-targeting (left) or *RABGGTB*-targeting (right) sgRNA abundances from genome-scale CRISPR/Cas9 screen performed in quadruplicate in Cas9+ GM12878 LCLs (Ma *et al.*, 2017c). *RABGGTA* and *RABGGTB* encode GGT-II subunits. Each sgRNA targets a distinct exon. The y-axis value refers to the log2-transformed number of reads for each sgRNA normalized to the total number of reads. Nomenclature of sgRNAs here is not related to that in Figure IV.21.

EBNA3C-induced RAB13 is critical for LMP1/2A trafficking and, LCL growth and survival

We hypothesized that GGPP-modified Rab proteins(s) important for EBV-mediated B-cell outgrowth would be upregulated upon primary B-cell infection. Of the 37 Rab proteins detected in our recent temporal proteomic analysis of EBV-mediated B-cell remodeling, 24 were upregulated at ≥ 1 time point (Figure IV.23A). Of these, sgRNAs targeting *RAB13* were most strongly selected against in our 21-day Cas9+ LCL screen (Ma *et al.*, 2017c) (Figure IV.23B).

Since RAB13 abundance appeared to be closely correlated with that of EBNA3C in our proteomic analysis (Figures IV.24A-B) and LCL ChIP-seq (Davis *et al.*, 2018; Consortium, 2012; Jiang *et al.*, 2017) identified that EBNA3C occupies the *RAB13* promoter (Figure IV.24C), we hypothesized that EBNA3C is important for *RAB13* induction by EBV. Indeed, conditional EBNA3C inactivation strongly downmodulated RAB13 expression in C19 LCLs, which express an EBNA3C/4HT-binding domain fusion protein (Maruo *et al.*, 2006) (Figure IV.24D). These results agree with prior microarray analyses, which found significant downmodulation of *RAB13* transcript abundance upon EBNA3C inactivation in C19 cells (Zhao *et al.*, 2011a).

Figure IV.23 Rab proteins are dynamically regulated during EBV infection of primary human B-cells. (A) Heatmap representation of relative abundance profiles for all Rab family proteins detected in whole cell proteomic analysis of primary human B-cells infected by EBV at the indicated DPI. Mean values from biological triplicate measurements are shown. (B) (A) Mean + SEM of input versus day 21 *RAB13*-targeting sgRNA abundances from genome-scale CRISPR/Cas9 screen performed in quadruplicate in Cas9+ GM12878 LCLs (Ma *et al.*, 2017c). Each sgRNA targets an independent exon region. The y-axis value refers to the log2-transformed number of reads for each sgRNA normalized to the total number of reads.

Figure IV.23 (Continued)

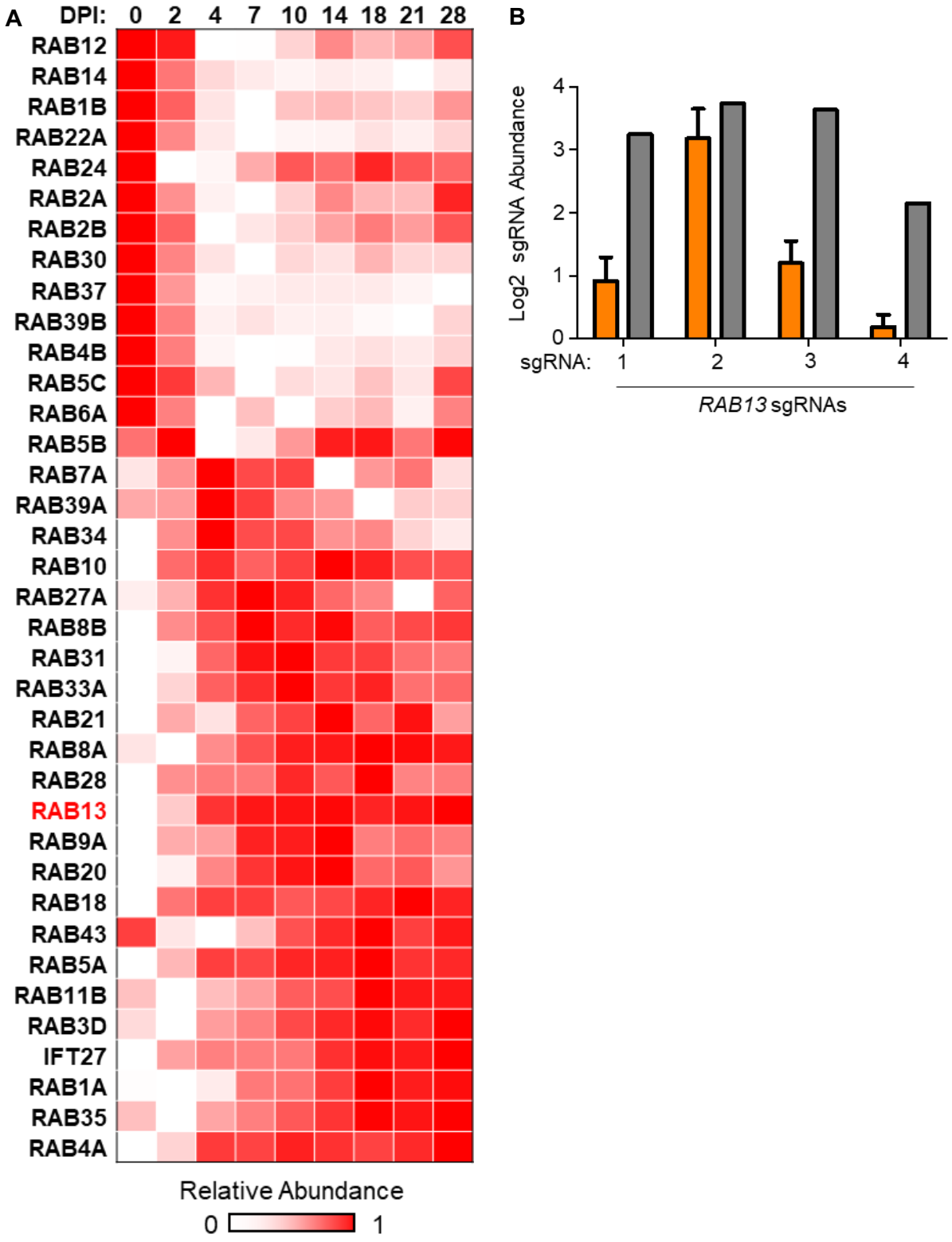

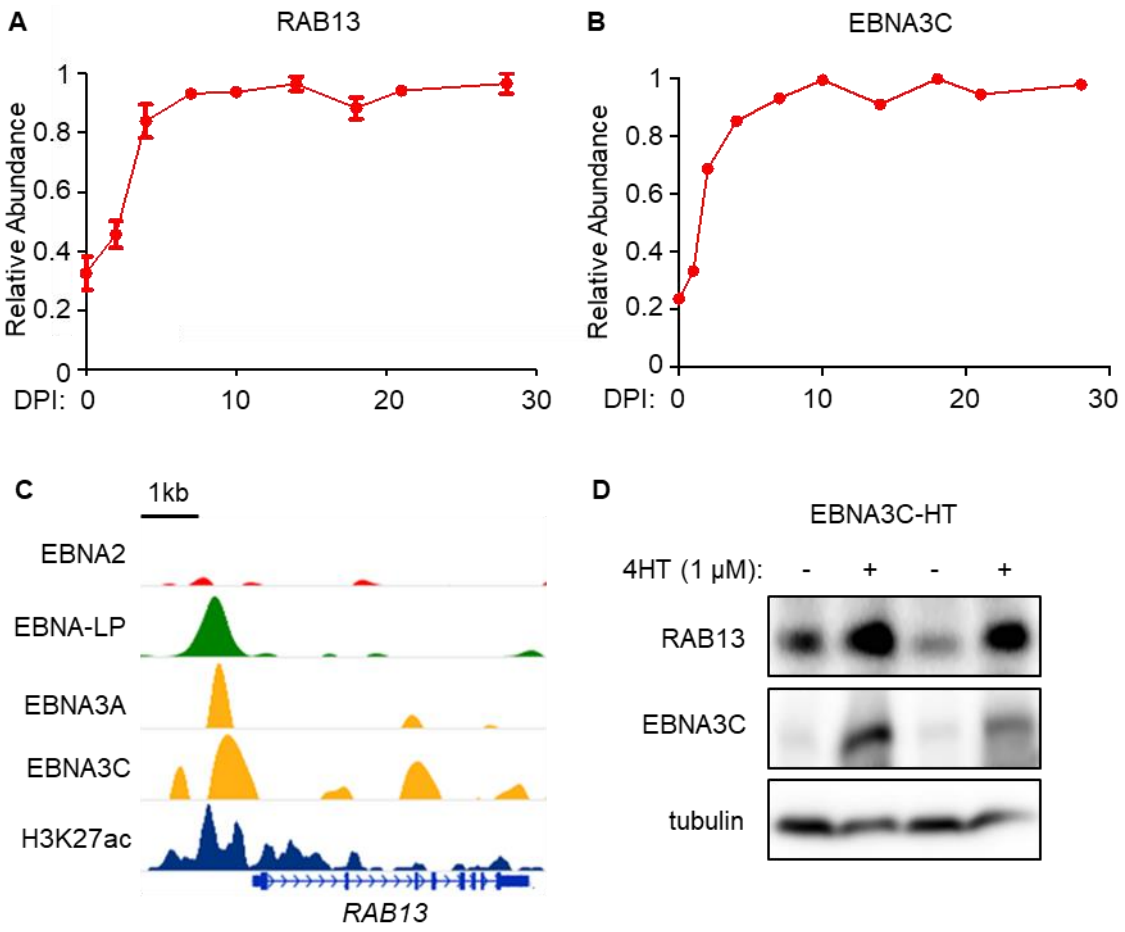

Figure IV.24 EBNA3C activates RAB13 expression. (A) Temporal proteomic trace of RAB13 protein relative abundance at the indicated DPI of primary human B-cell EBV infection. Mean + SEM levels for three biological replicates are shown. (B) Temporal proteomic trace of EBNA3C protein relative abundance at the indicated DPI of primary human B-cell EBV infection. (C) LCL ChIP-seq tracks for the indicated EBNAs or H3K27Ac epigenetic mark at the LCL *RAB13* locus. (D) Immunoblot analysis of conditional EBNA3C-HT LCLs grown in the presence of 4HT (1 μM) (EBNA3C permissive) or absence of 4HT (EBNA3C non-permissive) for 14 days. Representative blots of n=5 experiments are shown.

Immunofluorescence microscopy confirmed that RAB13 was upregulated by four days post EBV primary B-cell infection, at which point RAB13 colocalized with LMP2A (Figure IV.25). At this timepoint, RAB13 formed large aggregates with LMP2A, reminiscent of BCR micro-clusters that form during antigen-dependent reactions (Figure IV.25). We therefore hypothesized that RAB13 might be important for trafficking and activation of LMP1 and LMP2A, which co-localize with each other in EBV-infected lymphocytes (Longnecker and Kieff, 1990) and signal from lipid raft sites (Meckes, Menaker and Raab-Traub, 2013; Higuchi, Izumi and Kieff, 2001; Lam and Sugden, 2003; Lee and Sugden, 2007).

Figure IV.25 RAB13 co-localizes with LMP2A in newly infected cells. Immunofluorescence micrographs of LMP2A, RAB13 and nuclear DNA (stained with Hoechst 33528) stained uninfected versus newly infected primary human B-cells at 4 DPI. Merged images are shown with white boxes indicating inset images that have been further magnified. The asterisk denotes an area of strong RAB13 and LMP2A colocalization. Scale bars are indicated (50 μm for single-channel and merged images; 5 μm for inset images). Image acquisition and analysis were jointly performed by L.W. Wang and Z. Wang.

Figure IV.25 (Continued)

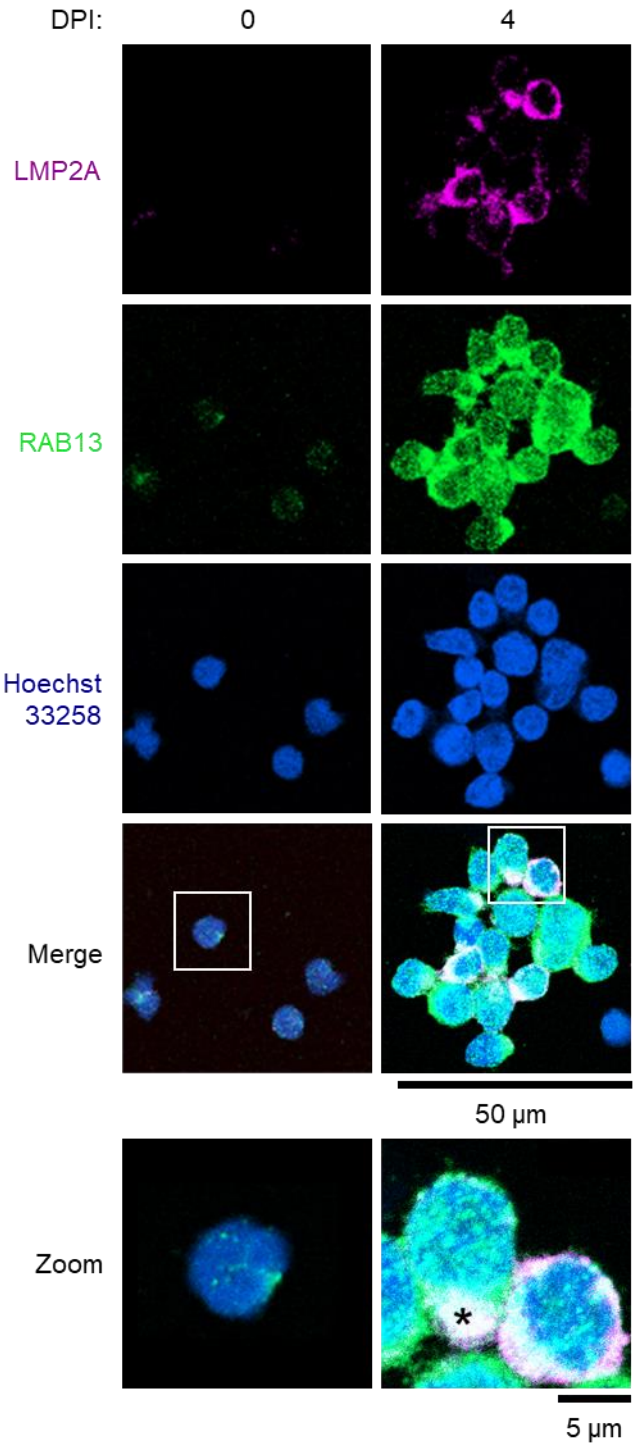

To further characterize RAB13 roles in LMP1 and LMP2A function, we first used CRISPR to test whether RAB13 was important for LCL growth and/or survival, as suggested by our recent CRISPR screen, where three independent sgRNAs targeting *RAB13* were strongly selected against in a 21-day outgrowth assay (Figure IV.23B). A *RAB13*-targeting sgRNA depleted endogenous RAB13 expression and strongly reduced Cas9+ LCL numbers in a 7-day outgrowth assay in comparison with a non-targeting sgRNA (Figure IV.26A); on-target CRISPR effects were validated by cDNA rescue (Figure IV.26B). Interestingly, RAB13 depletion decreased expression of the LMP1 target TRAF1 and similarly diminished activation of the LMP2A target mTOR, as judged by serine 2448 (S2448)-phosphorylation status (Figures IV.26C-D). Yet, RAB13 loss did not significantly change LMP1 or LMP2A abundance (Figure IV.26E), suggesting that RAB13 controls LMP activity at the post-translational level. Indeed, *RAB13* targeting by independent sgRNAs substantially altered LMP1 and LMP2A subcellular localization, with loss of LMP1 and LMP2A co-localized foci (Figure IV.27). Taken together, these observations indicate an important RAB13 role in LMP1 and LMP2A trafficking, likely to lipid raft signaling sites (Figure IV.28).

Figure IV.26 RAB13 regulates LMP1 and LMP2A signaling. (A) Growth curve analysis of Cas9+ GM12878 LCL that express either control GFP or rescue *RAB13* ($RAB13^R$) cDNAs and either control or *RAB13*-targeting sgRNA. A silent mutation at the CRISPR PAM site abrogates Cas9 cleavage of the $RAB13^R$ cDNA. Data show the mean + SEM fold change live cell values at the indicated timepoints for n=3 replicates. (B) Representative immunoblots from n=3 replicates of WCL from LCLs expressing the indicated cDNA and sgRNA are shown. (C) Immunoblot analysis of WCL from Cas9+ GM12878 LCL that express either control or independent *RAB13*-targeting sgRNAs. Representative blots from n=2 experiments are shown. Phospho-serine-2448 (S2448) mTOR is a marker of LMP2A activation, whereas TRAF1 is an LMP1-induced LCL target gene. (D) Quantitative PCR analysis of TRAF1 expression in Cas9+ GM12878 LCL that express either control or independent *RAB13*-targeting sgRNAs. Data show the mean with SEM, n=3. *, $p<0.05$ (one-sample t-test). (E) Immunoblot analysis of WCL from Cas9+ GM12878 LCL that express either control or independent *RAB13*-targeting sgRNAs to determine overall LMP1 and LMP2A levels. Representative blots from n=2 experiments are shown. Z. Wang performed RAB13 CRISPR KO and rescue growth curve and immunoblot analyses.

Figure IV.26 (Continued)

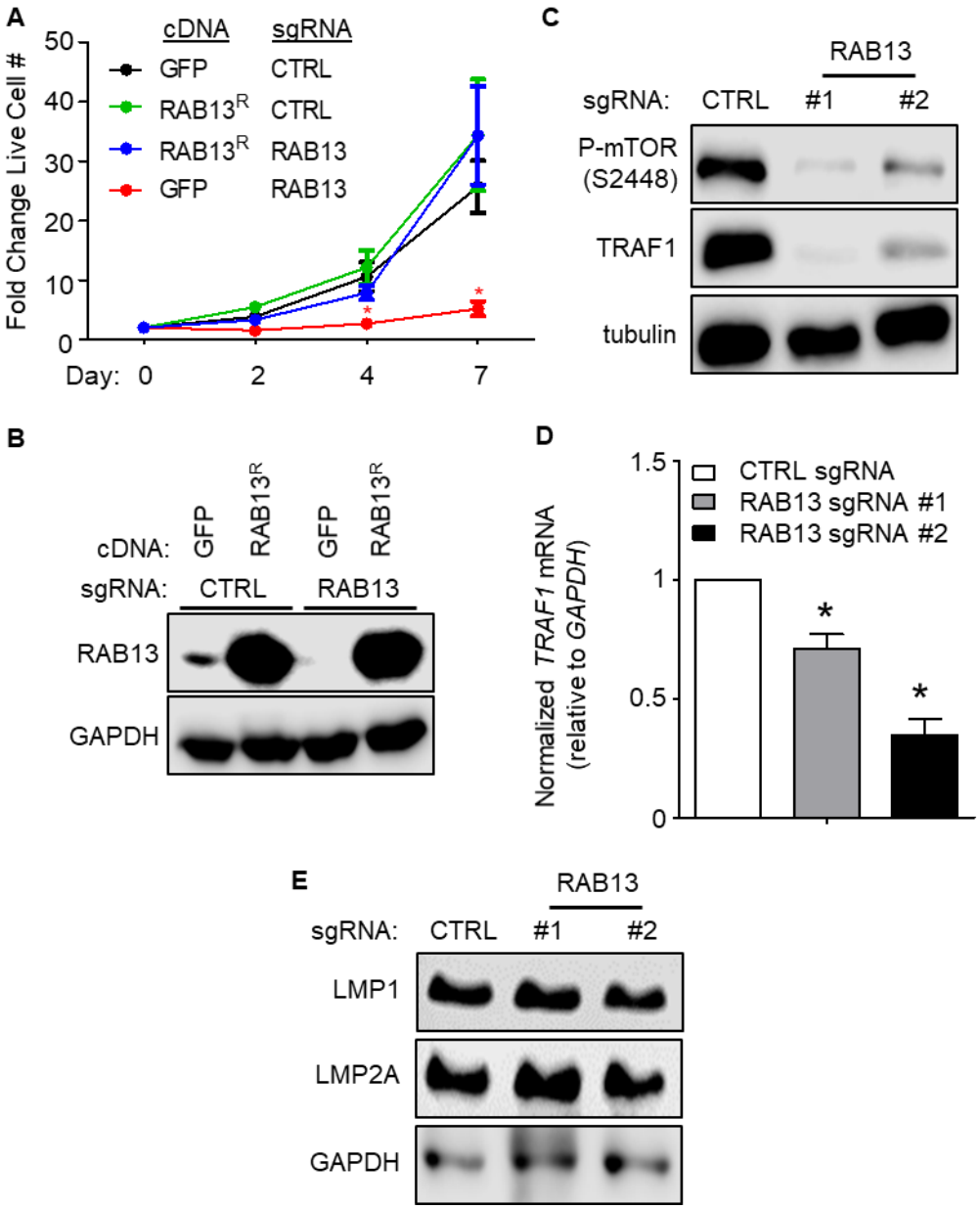

Figure IV.27 RAB13 colocalizes with LMP1 and LMP2A in LCLs. Immunofluorescence micrographs of Cas9+ GM12878 LCL that express either control or *RAB13*-targeting sgRNAs, showing localization patterns of RAB13, LMP1 or LMP2A. Merged images are shown with white boxes indicating inset images that have been further magnified. Scale bars are indicated (50 μm for single-channel and merged images; 5 μm for inset images). Z. Wang performed CRISPR KO of RAB13 and slide preparation, and acquired the images shown in this figure.

Figure IV.27 (Continued)

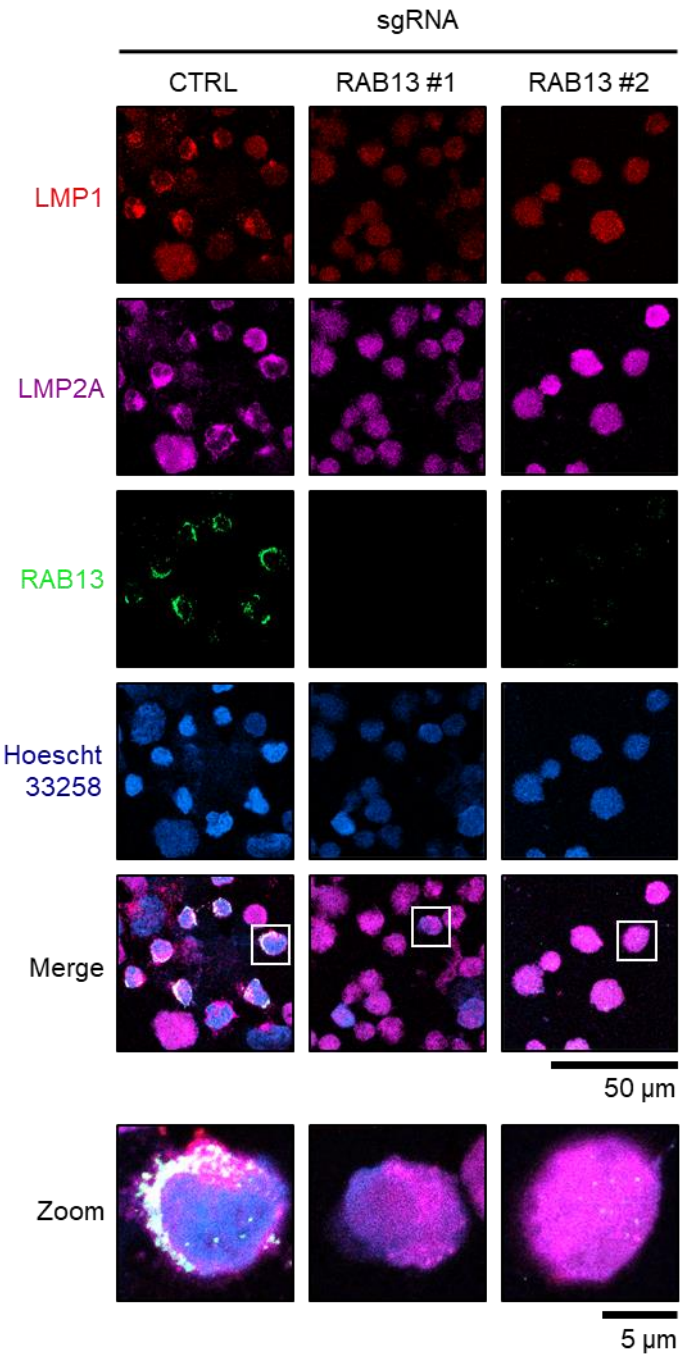

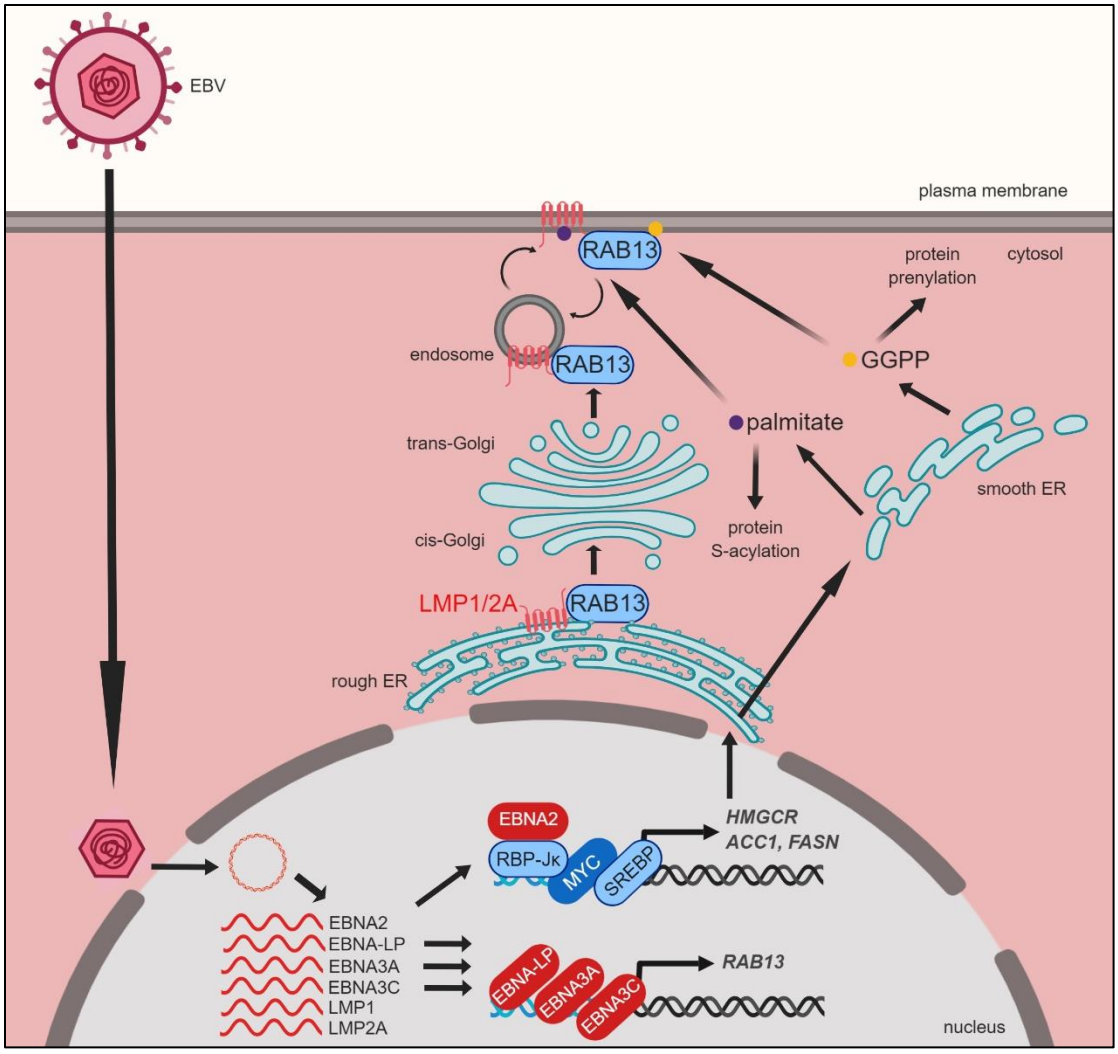

Figure IV.28 Model of EBV-induced cholesterol and lipid biosynthesis pathways remodeling and roles in LMP trafficking. EBV-encoded EBNA2 targets growth-promoting transcription factors such as MYC and SREBPs, which together with EBNA2 drive expression of key cholesterol and lipid biosynthesis genes. These metabolic programs induce mevalonate and fatty acid synthesis for B-cell remodeling and post-translational activation of target proteins. GGPP and palmitate support Rab geranylgeranylation and, protein palmitoylation and phospholipid synthesis, respectively. EBNA3C upregulates the expression of RAB13, a small GTPase protein that serves key chaperone roles in LMP1 and LMP2A trafficking and signaling.

Discussion

Diverse DNA viruses subvert host lipid biosynthesis pathways to support viral replication, including Kaposi's sarcoma-associated herpesvirus (KSHV) (Lange, Lagunoff and Tarakanova, 2019; Sychev *et al.*, 2017), human cytomegalovirus (HCMV) (Rodriguez-Sanchez and Munger, 2019; Shenk and Alwine, 2014; Purdy, Shenk and Rabinowitz, 2015), herpes simplex virus (HSV) (Jean Beltran *et al.*, 2018; Sanchez and Lagunoff, 2015) and vaccinia virus (VACV) (Greseth and Traktman, 2014). Interestingly, KSHV subverts hypoxia-inducible factors (HIF) to induce metabolic remodeling in B-cells (Singh *et al.*, 2018), whereas in epithelial cells, it targets glutamine and asparagine metabolic pathways while suppressing glycolysis to support transformed cell growth (Zhu *et al.*, 2017; Zhu *et al.*, 2016). Comparatively less is known about how EBV remodels lymphocyte metabolic pathways to support cell transformation, growth and survival. While EBV strongly upregulates aerobic glycolysis in newly infected B-cells (McFadden *et al.*, 2016), presumably to supply building blocks for anabolic pathways, key downstream lipid biosynthesis pathways upregulated by latent EBV infection have remained to be identified.

The studies presented here highlight EBV-induced mevalonate, GGPP, fatty acid biosynthetic and downstream RAB13 pathways as being critical for newly infected B-cell outgrowth (Figure IV.28). EBNA2 and its targets MYC and SREBP2 were found to play major roles in the induction of these key metabolic pathways in early B-cell transformation. Further studies are required to fully define how these host and viral transcription factors may function together on DNA to induce target genes. SREBPs interact with MYC at promoters of stemness-controlling genes (Li *et al.*, 2016; Wu *et al.*, 2016), and LCL ChIP-seq identifies them as co-occupants on promoters of LCL cholesterol and lipid metabolism pathway genes, together with EBNA2. Further suggesting interdependent roles, EBNA2, MYC and the SCAP/SREBP axis were found to cross-regulate one another's abundance in LCLs. We speculate that EBNA2 and SREBPs may initially

induce cholesterol and lipid pathway target genes, and that this activity is then amplified by MYC, analogous to that which has been previously described (Lin *et al.*, 2012).

LMP1 has been reported to activate lipogenesis via mTOR and SREBP1 in nasopharyngeal carcinoma (NPC) cells, which typically express the latency II program (Lo *et al.*, 2018). In contrast, our studies point to important EBNA roles in lipid pathway remodeling in newly infected B-cells. First, newly infected cells do not have high levels of LMP1 over the first several days post-infection when key targets such as HMGCR and ACC1 are initially upregulated. Second, LCL ChIP-seq demonstrates only modest NF-κB subunit occupancy at the *HMGCR* and *ACACA* promoters. Instead, EBNA2, MYC and SREBPs co-occupy these key promoters. LMP2A may also fulfill critical roles in maintaining cholesterogenic and lipogenic programs at later timepoints by stimulating PI3K/AKT/mTOR flux (Moody *et al.*, 2005).

We initially suspected that EBV upregulates mevalonate synthesis to supply cholesterol for lipid raft and membrane synthesis in support of B-cell lymphoblast transformation. However, using a chemical epistasis approach (Wagner *et al.*, 2011), we unexpectedly found that simvastatin impaired EBV-infected primary B-cell outgrowth by preventing GGPP synthesis and Rab protein activation. While off-target simvastatin effects on LFA-1 and LMP1 dissociation from lipid rafts have previously been reported in LCLs (Katano, Pesnicak and Cohen, 2004), simvastatin effects on EBV primary B-cell outgrowth and survival could nearly be completely rescued by GGPP supplementation. In further support of on-target statin activity underlying effects on EBV-driven B-cell outgrowth, a chemically distinct statin, atorvastatin, similarly blocked EBV-infected B-cell outgrowth. Lower LMP1 and LMP1-induced LFA-1 expression in newly infected B-cells (Price *et al.*, 2012) may have reduced the impact of the previously reported HMGCR-independent effects of simvastatin (Katano, Pesnicak and Cohen, 2004) in our experiments. Cholesterol also plays important roles in LMP1 and LMP2A trafficking (Katano, Pesnicak and Cohen, 2004; Meckes, Menaker and Raab-Traub, 2013; Ikeda and Longnecker, 2007; Verweij

et al., 2011). The mevalonate pathway may therefore also support this key aspect of EBV oncoprotein function in microenvironments where extracellular LDL is limiting.

While to our knowledge GGPP has not previously been studied in EBV-infected cells, key mevalonate pathway and GGPP roles have been identified in other B-cell contexts. Importantly, CD40-mediated B-cell activation upregulates the mevalonate pathway in primary B-cells, where GGPP supports antigen-presenting cell function and T-cell activation by mediating CD80, CD86 and HLA-DR upregulation (Shimabukuro-Vornhagen *et al.*, 2014). However, specific GGPP targets, such as Rab proteins that may function in trafficking of CD40 or of T-cell stimulatory molecules, remain to be identified. Given how closely LMP1 mimics CD40, we hypothesize that LMP1 may reinforce EBNA2-driven mevalonate metabolism and GGPP upregulation in the lymphoblastoid phase of B-cell transformation. Additional B-cell GGPP roles appear likely, since geranylgeranylation supports proliferative capacity and survival of multiple EBV-negative lymphomas and multiple myeloma B-cells in culture (Ageberg *et al.*, 2011; van de Donk *et al.*, 2003; van de Donk *et al.*, 2005; Fuchs *et al.*, 2008).

Our results highlight the interplay between RAB13, LMP1 and LMP2A in B-cell transformation and in transformed cell growth and survival. RAB13 has pleiotropic roles, including the regulation of glucose transporter 4 (GLUT4) trafficking (Deng *et al.*, 2018), macrophage phagocytosis (Yeo *et al.*, 2016; Condon *et al.*, 2018), autophagy (Zhang *et al.*, 2017c), lymphocyte trafficking (Nishikimi *et al.*, 2014), anoikis and metastasis (Ioannou *et al.*, 2015; Köhler, Louvard and Zahraoui, 2004; Ioannou and McPherson, 2016). Notably, LMP1 traffics to intracellular membranes to initiate signaling or to be secreted in exosomes (Hurwitz *et al.*, 2017; Ikeda and Longnecker, 2007; Liu, Wu and Chang, 2006; Meckes, Menaker and Raab-Traub, 2013; Verweij *et al.*, 2011; Verweij *et al.*, 2015; Nkosi *et al.*, 2018). However, the chaperone protein(s) required for intracellular sorting are incompletely defined. Our results suggest that EBV co-opts RAB13 to chaperone oncogenic LMP1 and LMP2A to appropriate sub-cellular

compartments where they can then activate downstream pathways. RAB13+ punctate structures observed in newly infected cells may represent unprenylated, inactive RAB13 pools that are subsequently activated by guanine exchange factors at the cell membrane (Ioannou, Girard and McPherson, 2016).

Given that both LMP1 and LMP2A can signal from intracellular membranes (Verweij *et al.*, 2015; Lynch, Zimmerman and Rowe, 2002; Dawson *et al.*, 2001; Lam and Sugden, 2003), it is possible that RAB13 functions to directly promote LMP movement to the plasma membrane and endosomal compartments. Alternatively, RAB13 may undergo cycles of activation and inactivation to facilitate LMP recycling between the plasma membrane and endosomes, in a manner similar to that with occludin in epithelial cells (Morimoto *et al.*, 2005). Notably, the prenylated Rab acceptor 1 (PRA1/RABAC1) associates with LMP1 at the Golgi apparatus and prevents LMP1 retrograde translocation back to the ER (Liu, Wu and Chang, 2006). PRA1 interacts with multiple prenylated Rab GTPases (Martincic, Peralta and Ngsee, 1997; Hutt *et al.*, 2000) and facilitates their delivery to cell membranes by counteracting the guanine nucleotide dissociation inhibitor GDI, a protein that actively solubilizes membrane-bound Rab proteins (Sivars, Aivazian and Pfeffer, 2003). We speculate that LMP1 association with PRA1 may require RAB13 as an intermediary binding partner.

The crucial EBNA3C role in support of LCL RAB13 expression raises the interesting question of how LMP1 and LMP2A traffic and signal in cells with latency II expression where EBNA3C is not expressed, such as in germinal center B-cells, Hodgkin Reed Sternberg (RS) or nasopharyngeal carcinoma tumor cells (Thorley-Lawson, 2015; Wang, Jiang and Gewurz, 2017; Kieser and Sterz, 2015; Lam and Sugden, 2003; Stunz and Bishop, 2014). Interestingly, RNA profiling datasets from classic Hodgkin's lymphoma, the HL subtype most closely associated with EBV, indicate active transcription of *RAB13* in RS cells (Küppers *et al.*, 2003). Since germinal center B-cells are the RS cell of origin and support the viral latency II program,

alternative mechanisms for RAB13 induction may therefore be operative in this important B-cell developmental state. Alternatively, other Rab protein(s) may act redundantly with RAB13 to support LMP1 and LMP2A transport in B and epithelial cells with EBV latency II expression. For instance, LMP1 was recently found to upregulate Rab11 (DeKroon *et al.*, 2018), which can have major roles in protein trafficking (Johnson *et al.*, 2016; Welz, Wellbourne-Wood and Kerkhoff, 2014).

These studies identify multiple EBV-induced metabolic pathway enzymes that may serve as attractive therapeutic targets to prevent or halt EBV-driven lymphoproliferative disease, which could be targeted by available small-molecule inhibitors as prophylaxis during periods of profound immunosuppression. These may include key druggable enzymes in the mevalonate, GGPP or fatty acid biosynthetic pathways. Of particular interest are simvastatin and atorvastatin, since the concentrations of these widely prescribed statins at which we observed inhibition of EBV-mediated B-cell outgrowth in vitro can likewise be achieved in humans in vivo (Thibault *et al.*, 1996). Simvastatin multi-target effects on LFA-1 and LMP1 lipid raft dissociation (Katano, Pesnicak and Cohen, 2004) further underscore its potential in counteracting EBV transformed lymphoblastoid B-cell growth. It will be of significant interest to test statin targets identified herein with recently developed humanized mouse models of EBV lymphoproliferative disease (Munz, 2017).

Chapter V: Dissertation Perspectives

Summary of Results

This work was aimed at understanding how EBV modulates host cell metabolic programs to promote long-term carriage, characterized by persistent growth, proliferation and survival. Through multiplexed proteomics, we discovered mitochondrial 1C metabolism and de novo synthesis of serine, cholesterol and lipids to be crucial for outgrowth and long-term transformation. Mitochondrial 1C metabolism functioned mainly to supply newly infected cells with one-carbon units for nucleotide synthesis, and also served roles in generating glycine for glutathione production and reducing power in the form of intramitochondrial NADPH. Mitochondrial 1C ablation in LCLs via MTHFD2 CRISPR KO demonstrated a novel requirement for intramitochondrial NADPH. De novo serine synthesis from the glycolytic intermediate 3-PG was crucial for transforming cell and LCL growth and/or survival, even with sufficient serine in the growth medium; however, its function remains poorly defined and is likely linked to cell-intrinsic serine production where certain environments in vivo may limit serine availability. De novo mevalonate metabolism and lipid synthesis supported protein post-translational modifications by supplying GGPP and palmitate for conjugation to target protein cysteine residues, thereby remodeling the signaling milieu of the newly infected cell. In particular, we discovered a positive regulatory role for EBNA3C-induced RAB13, a small GTPase protein that can be geranylgeranylated at its C-terminus, in the intracellular trafficking of LMP1 and LMP2A.

Early induction of these pathways is dependent on EBNA2 and its target gene MYC. Although these pathways have been variously described to be regulated by a number of different transcription factors, in our system i.e. B-cells, EBNA2 and MYC are central transcription factors governing metabolic remodeling of newly infected cells and maintenance of anabolism in LCLs.

Discussion

MYC, NF-κB and mTOR pathways co-regulate EBV-infected cell metabolism

Broadly speaking, EBV uses different transcriptional programs at various phases of its latent life cycle to support anabolic metabolism. Early in infection, the virus-infected cell's metabolism is heavily influenced by EBNA2-induced MYC. As the infection progresses, NF-κB (driven by LMP1) and PI3K/AKT/mTOR (driven by LMP2A) co-inhabit the metabolic landscape. It is worth noting that even though MYC abundance is lower in the stably transformed state compared to initial infection, MYC retains an indispensable role in sustaining proliferation and survival in LCLs. This might be related to the fact that MYC is not simply an oncogenic transcription factor that binds a new subset of growth-promoting genes; it also acts to augment existing transcriptional programs (Lin *et al.*, 2012) and likely reinforces LMP1 and LMP2A dependent signaling pathways. Similarly, while LMP2A is the major mTOR activator in stably transformed EBV-infected cells (Anderson and Longnecker, 2008; Portis and Longnecker, 2004; Moody *et al.*, 2005), the observed early activation of mTOR is presumably independent of LMP2A and is required for outgrowth (McFadden *et al.*, 2016). Although the mTOR stimulus is not well-defined, it likely involves an initial influx of amino acids through SLC3A2/SLC7A5 (Nicklin *et al.*, 2009).

MYC is known to strongly upregulate mitochondrial biogenesis by transactivating genes that encode mitochondrial proteins and binding at the promoter of transcription factor A, mitochondrial (*TFAM*), a mitochondrial DNA replication factor (Li *et al.*, 2005). While high MYC expression might be advantageous in terms of promoting the BL-like expansion of the newly infected cells and overcoming immune killing, it also sensitizes the cells to apoptosis (Cutrona *et al.*, 1995; Kelly *et al.*, 2009; McMahon, 2014), which is transiently mitigated by the virus-encoded BCL-2 molecules BHRF1 and BALF1 (Altmann and Hammerschmidt, 2005) and EBNA3A-induced host-encoded MCL-1 and BCL-2 (Price *et al.*, 2017). Expression of LMP1 and

LMP2A to drive pro-survival NF-κB and PI3K/AKT signaling likely reduces the apoptosis sensitivity of the newly infected cells, akin to the way follicular T helper cells and follicular dendritic cells rescue germinal center B-cells from 'death by neglect' (Hennino *et al.*, 2001; Rathmell and Thompson, 2002). In support of that idea, CD40L treatment of MYC-overexpressing cells reduced the propensity of the cells to undergo apoptosis (Cutrona *et al.*, 1995). Dampening of MYC-induced mitochondrial biogenesis at later time points could also be observed in our proteomic dataset; TFAM and peroxisome proliferator-activated receptor gamma coactivator 1-alpha (PGC-1α), a master regulator of mitochondrial biogenesis and oxidative function (Cunningham *et al.*, 2007), both decreased in abundance to a lower, non-zero set point over the infection time course (data not shown). Further, de novo infection of B-cells appears to skew mitochondrial biogenesis towards a fission phenotype over time, with the fission-promoting proteins mitofusin-1 (MFN1) and dynamin-1 like (DNM1L) increasing in abundance and the fusion-promoting factor optic atrophy protein 1 (OPA1) protein decreasing in abundance (data not shown). Notably, the expression kinetics of these fission/fusion regulators do not strictly track with MYC expression. In an earlier published dataset, there was no detectable change in expression of these genes with MYC loss in P493-6 cells (Li *et al.*, 2005). Finally, LMP1 and LMP2A both have well-characterized roles in the upregulation of glycolysis and OXPHOS in EBV-infected cells, even in the presence of transformed cell-level MYC (Chen *et al.*, 2010; DeKroon *et al.*, 2018; Lambert and Martinez, 2007; Minamitani *et al.*, 2017; Wakisaka *et al.*, 2004; Yun, Kim and Hur, 2019; Zhang *et al.*, 2017b). Taken together, while MYC is likely the primary driver of aerobic glycolysis and OXPHOS (Graves *et al.*, 2012) in early infection, NF-κB and mTOR pathways function as co-organizers of those pathways in the LCL state. There is a clear advantage to the virus in coupling the germinal center survival signals LMP1 and LMP2A with an appropriate mode of metabolism that avoids excessive proliferation which may elicit host immune cytotoxic responses and/or induce potential dysregulation of normal lymphoid tissue architecture and function.

The same paradigm applies to the other metabolic pathways described in this work i.e. 1C metabolism, DNSS, and mevalonate and lipid biosyntheses. EBNA2 and its target gene MYC activate these pathways early in infection as well as in the LCL state (Li *et al.*, 2005; Zeller *et al.*, 2003; Zeller *et al.*, 2006). However, the maintenance of the pathways in EBV-positive transformed cells is also significantly co-regulated by other non-MYC transcription factors. LCL induction of a genetically encoded dominant negative IκBα (ΔN-IκBα) (Cahir-McFarland *et al.*, 2000; Sommermann *et al.*, 2011) ablated cellular expression of SHMT2 and MTHFD2 (data not shown). SREBP inhibition by fatostatin treatment of newly infected cells or SCAP CRISPR ablation in LCLs diminished the expression of cholesterogenic and lipogenic genes as expected. However, SCAP CRISPR also led to an unexpected loss of MYC in our hands, suggesting interplay and likely positive feedback between the two pathways in LCLs. Curiously, P3HR-1 BL cells did not suffer proliferative defects with SCAP ablation despite expressing much higher levels of MYC (Ma *et al.*, 2017c), indicating that, in contrast to latency III-expressing LCLs, there is functional uncoupling between MYC and the SCAP/SREBP axis in latency I-expressing BL cells.

Many of the metabolic phenomena reported in this work are underpinned by mTOR-mediated pathways. Rapamycin treatment of newly infected cells and LCLs alike significantly reduced the expression of SHMT2, MTHFD2 and FASN (data not shown), which we have shown to also be MYC-dependent in this work. Our observations agree with previously published data that high mTOR activity is required for successful outgrowth and that cell cycle arrest in newly infected cells can be attributed to defects in mTOR signaling and autophagic flux (McFadden *et al.*, 2016). To add to the complexity of these regulatory networks, the protein abundance of PDCD4, a known substrate of the mTOR pathway effector S6K1 (Dorrello *et al.*, 2006) and a negative regulator of eukaryotic translation initiation factor 4A (eIF4A) (Suzuki *et al.*, 2008; Yang *et al.*, 2003), was significantly downregulated over the course of infection, which may augment cap-

dependent translation of MYC protein (Wolfe *et al.*, 2014) downstream of EBNA2. Thus, MYC, NF-κB and mTOR cross-regulate and collaborate to varying extents over the course of cellular transformation to achieve specific evolutionary objectives, namely successful colonization of the immunocompetent host at early time points and long-term maintenance of virus carriage at late time points.

Additional roles for mitochondrial 1C and mevalonate metabolism

In this work, we describe the main function of mitochondrial 1C metabolism as being a key source of 1C units for purine and thymidylate synthesis. Yet, we also found important roles for intramitochondrial NADPH and glutathione in maintaining the proliferative capacity and viability of EBV-infected cells; these metabolites may contribute to functions beyond the sustenance of in vitro transformation. How might intramitochondrial NADPH and glutathione be important? In our analysis, we observed that mitochondrial fatty acid synthesis was also strongly upregulated early in infection. It is possible that intramitochondrial NADPH might be directed towards the reduction of acyl carrier protein (ACP)-conjugated acyl chains for the production of larger lipid molecules, such as lipoic acid, which are crucial for respiratory chain function. In fact, when we performed C75 (a small-molecule inhibitor of cytosolic and mitochondrial fatty acid synthases) treatment (Kuhajda *et al.*, 2000; Chen *et al.*, 2014) of newly infected cells and LCL CRISPR KO of lipoic acid synthase (LIAS), we detected proliferative defects and loss of oxidative capacity (data not shown). Iron-sulfur (Fe-S) cluster-containing proteins, which feature prominently in the mitochondrial ETC, require lipoic acid and glutathione for proper function (Van Vranken *et al.*, 2016; Paul and Lill, 2014). These are consistent with the observed sensitivity of EBV-infected cells to mitochondrial ETC poisons and MitoTPNOX-mediated wasting of intramitochondrial NADPH.

While EBV infection induces mevalonate metabolism, the transformation-crucial activity lies in the production of GGPP. Isoprenoid synthesis is much less dependent on NADPH than de novo

cholesterol synthesis from squalene; FPP conversion to GGPP does not require NADPH input while chemical transformation of each mevalonate molecule into cholesterol requires 20 NADPH. Virus-induced upregulation of LDLR likely also allows the cell to survive by cholesterol scavenging even in the presence of statins (Goldstein and Brown, 2015; Uauy *et al.*, 1988). These are consistent with our observations that cytosolic expression of TPNOX, which likely prevents efficient reduction of acetyl-CoA to cholesterol, had no effect on LCL proliferation and survival.

Recently, S-geranylgeranyl-L-glutathione (GGG) has been described to be important for germinal center B-cell confinement (Lu *et al.*, 2019). Given that both GGPP and glutathione production are highly induced during EBV infection, GGG would likely be made at high levels and, in theory, cause confinement of EBV-infected B-cells to the germinal center by binding P2RY purinoreceptor family members. However, the virus has apparently evolved to bypass this checkpoint event by downregulating surface P2RY10 and the signal transducing GTPase protein Gα13 (data not shown), likely enabling the infected cell to undergo GC egress more effectively even in the presence of a confinement-inducing molecule. In addition, the downmodulation of Gα13 expression also confers a cell-intrinsic growth advantage to the infected cell; re-expression of Gα13 via lentiviral transduction caused rapid, profound, caspase-dependent cell death (data not shown), consistent with previously published work where multiple B-cell cancers carry inactivating mutations of Gα13 to stymie its tumor suppressor function (O'Hayre *et al.*, 2016).

Concluding Remarks

The evolutionary success of EBV can be attributed to its ability to subvert host B-cell physiological processes to maintain its long-term carriage. In the absence of a competent immune system, its immense potential to grow and survive is realized, leading to unchecked proliferation that culminates in lymphoproliferative disorders. The latent capacity of the infected

B-cell to expand so rapidly is undergirded by viral oncoprotein-guided remodeling of cellular and organellar metabolism to mimic normal B-cell physiology. To support B-cell proliferation and survival, virus-encoded EBNA2 and LMPs have evolved to hijack host transcription factors such as MYC and SREBPs to mediate potent activation of myriad metabolic programs, including glycolysis, mitochondrial 1C metabolism, DNSS, and cholesterol and lipid biosyntheses. These pathways enable the generation and utilization of key intermediates and reducing power that are needed for assembling complex molecules, such as nucleic acids, proteins and signaling molecules e.g. GGPP and palmitate, that support B-cell reorganization and growth.

Appendices

Table S1 Full details of enriched terms in Figure II.7.

Category	Enriched term	Parent term, where re-assigned	Fold Enrichment	Benjamini p-value
UP_KEYWORDS	Cell cycle		3.8	2.22E-34
UP_KEYWORDS	Nucleotide-binding		2.4	7.38E-30
UP_KEYWORDS	DNA replication		9.2	8.96E-27
GOTERM_BP_DIRECT	Sister chromatid cohesion	Cell cycle	5.5	3.15E-11
UP_KEYWORDS	DNA repair		3.1	1.98E-09
GOTERM_BP_DIRECT	Cell-cell adhesion		2.6	5.61E-05
UP_KEYWORDS	Helicase	Nucleotide-binding	5.0	5.02E-13
GOTERM_BP_DIRECT	DNA damage response, detection of DNA damage	DNA repair	7.8	3.91E-07
UP_KEYWORDS	Nucleotidyl-transferase	DNA replication	4.6	7.92E-06
GOTERM_CC_DIRECT	MCM complex	DNA replication	19.6	2.27E-08
INTERPRO	IPR003593:AAA + ATPase domain	AAA+ ATPase domain	3.1	0.001799134
UP_KEYWORDS	Antiviral defense		4.9	3.95E-10
INTERPRO	Tetratricopeptide-like helical	Tetratricopeptide-like helical domain	2.9	6.16E-05
INTERPRO	Kinesin, motor domain	Cell cycle	5.3	0.001351141

Table S1 (Continued)

UP_SEQ_FEATURE	domain:RAP	Nucleoside binding	17.3	0.013212799
GOTERM_MF_DIRECT	GTP binding	Nucleotide-binding	2.1	4.09E-04
UP_KEYWORDS	DNA condensation	Cell cycle	10.6	2.21E-04
GOTERM_BP_DIRECT	Anaphase-promoting complex-dependent catabolic process	Cell cycle	4.0	3.72E-04
GOTERM_CC_DIRECT	Alpha DNA polymerase: primase complex	DNA replication	19.6	4.59E-05
GOTERM_BP_DIRECT	Regulation of ubiquitin-protein ligase activity involved in mitotic cell cycle	Cell cycle	6.5	0.008330793
GOTERM_CC_DIRECT	SMN complex	mRNA processing	10.6	4.34E-04
UP_KEYWORDS	Purine biosynthesis	Nucleotide metabolism	11.4	1.35E-04
GOTERM_BP_DIRECT	tRNA processing		5.6	0.001423696
UP_KEYWORDS	Glutamine amido-transferase		9.4	0.037576209
INTERPRO	Armadillo-like helical		2.7	4.78E-04
UP_KEYWORDS	4Fe-4S	Metal binding	5.1	0.001925796
SMART	DSRM	Nucleoside binding	7.2	0.039491156
UP_KEYWORDS	DNA-directed RNA polymerase		4.9	0.002725971

Table S1 (Continued)

GOTERM_BP_DIRECT	Mismatch repair	DNA repair	4.8	0.020222815
GOTERM_BP_DIRECT	Nucleobase-containing small molecule interconversion	Nucleotide metabolism	6.8	0.00240859
KEGG_PATHWAY	p53 signaling pathway	Cell cycle	3.9	4.25E-04
UP_KEYWORDS	Protein biosynthesis		2.8	8.11E-04
GOTERM_BP_DIRECT	tRNA aminoacylation for protein translation	Protein biosynthesis	4.2	0.045821171
GOTERM_BP_DIRECT	Negative regulation of ubiquitin-protein ligase activity involved in mitotic cell cycle	Cell cycle	3.7	0.005388012
UP_KEYWORDS	Mitochondrion		2.5	1.24E-20
GOTERM_CC_DIRECT	Mitochondrial small ribosomal subunit	Mitochondrion	9.4	5.84E-07
UP_KEYWORDS	Cholesterol biosynthesis		10.0	1.21E-05
GOTERM_BP_DIRECT	Protein import into mitochondrial matrix	Mitochondrion	9.9	1.32E-04
UP_KEYWORDS	Mitochondrion nucleoid	Mitochondrion	8.2	9.60E-04
UP_KEYWORDS	One-carbon metabolism		6.2	0.037422669
UP_KEYWORDS	Serine biosynthesis		21.2	0.034673098

Table S2 Full details of "Mitochondrion" enriched clusters and their components amongst upregulated proteins in Figure II.22. The leftmost column contains the protein's Uniprot accession numbers. The middle column contains the protein's symbols. The rightmost column contains the full names of the proteins. Bold text indicates the enriched clusters and the associated p-values.

Ribosome, 6.6 fold enrichment, p=1.4e-5

P82912	MRPS11	28S ribosomal protein S11, mitochondrial
P82914	MRPS15	28S ribosomal protein S15, mitochondrial
Q9NZE8	MRPL35	39S ribosomal protein L35, mitochondrial
Q9Y2R9	MRPS7	28S ribosomal protein S7, mitochondrial
Q9Y2R5	MRPS17	28S ribosomal protein S17, mitochondrial
P82675	MRPS5	28S ribosomal protein S5, mitochondrial
P82664	MRPS10	28S ribosomal protein S10, mitochondrial
P82932	MRPS6	28S ribosomal protein S6, mitochondrial
Q7Z7H8	MRPL10	Isoform 2 of 39S ribosomal protein L10, mitochondrial
Q9Y3D3	MRPS16	28S ribosomal protein S16, mitochondrial
P82933	MRPS9	28S ribosomal protein S9, mitochondrial
P82921	MRPS21	28S ribosomal protein S21, mitochondrial
O60783	MRPS14	28S ribosomal protein S14, mitochondrial

One-carbon metabolism, 31.9 fold enrichment, p=1.5e-5

Q3SY69	ALDH1L2	Mitochondrial 10-formyltetrahydrofolate dehydrogenase
P13995	MTHFD2	Bifunctional methylenetetrahydrofolate dehydrogenase/cyclohydrolase, mitochondrial
F5H2F4	MTHFD1	C-1-tetrahydrofolate synthase, cytoplasmic
P34896	SHMT1	Serine hydroxymethyltransferase, cytosolic
P34897	SHMT2	Serine hydroxymethyltransferase, mitochondrial
Q6UB35	MTHFD1L	Monofunctional C1-tetrahydrofolate synthase, mitochondrial
P11586	MTHFD1	C-1-tetrahydrofolate synthase, cytoplasmic

Table S2 (Continued)

Fatty acid metabolism, 7.2 fold enrichment, p=1.1e-4

Q13085	ACACA	Isoform 4 of Acetyl-CoA carboxylase 1
P11310	ACADM	Isoform 2 of Medium-chain specific acyl-CoA dehydrogenase, mitochondrial
Q9UKG9	CROT	Isoform 3 of Peroxisomal carnitine O-octanoyltransferase
P49327	FASN	Fatty acid synthase
Q8IVS2	MCAT	Malonyl-CoA-acyl carrier protein transacylase, mitochondrial
Q53FZ2	ACSM3	Acyl-coenzyme A synthetase ACSM3, mitochondrial
P33121	ACSL1	Long-chain-fatty-acid--CoA ligase 1
O60488	ACSL4	Long-chain-fatty-acid--CoA ligase 4
Q08426	EHHADH	Peroxisomal bifunctional enzyme
Q15067	ACOX1	Peroxisomal acyl-coenzyme A oxidase 1

Fatty acid biosynthesis, 26.6 fold enrichment, p=3.5e-4

Q13085	ACACA	Isoform 4 of Acetyl-CoA carboxylase 1
P49327	FASN	Fatty acid synthase
Q8IVS2	MCAT	Malonyl-CoA-acyl carrier protein transacylase, mitochondrial
P33121	ACSL1	Long-chain-fatty-acid--CoA ligase 1
O60488	ACSL4	Long-chain-fatty-acid--CoA ligase 4

Cellular respiration, 22.6 fold enrichment, p=3.5e-4

Q14CZ7	FASTKD3	FAST kinase domain-containing protein 3
Q969Z0	TBRG4	Protein TBRG4
Q9NYY8	FASTKD2	FAST kinase domain-containing protein 2
Q7L8L6	FASTKD5	FAST kinase domain-containing protein 5
Q53R41	FASTKD1	FAST kinase domain-containing protein 1
Q9UJS0	SLC25A13	Isoform 2 of Calcium-binding mitochondrial carrier protein Aralar2

NADP, 5.3 fold enrichment, p=4.2e-4

Q3SY69	ALDH1L2	Mitochondrial 10-formyltetrahydrofolate dehydrogenase
Q15392	DHCR24	Delta(24)-sterol reductase
Q96C36	PYCR2	Pyrroline-5-carboxylate reductase 2
F5H2F4	MTHFD1	C-1-tetrahydrofolate synthase, cytoplasmic
P49327	FASN	Fatty acid synthase
P32322	PYCR1	Pyrroline-5-carboxylate reductase 1, mitochondrial
P54886	ALDH18A1	Delta-1-pyrroline-5-carboxylate synthase
P48163	ME1	NADP-dependent malic enzyme
P35270	SPR	Sepiapterin reductase
P22570	FDXR	Isoform 3 of NADPH:adrenodoxin oxidoreductase, mitochondrial
P11586	MTHFD1	C-1-tetrahydrofolate synthase, cytoplasmic
Q6IAN0	DHRS7B	Dehydrogenase/reductase SDR family member 7B

Table S2 (Continued)

Biosynthesis of amino acids, 7.5 fold enrichment, p=9.3e-4

P11498	PC	Pyruvate carboxylase, mitochondrial
P30613	PKLR	Pyruvate kinase PKLR
Q96C36	PYCR2	Pyrroline-5-carboxylate reductase 2
P34896	SHMT1	Serine hydroxymethyltransferase, cytosolic
P34897	SHMT2	Serine hydroxymethyltransferase, mitochondrial
P32322	PYCR1	Pyrroline-5-carboxylate reductase 1, mitochondrial
P54886	ALDH18A1	Delta-1-pyrroline-5-carboxylate synthase
P49419	ALDH7A1	Alpha-aminoadipic semialdehyde dehydrogenase

Lipid metabolism, 5.7 fold enrichment, p=0.011

Q709F0	ACAD11	Acyl-CoA dehydrogenase family member 11
Q13085	ACACA	Isoform 4 of Acetyl-CoA carboxylase 1
P11310	ACADM	Isoform 2 of Medium-chain specific acyl-CoA dehydrogenase, mitochondrial
Q53FZ2	ACSM3	Acyl-coenzyme A synthetase ACSM3, mitochondrial
P33121	ACSL1	Long-chain-fatty-acid--CoA ligase 1
O60488	ACSL4	Long-chain-fatty-acid--CoA ligase 4
Q6JQN1	ACAD10	Isoform 5 of Acyl-CoA dehydrogenase family member 10

Fatty acid beta-oxidation, 12.6 fold enrichment, p=1.0e-4

Q709F0	ACAD11	Acyl-CoA dehydrogenase family member 11
P11310	ACADM	Isoform 2 of Medium-chain specific acyl-CoA dehydrogenase, mitochondrial
Q9UKG9	CROT	Isoform 3 of Peroxisomal carnitine O-octanoyltransferase
O43808	SLC25A17	Peroxisomal membrane protein PMP34
Q08426	EHHADH	Peroxisomal bifunctional enzyme
Q6JQN1	ACAD10	Isoform 5 of Acyl-CoA dehydrogenase family member 10
Q15067	ACOX1	Peroxisomal acyl-coenzyme A oxidase 1

Glycine, serine and threonine metabolism, 10.6 fold enrichment, p=0.002

P23378	GLDC	Glycine dehydrogenase (decarboxylating), mitochondrial
P34896	SHMT1	Serine hydroxymethyltransferase, cytosolic
P34897	SHMT2	Serine hydroxymethyltransferase, mitochondrial
P50440	GATM	Isoform 2 of Glycine amidinotransferase, mitochondrial
P49419	ALDH7A1	Alpha-aminoadipic semialdehyde dehydrogenase
P13196	ALAS1	5-aminolevulinate synthase, nonspecific, mitochondrial

Table S2 (Continued)

Peptidase M16 domain, 47.8 fold enrichment, p=0.0056

Q10713	PMPCA	Mitochondrial-processing peptidase subunit alpha
O75439	PMPCB	Mitochondrial-processing peptidase subunit beta
O43847	NRD1	Isoform 2 of Nardilysin
P14735	IDE	Insulin-degrading enzyme

Mitochondrial inner membrane translocase subunit Tim17/Tim22/Tim23/peroxisomal protein PMP24, 41.8 fold enrichment, p=0.0063

O60830	TIMM17B	Isoform 2 of Mitochondrial import inner membrane translocase subunit Tim17-B
O14925	TIMM23	Mitochondrial import inner membrane translocase subunit Tim23
Q99595	TIMM17A	Mitochondrial import inner membrane translocase subunit Tim17-A
Q9NPL8	TIMMDC1	Complex I assembly factor TIMMDC1, mitochondrial

Glycolysis / Gluconeogenesis, 7.2 fold enrichment, p=0.0034

P51648	ALDH3A2	Isoform 2 of Fatty aldehyde dehydrogenase
P30613	PKLR	Pyruvate kinase PKLR
P52789	HK2	Hexokinase-2
P06744	GPI	Isoform 2 of Glucose-6-phosphate isomerase
P07195	LDHB	L-lactate dehydrogenase B chain
P49419	ALDH7A1	Alpha-aminoadipic semialdehyde dehydrogenase
P05091	ALDH2	Aldehyde dehydrogenase, mitochondrial

Table S3 GSEA re-analysis of metabolism-related proteins detected in the transformation QTV. Blue highlights the processes of interest.

Category	Term	Fold Enrichment	Benjamini p-value
UP_KEYWORDS	Cholesterol biosynthesis	28.08503	5.97E-09
UP_KEYWORDS	Purine biosynthesis	29.78715	5.70E-07
UP_KEYWORDS	Dioxygenase	9.535041	2.29E-06
UP_KEYWORDS	Transmembrane helix	1.951802	4.53E-06
UP_KEYWORDS	ATP-binding	2.296673	4.69E-06
UP_KEYWORDS	Mitochondrion	2.267735	1.66E-05
UP_KEYWORDS	One-carbon metabolism	23.40419	3.13E-05
UP_KEYWORDS	Allosteric enzyme	11.7021	3.87E-05
UP_KEYWORDS	Pyridoxal phosphate	11.01374	5.72E-05
UP_KEYWORDS	Metal-binding	1.690851	1.26E-04
UP_SEQ_FEATURE	Transmembrane region	2.042524	1.84E-04
GOTERM_BP_DIRECT	Glutamine metabolic process	18.21932	2.01E-04
GOTERM_BP_DIRECT	Nucleobase-containing small molecule interconversion	18.21932	2.01E-04
GOTERM_BP_DIRECT	Amino acid transport	20.42165	7.29E-04
GOTERM_BP_DIRECT	Amino acid transport	20.42165	7.29E-04
UP_KEYWORDS	NAD	4.812077	7.30E-04
GOTERM_BP_DIRECT	Cellular amino acid biosynthetic process	17.69877	1.28E-03
GOTERM_BP_DIRECT	L-serine biosynthetic process	44.24691	3.73E-03
UP_KEYWORDS	Fatty acid metabolism	5.34953	5.02E-03
INTERPRO	2-5-oligoadenylate synthetase, conserved site	45.28313	6.67E-03
GOTERM_BP_DIRECT	Transport	4.213992	8.10E-03

Table S4 Full details of enriched terms as shown in Table S3. The left column contains the Uniprot accession numbers for the enriched proteins. The right column contains the symbols for the enriched proteins. Bold text indicates the enriched terms.

Cholesterol biosynthesis	
P14324	FDPS
Q01581	HMGCS1
Q15738	NSDHL
Q16850	CYP51A1
Q13907	IDI1
Q9UBM7	DHCR7
Q03426	MVK
P04035	HMGCR
P37268	FDFT1
Purine biosynthesis	
P20839	IMPDH1
P22234	PAICS
P22102	GART
P30520	ADSS
P12268	IMPDH2
P49915	GMPS
P11586	MTHFD1
Dioxygenase	
P41229	KDM5C
Q02809	PLOD1
Q9BV57	ADI1
Q13686	ALKBH1
O00625	PIR
P13674	P4HA1
Q8N543	OGFOD1
Q6N021	TET2
O43151	TET3
Q9H3R0	KDM4C
O60568	PLOD3

Table S4 (Continued)

Transmembrane helix

P36551	CPOX
P01130	LDLR
Q96BD0	SLCO4A1
Q9NS00	C1GALT1
Q92536	SLC7A6
P14324	FDPS
Q15070	OXA1L
Q15758	SLC1A5
P49961	ENTPD1
Q8TB61	SLC35B2
O43808	SLC25A17
P05023	ATP1A1
O15269	SPTLC1
Q96HS1	PGAM5
Q14534	SQLE
Q5T8D3	ACBD5
Q8IZK6	MCOLN2
P30825	SLC7A1
P04035	HMGCR
P23921	RRM1
Q8N8Q8	COX18
O15270	SPTLC2
Q9H936	SLC25A22
Q8WUM9	SLC20A1
Q9P0S2	COX16
Q9BRQ8	AIFM2
Q9Y6K5	OAS3
Q16850	CYP51A1
P52429	DGKE
P16615	ATP2A2
Q643R3	LPCAT4
Q15738	NSDHL
P06756	ITGAV
P22102	GART
P08195	SLC3A2
Q9H2D1	SLC25A32
P37268	FDFT1
Q9UJS0	SLC25A13
P98194	ATP2C1
Q9BW60	ELOVL1
P43007	SLC1A4
Q9UBM7	DHCR7

Table S4 (Continued)

Transmembrane helix	
O15247	CLIC2
P00338	LDHA
P54709	ATP1B3
Q9UBX3	SLC25A10
Q99808	SLC29A1
Q96CU9	FOXRED1
Q9H2H9	SLC38A1
Q9HBU6	ETNK1
Q96G23	CERS2
O95864	FADS2
P53985	SLC16A1
Q5SRI9	MANEA
Q9H7F0	ATP13A3
A1L0T0	ILVBL
ATP-binding	
P17812	CTPS1
P00973	OAS1
Q9Y6K5	OAS3
Q01813	PFKP
P30613	PKLR
P31153	MAT2A
P49915	GMPS
P52429	DGKE
Q9GZT4	SRR
Q6UB35	MTHFD1L
P29728	OAS2
P16615	ATP2A2
P11586	MTHFD1
Q9UG63	ABCF2
Q96EY8	MMAB
P22392	NME2
P22102	GART
P08243	ASNS
P49961	ENTPD1
P27708	CAD
P52789	HK2
P05023	ATP1A1
Q16877	PFKFB4
P04183	TK1
Q9NQX3	GPHN
P98194	ATP2C1

Table S4 (Continued)

ATP-binding	
Q9BZX2	UCK2
Q86V21	AACS
P00966	ASS1
Q03426	MVK
P54886	ALDH18A1
P15531	NME1
P27144	AK4
P23921	RRM1
Q13085	ACACA
P22234	PAICS
Q9H999	PANK3
Q9HBU6	ETNK1
P08237	PFKM
Q53FZ2	ACSM3
O00746	NME4
Q9H7F0	ATP13A3
Mitochondrion	
P00973	OAS1
Q13686	ALKBH1
P36551	CPOX
Q6UB35	MTHFD1L
P29728	OAS2
Q96EY8	MMAB
Q15070	OXA1L
Q9Y375	NDUFAF1
Q9H2D1	SLC25A32
P52789	HK2
P32322	PYCR1
Q8IVS2	MCAT
Q86YH6	PDSS2
P50440	GATM
O43766	LIAS
Q9UJS0	SLC25A13
Q96HS1	PGAM5
Q96C36	PYCR2
P13995	MTHFD2
O94925	GLS
P34897	SHMT2
Q9UBX3	SLC25A10
P54886	ALDH18A1
Q96CU9	FOXRED1

Table S4 (Continued)

Mitochondrion	
P04181	OAT
P27144	AK4
O43819	SCO2
Q7L5Y1	ENOSF1
Q16762	TST
Q8N8Q8	COX18
Q9P0S2	COX16
Q9H936	SLC25A22
P36639	NUDT1
Q53FZ2	ACSM3
O00746	NME4
Q14061	COX17
Q9BRQ8	AIFM2
O00154	ACOT7
P53701	HCCS
One-carbon metabolism	
P13995	MTHFD2
P31153	MAT2A
P34897	SHMT2
Q6UB35	MTHFD1L
P11586	MTHFD1
P00374	DHFR
Allosteric enzyme	
Q13085	ACACA
P23921	RRM1
Q01813	PFKP
P30613	PKLR
P08237	PFKM
P52789	HK2
P27708	CAD
Q9GZT4	SRR

Table S4 (Continued)

Pyridoxal phosphate	
O15269	SPTLC1
Q9Y617	PSAT1
Q6P996	PDXDC1
P34897	SHMT2
P49327	FASN
O15270	SPTLC2
Q9GZT4	SRR
P04181	OAT
Metal-binding	
P00973	OAS1
P30613	PKLR
Q9NS00	C1GALT1
P31153	MAT2A
P12268	IMPDH2
Q8N543	OGFOD1
Q15181	PPA1
Q9GZT4	SRR
P31350	RRM2
P14324	FDPS
P05023	ATP1A1
Q86UY8	NT5DC3
P16930	FAH
P04183	TK1
Q9NQX3	GPHN
O00625	PIR
O43151	TET3
Q9H3R0	KDM4C
P47712	PLA2G4A
Q9BV57	ADI1
P20839	IMPDH1
Q7L5Y1	ENOSF1
P08237	PFKM
Q8WV74	NUDT8
Q6N021	TET2
O76003	GLRX3
P36639	NUDT1
Q14061	COX17
P78330	PSPH
P41229	KDM5C
Q9Y6K5	OAS3
Q13686	ALKBH1

Table S4 (Continued)

Metal-binding

Q01813	PFKP
Q16850	CYP51A1
P30520	ADSS
P52429	DGKE
P29728	OAS2
P16615	ATP2A2
O60568	PLOD3
O00754	MAN2B1
P22392	NME2
P06756	ITGAV
P22102	GART
Q13907	IDI1
P27708	CAD
Q9BQG2	NUDT12
O43766	LIAS
Q9UJS0	SLC25A13
Q02809	PLOD1
P98194	ATP2C1
P15531	NME1
Q13085	ACACA
O43819	SCO2
P13674	P4HA1
Q53FZ2	ACSM3
O00746	NME4
Q9H857	NT5DC2
Q9H7F0	ATP13A3
P53701	HCCS
A1L0T0	ILVBL

Transmembrane region

Q16850	CYP51A1
P01130	LDLR
Q96BD0	SLCO4A1
Q9NS00	C1GALT1
Q92536	SLC7A6
P52429	DGKE
P16615	ATP2A2
Q643R3	LPCAT4
Q15738	NSDHL
Q15758	SLC1A5
Q15070	OXA1L
P06756	ITGAV

Table S4 (Continued)

Transmembrane region

P08195	SLC3A2
P49961	ENTPD1
Q9H2D1	SLC25A32
Q8TB61	SLC35B2
P05023	ATP1A1
O43808	SLC25A17
P37268	FDFT1
Q9UJS0	SLC25A13
P98194	ATP2C1
O15269	SPTLC1
Q96HS1	PGAM5
Q9BW60	ELOVL1
Q14534	SQLE
Q5T8D3	ACBD5
O15247	CLIC2
Q9UBM7	DHCR7
P43007	SLC1A4
Q8IZK6	MCOLN2
P54709	ATP1B3
P30825	SLC7A1
Q9UBX3	SLC25A10
P04035	HMGCR
Q99808	SLC29A1
Q96CU9	FOXRED1
Q9H2H9	SLC38A1
Q96G23	CERS2
O95864	FADS2
P53985	SLC16A1
Q8N8Q8	COX18
Q5SRI9	MANEA
O15270	SPTLC2
Q9P0S2	COX16
Q8WUM9	SLC20A1
Q9H936	SLC25A22
Q9H7F0	ATP13A3
Q9BRQ8	AIFM2
A1L0T0	ILVBL

Table S4 (Continued)

Glutamine metabolic process

P17812	CTPS1
Q06210	GFPT1
P08243	ASNS
O94925	GLS
P27708	CAD
P49915	GMPS
O43175	PHGDH

Nucleobase-containing small molecule interconversion

P17812	CTPS1
P23921	RRM1
P27144	AK4
P22392	NME2
O00746	NME4
P31350	RRM2
P15531	NME1

Amino acid transport

Q9H2H9	SLC38A1
Q15758	SLC1A5
P08195	SLC3A2
P43007	SLC1A4
P30825	SLC7A1
Q92536	SLC7A6

NAD

Q15738	NSDHL
P20839	IMPDH1
Q9NPH2	ISYNA1
P13995	MTHFD2
Q6NUM9	RETSAT
P00338	LDHA
P49327	FASN
P12268	IMPDH2
Q9BQG2	NUDT12
P07195	LDHB
O43175	PHGDH

Table S4 (Continued)

Cellular amino acid biosynthetic process	
P08243	ASNS
Q96C36	PYCR2
O94925	GLS
P32322	PYCR1
P54886	ALDH18A1
P04181	OAT
L-serine biosynthetic process	
Q9Y617	PSAT1
P34897	SHMT2
O43175	PHGDH
P78330	PSPH
Fatty acid metabolism	
Q86V21	AACS
Q13085	ACACA
Q9BW60	ELOVL1
O95864	FADS2
P49327	FASN
Q8IVS2	MCAT
Q53FZ2	ACSM3
Q15067	ACOX1
2-5-oligoadenylate synthetase, conserved site	
Q9Y6K5	OAS3
P00973	OAS1
Q15646	OASL
P29728	OAS2
Transport	
Q5T8D3	ACBD5
O15247	CLIC2
Q9H2D1	SLC25A32
P54709	ATP1B3
P30825	SLC7A1
Q92536	SLC7A6
Q9UBX3	SLC25A10
Q8WUM9	SLC20A1
Q9H936	SLC25A22
O43808	SLC25A17
Q9UG63	ABCF2
Q9UJS0	SLC25A13

References

Acuna-Hidalgo, R., Schanze, D., Kariminejad, A., Nordgren, A., Kariminejad, M. H., Conner, P., Grigelioniene, G., Nilsson, D., Nordenskjöld, M., Wedell, A., Freyer, C., Wredenberg, A., Wieczorek, D., Gillessen-Kaesbach, G., Kayserili, H., Elcioglu, N., Ghaderi-Sohi, S., Goodarzi, P., Setayesh, H., van de Vorst, M., Steehouwer, M., Pfundt, R., Krabichler, B., Curry, C., MacKenzie, M. G., Boycott, K. M., Gilissen, C., Janecke, A. R., Hoischen, A. and Zenker, M. (2014) 'Neu-Laxova syndrome is a heterogeneous metabolic disorder caused by defects in enzymes of the L-serine biosynthesis pathway', *Am J Hum Genet,* 95(3), pp. 285-93.

Adamus, A., Muller, P., Nissen, B., Kasten, A., Timm, S., Bauwe, H., Seitz, G. and Engel, N. (2018) 'GCSH antisense regulation determines breast cancer cells' viability', *Sci Rep,* 8(1), pp. 15399.

Ageberg, M., Rydström, K., Lindén, O., Linderoth, J., Jerkeman, M. and Drott, K. (2011) 'Inhibition of geranylgeranylation mediates sensitivity to CHOP-induced cell death of DLBCL cell lines', *Exp Cell Res,* 317(8), pp. 1179-91.

Alfieri, C., Birkenbach, M. and Kieff, E. (1991) 'Early events in Epstein-Barr virus infection of human B lymphocytes', *Virology,* 181(2), pp. 595-608.

Allevato, M., Bolotin, E., Grossman, M., Mane-Padros, D., Sladek, F. M. and Martinez, E. (2017) 'Sequence-specific DNA binding by MYC/MAX to low-affinity non-E-box motifs', *PLoS One,* 12(7), pp. e0180147.

Altmann, M. and Hammerschmidt, W. (2005) 'Epstein-Barr virus provides a new paradigm: a requirement for the immediate inhibition of apoptosis', *PLoS Biol,* 3(12), pp. e404.

Amemiya-Kudo, M., Shimano, H., Hasty, A. H., Yahagi, N., Yoshikawa, T., Matsuzaka, T., Okazaki, H., Tamura, Y., Iizuka, Y., Ohashi, K., Osuga, J., Harada, K., Gotoda, T., Sato, R., Kimura, S., Ishibashi, S. and Yamada, N. (2002) 'Transcriptional activities of nuclear SREBP-1a, -1c, and -2 to different target promoters of lipogenic and cholesterogenic genes', *J Lipid Res,* 43(8), pp. 1220-35.

Anagnostopoulos, I., Herbst, H., Niedobitek, G. and Stein, H. (1989) 'Demonstration of monoclonal EBV genomes in Hodgkin's disease and Ki-1-positive anaplastic large cell lymphoma by combined Southern blot and in situ hybridization', *Blood,* 74(2), pp. 810-6.

Anderson, D. D. and Stover, P. J. (2009) 'SHMT1 and SHMT2 are functionally redundant in nuclear de novo thymidylate biosynthesis', *PLoS One,* 4(6), pp. e5839.

Anderson, D. D., Woeller, C. F., Chiang, E. P., Shane, B. and Stover, P. J. (2012) 'Serine hydroxymethyltransferase anchors de novo thymidylate synthesis pathway to nuclear lamina for DNA synthesis', *J Biol Chem,* 287(10), pp. 7051-62.

Anderson, L. J. and Longnecker, R. (2008) 'EBV LMP2A provides a surrogate pre-B cell receptor signal through constitutive activation of the ERK/MAPK pathway', *J Gen Virol,* 89(Pt 7), pp. 1563-8.

Anighoro, A., Bajorath, J. and Rastelli, G. (2014) 'Polypharmacology: challenges and opportunities in drug discovery', *J Med Chem,* 57(19), pp. 7874-87.

Arvey, A., Tempera, I., Tsai, K., Chen, H. S., Tikhmyanova, N., Klichinsky, M., Leslie, C. and Lieberman, P. M. (2012) 'An atlas of the Epstein-Barr virus transcriptome and epigenome reveals host-virus regulatory interactions', *Cell Host Microbe,* 12(2), pp. 233-45.

Baer, R., Bankier, A. T., Biggin, M. D., Deininger, P. L., Farrell, P. J., Gibson, T. J., Hatfull, G., Hudson, G. S., Satchwell, S. C., Seguin, C. and et al. (1984) 'DNA sequence and expression of the B95-8 Epstein-Barr virus genome', *Nature,* 310(5974), pp. 207-11.

Baggott, J. E. and Tamura, T. (2015) 'Folate-Dependent Purine Nucleotide Biosynthesis in Humans', *Adv Nutr,* 6(5), pp. 564-71.

Bao, X. R., Ong, S. E., Goldberger, O., Peng, J., Sharma, R., Thompson, D. A., Vafai, S. B., Cox, A. G., Marutani, E., Ichinose, F., Goessling, W., Regev, A., Carr, S. A., Clish, C. B. and Mootha, V. K. (2016) 'Mitochondrial dysfunction remodels one-carbon metabolism in human cells', *Elife,* 5.

Ben-Sahra, I., Hoxhaj, G., Ricoult, S. J., Asara, J. M. and Manning, B. D. (2016) 'mTORC1 induces purine synthesis through control of the mitochondrial tetrahydrofolate cycle', *Science,* 351(6274), pp. 728-33.

Berberich, S., Hyde-DeRuyscher, N., Espenshade, P. and Cole, M. (1992) 'max encodes a sequence-specific DNA-binding protein and is not regulated by serum growth factors', *Oncogene,* 7(4), pp. 775-9.

Berndt, N., Hamilton, A. D. and Sebti, S. M. (2011) 'Targeting protein prenylation for cancer therapy', *Nat Rev Cancer,* 11(11), pp. 775-91.

Beroukhim, R., Mermel, C. H., Porter, D., Wei, G., Raychaudhuri, S., Donovan, J., Barretina, J., Boehm, J. S., Dobson, J., Urashima, M., Mc Henry, K. T., Pinchback, R. M., Ligon, A. H., Cho, Y. J., Haery, L., Greulich, H., Reich, M., Winckler, W., Lawrence, M. S., Weir, B. A., Tanaka, K. E., Chiang, D. Y., Bass, A. J., Loo, A., Hoffman, C., Prensner, J., Liefeld, T., Gao, Q., Yecies,

D., Signoretti, S., Maher, E., Kaye, F. J., Sasaki, H., Tepper, J. E., Fletcher, J. A., Tabernero, J., Baselga, J., Tsao, M. S., Demichelis, F., Rubin, M. A., Janne, P. A., Daly, M. J., Nucera, C., Levine, R. L., Ebert, B. L., Gabriel, S., Rustgi, A. K., Antonescu, C. R., Ladanyi, M., Letai, A., Garraway, L. A., Loda, M., Beer, D. G., True, L. D., Okamoto, A., Pomeroy, S. L., Singer, S., Golub, T. R., Lander, E. S., Getz, G., Sellers, W. R. and Meyerson, M. (2010) 'The landscape of somatic copy-number alteration across human cancers', *Nature,* 463(7283), pp. 899-905.

Berrios, C., Padi, M., Keibler, M. A., Park, D. E., Molla, V., Cheng, J., Lee, S. M., Stephanopoulos, G., Quackenbush, J. and DeCaprio, J. A. (2016) 'Merkel Cell Polyomavirus Small T Antigen Promotes Pro-Glycolytic Metabolic Perturbations Required for Transformation', *PLoS Pathog,* 12(11), pp. e1006020.

Birsoy, K., Wang, T., Chen, W. W., Freinkman, E., Abu-Remaileh, M. and Sabatini, D. M. (2015) 'An Essential Role of the Mitochondrial Electron Transport Chain in Cell Proliferation Is to Enable Aspartate Synthesis', *Cell,* 162(3), pp. 540-51.

Brugarolas, J., Lei, K., Hurley, R. L., Manning, B. D., Reiling, J. H., Hafen, E., Witters, L. A., Ellisen, L. W. and Kaelin, W. G., Jr. (2004) 'Regulation of mTOR function in response to hypoxia by REDD1 and the TSC1/TSC2 tumor suppressor complex', *Genes Dev,* 18(23), pp. 2893-904.

Bryant, J. D., Sweeney, S. R., Sentandreu, E., Shin, M., Ipas, H., Xhemalce, B., Momb, J., Tiziani, S. and Appling, D. R. (2018a) 'Deletion of the neural tube defect-associated gene', *J Biol Chem*.

Bryant, J. D., Sweeney, S. R., Sentandreu, E., Shin, M., Ipas, H., Xhemalce, B., Momb, J., Tiziani, S. and Appling, D. R. (2018b) 'Deletion of the neural tube defect-associated gene Mthfd1l disrupts one-carbon and central energy metabolism in mouse embryos', *J Biol Chem,* 293(16), pp. 5821-5833.

Cahir-McFarland, E. D., Davidson, D. M., Schauer, S. L., Duong, J. and Kieff, E. (2000) 'NF-kappa B inhibition causes spontaneous apoptosis in Epstein-Barr virus-transformed lymphoblastoid cells', *Proc Natl Acad Sci U S A,* 97(11), pp. 6055-60.

Calderwood, M. A., Holthaus, A. M. and Johannsen, E. (2008) 'The Epstein-Barr virus LF2 protein inhibits viral replication', *J Virol,* 82(17), pp. 8509-19.

Caldwell, R. G., Wilson, J. B., Anderson, S. J. and Longnecker, R. (1998) 'Epstein-Barr virus LMP2A drives B cell development and survival in the absence of normal B cell receptor signals', *Immunity,* 9(3), pp. 405-11.

Calvo, S. E., Clauser, K. R. and Mootha, V. K. (2016) 'MitoCarta2.0: an updated inventory of mammalian mitochondrial proteins', *Nucleic Acids Res,* 44(D1), pp. D1251-7.

Carbone, A. (2003) 'Emerging pathways in the development of AIDS-related lymphomas', *Lancet Oncol,* 4(1), pp. 22-9.

Carta, G., Murru, E., Banni, S. and Manca, C. (2017) 'Palmitic Acid: Physiological Role, Metabolism and Nutritional Implications', *Front Physiol,* 8, pp. 902.

Casey, P. J. and Seabra, M. C. (1996) 'Protein prenyltransferases', *J Biol Chem,* 271(10), pp. 5289-92.

Cen, O., Kannan, K., Huck Sappal, J., Yu, J., Zhang, M., Arikan, M., Ucur, A., Ustek, D., Cen, Y., Gordon, L. and Longnecker, R. (2018) 'Spleen Tyrosine Kinase Inhibitor TAK-659 Prevents Splenomegaly and Tumor Development in a Murine Model of Epstein-Barr Virus-Associated Lymphoma', *mSphere,* 3(4).

Cen, O. and Longnecker, R. (2015) 'Latent Membrane Protein 2 (LMP2)', *Curr Top Microbiol Immunol,* 391, pp. 151-80.

Chandrasekaran, S., Zhang, J., Sun, Z., Zhang, L., Ross, C. A., Huang, Y. C., Asara, J. M., Li, H., Daley, G. Q. and Collins, J. J. (2017) 'Comprehensive Mapping of Pluripotent Stem Cell Metabolism Using Dynamic Genome-Scale Network Modeling', *Cell Rep,* 21(10), pp. 2965-2977.

Chaneton, B., Hillmann, P., Zheng, L., Martin, A. C. L., Maddocks, O. D. K., Chokkathukalam, A., Coyle, J. E., Jankevics, A., Holding, F. P., Vousden, K. H., Frezza, C., O'Reilly, M. and Gottlieb, E. (2012) 'Serine is a natural ligand and allosteric activator of pyruvate kinase M2', *Nature,* 491(7424), pp. 458-462.

Chen, C., Han, X., Zou, X., Li, Y., Yang, L., Cao, K., Xu, J., Long, J., Liu, J. and Feng, Z. (2014) '4-methylene-2-octyl-5-oxotetrahydrofuran-3-carboxylic acid (C75), an inhibitor of fatty-acid synthase, suppresses the mitochondrial fatty acid synthesis pathway and impairs mitochondrial function', *J Biol Chem,* 289(24), pp. 17184-94.

Chen, H., Lee, J. M., Zong, Y., Borowitz, M., Ng, M. H., Ambinder, R. F. and Hayward, S. D. (2001) 'Linkage between STAT regulation and Epstein-Barr virus gene expression in tumors', *J Virol,* 75(6), pp. 2929-37.

Chen, J., Hu, C. F., Hou, J. H., Shao, Q., Yan, L. X., Zhu, X. F., Zeng, Y. X. and Shao, J. Y. (2010) 'Epstein-Barr virus encoded latent membrane protein 1 regulates mTOR signaling pathway genes which predict poor prognosis of nasopharyngeal carcinoma', *J Transl Med,* 8, pp. 30.

Chen, X., Kamranvar, S. A. and Masucci, M. G. (2016) 'Oxidative stress enables Epstein-Barr virus-induced B-cell transformation by posttranscriptional regulation of viral and cellular growth-promoting factors', *Oncogene,* 35(29), pp. 3807-16.

Cheng, S. C., Quintin, J., Cramer, R. A., Shepardson, K. M., Saeed, S., Kumar, V., Giamarellos-Bourboulis, E. J., Martens, J. H., Rao, N. A., Aghajanirefah, A., Manjeri, G. R., Li, Y., Ifrim, D. C., Arts, R. J., van der Veer, B. M., Deen, P. M., Logie, C., O'Neill, L. A., Willems, P., van de Veerdonk, F. L., van der Meer, J. W., Ng, A., Joosten, L. A., Wijmenga, C., Stunnenberg, H. G., Xavier, R. J. and Netea, M. G. (2014) 'mTOR- and HIF-1alpha-mediated aerobic glycolysis as metabolic basis for trained immunity', *Science,* 345(6204), pp. 1250684.

Christensen, K. E. and Mackenzie, R. E. (2008) 'Mitochondrial methylenetetrahydrofolate dehydrogenase, methenyltetrahydrofolate cyclohydrolase, and formyltetrahydrofolate synthetases', *Vitam Horm,* 79, pp. 393-410.

Condon, N. D., Heddleston, J. M., Chew, T. L., Luo, L., McPherson, P. S., Ioannou, M. S., Hodgson, L., Stow, J. L. and Wall, A. A. (2018) 'Macropinosome formation by tent pole ruffling in macrophages', *J Cell Biol,* 217(11), pp. 3873-3885.

Consortium, E. P. (2012) 'An integrated encyclopedia of DNA elements in the human genome', *Nature,* 489(7414), pp. 57-74.

Cracan, V., Titov, D. V., Shen, H., Grabarek, Z. and Mootha, V. K. (2017) 'A genetically encoded tool for manipulation of NADP(+)/NADPH in living cells', *Nat Chem Biol*.

Crumpton, M. J., Owens, R. J., Gallagher, C. J. and Davies, A. A. (1983) 'The cell surface and its metabolism', *J Pathol,* 141(3), pp. 235-48.

Cunningham, J. T., Rodgers, J. T., Arlow, D. H., Vazquez, F., Mootha, V. K. and Puigserver, P. (2007) 'mTOR controls mitochondrial oxidative function through a YY1-PGC-1alpha transcriptional complex', *Nature,* 450(7170), pp. 736-40.

Cutrona, G., Ulivi, M., Fais, F., Roncella, S. and Ferrarini, M. (1995) 'Transfection of the c-myc oncogene into normal Epstein-Barr virus-harboring B cells results in new phenotypic and functional features resembling those of Burkitt lymphoma cells and normal centroblasts', *J Exp Med,* 181(2), pp. 699-711.

Dalenc, F., Poirot, M. and Silvente-Poirot, S. (2015) 'Dendrogenin A: A Mammalian Metabolite of Cholesterol with Tumor Suppressor and Neurostimulating Properties', *Curr Med Chem,* 22(30), pp. 3533-49.

Dang, C. V. (1999) 'c-Myc target genes involved in cell growth, apoptosis, and metabolism', *Mol Cell Biol,* 19(1), pp. 1-11.

Dang, C. V. (2012) 'MYC on the path to cancer', *Cell,* 149(1), pp. 22-35.

Dang, C. V. (2013) 'MYC, metabolism, cell growth, and tumorigenesis', *Cold Spring Harb Perspect Med,* 3(8).

Daniel, E. (1990) 'Burkitt's lymphoma in Ethiopian children', *Trop Geogr Med,* 42(3), pp. 255-60.

Darekar, S., Georgiou, K., Yurchenko, M., Yenamandra, S. P., Chachami, G., Simos, G., Klein, G. and Kashuba, E. (2012) 'Epstein-Barr virus immortalization of human B-cells leads to stabilization of hypoxia-induced factor 1 alpha, congruent with the Warburg effect', *PLoS One,* 7(7), pp. e42072.

Davda, D., El Azzouny, M. A., Tom, C. T., Hernandez, J. L., Majmudar, J. D., Kennedy, R. T. and Martin, B. R. (2013) 'Profiling targets of the irreversible palmitoylation inhibitor 2-bromopalmitate', *ACS Chem Biol,* 8(9), pp. 1912-7.

Davis, C. A., Hitz, B. C., Sloan, C. A., Chan, E. T., Davidson, J. M., Gabdank, I., Hilton, J. A., Jain, K., Baymuradov, U. K., Narayanan, A. K., Onate, K. C., Graham, K., Miyasato, S. R., Dreszer, T. R., Strattan, J. S., Jolanki, O., Tanaka, F. Y. and Cherry, J. M. (2018) 'The Encyclopedia of DNA elements (ENCODE): data portal update', *Nucleic Acids Res,* 46(D1), pp. D794-d801.

Dawson, C. W., George, J. H., Blake, S. M., Longnecker, R. and Young, L. S. (2001) 'The Epstein-Barr virus encoded latent membrane protein 2A augments signaling from latent membrane protein 1', *Virology,* 289(2), pp. 192-207.

de Medina, P., Paillasse, M. R., Segala, G., Voisin, M., Mhamdi, L., Dalenc, F., Lacroix-Triki, M., Filleron, T., Pont, F., Saati, T. A., Morisseau, C., Hammock, B. D., Silvente-Poirot, S. and Poirot, M. (2013) 'Dendrogenin A arises from cholesterol and histamine metabolism and shows cell differentiation and anti-tumour properties', *Nat Commun,* 4, pp. 1840.

DeKroon, R. M., Gunawardena, H. P., Edwards, R. and Raab-Traub, N. (2018) 'Global Proteomic Changes Induced by the Epstein-Barr Virus Oncoproteins Latent Membrane Protein 1 and 2A', *MBio,* 9(3).

Delgado, T., Carroll, P. A., Punjabi, A. S., Margineantu, D., Hockenbery, D. M. and Lagunoff, M. (2010) 'Induction of the Warburg effect by Kaposi's sarcoma herpesvirus is required for the maintenance of latently infected endothelial cells', *Proc Natl Acad Sci U S A,* 107(23), pp. 10696-701.

Delgado, T., Sanchez, E. L., Camarda, R. and Lagunoff, M. (2012) 'Global metabolic profiling of infection by an oncogenic virus: KSHV induces and requires lipogenesis for survival of latent infection', *PLoS Pathog,* 8(8), pp. e1002866.

Deng, B., Zhu, X., Zhao, Y., Zhang, D., Pannu, A., Chen, L. and Niu, W. (2018) 'PKC and Rab13 mediate Ca', *Biochem Biophys Res Commun,* 495(2), pp. 1956-1963.

DeNicola, G. M., Chen, P. H., Mullarky, E., Sudderth, J. A., Hu, Z., Wu, D., Tang, H., Xie, Y., Asara, J. M., Huffman, K. E., Wistuba, I. I., Minna, J. D., DeBerardinis, R. J. and Cantley, L. C. (2015) 'NRF2 regulates serine biosynthesis in non-small cell lung cancer', *Nat Genet,* 47(12), pp. 1475-81.

Dennis, M. D., Jefferson, L. S. and Kimball, S. R. (2012) 'Role of p70S6K1-mediated phosphorylation of eIF4B and PDCD4 proteins in the regulation of protein synthesis', *J Biol Chem,* 287(51), pp. 42890-9.

Dharnidharka, V. R., Webster, A. C., Martinez, O. M., Preiksaitis, J. K., Leblond, V. and Choquet, S. (2016) 'Post-transplant lymphoproliferative disorders', *Nat Rev Dis Primers,* 2, pp. 15088.

Di Pietro, E., Sirois, J., Tremblay, M. L. and MacKenzie, R. E. (2002) 'Mitochondrial NAD-dependent methylenetetrahydrofolate dehydrogenase-methenyltetrahydrofolate cyclohydrolase is essential for embryonic development', *Mol Cell Biol,* 22(12), pp. 4158-66.

Di Pietro, E., Wang, X. L. and MacKenzie, R. E. (2004) 'The expression of mitochondrial methylenetetrahydrofolate dehydrogenase-cyclohydrolase supports a role in rapid cell growth', *Biochim Biophys Acta,* 1674(1), pp. 78-84.

Ding, J., Li, T., Wang, X., Zhao, E., Choi, J. H., Yang, L., Zha, Y., Dong, Z., Huang, S., Asara, J. M., Cui, H. and Ding, H. F. (2013) 'The histone H3 methyltransferase G9A epigenetically activates the serine-glycine synthesis pathway to sustain cancer cell survival and proliferation', *Cell Metab,* 18(6), pp. 896-907.

Doench, J. G., Fusi, N., Sullender, M., Hegde, M., Vaimberg, E. W., Donovan, K. F., Smith, I., Tothova, Z., Wilen, C., Orchard, R., Virgin, H. W., Listgarten, J. and Root, D. E. (2016) 'Optimized sgRNA design to maximize activity and minimize off-target effects of CRISPR-Cas9', *Nat Biotechnol,* 34(2), pp. 184-91.

Doherty, J. R., Yang, C., Scott, K. E., Cameron, M. D., Fallahi, M., Li, W., Hall, M. A., Amelio, A. L., Mishra, J. K., Li, F., Tortosa, M., Genau, H. M., Rounbehler, R. J., Lu, Y., Dang, C. V., Kumar, K. G., Butler, A. A., Bannister, T. D., Hooper, A. T., Unsal-Kacmaz, K., Roush, W. R. and Cleveland, J. L. (2014) 'Blocking lactate export by inhibiting the Myc target MCT1 Disables glycolysis and glutathione synthesis', *Cancer Res,* 74(3), pp. 908-20.

Dorrello, N. V., Peschiaroli, A., Guardavaccaro, D., Colburn, N. H., Sherman, N. E. and Pagano, M. (2006) 'S6K1- and betaTRCP-mediated degradation of PDCD4 promotes protein translation and cell growth', *Science,* 314(5798), pp. 467-71.

Ducker, G. S., Chen, L., Morscher, R. J., Ghergurovich, J. M., Esposito, M., Teng, X., Kang, Y. and Rabinowitz, J. D. (2016) 'Reversal of Cytosolic One-Carbon Flux Compensates for Loss of the Mitochondrial Folate Pathway', *Cell Metab,* 23(6), pp. 1140-53.

Ducker, G. S., Ghergurovich, J. M., Mainolfi, N., Suri, V., Jeong, S. K., Hsin-Jung Li, S., Friedman, A., Manfredi, M. G., Gitai, Z., Kim, H. and Rabinowitz, J. D. (2017) 'Human SHMT inhibitors reveal defective glycine import as a targetable metabolic vulnerability of diffuse large B-cell lymphoma', *Proc Natl Acad Sci U S A,* 114(43), pp. 11404-11409.

Ducker, G. S. and Rabinowitz, J. D. (2017) 'One-Carbon Metabolism in Health and Disease', *Cell Metab,* 25(1), pp. 27-42.

Dudman, N. P., Tyrrell, P. A. and Wilcken, D. E. (1987) 'Homocysteinemia: depressed plasma serine levels', *Metabolism,* 36(2), pp. 198-201.

Düvel, K., Yecies, J. L., Menon, S., Raman, P., Lipovsky, A. I., Souza, A. L., Triantafellow, E., Ma, Q., Gorski, R., Cleaver, S., Vander Heiden, M. G., MacKeigan, J. P., Finan, P. M., Clish, C. B., Murphy, L. O. and Manning, B. D. (2010) 'Activation of a metabolic gene regulatory network downstream of mTOR complex 1', *Mol Cell,* 39(2), pp. 171-83.

Ehlin-Henriksson, B., Gordon, J. and Klein, G. (2003) 'B-lymphocyte subpopulations are equally susceptible to Epstein-Barr virus infection, irrespective of immunoglobulin isotype expression', *Immunology,* 108(4), pp. 427-30.

Elias, J. E. and Gygi, S. P. (2007) 'Target-decoy search strategy for increased confidence in large-scale protein identifications by mass spectrometry', *Nat Methods,* 4(3), pp. 207-14.

Elias, J. E. and Gygi, S. P. (2010) 'Target-decoy search strategy for mass spectrometry-based proteomics', *Methods Mol Biol,* 604, pp. 55-71.

Engelking, L. J., Kuriyama, H., Hammer, R. E., Horton, J. D., Brown, M. S., Goldstein, J. L. and Liang, G. (2004) 'Overexpression of Insig-1 in the livers of transgenic mice inhibits SREBP processing and reduces insulin-stimulated lipogenesis', *J Clin Invest,* 113(8), pp. 1168-75.

Epstein, M. A., Achong, B. G. and Barr, Y. M. (1964) 'VIRUS PARTICLES IN CULTURED LYMPHOBLASTS FROM BURKITT'S LYMPHOMA', *Lancet,* 1(7335), pp. 702-3.

Epstein, M. A., Barr, Y. M. and Achong, B. G. (1965) 'The Behaviour and Morphology of a Second Tissue Culture Strain (EB2) of Lymphoblasts from Burkitt's Lymphoma', *Br J Cancer,* 19(1), pp. 108-15.

Epstein, M. A., Henle, G., Achong, B. G. and Barr, Y. M. (1965) 'MORPHOLOGICAL AND BIOLOGICAL STUDIES ON A VIRUS IN CULTURED LYMPHOBLASTS FROM BURKITT'S LYMPHOMA', *J Exp Med,* 121(5), pp. 761-70.

Ersing, I., Nobre, L., Wang, L. W., Soday, L., Ma, Y., Paulo, J. A., Narita, Y., Ashbaugh, C. W., Jiang, C., Grayson, N. E., Kieff, E., Gygi, S. P., Weekes, M. P. and Gewurz, B. E. (2017) 'A Temporal Proteomic Map of Epstein-Barr Virus Lytic Replication in B Cells', *Cell Rep,* 19(7), pp. 1479-1493.

Fan, J., Teng, X., Liu, L., Mattaini, K. R., Looper, R. E., Vander Heiden, M. G. and Rabinowitz, J. D. (2015) 'Human phosphoglycerate dehydrogenase produces the oncometabolite D-2-hydroxyglutarate', *ACS Chem Biol,* 10(2), pp. 510-6.

Fan, J., Ye, J., Kamphorst, J. J., Shlomi, T., Thompson, C. B. and Rabinowitz, J. D. (2014) 'Quantitative flux analysis reveals folate-dependent NADPH production', *Nature,* 510(7504), pp. 298-302.

Fassone, L., Cingolani, A., Martini, M., Migliaretti, G., Oreste, P. L., Capello, D., Gloghini, A., Vivenza, D., Dolcetti, R., Carbone, A., Antinori, A., Gaidano, G. and Larocca, L. M. (2002) 'Characterization of Epstein-Barr virus genotype in AIDS-related non-Hodgkin's lymphoma', *AIDS Res Hum Retroviruses,* 18(1), pp. 19-26.

Feederle, R., Neuhierl, B., Baldwin, G., Bannert, H., Hub, B., Mautner, J., Behrends, U. and Delecluse, H. J. (2006) 'Epstein-Barr virus BNRF1 protein allows efficient transfer from the endosomal compartment to the nucleus of primary B lymphocytes', *J Virol,* 80(19), pp. 9435-43.

Fernandez, C. A., Des Rosiers, C., Previs, S. F., David, F. and Brunengraber, H. (1996) 'Correction of 13C mass isotopomer distributions for natural stable isotope abundance', *J Mass Spectrom,* 31(3), pp. 255-62.

Fernandez, P. C., Frank, S. R., Wang, L., Schroeder, M., Liu, S., Greene, J., Cocito, A. and Amati, B. (2003) 'Genomic targets of the human c-Myc protein', *Genes Dev,* 17(9), pp. 1115-29.

Findlay, J. S. and Ulaeto, D. (2015) 'Semliki Forest virus and Sindbis virus, but not vaccinia virus, require glycolysis for optimal replication', *J Gen Virol,* 96(9), pp. 2693-6.

Fingar, D. C., Salama, S., Tsou, C., Harlow, E. and Blenis, J. (2002) 'Mammalian cell size is controlled by mTOR and its downstream targets S6K1 and 4EBP1/eIF4E', *Genes Dev,* 16(12), pp. 1472-87.

Fingeroth, J. D., Weis, J. J., Tedder, T. F., Strominger, J. L., Biro, P. A. and Fearon, D. T. (1984) 'Epstein-Barr virus receptor of human B lymphocytes is the C3d receptor CR2', *Proc Natl Acad Sci U S A,* 81(14), pp. 4510-4.

Fontaine, K. A., Camarda, R. and Lagunoff, M. (2014) 'Vaccinia virus requires glutamine but not glucose for efficient replication', *J Virol,* 88(8), pp. 4366-74.

Foretz, M., Guichard, C., Ferre, P. and Foufelle, F. (1999) 'Sterol regulatory element binding protein-1c is a major mediator of insulin action on the hepatic expression of glucokinase and lipogenesis-related genes', *Proc Natl Acad Sci U S A,* 96(22), pp. 12737-42.

Fruehling, S. and Longnecker, R. (1997) 'The immunoreceptor tyrosine-based activation motif of Epstein-Barr virus LMP2A is essential for blocking BCR-mediated signal transduction', *Virology,* 235(2), pp. 241-51.

Fuchs, D., Berges, C., Opelz, G., Daniel, V. and Naujokat, C. (2008) 'HMG-CoA reductase inhibitor simvastatin overcomes bortezomib-induced apoptosis resistance by disrupting a geranylgeranyl pyrophosphate-dependent survival pathway', *Biochem Biophys Res Commun,* 374(2), pp. 309-14.

Fukuda, M. and Kawaguchi, Y. (2014) 'Role of the immunoreceptor tyrosine-based activation motif of latent membrane protein 2A (LMP2A) in Epstein-Barr virus LMP2A-induced cell transformation', *J Virol,* 88(9), pp. 5189-94.

Gao, X., Lin, S. H., Ren, F., Li, J. T., Chen, J. J., Yao, C. B., Yang, H. B., Jiang, S. X., Yan, G. Q., Wang, D., Wang, Y., Liu, Y., Cai, Z., Xu, Y. Y., Chen, J., Yu, W., Yang, P. Y. and Lei, Q. Y. (2016) 'Acetate functions as an epigenetic metabolite to promote lipid synthesis under hypoxia', *Nat Commun,* 7, pp. 11960.

Gholkar, A. A., Cheung, K., Williams, K. J., Lo, Y. C., Hamideh, S. A., Nnebe, C., Khuu, C., Bensinger, S. J. and Torres, J. Z. (2016) 'Fatostatin Inhibits Cancer Cell Proliferation by Affecting Mitotic Microtubule Spindle Assembly and Cell Division', *J Biol Chem,* 291(33), pp. 17001-8.

Giandomenico, V., Simonsson, M., Gronroos, E. and Ericsson, J. (2003) 'Coactivator-dependent acetylation stabilizes members of the SREBP family of transcription factors', *Mol Cell Biol,* 23(7), pp. 2587-99.

Giulino-Roth, L. and Goldman, S. (2016) 'Recent molecular and therapeutic advances in B-cell non-Hodgkin lymphoma in children', *Br J Haematol,* 173(4), pp. 531-44.

Goldstein, J. L. and Brown, M. S. (1990) 'Regulation of the mevalonate pathway', *Nature,* 343(6257), pp. 425-30.

Goldstein, J. L. and Brown, M. S. (2015) 'A century of cholesterol and coronaries: from plaques to genes to statins', *Cell,* 161(1), pp. 161-172.

Gordadze, A. V., Peng, R., Tan, J., Liu, G., Sutton, R., Kempkes, B., Bornkamm, G. W. and Ling, P. D. (2001) 'Notch1IC partially replaces EBNA2 function in B cells immortalized by Epstein-Barr virus', *J Virol,* 75(13), pp. 5899-912.

Graves, J. A., Wang, Y., Sims-Lucas, S., Cherok, E., Rothermund, K., Branca, M. F., Elster, J., Beer-Stolz, D., Van Houten, B., Vockley, J. and Prochownik, E. V. (2012) 'Mitochondrial structure, function and dynamics are temporally controlled by c-Myc', *PLoS One,* 7(5), pp. e37699.

Green, M. and Michaels, M. G. (2013) 'Epstein-Barr virus infection and posttransplant lymphoproliferative disorder', *Am J Transplant,* 13 Suppl 3, pp. 41-54; quiz 54.

Greseth, M. D. and Traktman, P. (2014) 'De novo fatty acid biosynthesis contributes significantly to establishment of a bioenergetically favorable environment for vaccinia virus infection', *PLoS Pathog,* 10(3), pp. e1004021.

Gulley, M. L., Eagan, P. A., Quintanilla-Martinez, L., Picado, A. L., Smir, B. N., Childs, C., Dunn, C. D., Craig, F. E., Williams, J. W., Jr. and Banks, P. M. (1994) 'Epstein-Barr virus DNA is abundant and monoclonal in the Reed-Sternberg cells of Hodgkin's disease: association with mixed cellularity subtype and Hispanic American ethnicity', *Blood,* 83(6), pp. 1595-602.

Gunnell, A., Webb, H. M., Wood, C. D., McClellan, M. J., Wichaidit, B., Kempkes, B., Jenner, R. G., Osborne, C., Farrell, P. J. and West, M. J. (2016) 'RUNX super-enhancer control through the Notch pathway by Epstein-Barr virus transcription factors regulates B cell growth', *Nucleic Acids Res,* 44(10), pp. 4636-50.

Guri, Y., Colombi, M., Dazert, E., Hindupur, S. K., Roszik, J., Moes, S., Jenoe, P., Heim, M. H., Riezman, I., Riezman, H. and Hall, M. N. (2017) 'mTORC2 Promotes Tumorigenesis via Lipid Synthesis', *Cancer Cell,* 32(6), pp. 807-823.e12.

Gustafsson, R., Jemth, A. S., Gustafsson, N. M., Färnegårdh, K., Loseva, O., Wiita, E., Bonagas, N., Dahllund, L., Llona-Minguez, S., Häggblad, M., Henriksson, M., Andersson, Y.,

Homan, E., Helleday, T. and Stenmark, P. (2017) 'Crystal Structure of the Emerging Cancer Target MTHFD2 in Complex with a Substrate-Based Inhibitor', *Cancer Res,* 77(4), pp. 937-948.

Gustafsson Sheppard, N., Jarl, L., Mahadessian, D., Strittmatter, L., Schmidt, A., Madhusudan, N., Tegnér, J., Lundberg, E. K., Asplund, A., Jain, M. and Nilsson, R. (2015) 'The folate-coupled enzyme MTHFD2 is a nuclear protein and promotes cell proliferation', *Sci Rep,* 5, pp. 15029.

Hafez, A. Y., Messinger, J. E., McFadden, K., Fenyofalvi, G., Shepard, C. N., Lenzi, G. M., Kim, B. and Luftig, M. A. (2017) 'Limited nucleotide pools restrict Epstein-Barr virus-mediated B-cell immortalization', *Oncogenesis,* 6(6), pp. e349.

Hammerschmidt, W. and Sugden, B. (2004) 'Epstein-Barr virus sustains Burkitt's lymphomas and Hodgkin's disease', *Trends Mol Med,* 10(7), pp. 331-6.

Han, J., Li, E., Chen, L., Zhang, Y., Wei, F., Liu, J., Deng, H. and Wang, Y. (2015) 'The CREB coactivator CRTC2 controls hepatic lipid metabolism by regulating SREBP1', *Nature,* 524(7564), pp. 243-6.

Hanahan, D. and Weinberg, R. A. (2011) 'Hallmarks of cancer: the next generation', *Cell,* 144(5), pp. 646-74.

Hatton, O., Phillips, L. K., Vaysberg, M., Hurwich, J., Krams, S. M. and Martinez, O. M. (2011) 'Syk activation of phosphatidylinositol 3-kinase/Akt prevents HtrA2-dependent loss of X-linked inhibitor of apoptosis protein (XIAP) to promote survival of Epstein-Barr virus+ (EBV+) B cell lymphomas', *J Biol Chem,* 286(43), pp. 37368-78.

Henderson, E., Miller, G., Robinson, J. and Heston, L. (1977) 'Efficiency of transformation of lymphocytes by Epstein-Barr virus', *Virology,* 76(1), pp. 152-63.

Hennino, A., Berard, M., Krammer, P. H. and Defrance, T. (2001) 'FLICE-inhibitory protein is a key regulator of germinal center B cell apoptosis', *J Exp Med,* 193(4), pp. 447-58.

Higuchi, M., Izumi, K. M. and Kieff, E. (2001) 'Epstein-Barr virus latent-infection membrane proteins are palmitoylated and raft-associated: protein 1 binds to the cytoskeleton through TNF receptor cytoplasmic factors', *Proc Natl Acad Sci U S A,* 98(8), pp. 4675-80.

Hofelmayr, H., Strobl, L. J., Marschall, G., Bornkamm, G. W. and Zimber-Strobl, U. (2001) 'Activated Notch1 can transiently substitute for EBNA2 in the maintenance of proliferation of LMP1-expressing immortalized B cells', *J Virol,* 75(5), pp. 2033-40.

Hoppe-Seyler, K., Honegger, A., Bossler, F., Sponagel, J., Bulkescher, J., Lohrey, C. and Hoppe-Seyler, F. (2017) 'Viral E6/E7 oncogene and cellular hexokinase 2 expression in HPV-positive cancer cell lines', *Oncotarget,* 8(63), pp. 106342-106351.

Horton, J. D., Shah, N. A., Warrington, J. A., Anderson, N. N., Park, S. W., Brown, M. S. and Goldstein, J. L. (2003) 'Combined analysis of oligonucleotide microarray data from transgenic and knockout mice identifies direct SREBP target genes', *Proc Natl Acad Sci U S A: Vol. 21*, pp. 12027-32.

Hsieh, A. L., Walton, Z. E., Altman, B. J., Stine, Z. E. and Dang, C. V. (2015) 'MYC and metabolism on the path to cancer', *Semin Cell Dev Biol,* 43, pp. 11-21.

Hsieh, J. J. and Hayward, S. D. (1995) 'Masking of the CBF1/RBPJ kappa transcriptional repression domain by Epstein-Barr virus EBNA2', *Science,* 268(5210), pp. 560-3.

Hsieh, J. J., Henkel, T., Salmon, P., Robey, E., Peterson, M. G. and Hayward, S. D. (1996) 'Truncated mammalian Notch1 activates CBF1/RBPJk-repressed genes by a mechanism resembling that of Epstein-Barr virus EBNA2', *Mol Cell Biol,* 16(3), pp. 952-9.

Huang da, W., Sherman, B. T. and Lempicki, R. A. (2009) 'Systematic and integrative analysis of large gene lists using DAVID bioinformatics resources', *Nat Protoc,* 4(1), pp. 44-57.

Huang, d. W., Sherman, B. T. and Lempicki, R. A. (2009a) 'Bioinformatics enrichment tools: paths toward the comprehensive functional analysis of large gene lists', *Nucleic Acids Res,* 37(1), pp. 1-13.

Huang, d. W., Sherman, B. T. and Lempicki, R. A. (2009b) 'Systematic and integrative analysis of large gene lists using DAVID bioinformatics resources', *Nat Protoc,* 4(1), pp. 44-57.

Hudson, C. C., Liu, M., Chiang, G. G., Otterness, D. M., Loomis, D. C., Kaper, F., Giaccia, A. J. and Abraham, R. T. (2002) 'Regulation of hypoxia-inducible factor 1alpha expression and function by the mammalian target of rapamycin', *Mol Cell Biol,* 22(20), pp. 7004-14.

Hughes, D. J., Marendy, E. M., Dickerson, C. A., Yetming, K. D., Sample, C. E. and Sample, J. T. (2012) 'Contributions of CTCF and DNA methyltransferases DNMT1 and DNMT3B to Epstein-Barr virus restricted latency', *J Virol,* 86(2), pp. 1034-45.

Hui, S., Ghergurovich, J. M., Morscher, R. J., Jang, C., Teng, X., Lu, W., Esparza, L. A., Reya, T., Zhan, L., Guo, J. Y., White, E. and Rabinowitz, J. D. (2017) 'Glucose feeds the TCA cycle via circulating lactate', *Nature,* 551(7678), pp. 115-8.

Hulse, M., Caruso, L. B., Madzo, J., Tan, Y., Johnson, S. and Tempera, I. (2018) 'Poly(ADP-ribose) polymerase 1 is necessary for coactivating hypoxia-inducible factor-1-dependent gene expression by Epstein-Barr virus latent membrane protein 1', *PLoS Pathog,* 14(11), pp. e1007394.

Hurwitz, S. N., Nkosi, D., Conlon, M. M., York, S. B., Liu, X., Tremblay, D. C. and Meckes, D. G. (2017) 'CD63 Regulates Epstein-Barr Virus LMP1 Exosomal Packaging, Enhancement of Vesicle Production, and Noncanonical NF-κB Signaling', *J Virol,* 91(5).

Hutagalung, A. H. and Novick, P. J. (2011) 'Role of Rab GTPases in membrane traffic and cell physiology', *Physiol Rev,* 91(1), pp. 119-49.

Hutt, D. M., Da-Silva, L. F., Chang, L. H., Prosser, D. C. and Ngsee, J. K. (2000) 'PRA1 inhibits the extraction of membrane-bound rab GTPase by GDI1', *J Biol Chem,* 275(24), pp. 18511-9.

Huttlin, E. L., Jedrychowski, M. P., Elias, J. E., Goswami, T., Rad, R., Beausoleil, S. A., Villen, J., Haas, W., Sowa, M. E. and Gygi, S. P. (2010) 'A tissue-specific atlas of mouse protein phosphorylation and expression', *Cell,* 143(7), pp. 1174-89.

Höfelmayr, H., Strobl, L. J., Stein, C., Laux, G., Marschall, G., Bornkamm, G. W. and Zimber-Strobl, U. (1999) 'Activated Mouse Notch1 Transactivates Epstein-Barr Virus Nuclear Antigen 2-Regulated Viral Promoters', *J Virol: Vol. 4*, pp. 2770-80.

Ikeda, M. and Longnecker, R. (2007) 'Cholesterol is critical for Epstein-Barr virus latent membrane protein 2A trafficking and protein stability', *Virology,* 360(2), pp. 461-8.

Ioannou, M. S., Bell, E. S., Girard, M., Chaineau, M., Hamlin, J. N., Daubaras, M., Monast, A., Park, M., Hodgson, L. and McPherson, P. S. (2015) 'DENND2B activates Rab13 at the leading edge of migrating cells and promotes metastatic behavior', *J Cell Biol,* 208(5), pp. 629-48.

Ioannou, M. S., Girard, M. and McPherson, P. S. (2016) 'Rab13 Traffics on Vesicles Independent of Prenylation', *J Biol Chem,* 291(20), pp. 10726-35.

Ioannou, M. S. and McPherson, P. S. (2016) 'Regulation of Cancer Cell Behavior by the Small GTPase Rab13', *J Biol Chem,* 291(19), pp. 9929-37.

Jain, M., Nilsson, R., Sharma, S., Madhusudhan, N., Kitami, T., Souza, A. L., Kafri, R., Kirschner, M. W., Clish, C. B. and Mootha, V. K. (2012) 'Metabolite profiling identifies a key role for glycine in rapid cancer cell proliferation', *Science,* 336(6084), pp. 1040-4.

Jazayeri, M., Andreyev, A., Will, Y., Ward, M., Anderson, C. M. and Clevenger, W. (2003) 'Inducible expression of a dominant negative DNA polymerase-gamma depletes mitochondrial DNA and produces a rho0 phenotype', *J Biol Chem,* 278(11), pp. 9823-30.

Jean Beltran, P. M., Cook, K. C., Hashimoto, Y., Galitzine, C., Murray, L. A., Vitek, O. and Cristea, I. M. (2018) 'Infection-Induced Peroxisome Biogenesis Is a Metabolic Strategy for Herpesvirus Replication', *Cell Host Microbe,* 24(4), pp. 526-541.e7.

Jiang, S., Wang, L. W., Walsh, M. J., Trudeau, S. J., Gerdt, C., Zhao, B. and Gewurz, B. E. (2018) 'CRISPR/Cas9-Mediated Genome Editing in Epstein-Barr Virus-Transformed Lymphoblastoid B-Cell Lines', *Curr Protoc Mol Biol,* 121, pp. 31.12.1-31.12.23.

Jiang, S., Willox, B., Zhou, H., Holthaus, A. M., Wang, A., Shi, T. T., Maruo, S., Kharchenko, P. V., Johannsen, E. C., Kieff, E. and Zhao, B. (2014) 'Epstein-Barr virus nuclear antigen 3C binds to BATF/IRF4 or SPI1/IRF4 composite sites and recruits Sin3A to repress CDKN2A', *Proc Natl Acad Sci U S A,* 111(1), pp. 421-6.

Jiang, S., Zhou, H., Liang, J., Gerdt, C., Wang, C., Ke, L., Schmidt, S. C. S., Narita, Y., Ma, Y., Wang, S., Colson, T., Gewurz, B., Li, G., Kieff, E. and Zhao, B. (2017) 'The Epstein-Barr Virus Regulome in Lymphoblastoid Cells', *Cell Host Microbe,* 22(4), pp. 561-573.e4.

Johannsen, E., Koh, E., Mosialos, G., Tong, X., Kieff, E. and Grossman, S. R. (1995) 'Epstein-Barr virus nuclear protein 2 transactivation of the latent membrane protein 1 promoter is mediated by J kappa and PU.1', *J Virol,* 69(1), pp. 253-62.

Johannsen, E., Luftig, M., Chase, M. R., Weicksel, S., Cahir-McFarland, E., Illanes, D., Sarracino, D. and Kieff, E. (2004) 'Proteins of purified Epstein-Barr virus', *Proc Natl Acad Sci U S A,* 101(46), pp. 16286-91.

Johnson, J. L., He, J., Ramadass, M., Pestonjamasp, K., Kiosses, W. B., Zhang, J. and Catz, S. D. (2016) 'Munc13-4 Is a Rab11-binding Protein That Regulates Rab11-positive Vesicle Trafficking and Docking at the Plasma Membrane', *J Biol Chem,* 291(7), pp. 3423-38.

Ju, H. Q., Lu, Y. X., Chen, D. L., Zuo, Z. X., Liu, Z. X., Wu, Q. N., Mo, H. Y., Wang, Z. X., Wang, D. S., Pu, H. Y., Zeng, Z. L., Li, B., Xie, D., Huang, P., Hung, M. C., Chiao, P. J. and Xu, R. H. (2018) 'Modulation of Redox Homeostasis by Inhibition of MTHFD2 in Colorectal Cancer: Mechanisms and Therapeutic Implications', *J Natl Cancer Inst*.

Jun, D. Y., Park, H. S., Lee, J. Y., Baek, J. Y., Park, H. K., Fukui, K. and Kim, Y. H. (2008) 'Positive regulation of promoter activity of human 3-phosphoglycerate dehydrogenase (PHGDH) gene is mediated by transcription factors Sp1 and NF-Y', *Gene,* 414(1-2), pp. 106-14.

Kaiser, C., Laux, G., Eick, D., Jochner, N., Bornkamm, G. W. and Kempkes, B. (1999) 'The proto-oncogene c-myc is a direct target gene of Epstein-Barr virus nuclear antigen 2', *J Virol,* 73(5), pp. 4481-4.

Kalla, M., Göbel, C. and Hammerschmidt, W. (2012) 'The lytic phase of epstein-barr virus requires a viral genome with 5-methylcytosine residues in CpG sites', *J Virol,* 86(1), pp. 447-58.

Kalla, M., Schmeinck, A., Bergbauer, M., Pich, D. and Hammerschmidt, W. (2010) 'AP-1 homolog BZLF1 of Epstein-Barr virus has two essential functions dependent on the epigenetic state of the viral genome', *Proc Natl Acad Sci U S A,* 107(2), pp. 850-5.

Kamisuki, S., Mao, Q., Abu-Elheiga, L., Gu, Z., Kugimiya, A., Kwon, Y., Shinohara, T., Kawazoe, Y., Sato, S., Asakura, K., Choo, H. Y., Sakai, J., Wakil, S. J. and Uesugi, M. (2009) 'A small molecule that blocks fat synthesis by inhibiting the activation of SREBP', *Chem Biol,* 16(8), pp. 882-92.

Kang, M. S. and Kieff, E. (2015) 'Epstein-Barr virus latent genes', *Exp Mol Med,* 47, pp. e131.

Katano, H., Pesnicak, L. and Cohen, J. I. (2004) 'Simvastatin induces apoptosis of Epstein-Barr virus (EBV)-transformed lymphoblastoid cell lines and delays development of EBV lymphomas', *Proc Natl Acad Sci U S A,* 101(14), pp. 4960-5.

Kataoka, K., Miyoshi, H., Sakata, S., Dobashi, A., Couronne, L., Kogure, Y., Sato, Y., Nishida, K., Gion, Y., Shiraishi, Y., Tanaka, H., Chiba, K., Watatani, Y., Kakiuchi, N., Shiozawa, Y., Yoshizato, T., Yoshida, K., Makishima, H., Sanada, M., Onozawa, M., Teshima, T., Yoshiki, Y., Ishida, T., Suzuki, K., Shimada, K., Tomita, A., Kato, M., Ota, Y., Izutsu, K., Demachi-Okamura, A., Akatsuka, Y., Miyano, S., Yoshino, T., Gaulard, P., Hermine, O., Takeuchi, K., Ohshima, K. and Ogawa, S. (2019) 'Frequent structural variations involving programmed death ligands in Epstein-Barr virus-associated lymphomas', *Leukemia*.

Kelly, G. L., Long, H. M., Stylianou, J., Thomas, W. A., Leese, A., Bell, A. I., Bornkamm, G. W., Mautner, J., Rickinson, A. B. and Rowe, M. (2009) 'An Epstein-Barr virus anti-apoptotic protein constitutively expressed in transformed cells and implicated in burkitt lymphomagenesis: the Wp/BHRF1 link', *PLoS Pathog,* 5(3), pp. e1000341.

Kieser, A. and Sterz, K. R. (2015) 'The Latent Membrane Protein 1 (LMP1)', *Curr Top Microbiol Immunol,* 391, pp. 119-49.

Kim, D., Fiske, B. P., Birsoy, K., Freinkman, E., Kami, K., Possemato, R. L., Chudnovsky, Y., Pacold, M. E., Chen, W. W., Cantor, J. R., Shelton, L. M., Gui, D. Y., Kwon, M., Ramkissoon, S. H., Ligon, K. L., Kang, S. W., Snuderl, M., Vander Heiden, M. G. and Sabatini, D. M. (2015) 'SHMT2 drives glioma cell survival in ischaemia but imposes a dependence on glycine clearance', *Nature,* 520(7547), pp. 363-7.

Kim, J. W., Zeller, K. I., Wang, Y., Jegga, A. G., Aronow, B. J., O'Donnell, K. A. and Dang, C. V. (2004) 'Evaluation of myc E-box phylogenetic footprints in glycolytic genes by chromatin immunoprecipitation assays', *Mol Cell Biol,* 24(13), pp. 5923-36.

Kis, L. L., Salamon, D., Persson, E. K., Nagy, N., Scheeren, F. A., Spits, H., Klein, G. and Klein, E. (2010) 'IL-21 imposes a type II EBV gene expression on type III and type I B cells by the repression of C- and activation of LMP-1-promoter', *Proc Natl Acad Sci U S A,* 107(2), pp. 872-7.

Kis, L. L., Takahara, M., Nagy, N., Klein, G. and Klein, E. (2006) 'IL-10 can induce the expression of EBV-encoded latent membrane protein-1 (LMP-1) in the absence of EBNA-2 in B lymphocytes and in Burkitt lymphoma- and NK lymphoma-derived cell lines', *Blood,* 107(7), pp. 2928-35.

Klein, E., Nagy, N. and Rasul, A. E. (2013) 'EBV genome carrying B lymphocytes that express the nuclear protein EBNA-2 but not LMP-1: Type IIb latency', *Oncoimmunology,* 2(2), pp. e23035.

Knutson, S. K., Chyla, B. J., Amann, J. M., Bhaskara, S., Huppert, S. S. and Hiebert, S. W. (2008) 'Liver-specific deletion of histone deacetylase 3 disrupts metabolic transcriptional networks', *Embo j,* 27(7), pp. 1017-28.

Ko, M., An, J., Pastor, W. A., Koralov, S. B., Rajewsky, K. and Rao, A. (2015) 'TET proteins and 5-methylcytosine oxidation in hematological cancers', *Immunol Rev,* 263(1), pp. 6-21.

Koboldt, D. C., Zhang, Q., Larson, D. E., Shen, D., McLellan, M. D., Lin, L., Miller, C. A., Mardis, E. R., Ding, L. and Wilson, R. K. (2012) 'VarScan 2: somatic mutation and copy number alteration discovery in cancer by exome sequencing', *Genome Res,* 22(3), pp. 568-76.

Kory, N., Wyant, G. A., Prakash, G., Uit de Bos, J., Bottanelli, F., Pacold, M. E., Chan, S. H., Lewis, C. A., Wang, T., Keys, H. R., Guo, Y. E. and Sabatini, D. M. (2018) 'SFXN1 is a mitochondrial serine transporter required for one-carbon metabolism', *Science,* 362(6416).

Koufaris, C. and Nilsson, R. (2018) 'Protein interaction and functional data indicate MTHFD2 involvement in RNA processing and translation', *Cancer Metab,* 6, pp. 12.

Krupenko, N. I., Dubard, M. E., Strickland, K. C., Moxley, K. M., Oleinik, N. V. and Krupenko, S. A. (2010) 'ALDH1L2 is the mitochondrial homolog of 10-formyltetrahydrofolate dehydrogenase', *J Biol Chem,* 285(30), pp. 23056-63.

Kuhajda, F. P., Pizer, E. S., Li, J. N., Mani, N. S., Frehywot, G. L. and Townsend, C. A. (2000) 'Synthesis and antitumor activity of an inhibitor of fatty acid synthase', *Proc Natl Acad Sci U S A,* 97(7), pp. 3450-4.

Kurth, J., Hansmann, M. L., Rajewsky, K. and Kuppers, R. (2003) 'Epstein-Barr virus-infected B cells expanding in germinal centers of infectious mononucleosis patients do not participate in the germinal center reaction', *Proc Natl Acad Sci U S A,* 100(8), pp. 4730-5.

Kurth, J., Spieker, T., Wustrow, J., Strickler, G. J., Hansmann, L. M., Rajewsky, K. and Kuppers, R. (2000) 'EBV-infected B cells in infectious mononucleosis: viral strategies for spreading in the B cell compartment and establishing latency', *Immunity,* 13(4), pp. 485-95.

Kuzu, O. F., Noory, M. A. and Robertson, G. P. (2016) 'The role of cholesterol in cancer', *Cancer Res,* 76(8), pp. 2063-70.

Kwok, H., Tong, A. H., Lin, C. H., Lok, S., Farrell, P. J., Kwong, D. L. and Chiang, A. K. (2012) 'Genomic sequencing and comparative analysis of Epstein-Barr virus genome isolated from primary nasopharyngeal carcinoma biopsy', *PLoS One,* 7(5), pp. e36939.

Köhler, K., Louvard, D. and Zahraoui, A. (2004) 'Rab13 regulates PKA signaling during tight junction assembly', *J Cell Biol,* 165(2), pp. 175-80.

Küppers, R., Klein, U., Schwering, I., Distler, V., Bräuninger, A., Cattoretti, G., Tu, Y., Stolovitzky, G. A., Califano, A., Hansmann, M. L. and Dalla-Favera, R. (2003) 'Identification of Hodgkin and Reed-Sternberg cell-specific genes by gene expression profiling', *J Clin Invest: Vol. 4*, pp. 529-37.

Labuschagne, C. F., van den Broek, N. J., Mackay, G. M., Vousden, K. H. and Maddocks, O. D. (2014) 'Serine, but not glycine, supports one-carbon metabolism and proliferation of cancer cells', *Cell Rep,* 7(4), pp. 1248-58.

LaCasce, A. S. (2006) 'Post-transplant lymphoproliferative disorders', *Oncologist,* 11(6), pp. 674-80.

Lackner, M. R., Kindt, R. M., Carroll, P. M., Brown, K., Cancilla, M. R., Chen, C., de Silva, H., Franke, Y., Guan, B., Heuer, T., Hung, T., Keegan, K., Lee, J. M., Manne, V., O'Brien, C., Parry, D., Perez-Villar, J. J., Reddy, R. K., Xiao, H., Zhan, H., Cockett, M., Plowman, G., Fitzgerald, K., Costa, M. and Ross-Macdonald, P. (2005) 'Chemical genetics identifies Rab geranylgeranyl transferase as an apoptotic target of farnesyl transferase inhibitors', *Cancer Cell,* 7(4), pp. 325-36.

Lam, N. and Sugden, B. (2003) 'LMP1, a viral relative of the TNF receptor family, signals principally from intracellular compartments', *Embo j,* 22(12), pp. 3027-38.

Lambert, S. L. and Martinez, O. M. (2007) 'Latent membrane protein 1 of EBV activates phosphatidylinositol 3-kinase to induce production of IL-10', *J Immunol,* 179(12), pp. 8225-34.

Lange, P. T., Lagunoff, M. and Tarakanova, V. L. (2019) 'Chewing the Fat: The Conserved Ability of DNA Viruses to Hijack Cellular Lipid Metabolism', *Viruses,* 11(2).

Lee, G., Zheng, Y., Cho, S., Jang, C., England, C., Dempsey, J. M., Yu, Y., Liu, X., He, L., Cavaliere, P. M., Chavez, A., Zhang, E., Isik, M., Couvillon, A., Dephoure, N. E., Blackwell, T. K., Yu, J. J., Rabinowitz, J. D., Cantley, L. C. and Blenis, J. (2017) 'Post-transcriptional Regulation of De Novo Lipogenesis by mTORC1-S6K1-SRPK2 Signaling', *Cell,* 171(7), pp. 1545-1558.e18.

Lee, J. and Sugden, B. (2007) 'A membrane leucine heptad contributes to trafficking, signaling, and transformation by latent membrane protein 1', *J Virol,* 81(17), pp. 9121-30.

Li, F., Wang, Y., Zeller, K. I., Potter, J. J., Wonsey, D. R., O'Donnell, K. A., Kim, J. W., Yustein, J. T., Lee, L. A. and Dang, C. V. (2005) 'Myc stimulates nuclearly encoded mitochondrial genes and mitochondrial biogenesis', *Mol Cell Biol,* 25(14), pp. 6225-34.

Li, X., Wu, J. B., Li, Q., Shigemura, K., Chung, L. W. and Huang, W. C. (2016) 'SREBP-2 promotes stem cell-like properties and metastasis by transcriptional activation of c-Myc in prostate cancer', *Oncotarget,* 7(11), pp. 12869-84.

Liberti, M. V. and Locasale, J. W. (2016) 'The Warburg Effect: How Does it Benefit Cancer Cells?', *Trends Biochem Sci,* 41(3), pp. 211-8.

Lin, C. Y., Lovén, J., Rahl, P. B., Paranal, R. M., Burge, C. B., Bradner, J. E., Lee, T. I. and Young, R. A. (2012) 'Transcriptional amplification in tumor cells with elevated c-Myc', *Cell,* 151(1), pp. 56-67.

Ling, P. D. and Hayward, S. D. (1995) 'Contribution of conserved amino acids in mediating the interaction between EBNA2 and CBF1/RBPJk', *J Virol,* 69(3), pp. 1944-50.

Ling, P. D., Hsieh, J. J., Ruf, I. K., Rawlins, D. R. and Hayward, S. D. (1994) 'EBNA-2 upregulation of Epstein-Barr virus latency promoters and the cellular CD23 promoter utilizes a common targeting intermediate, CBF1', *J Virol,* 68(9), pp. 5375-83.

Liu, H., Liu, J. Y., Wu, X. and Zhang, J. T. (2010) 'Biochemistry, molecular biology, and pharmacology of fatty acid synthase, an emerging therapeutic target and diagnosis/prognosis marker', *Int J Biochem Mol Biol,* 1(1), pp. 69-89.

Liu, H. P., Wu, C. C. and Chang, Y. S. (2006) 'PRA1 promotes the intracellular trafficking and NF-kappaB signaling of EBV latent membrane protein 1', *EMBO J,* 25(17), pp. 4120-30.

Liu, P., Fang, X., Feng, Z., Guo, Y. M., Peng, R. J., Liu, T., Huang, Z., Feng, Y., Sun, X., Xiong, Z., Guo, X., Pang, S. S., Wang, B., Lv, X., Feng, F. T., Li, D. J., Chen, L. Z., Feng, Q. S., Huang, W. L., Zeng, M. S., Bei, J. X., Zhang, Y. and Zeng, Y. X. (2011) 'Direct sequencing and characterization of a clinical isolate of Epstein-Barr virus from nasopharyngeal carcinoma tissue by using next-generation sequencing technology', *J Virol,* 85(21), pp. 11291-9.

Lo, A. K., Dawson, C. W., Young, L. S., Ko, C. W., Hau, P. M. and Lo, K. W. (2015) 'Activation of the FGFR1 signalling pathway by the Epstein-Barr virus-encoded LMP1 promotes aerobic glycolysis and transformation of human nasopharyngeal epithelial cells', *J Pathol,* 237(2), pp. 238-48.

Lo, A. K., Lung, R. W., Dawson, C. W., Young, L. S., Ko, C., Yeung, W. W., Kang, W., To, K. and Lo, K. (2018) 'Activation of sterol regulatory element‐binding protein 1 (SREBP1)‐mediated lipogenesis by the Epstein–Barr virus‐encoded latent membrane protein 1 (LMP1) promotes cell proliferation and progression of nasopharyngeal carcinoma', *J Pathol: Vol. 2*, pp. 180-90.

Locasale, J. W. (2013) 'Serine, glycine and one-carbon units: cancer metabolism in full circle', *Nat Rev Cancer,* 13(8), pp. 572-83.

Locasale, J. W., Grassian, A. R., Melman, T., Lyssiotis, C. A., Mattaini, K. R., Bass, A. J., Heffron, G., Metallo, C. M., Muranen, T., Sharfi, H., Sasaki, A. T., Anastasiou, D., Mullarky, E., Vokes, N. I., Sasaki, M., Beroukhim, R., Stephanopoulos, G., Ligon, A. H., Meyerson, M., Richardson, A. L., Chin, L., Wagner, G., Asara, J. M., Brugge, J. S., Cantley, L. C. and Vander Heiden, M. G. (2011) 'Phosphoglycerate dehydrogenase diverts glycolytic flux and contributes to oncogenesis', *Nat Genet,* 43(9), pp. 869-74.

Longnecker, R. and Kieff, E. (1990) 'A second Epstein-Barr virus membrane protein (LMP2) is expressed in latent infection and colocalizes with LMP1', *J Virol,* 64(5), pp. 2319-26.

Longnecker, R., Kieff, E and Cohen, JI (2013) 'Epstein-Barr Virus', in Knipe, D.M.a.H., P.M. (ed.) *Fields Virology.* 6 ed. Philadelphia: Lippincott, Williams and Wilkins, pp. 1898-1959.

Longnecker, R., Miller, C. L., Miao, X. Q., Marchini, A. and Kieff, E. (1992) 'The only domain which distinguishes Epstein-Barr virus latent membrane protein 2A (LMP2A) from LMP2B is

dispensable for lymphocyte infection and growth transformation in vitro; LMP2A is therefore nonessential', *J Virol,* 66(11), pp. 6461-9.

Lopaschuk, G. D., Wall, S. R., Olley, P. M. and Davies, N. J. (1988) 'Etomoxir, a carnitine palmitoyltransferase I inhibitor, protects hearts from fatty acid-induced ischemic injury independent of changes in long chain acylcarnitine', *Circ Res,* 63(6), pp. 1036-43.

Lu, E., Wolfreys, F. D., Muppidi, J. R., Xu, Y. and Cyster, J. G. (2019) 'S-Geranylgeranyl-L-glutathione is a ligand for human B cell-confinement receptor P2RY8', *Nature,* 567(7747), pp. 244-248.

Lu, F., Wiedmer, A., Martin, K. A., Wickramasinghe, P., Kossenkov, A. V. and Lieberman, P. M. (2017) 'Coordinate Regulation of TET2 and EBNA2 Controls the DNA Methylation State of Latent Epstein-Barr Virus', *J Virol,* 91(20).

Luftig, M., Prinarakis, E., Yasui, T., Tsichritzis, T., Cahir-McFarland, E., Inoue, J., Nakano, H., Mak, T. W., Yeh, W. C., Li, X., Akira, S., Suzuki, N., Suzuki, S., Mosialos, G. and Kieff, E. (2003) 'Epstein-Barr virus latent membrane protein 1 activation of NF-kappaB through IRAK1 and TRAF6', *Proc Natl Acad Sci U S A,* 100(26), pp. 15595-600.

Lynch, D. T., Zimmerman, J. S. and Rowe, D. T. (2002) 'Epstein-Barr virus latent membrane protein 2B (LMP2B) co-localizes with LMP2A in perinuclear regions in transiently transfected cells', *J Gen Virol,* 83(Pt 5), pp. 1025-35.

Ma, E. H., Bantug, G., Griss, T., Condotta, S., Johnson, R. M., Samborska, B., Mainolfi, N., Suri, V., Guak, H., Balmer, M. L., Verway, M. J., Raissi, T. C., Tsui, H., Boukhaled, G., Henriques da Costa, S., Frezza, C., Krawczyk, C. M., Friedman, A., Manfredi, M., Richer, M. J., Hess, C. and Jones, R. G. (2017a) 'Serine Is an Essential Metabolite for Effector T Cell Expansion', *Cell Metab,* 25(2), pp. 345-357.

Ma, L., Tao, Y., Duran, A., Llado, V., Galvez, A., Barger, J. F., Castilla, E. A., Chen, J., Yajima, T., Porollo, A., Medvedovic, M., Brill, L. M., Plas, D. R., Riedl, S. J., Leitges, M., Diaz-Meco, M. T., Richardson, A. D. and Moscat, J. (2013) 'Control of nutrient stress-induced metabolic reprogramming by PKCzeta in tumorigenesis', *Cell,* 152(3), pp. 599-611.

Ma, S. D., Tsai, M. H., Romero-Masters, J. C., Ranheim, E. A., Huebner, S. M., Bristol, J. A., Delecluse, H. J. and Kenney, S. C. (2017b) 'Latent Membrane Protein 1 (LMP1) and LMP2A Collaborate To Promote Epstein-Barr Virus-Induced B Cell Lymphomas in a Cord Blood-Humanized Mouse Model but Are Not Essential', *J Virol,* 91(7).

Ma, Y., Walsh, M. J., Bernhardt, K., Ashbaugh, C. W., Trudeau, S. J., Ashbaugh, I. Y., Jiang, S., Jiang, C., Zhao, B., Root, D. E., Doench, J. G. and Gewurz, B. E. (2017c) 'CRISPR/Cas9

Screens Reveal Epstein-Barr Virus-Transformed B Cell Host Dependency Factors', *Cell Host Microbe,* 21(5), pp. 580-591.e7.

Maddocks, O. D., Labuschagne, C. F., Adams, P. D. and Vousden, K. H. (2016) 'Serine Metabolism Supports the Methionine Cycle and DNA/RNA Methylation through De Novo ATP Synthesis in Cancer Cells', *Mol Cell,* 61(2), pp. 210-21.

Maeda, M., Constantoulakis, P., Chen, C. S., Stamatoyannopoulos, G. and Yoshida, A. (1992) 'Molecular abnormalities of a human glucose-6-phosphate dehydrogenase variant associated with undetectable enzyme activity and immunologically cross-reacting material', *Am J Hum Genet,* 51(2), pp. 386-95.

Majumder, P. K., Febbo, P. G., Bikoff, R., Berger, R., Xue, Q., McMahon, L. M., Manola, J., Brugarolas, J., McDonnell, T. J., Golub, T. R., Loda, M., Lane, H. A. and Sellers, W. R. (2004) 'mTOR inhibition reverses Akt-dependent prostate intraepithelial neoplasia through regulation of apoptotic and HIF-1-dependent pathways', *Nature Medicine,* 10(6), pp. 594.

Makata, A. M., Toriyama, K., Kamidigo, N. O., Eto, H. and Itakura, H. (1996) 'The pattern of pediatric solid malignant tumors in western Kenya, east Africa, 1979-1994: an analysis based on histopathologic study', *Am J Trop Med Hyg,* 54(4), pp. 343-7.

Mancao, C., Altmann, M., Jungnickel, B. and Hammerschmidt, W. (2005) 'Rescue of "crippled" germinal center B cells from apoptosis by Epstein-Barr virus', *Blood,* 106(13), pp. 4339-44.

Mancao, C. and Hammerschmidt, W. (2007) 'Epstein-Barr virus latent membrane protein 2A is a B-cell receptor mimic and essential for B-cell survival', *Blood,* 110(10), pp. 3715-21.

Marshall, D. and Sample, C. (1995) 'Epstein-Barr virus nuclear antigen 3C is a transcriptional regulator', *J Virol,* 69(6), pp. 3624-30.

Martincic, I., Peralta, M. E. and Ngsee, J. K. (1997) 'Isolation and characterization of a dual prenylated Rab and VAMP2 receptor', *J Biol Chem,* 272(43), pp. 26991-8.

Martinez, O. M. and Krams, S. M. (2017) 'The Immune Response to Epstein Barr Virus and Implications for Posttransplant Lymphoproliferative Disorder', *Transplantation,* 101(9), pp. 2009-2016.

Maruo, S., Wu, Y., Ishikawa, S., Kanda, T., Iwakiri, D. and Takada, K. (2006) 'Epstein-Barr virus nuclear protein EBNA3C is required for cell cycle progression and growth maintenance of lymphoblastoid cells', *Proc Natl Acad Sci U S A,* 103(51), pp. 19500-5.

Mattos, E. P., Silva, A. A., Magalhães, J. A., Leite, J. C., Leistner-Segal, S., Gus-Kessler, R., Perez, J. A., Vedolin, L. M., Torreblanca-Zanca, A., Lapunzina, P., Ruiz-Perez, V. L. and Sanseverino, M. T. (2015) 'Identification of a premature stop codon mutation in the PHGDH gene in severe Neu-Laxova syndrome-evidence for phenotypic variability', *Am J Med Genet A,* 167(6), pp. 1323-9.

McAlister, G. C., Huttlin, E. L., Haas, W., Ting, L., Jedrychowski, M. P., Rogers, J. C., Kuhn, K., Pike, I., Grothe, R. A., Blethrow, J. D. and Gygi, S. P. (2012) 'Increasing the multiplexing capacity of TMTs using reporter ion isotopologues with isobaric masses', *Anal Chem,* 84(17), pp. 7469-78.

McFadden, K., Hafez, A. Y., Kishton, R., Messinger, J. E., Nikitin, P. A., Rathmell, J. C. and Luftig, M. A. (2016) 'Metabolic stress is a barrier to Epstein-Barr virus-mediated B-cell immortalization', *Proc Natl Acad Sci U S A,* 113(6), pp. E782-90.

McMahon, S. B. (2014) 'MYC and the Control of Apoptosis', *Cold Spring Harb Perspect Med: Vol. 7*.

Meckes, D. G., Menaker, N. F. and Raab-Traub, N. (2013) 'Epstein-Barr virus LMP1 modulates lipid raft microdomains and the vimentin cytoskeleton for signal transduction and transformation', *J Virol,* 87(3), pp. 1301-11.

Meija, J., Coplen Tyler, B., Berglund, M., Brand Willi, A., De Bièvre, P., Gröning, M., Holden Norman, E., Irrgeher, J., Loss Robert, D., Walczyk, T. and Prohaska, T. 2016. Isotopic compositions of the elements 2013 (IUPAC Technical Report). *Pure and Applied Chemistry.*

Meiser, J., Tumanov, S., Maddocks, O., Labuschagne, C. F., Athineos, D., Van Den Broek, N., Mackay, G. M., Gottlieb, E., Blyth, K., Vousden, K., Kamphorst, J. J. and Vazquez, A. (2016) 'Serine one-carbon catabolism with formate overflow', *Sci Adv,* 2(10), pp. e1601273.

Merchant, M., Caldwell, R. G. and Longnecker, R. (2000) 'The LMP2A ITAM is essential for providing B cells with development and survival signals in vivo', *J Virol,* 74(19), pp. 9115-24.

Midani, F. S., Wynn, M. L. and Schnell, S. (2017) 'The importance of accurately correcting for the natural abundance of stable isotopes', *Anal Biochem,* 520, pp. 27-43.

Miller, G., Robinson, J. and Heston, L. (1975) 'Immortalizing and nonimmortalizing laboratory strains of Epstein-Barr Virus', *Cold Spring Harb Symp Quant Biol,* 39 Pt 2, pp. 773-81.

Miller, G., Robinson, J., Heston, L. and Lipman, M. (1974) 'Differences between laboratory strains of Epstein-Barr virus based on immortalization, abortive infection, and interference', *Proc Natl Acad Sci U S A,* 71(10), pp. 4006-10.

Minamitani, T., Ma, Y., Zhou, H., Kida, H., Tsai, C. Y., Obana, M., Okuzaki, D., Fujio, Y., Kumanogoh, A., Zhao, B., Kikutani, H., Kieff, E., Gewurz, B. E. and Yasui, T. (2017) 'Mouse model of Epstein-Barr virus LMP1- and LMP2A-driven germinal center B-cell lymphoproliferative disease', *Proc Natl Acad Sci U S A,* 114(18), pp. 4751-4756.

Minton, D. R., Nam, M., McLaughlin, D. J., Shin, J., Bayraktar, E. C., Alvarez, S. W., Sviderskiy, V. O., Papagiannakopoulos, T., Sabatini, D. M., Birsoy, K. and Possemato, R. (2018) 'Serine Catabolism by SHMT2 Is Required for Proper Mitochondrial Translation Initiation and Maintenance of Formylmethionyl-tRNAs', *Mol Cell,* 69(4), pp. 610-621.e5.

Mollinedo, F. and Gajate, C. (2015) 'Lipid rafts as major platforms for signaling regulation in cancer', *Adv Biol Regul,* 57, pp. 130-46.

Molyneux, E. M., Rochford, R., Griffin, B., Newton, R., Jackson, G., Menon, G., Harrison, C. J., Israels, T. and Bailey, S. (2012) 'Burkitt's lymphoma', *Lancet,* 379(9822), pp. 1234-44.

Momb, J., Lewandowski, J. P., Bryant, J. D., Fitch, R., Surman, D. R., Vokes, S. A. and Appling, D. R. (2013) 'Deletion of Mthfd1l causes embryonic lethality and neural tube and craniofacial defects in mice', *Proc Natl Acad Sci U S A,* 110(2), pp. 549-54.

Montone, K. T., Litzky, L. A., Wurster, A., Kaiser, L., Bavaria, J., Kotloff, R., Palevsky, H., Pietra, G. G. and Tomaszewski, J. E. (1996) 'Analysis of Epstein-Barr virus-associated posttransplantation lymphoproliferative disorder after lung transplantation', *Surgery,* 119(5), pp. 544-51.

Moody, C. A., Scott, R. S., Amirghahari, N., Nathan, C. O., Young, L. S., Dawson, C. W. and Sixbey, J. W. (2005) 'Modulation of the cell growth regulator mTOR by Epstein-Barr virus-encoded LMP2A', *J Virol,* 79(9), pp. 5499-506.

Moosmann, A., Bigalke, I., Tischer, J., Schirrmann, L., Kasten, J., Tippmer, S., Leeping, M., Prevalsek, D., Jaeger, G., Ledderose, G., Mautner, J., Hammerschmidt, W., Schendel, D. J. and Kolb, H. J. (2010) 'Effective and long-term control of EBV PTLD after transfer of peptide-selected T cells', *Blood,* 115(14), pp. 2960-70.

Morimoto, S., Nishimura, N., Terai, T., Manabe, S., Yamamoto, Y., Shinahara, W., Miyake, H., Tashiro, S., Shimada, M. and Sasaki, T. (2005) 'Rab13 mediates the continuous endocytic recycling of occludin to the cell surface', *J Biol Chem,* 280(3), pp. 2220-8.

Morscher, R. J., Ducker, G. S., Li, S. H., Mayer, J. A., Gitai, Z., Sperl, W. and Rabinowitz, J. D. (2018) 'Mitochondrial translation requires folate-dependent tRNA methylation', *Nature,* 554(7690), pp. 128-132.

Mrozek-Gorska, P., Buschle, A., Pich, D., Schwarzmayr, T., Fechtner, R., Scialdone, A. and Hammerschmidt, W. (2018) 'Epstein-Barr virus reprograms human B-lymphocytes immediately in the pre-latent phase of infection'.

Mukherjee, A., Wu, J., Barbour, S. and Fang, X. (2012) 'Lysophosphatidic acid activates lipogenic pathways and de novo lipid synthesis in ovarian cancer cells', *J Biol Chem,* 287(30), pp. 24990-5000.

Mullarky, E., Lairson, L. L., Cantley, L. C. and Lyssiotis, C. A. (2016a) 'A novel small-molecule inhibitor of 3-phosphoglycerate dehydrogenase', *Mol Cell Oncol,* 3(4), pp. e1164280.

Mullarky, E., Lucki, N. C., Beheshti Zavareh, R., Anglin, J. L., Gomes, A. P., Nicolay, B. N., Wong, J. C., Christen, S., Takahashi, H., Singh, P. K., Blenis, J., Warren, J. D., Fendt, S. M., Asara, J. M., DeNicola, G. M., Lyssiotis, C. A., Lairson, L. L. and Cantley, L. C. (2016b) 'Identification of a small molecule inhibitor of 3-phosphoglycerate dehydrogenase to target serine biosynthesis in cancers', *Proc Natl Acad Sci U S A,* 113(7), pp. 1778-83.

Munz, C. (2016) 'Epstein Barr virus - a tumor virus that needs cytotoxic lymphocytes to persist asymptomatically', *Curr Opin Virol,* 20, pp. 34-39.

Munz, C. (2017) 'Humanized mouse models for Epstein Barr virus infection', *Curr Opin Virol,* 25, pp. 113-118.

Murray, P. and Bell, A. (2015) 'Contribution of the Epstein-Barr Virus to the Pathogenesis of Hodgkin Lymphoma', *Curr Top Microbiol Immunol,* 390(Pt 1), pp. 287-313.

Mushtaq, M., Darekar, S., Klein, G. and Kashuba, E. (2015) 'Different Mechanisms of Regulation of the Warburg Effect in Lymphoblastoid and Burkitt Lymphoma Cells', *PLoS One,* 10(8), pp. e0136142.

Nair, S. K. and Burley, S. K. (2003) 'X-ray structures of Myc-Max and Mad-Max recognizing DNA. Molecular bases of regulation by proto-oncogenic transcription factors', *Cell,* 112(2), pp. 193-205.

Nalesnik, M. A., Jaffe, R., Starzl, T. E., Demetris, A. J., Porter, K., Burnham, J. A., Makowka, L., Ho, M. and Locker, J. (1988) 'The pathology of posttransplant lymphoproliferative disorders occurring in the setting of cyclosporine A-prednisone immunosuppression', *Am J Pathol,* 133(1), pp. 173-92.

Nelson, E. R., Wardell, S. E., Jasper, J. S., Park, S., Suchindran, S., Howe, M. K., Carver, N. J., Pillai, R. V., Sullivan, P. M., Sondhi, V., Umetani, M., Geradts, J. and McDonnell, D. P. (2013)

'27-Hydroxycholesterol Links Hypercholesterolemia and Breast Cancer Pathophysiology', *Science*.

Nemerow, G. R. and Cooper, N. R. (1984) 'Early events in the infection of human B lymphocytes by Epstein-Barr virus: the internalization process', *Virology,* 132(1), pp. 186-98.

Neri, A., Barriga, F., Inghirami, G., Knowles, D. M., Neequaye, J., Magrath, I. T. and Dalla-Favera, R. (1991) 'Epstein-Barr virus infection precedes clonal expansion in Burkitt's and acquired immunodeficiency syndrome-associated lymphoma', *Blood,* 77(5), pp. 1092-5.

Newell, K. A., Alonso, E. M., Whitington, P. F., Bruce, D. S., Millis, J. M., Piper, J. B., Woodle, E. S., Kelly, S. M., Koeppen, H., Hart, J., Rubin, C. M. and Thistlethwaite, J. R., Jr. (1996) 'Posttransplant lymphoproliferative disease in pediatric liver transplantation. Interplay between primary Epstein-Barr virus infection and immunosuppression', *Transplantation,* 62(3), pp. 370-5.

Newman, A. C. and Maddocks, O. D. K. (2017) 'One-carbon metabolism in cancer', *Br J Cancer,* 116(12), pp. 1499-1504.

Nguyen, U. T., Guo, Z., Delon, C., Wu, Y., Deraeve, C., Franzel, B., Bon, R. S., Blankenfeldt, W., Goody, R. S., Waldmann, H., Wolters, D. and Alexandrov, K. (2009) 'Analysis of the eukaryotic prenylome by isoprenoid affinity tagging', *Nat Chem Biol,* 5(4), pp. 227-35.

Nicklin, P., Bergman, P., Zhang, B., Triantafellow, E., Wang, H., Nyfeler, B., Yang, H., Hild, M., Kung, C., Wilson, C., Myer, V. E., MacKeigan, J. P., Porter, J. A., Wang, Y. K., Cantley, L. C., Finan, P. M. and Murphy, L. O. (2009) 'Bidirectional Transport of Amino Acids Regulates mTOR and Autophagy', *Cell,* 136(3), pp. 521-34.

Nikitin, P. A., Yan, C. M., Forte, E., Bocedi, A., Tourigny, J. P., White, R. E., Allday, M. J., Patel, A., Dave, S. S., Kim, W., Hu, K., Guo, J., Tainter, D., Rusyn, E. and Luftig, M. A. (2010) 'An ATM/Chk2-mediated DNA damage-responsive signaling pathway suppresses Epstein-Barr virus transformation of primary human B cells', *Cell Host Microbe,* 8(6), pp. 510-22.

Nilsson, R., Jain, M., Madhusudhan, N., Sheppard, N. G., Strittmatter, L., Kampf, C., Huang, J., Asplund, A. and Mootha, V. K. (2014) 'Metabolic enzyme expression highlights a key role for MTHFD2 and the mitochondrial folate pathway in cancer', *Nat Commun,* 5, pp. 3128.

Nishikimi, A., Ishihara, S., Ozawa, M., Etoh, K., Fukuda, M., Kinashi, T. and Katagiri, K. (2014) 'Rab13 acts downstream of the kinase Mst1 to deliver the integrin LFA-1 to the cell surface for lymphocyte trafficking', *Sci Signal,* 7(336), pp. ra72.

Nkosi, D., Howell, L. A., Cheerathodi, M. R., Hurwitz, S. N., Tremblay, D. C., Liu, X. and Meckes, D. G. (2018) 'Transmembrane Domains Mediate Intra- and Extracellular Trafficking of Epstein-Barr Virus Latent Membrane Protein 1', *J Virol,* 92(17).

Nonkwelo, C., Skinner, J., Bell, A., Rickinson, A. and Sample, J. (1996) 'Transcription start sites downstream of the Epstein-Barr virus (EBV) Fp promoter in early-passage Burkitt lymphoma cells define a fourth promoter for expression of the EBV EBNA-1 protein', *J Virol,* 70(1), pp. 623-7.

O'Hayre, M., Inoue, A., Kufareva, I., Wang, Z., Mikelis, C. M., Drummond, R. A., Avino, S., Finkel, K., Kalim, K. W., DiPasquale, G., Guo, F., Aoki, J., Zheng, Y., Lionakis, M. S., Molinolo, A. A. and Gutkind, J. S. (2016) 'Inactivating mutations in GNA13 and RHOA in Burkitt's lymphoma and diffuse large B-cell lymphoma: a tumor suppressor function for the Gα13/RhoA axis in B cells', *Oncogene,* 35(29), pp. 3771-80.

Oettgen, H. F., Burkitt, D. and Burchenal, J. H. (1963) 'Malignant lymphoma involving the jaw in African children: treatment with Methotrexate', *Cancer,* 16, pp. 616-23.

Pacold, M. E., Brimacombe, K. R., Chan, S. H., Rohde, J. M., Lewis, C. A., Swier, L. J., Possemato, R., Chen, W. W., Sullivan, L. B., Fiske, B. P., Cho, S., Freinkman, E., Birsoy, K., Abu, M. R., Shaul, Y. D., Liu, C. M., Zhou, M., Koh, M. J., Chung, H., Davidson, S. M., Luengo, A., Wang, A. Q., Xu, X., Yasgar, A., Liu, L., Rai, G., Westover, K. D., Heiden, M. G., Shen, M., Gray, N. S., Boxer, M. B. and Sabatini, D. M. (2016a) 'Corrigendum: A PHGDH inhibitor reveals coordination of serine synthesis and one-carbon unit fate', *Nat Chem Biol,* 12(8), pp. 656.

Pacold, M. E., Brimacombe, K. R., Chan, S. H., Rohde, J. M., Lewis, C. A., Swier, L. J., Possemato, R., Chen, W. W., Sullivan, L. B., Fiske, B. P., Cho, S., Freinkman, E., Birsoy, K., Abu-Remaileh, M., Shaul, Y. D., Liu, C. M., Zhou, M., Koh, M. J., Chung, H., Davidson, S. M., Luengo, A., Wang, A. Q., Xu, X., Yasgar, A., Liu, L., Rai, G., Westover, K. D., Vander Heiden, M. G., Shen, M., Gray, N. S., Boxer, M. B. and Sabatini, D. M. (2016b) 'A PHGDH inhibitor reveals coordination of serine synthesis and one-carbon unit fate', *Nat Chem Biol,* 12(6), pp. 452-8.

Parikh, H., Carlsson, E., Chutkow, W. A., Johansson, L. E., Storgaard, H., Poulsen, P., Saxena, R., Ladd, C., Schulze, P. C., Mazzini, M. J., Jensen, C. B., Krook, A., Björnholm, M., Tornqvist, H., Zierath, J. R., Ridderstråle, M., Altshuler, D., Lee, R. T., Vaag, A., Groop, L. C. and Mootha, V. K. (2007) 'TXNIP regulates peripheral glucose metabolism in humans', *PLoS Med,* 4(5), pp. e158.

Patel, H., Di Pietro, E., Mejia, N. and MacKenzie, R. E. (2005) 'NAD- and NADP-dependent mitochondrially targeted methylenetetrahydrofolate dehydrogenase-cyclohydrolases can rescue mthfd2 null fibroblasts', *Arch Biochem Biophys,* 442(1), pp. 133-9.

Patel, H., Pietro, E. D. and MacKenzie, R. E. (2003) 'Mammalian fibroblasts lacking mitochondrial NAD+-dependent methylenetetrahydrofolate dehydrogenase-cyclohydrolase are glycine auxotrophs', *J Biol Chem,* 278(21), pp. 19436-41.

Patra, K. C. and Hay, N. (2014) 'The pentose phosphate pathway and cancer', *Trends Biochem Sci,* 39(8), pp. 347-54.

Paul, V. D. and Lill, R. (2014) 'SnapShot: eukaryotic Fe-S protein biogenesis', *Cell Metab,* 20(2), pp. 384-384.e1.

Pease, B. N., Huttlin, E. L., Jedrychowski, M. P., Talevich, E., Harmon, J., Dillman, T., Kannan, N., Doerig, C., Chakrabarti, R., Gygi, S. P. and Chakrabarti, D. (2013) 'Global analysis of protein expression and phosphorylation of three stages of Plasmodium falciparum intraerythrocytic development', *J Proteome Res,* 12(9), pp. 4028-45.

Pedley, A. M. and Benkovic, S. J. (2017) 'A New View into the Regulation of Purine Metabolism: The Purinosome', *Trends Biochem Sci,* 42(2), pp. 141-154.

Pedro, M. P., Vilcaes, A. A., Tomatis, V. M., Oliveira, R. G., Gomez, G. A. and Daniotti, J. L. (2013) '2-Bromopalmitate reduces protein deacylation by inhibition of acyl-protein thioesterase enzymatic activities', *PLoS One,* 8(10), pp. e75232.

Pegman, P. M., Smith, S. M., D'Souza, B. N., Loughran, S. T., Maier, S., Kempkes, B., Cahill, P. A., Simmons, M. J., Gelinas, C. and Walls, D. (2006) 'Epstein-Barr virus nuclear antigen 2 trans-activates the cellular antiapoptotic bfl-1 gene by a CBF1/RBPJ kappa-dependent pathway', *J Virol,* 80(16), pp. 8133-44.

Peterson, T. R., Sengupta, S. S., Harris, T. E., Carmack, A. E., Kang, S. A., Balderas, E., Guertin, D. A., Madden, K. L., Carpenter, A. E., Finck, B. N. and Sabatini, D. M. (2011) 'mTOR complex 1 regulates lipin 1 localization to control the SREBP pathway', *Cell,* 146(3), pp. 408-20.

Pikman, Y., Puissant, A., Alexe, G., Furman, A., Chen, L. M., Frumm, S. M., Ross, L., Fenouille, N., Bassil, C. F., Lewis, C. A., Ramos, A., Gould, J., Stone, R. M., DeAngelo, D. J., Galinsky, I., Clish, C. B., Kung, A. L., Hemann, M. T., Vander Heiden, M. G., Banerji, V. and Stegmaier, K. (2016) 'Targeting MTHFD2 in acute myeloid leukemia', *J Exp Med,* 213(7), pp. 1285-306.

Porstmann, T., Griffiths, B., Chung, Y. L., Delpuech, O., Griffiths, J. R., Downward, J. and Schulze, A. (2005) 'PKB/Akt induces transcription of enzymes involved in cholesterol and fatty acid biosynthesis via activation of SREBP', *Oncogene,* 24(43), pp. 6465-81.

Porstmann, T., Santos, C. R., Griffiths, B., Cully, M., Wu, M., Leevers, S., Griffiths, J. R., Chung, Y. L. and Schulze, A. (2008) 'SREBP activity is regulated by mTORC1 and contributes to Akt-dependent cell growth', *Cell Metab,* 8(3), pp. 224-36.

Portis, T. and Longnecker, R. (2004) 'Epstein-Barr virus (EBV) LMP2A mediates B-lymphocyte survival through constitutive activation of the Ras/PI3K/Akt pathway', *Oncogene,* 23(53), pp. 8619-28.

Possemato, R., Marks, K. M., Shaul, Y. D., Pacold, M. E., Kim, D., Birsoy, K., Sethumadhavan, S., Woo, H. K., Jang, H. G., Jha, A. K., Chen, W. W., Barrett, F. G., Stransky, N., Tsun, Z. Y., Cowley, G. S., Barretina, J., Kalaany, N. Y., Hsu, P. P., Ottina, K., Chan, A. M., Yuan, B., Garraway, L. A., Root, D. E., Mino-Kenudson, M., Brachtel, E. F., Driggers, E. M. and Sabatini, D. M. (2011) 'Functional genomics reveal that the serine synthesis pathway is essential in breast cancer', *Nature,* 476(7360), pp. 346-50.

Price, A. M., Dai, J., Bazot, Q., Patel, L., Nikitin, P. A., Djavadian, R., Winter, P. S., Salinas, C. A., Barry, A. P., Wood, K. C., Johannsen, E. C., Letai, A., Allday, M. J. and Luftig, M. A. (2017) 'Epstein-Barr virus ensures B cell survival by uniquely modulating apoptosis at early and late times after infection', *Elife,* 6.

Price, A. M. and Luftig, M. A. (2014) 'Dynamic Epstein-Barr Virus Gene Expression on the Path to B-Cell Transformation', *Adv Virus Res,* 88, pp. 279-313.

Price, A. M. and Luftig, M. A. (2015) 'To be or not IIb: a multi-step process for Epstein-Barr virus latency establishment and consequences for B cell tumorigenesis', *PLoS Pathog,* 11(3), pp. e1004656.

Price, A. M., Messinger, J. E. and Luftig, M. A. (2018) 'c-Myc Represses Transcription of Epstein-Barr Virus Latent Membrane Protein 1 Early after Primary B Cell Infection', *J Virol,* 92(2).

Price, A. M., Tourigny, J. P., Forte, E., Salinas, R. E., Dave, S. S. and Luftig, M. A. (2012) 'Analysis of Epstein-Barr virus-regulated host gene expression changes through primary B-cell outgrowth reveals delayed kinetics of latent membrane protein 1-mediated NF-κB activation', *J Virol,* 86(20), pp. 11096-106.

Puig, T., Aguilar, H., Cufí, S., Oliveras, G., Turrado, C., Ortega-Gutiérrez, S., Benhamú, B., López-Rodríguez, M. L., Urruticoechea, A. and Colomer, R. (2011) 'A novel inhibitor of fatty acid synthase shows activity against HER2+ breast cancer xenografts and is active in anti-HER2 drug-resistant cell lines', *Breast Cancer Res,* 13(6), pp. R131.

Puig, T., Turrado, C., Benhamú, B., Aguilar, H., Relat, J., Ortega-Gutiérrez, S., Casals, G., Marrero, P. F., Urruticoechea, A., Haro, D., López-Rodríguez, M. L. and Colomer, R. (2009)

'Novel Inhibitors of Fatty Acid Synthase with Anticancer Activity', *Clin Cancer Res,* 15(24), pp. 7608-7615.

Purdy, J. G., Shenk, T. and Rabinowitz, J. D. (2015) 'Fatty acid elongase 7 catalyzes lipidome remodeling essential for human cytomegalovirus replication', *Cell Rep,* 10(8), pp. 1375-85.

Rastelli, J., Hömig-Hölzel, C., Seagal, J., Müller, W., Hermann, A. C., Rajewsky, K. and Zimber-Strobl, U. (2008) 'LMP1 signaling can replace CD40 signaling in B cells in vivo and has unique features of inducing class-switch recombination to IgG1', *Blood,* 111(3), pp. 1448-55.

Rathmell, J. C. and Thompson, C. B. (2002) 'Pathways of apoptosis in lymphocyte development, homeostasis, and disease', *Cell,* 109 Suppl, pp. S97-107.

Reid, M. A., Allen, A. E., Liu, S., Liberti, M. V., Liu, P., Liu, X., Dai, Z., Gao, X., Wang, Q., Liu, Y., Lai, L. and Locasale, J. W. (2018) 'Serine synthesis through PHGDH coordinates nucleotide levels by maintaining central carbon metabolism', *Nat Commun,* 9(1), pp. 5442.

Reisman, D., Elkind, N. B., Roy, B., Beamon, J. and Rotter, V. (1993) 'c-Myc trans-activates the p53 promoter through a required downstream CACGTG motif', *Cell Growth Differ,* 4(2), pp. 57-65.

Ricoult, S. J., Yecies, J. L., Ben-Sahra, I. and Manning, B. D. (2016) 'Oncogenic PI3K and K-Ras stimulate de novo lipid synthesis through mTORC1 and SREBP', *Oncogene,* 35(10), pp. 1250-60.

Robertson, E. S., Grossman, S., Johannsen, E., Miller, C., Lin, J., Tomkinson, B. and Kieff, E. (1995) 'Epstein-Barr virus nuclear protein 3C modulates transcription through interaction with the sequence-specific DNA-binding protein J kappa', *J Virol,* 69(5), pp. 3108-16.

Robey, I. F., Lien, A. D., Welsh, S. J., Baggett, B. K. and Gillies, R. J. (2005) 'Hypoxia-Inducible Factor-1α and the Glycolytic Phenotype in Tumors1', *Neoplasia: Vol. 4*, pp. 324-30.

Robinson, J. E., Smith, D. and Niederman, J. (1981) 'Plasmacytic differentiation of circulating Epstein-Barr virus-infected B lymphocytes during acute infectious mononucleosis', *J Exp Med,* 153(2), pp. 235-44.

Rochford, R. and Moormann, A. M. (2015) 'Burkitt's Lymphoma', *Curr Top Microbiol Immunol: Vol. Pt 1.* 2015/10/02 ed, pp. 267-85.

Rodriguez, A. E., Ducker, G. S., Billingham, L. K., Martinez, C. A., Mainolfi, N., Suri, V., Friedman, A., Manfredi, M. G., Weinberg, S. E., Rabinowitz, J. D. and Chandel, N. S. (2019) 'Serine Metabolism Supports Macrophage IL-1beta Production', *Cell Metab*.

Rodriguez-Sanchez, I. and Munger, J. (2019) 'Meal for Two: Human Cytomegalovirus-Induced Activation of Cellular Metabolism', *Viruses,* 11(3).

Rohrig, F. and Schulze, A. (2016) 'The multifaceted roles of fatty acid synthesis in cancer', *Nat Rev Cancer,* 16(11), pp. 732-749.

Ron-Harel, N., Santos, D., Ghergurovich, J. M., Sage, P. T., Reddy, A., Lovitch, S. B., Dephoure, N., Satterstrom, F. K., Sheffer, M., Spinelli, J. B., Gygi, S., Rabinowitz, J. D., Sharpe, A. H. and Haigis, M. C. (2016) 'Mitochondrial Biogenesis and Proteome Remodeling Promote One-Carbon Metabolism for T Cell Activation', *Cell Metab,* 24(1), pp. 104-17.

Rosenblatt, J., Chinkes, D., Wolfe, M. and Wolfe, R. R. (1992) 'Stable isotope tracer analysis by GC-MS, including quantification of isotopomer effects', *Am J Physiol,* 263(3 Pt 1), pp. E584-96.

Rowe, D., Heston, L., Metlay, J. and Miller, G. (1985) 'Identification and expression of a nuclear antigen from the genomic region of the Jijoye strain of Epstein-Barr virus that is missing in its nonimmortalizing deletion mutant, P3HR-1', *Proc Natl Acad Sci U S A,* 82(21), pp. 7429-33.

Rymo, L., Klein, G. and Ricksten, A. (1985) 'Expression of a second Epstein-Barr virus-determined nuclear antigen in mouse cells after gene transfer with a cloned fragment of the viral genome', *Proc Natl Acad Sci U S A,* 82(10), pp. 3435-9.

Sabatini, D. M. (2017) 'Twenty-five years of mTOR: Uncovering the link from nutrients to growth', *Proc Natl Acad Sci U S A,* 114(45), pp. 11818-11825.

Saha, A., Jha, H. C., Upadhyay, S. K. and Robertson, E. S. (2015) 'Epigenetic silencing of tumor suppressor genes during in vitro Epstein-Barr virus infection', *Proc Natl Acad Sci U S A,* 112(37), pp. E5199-207.

Samanta, D., Park, Y., Andrabi, S. A., Shelton, L. M., Gilkes, D. M. and Semenza, G. L. (2016) 'PHGDH Expression Is Required for Mitochondrial Redox Homeostasis, Breast Cancer Stem Cell Maintenance, and Lung Metastasis', *Cancer Res,* 76(15), pp. 4430-42.

Sample, J., Henson, E. B. and Sample, C. (1992) 'The Epstein-Barr virus nuclear protein 1 promoter active in type I latency is autoregulated', *J Virol,* 66(8), pp. 4654-61.

Sanchez, E. L. and Lagunoff, M. (2015) 'Viral activation of cellular metabolism', *Virology,* 479-480, pp. 609-18.

Sanchez, E. L., Pulliam, T. H., Dimaio, T. A., Thalhofer, A. B., Delgado, T. and Lagunoff, M. (2017) 'Glycolysis, Glutaminolysis, and Fatty Acid Synthesis Are Required for Distinct Stages of Kaposi's Sarcoma-Associated Herpesvirus Lytic Replication', *J Virol,* 91(10).

Schaefer, B. C., Woisetschlaeger, M., Strominger, J. L. and Speck, S. H. (1991) 'Exclusive expression of Epstein-Barr virus nuclear antigen 1 in Burkitt lymphoma arises from a third promoter, distinct from the promoters used in latently infected lymphocytes', *Proc Natl Acad Sci U S A,* 88(15), pp. 6550-4.

Schlee, M., Krug, T., Gires, O., Zeidler, R., Hammerschmidt, W., Mailhammer, R., Laux, G., Sauer, G., Lovric, J. and Bornkamm, G. W. (2004) 'Identification of Epstein-Barr virus (EBV) nuclear antigen 2 (EBNA2) target proteins by proteome analysis: activation of EBNA2 in conditionally immortalized B cells reflects early events after infection of primary B cells by EBV', *J Virol,* 78(8), pp. 3941-52.

Schmid, T., Jansen, A. P., Baker, A. R., Hegamyer, G., Hagan, J. P. and Colburn, N. H. (2008) 'Translation inhibitor Pdcd4 is targeted for degradation during tumor promotion', *Cancer Res,* 68(5), pp. 1254-60.

Schmidt, S. C., Jiang, S., Zhou, H., Willox, B., Holthaus, A. M., Kharchenko, P. V., Johannsen, E. C., Kieff, E. and Zhao, B. (2015) 'Epstein-Barr virus nuclear antigen 3A partially coincides with EBNA3C genome-wide and is tethered to DNA through BATF complexes', *Proc Natl Acad Sci U S A,* 112(2), pp. 554-9.

Schuhmacher, M., Kohlhuber, F., Holzel, M., Kaiser, C., Burtscher, H., Jarsch, M., Bornkamm, G. W., Laux, G., Polack, A., Weidle, U. H. and Eick, D. (2001a) 'The transcriptional program of a human B cell line in response to Myc', *Nucleic Acids Res,* 29(2), pp. 397-406.

Schuhmacher, M., Kohlhuber, F., Hölzel, M., Kaiser, C., Burtscher, H., Jarsch, M., Bornkamm, G. W., Laux, G., Polack, A., Weidle, U. H. and Eick, D. (2001b) 'The transcriptional program of a human B cell line in response to Myc', *Nucleic Acids Res,* 29(2), pp. 397-406.

Schuhmacher, M., Staege, M. S., Pajic, A., Polack, A., Weidle, U. H., Bornkamm, G. W., Eick, D. and Kohlhuber, F. (1999) 'Control of cell growth by c-Myc in the absence of cell division', *Curr Biol,* 9(21), pp. 1255-8.

Segala, G., David, M., de Medina, P., Poirot, M. C., Serhan, N., Vergez, F., Mougel, A., Saland, E., Carayon, K., Leignadier, J., Caron, N., Voisin, M., Cherier, J., Ligat, L., Lopez, F., Noguer, E., Rives, A., Payre, B., Saati, T. A., Lamaziere, A., Despres, G., Lobaccaro, J. M., Baron, S., Demur, C., de Toni, F., Larrue, C., Boutzen, H., Thomas, F., Sarry, J. E., Tosolini, M., Picard,

D., Record, M., Recher, C., Poirot, M. and Silvente-Poirot, S. (2017) 'Dendrogenin A drives LXR to trigger lethal autophagy in cancers', *Nat Commun,* 8(1), pp. 1903.

Semenza, G. L. (2013) 'HIF-1 mediates metabolic responses to intratumoral hypoxia and oncogenic mutations', *J Clin Invest: Vol. 9*, pp. 3664-71.

Shaheen, R., Rahbeeni, Z., Alhashem, A., Faqeih, E., Zhao, Q., Xiong, Y., Almoisheer, A., Al-Qattan, S. M., Almadani, H. A., Al-Onazi, N., Al-Baqawi, B. S., Saleh, M. A. and Alkuraya, F. S. (2014) 'Neu-Laxova syndrome, an inborn error of serine metabolism, is caused by mutations in PHGDH', *Am J Hum Genet,* 94(6), pp. 898-904.

Shalem, O., Sanjana, N. E., Hartenian, E., Shi, X., Scott, D. A., Mikkelson, T., Heckl, D., Ebert, B. L., Root, D. E., Doench, J. G. and Zhang, F. (2014) 'Genome-scale CRISPR-Cas9 knockout screening in human cells', *Science,* 343(6166), pp. 84-87.

Shannon-Lowe, C., Rickinson, A. B. and Bell, A. I. (2017) 'Epstein-Barr virus-associated lymphomas', *Philos Trans R Soc Lond B Biol Sci,* 372(1732).

Shao, W., Machamer, C. E. and Espenshade, P. J. (2016) 'Fatostatin blocks ER exit of SCAP but inhibits cell growth in a SCAP-independent manner', *J Lipid Res,* 57(8), pp. 1564-73.

Shenk, T. and Alwine, J. C. (2014) 'Human Cytomegalovirus: Coordinating Cellular Stress, Signaling, and Metabolic Pathways', *Annu Rev Virol,* 1(1), pp. 355-74.

Sherbet, G. V. (1989) 'Membrane fluidity and cancer metastasis', *Exp Cell Biol,* 57(4), pp. 198-205.

Shim, H., Dolde, C., Lewis, B. C., Wu, C. S., Dang, G., Jungmann, R. A., Dalla-Favera, R. and Dang, C. V. (1997) 'c-Myc transactivation of LDH-A: implications for tumor metabolism and growth', *Proc Natl Acad Sci U S A,* 94(13), pp. 6658-63.

Shimabukuro-Vornhagen, A., Zoghi, S., Liebig, T. M., Wennhold, K., Chemitz, J., Draube, A., Kochanek, M., Blaschke, F., Pallasch, C., Holtick, U., Scheid, C., Theurich, S., Hallek, M. and von Bergwelt-Baildon, M. S. (2014) 'Inhibition of protein geranylgeranylation specifically interferes with CD40-dependent B cell activation, resulting in a reduced capacity to induce T cell immunity', *J Immunol,* 193(10), pp. 5294-305.

Shimano, H., Yahagi, N., Amemiya-Kudo, M., Hasty, A. H., Osuga, J., Tamura, Y., Shionoiri, F., Iizuka, Y., Ohashi, K., Harada, K., Gotoda, T., Ishibashi, S. and Yamada, N. (1999) 'Sterol regulatory element-binding protein-1 as a key transcription factor for nutritional induction of lipogenic enzyme genes', *J Biol Chem,* 274(50), pp. 35832-9.

Shin, M., Bryant, J. D., Momb, J. and Appling, D. R. (2014) 'Mitochondrial MTHFD2L is a dual redox cofactor-specific methylenetetrahydrofolate dehydrogenase/methenyltetrahydrofolate cyclohydrolase expressed in both adult and embryonic tissues', *J Biol Chem,* 289(22), pp. 15507-17.

Shin, M., Momb, J. and Appling, D. R. (2017) 'Human mitochondrial MTHFD2 is a dual redox cofactor-specific methylenetetrahydrofolate dehydrogenase/methenyltetrahydrofolate cyclohydrolase', *Cancer Metab,* 5, pp. 11.

Shumilov, A., Tsai, M. H., Schlosser, Y. T., Kratz, A. S., Bernhardt, K., Fink, S., Mizani, T., Lin, X., Jauch, A., Mautner, J., Kopp-Schneider, A., Feederle, R., Hoffmann, I. and Delecluse, H. J. (2017) 'Epstein-Barr virus particles induce centrosome amplification and chromosomal instability', *Nat Commun,* 8, pp. 14257.

Singh, R. K., Lang, F., Pei, Y., Jha, H. C. and Robertson, E. S. (2018) 'Metabolic reprogramming of Kaposi's sarcoma associated herpes virus infected B-cells in hypoxia', *PLoS Pathog,* 14(5), pp. e1007062.

Sivars, U., Aivazian, D. and Pfeffer, S. R. (2003) 'Yip3 catalyses the dissociation of endosomal Rab-GDI complexes', *Nature,* 425(6960), pp. 856-9.

Sommermann, T. G., O'Neill, K., Plas, D. R. and Cahir-McFarland, E. (2011) 'IKKβ and NF-κB transcription govern lymphoma cell survival through AKT-induced plasma membrane trafficking of GLUT1', *Cancer Res,* 71(23), pp. 7291-300.

Spencer, C. M., Schafer, X. L., Moorman, N. J. and Munger, J. (2011) 'Human cytomegalovirus induces the activity and expression of acetyl-coenzyme A carboxylase, a fatty acid biosynthetic enzyme whose inhibition attenuates viral replication', *J Virol,* 85(12), pp. 5814-24.

Stine, Z. E., Walton, Z. E., Altman, B. J., Hsieh, A. L. and Dang, C. V. (2015) 'MYC, Metabolism, and Cancer', *Cancer Discov,* 5(10), pp. 1024-39.

Strobl, L. J., Hofelmayr, H., Marschall, G., Brielmeier, M., Bornkamm, G. W. and Zimber-Strobl, U. (2000) 'Activated Notch1 modulates gene expression in B cells similarly to Epstein-Barr viral nuclear antigen 2', *J Virol,* 74(4), pp. 1727-35.

Stunz, L. L. and Bishop, G. A. (2014) 'Latent membrane protein 1 and the B lymphocyte-a complex relationship', *Crit Rev Immunol,* 34(3), pp. 177-98.

Subramanian, A., Tamayo, P., Mootha, V. K., Mukherjee, S., Ebert, B. L., Gillette, M. A., Paulovich, A., Pomeroy, S. L., Golub, T. R., Lander, E. S. and Mesirov, J. P. (2005) 'Gene set

enrichment analysis: a knowledge-based approach for interpreting genome-wide expression profiles', *Proc Natl Acad Sci U S A,* 102(43), pp. 15545-50.

Sullivan, L. B., Gui, D. Y., Hosios, A. M., Bush, L. N., Freinkman, E. and Vander Heiden, M. G. (2015) 'Supporting Aspartate Biosynthesis Is an Essential Function of Respiration in Proliferating Cells', *Cell,* 162(3), pp. 552-63.

Sullivan, M. R., Mattaini, K. R., Dennstedt, E. A., Nguyen, A. A., Sivanand, S., Reilly, M. F., Meeth, K., Muir, A., Darnell, A. M., Bosenberg, M. W., Lewis, C. A. and Vander Heiden, M. G. (2019) 'Increased Serine Synthesis Provides an Advantage for Tumors Arising in Tissues Where Serine Levels Are Limiting', *Cell Metab*.

Sun, Q., Chen, X., Ma, J., Peng, H., Wang, F., Zha, X., Wang, Y., Jing, Y., Yang, H., Chen, R., Chang, L., Zhang, Y., Goto, J., Onda, H., Chen, T., Wang, M. R., Lu, Y., You, H., Kwiatkowski, D. and Zhang, H. (2011) 'Mammalian target of rapamycin up-regulation of pyruvate kinase isoenzyme type M2 is critical for aerobic glycolysis and tumor growth', *Proc Natl Acad Sci U S A,* 108(10), pp. 4129-34.

Sung, W. W., Chen, P. R., Liao, M. H. and Lee, J. W. (2017) 'Enhanced aerobic glycolysis of nasopharyngeal carcinoma cells by Epstein-Barr virus latent membrane protein 1', *Exp Cell Res,* 359(1), pp. 94-100.

Suzuki, C., Garces, R. G., Edmonds, K. A., Hiller, S., Hyberts, S. G., Marintchev, A. and Wagner, G. (2008) 'PDCD4 inhibits translation initiation by binding to eIF4A using both its MA3 domains', *Proc Natl Acad Sci U S A,* 105(9), pp. 3274-9.

Swart, R., Ruf, I. K., Sample, J. and Longnecker, R. (2000) 'Latent membrane protein 2A-mediated effects on the phosphatidylinositol 3-Kinase/Akt pathway', *J Virol,* 74(22), pp. 10838-45.

Sychev, Z. E., Hu, A., DiMaio, T. A., Gitter, A., Camp, N. D., Noble, W. S., Wolf-Yadlin, A. and Lagunoff, M. (2017) 'Integrated systems biology analysis of KSHV latent infection reveals viral induction and reliance on peroxisome mediated lipid metabolism', *PLoS Pathog,* 13(3), pp. e1006256.

Tani, H., Ohnishi, S., Shitara, H., Mito, T., Yamaguchi, M., Yonekawa, H., Hashizume, O., Ishikawa, K., Nakada, K. and Hayashi, J. I. (2018) 'Mice deficient in the Shmt2 gene have mitochondrial respiration defects and are embryonic lethal', *Sci Rep,* 8(1), pp. 425.

Tanner, J., Weis, J., Fearon, D., Whang, Y. and Kieff, E. (1987) 'Epstein-Barr virus gp350/220 binding to the B lymphocyte C3d receptor mediates adsorption, capping, and endocytosis', *Cell,* 50(2), pp. 203-13.

Tanner, J. M., Bensard, C., Wei, P., Krah, N. M., Schell, J. C., Gardiner, J., Schiffman, J., Lessnick, S. L. and Rutter, J. (2017) 'EWS/FLI is a Master Regulator of Metabolic Reprogramming in Ewing Sarcoma', *Mol Cancer Res,* 15(11), pp. 1517-1530.

Taylor, G. S., Long, H. M., Brooks, J. M., Rickinson, A. B. and Hislop, A. D. (2015) 'The immunology of Epstein-Barr virus-induced disease', *Annu Rev Immunol,* 33, pp. 787-821.

Tedeschi, P. M., Markert, E. K., Gounder, M., Lin, H., Dvorzhinski, D., Dolfi, S. C., Chan, L. L., Qiu, J., DiPaola, R. S., Hirshfield, K. M., Boros, L. G., Bertino, J. R., Oltvai, Z. N. and Vazquez, A. (2013) 'Contribution of serine, folate and glycine metabolism to the ATP, NADPH and purine requirements of cancer cells', *Cell Death Dis,* 4, pp. e877.

Thibault, A., Samid, D., Tompkins, A. C., Figg, W. D., Cooper, M. R., Hohl, R. J., Trepel, J., Liang, B., Patronas, N., Venzon, D. J., Reed, E. and Myers, C. E. (1996) 'Phase I study of lovastatin, an inhibitor of the mevalonate pathway, in patients with cancer', *Clin Cancer Res,* 2(3), pp. 483-91.

Thorley-Lawson, D. A. (2015) 'EBV Persistence--Introducing the Virus', *Curr Top Microbiol Immunol,* 390(Pt 1), pp. 151-209.

Thorley-Lawson, D. A. and Gross, A. (2004) 'Persistence of the Epstein-Barr virus and the origins of associated lymphomas', *N Engl J Med,* 350(13), pp. 1328-37.

Thorley-Lawson, D. A. and Mann, K. P. (1985) 'Early events in Epstein-Barr virus infection provide a model for B cell activation', *J Exp Med,* 162(1), pp. 45-59.

Ting, Y. S., Shaffer, S. A., Jones, J. W., Ng, W. V., Ernst, R. K. and Goodlett, D. R. (2011) 'Automated lipid A structure assignment from hierarchical tandem mass spectrometry data', *J Am Soc Mass Spectrom,* 22(5), pp. 856-66.

Titov, D. V., Cracan, V., Goodman, R. P., Peng, J., Grabarek, Z. and Mootha, V. K. (2016) 'Complementation of mitochondrial electron transport chain by manipulation of the NAD+/NADH ratio', *Science,* 352(6282), pp. 231-5.

Tsai, K., Chan, L., Gibeault, R., Conn, K., Dheekollu, J., Domsic, J., Marmorstein, R., Schang, L. M. and Lieberman, P. M. (2014) 'Viral reprogramming of the Daxx histone H3.3 chaperone during early Epstein-Barr virus infection', *J Virol,* 88(24), pp. 14350-63.

Tsai, K., Thikmyanova, N., Wojcechowskyj, J. A., Delecluse, H. J. and Lieberman, P. M. (2011) 'EBV tegument protein BNRF1 disrupts DAXX-ATRX to activate viral early gene transcription', *PLoS Pathog,* 7(11), pp. e1002376.

Tsang, S. F., Wang, F., Izumi, K. M. and Kieff, E. (1991) 'Delineation of the cis-acting element mediating EBNA-2 transactivation of latent infection membrane protein expression', *J Virol,* 65(12), pp. 6765-71.

Tsao, S. W., Tsang, C. M. and Lo, K. W. (2017) 'Epstein-Barr virus infection and nasopharyngeal carcinoma', *Philos Trans R Soc Lond B Biol Sci,* 372(1732).

Uauy, R., Vega, G. L., Grundy, S. M. and Bilheimer, D. M. (1988) 'Lovastatin therapy in receptor-negative homozygous familial hypercholesterolemia: lack of effect on low-density lipoprotein concentrations or turnover', *J Pediatr,* 113(2), pp. 387-92.

Uchida, J., Yasui, T., Takaoka-Shichijo, Y., Muraoka, M., Kulwichit, W., Raab-Traub, N. and Kikutani, H. (1999) 'Mimicry of CD40 signals by Epstein-Barr virus LMP1 in B lymphocyte responses', *Science,* 286(5438), pp. 300-3.

Valencia, S. M. and Hutt-Fletcher, L. M. (2012) 'Important but Differential Roles for Actin in Trafficking of Epstein-Barr Virus in B Cells and Epithelial Cells', *J Virol: Vol. 1*, pp. 2-10.

Valente, A. J., Morris, C. J. and Walton, K. W. (1980) 'Demonstration by a rosette-forming technique of surface receptors for low-density lipoproteins on lymphoblastoid cells', *Clin Sci (Lond),* 59(4), pp. 265-73.

van de Donk, N. W., Lokhorst, H. M., Nijhuis, E. H., Kamphuis, M. M. and Bloem, A. C. (2005) 'Geranylgeranylated proteins are involved in the regulation of myeloma cell growth', *Clin Cancer Res,* 11(2 Pt 1), pp. 429-39.

van de Donk, N. W., Schotte, D., Kamphuis, M. M., van Marion, A. M., van Kessel, B., Bloem, A. C. and Lokhorst, H. M. (2003) 'Protein geranylgeranylation is critical for the regulation of survival and proliferation of lymphoma tumor cells', *Clin Cancer Res,* 9(15), pp. 5735-48.

Van Vranken, J. G., Jeong, M. Y., Wei, P., Chen, Y. C., Gygi, S. P., Winge, D. R. and Rutter, J. (2016) 'The mitochondrial acyl carrier protein (ACP) coordinates mitochondrial fatty acid synthesis with iron sulfur cluster biogenesis', *Elife,* 5.

Vander Heiden, M. G., Cantley, L. C. and Thompson, C. B. (2009) 'Understanding the Warburg effect: the metabolic requirements of cell proliferation', *Science,* 324(5930), pp. 1029-33.

Vennstrom, B., Sheiness, D., Zabielski, J. and Bishop, J. M. (1982) 'Isolation and characterization of c-myc, a cellular homolog of the oncogene (v-myc) of avian myelocytomatosis virus strain 29', *J Virol,* 42(3), pp. 773-9.

Verweij, F. J., de Heus, C., Kroeze, S., Cai, H., Kieff, E., Piersma, S. R., Jimenez, C. R., Middeldorp, J. M. and Pegtel, D. M. (2015) 'Exosomal sorting of the viral oncoprotein LMP1 is restrained by TRAF2 association at signalling endosomes', *J Extracell Vesicles,* 4, pp. 26334.

Verweij, F. J., van Eijndhoven, M. A., Hopmans, E. S., Vendrig, T., Wurdinger, T., Cahir-McFarland, E., Kieff, E., Geerts, D., van der Kant, R., Neefjes, J., Middeldorp, J. M. and Pegtel, D. M. (2011) 'LMP1 association with CD63 in endosomes and secretion via exosomes limits constitutive NF-κB activation', *EMBO J,* 30(11), pp. 2115-29.

Villagra, A., Ulloa, N., Zhang, X., Yuan, Z., Sotomayor, E. and Seto, E. (2007) 'Histone deacetylase 3 down-regulates cholesterol synthesis through repression of lanosterol synthase gene expression', *J Biol Chem,* 282(49), pp. 35457-70.

Vysochan, A., Sengupta, A., Weljie, A. M., Alwine, J. C. and Yu, Y. (2017) 'ACSS2-mediated acetyl-CoA synthesis from acetate is necessary for human cytomegalovirus infection', *Proc Natl Acad Sci U S A: Vol. 8*, pp. E1528-35.

Wagner, B. K., Gilbert, T. J., Hanai, J., Imamura, S., Bodycombe, N. E., Bon, R. S., Waldmann, H., Clemons, P. A., Sukhatme, V. P. and Mootha, V. K. (2011) 'A small-molecule screening strategy to identify suppressors of statin myopathy', *ACS Chem Biol,* 6(9), pp. 900-4.

Wakisaka, N., Kondo, S., Yoshizaki, T., Murono, S., Furukawa, M. and Pagano, J. S. (2004) 'Epstein-Barr virus latent membrane protein 1 induces synthesis of hypoxia-inducible factor 1 alpha', *Mol Cell Biol,* 24(12), pp. 5223-34.

Walker, A. K., Yang, F., Jiang, K., Ji, J. Y., Watts, J. L., Purushotham, A., Boss, O., Hirsch, M. L., Ribich, S., Smith, J. J., Israelian, K., Westphal, C. H., Rodgers, J. T., Shioda, T., Elson, S. L., Mulligan, P., Najafi-Shoushtari, H., Black, J. C., Thakur, J. K., Kadyk, L. C., Whetstine, J. R., Mostoslavsky, R., Puigserver, P., Li, X., Dyson, N. J., Hart, A. C. and Näär, A. M. (2010) 'Conserved role of SIRT1 orthologs in fasting-dependent inhibition of the lipid/cholesterol regulator SREBP', *Genes Dev,* 24(13), pp. 1403-17.

Waltzer, L., Logeat, F., Brou, C., Israel, A., Sergeant, A. and Manet, E. (1994) 'The human J kappa recombination signal sequence binding protein (RBP-J kappa) targets the Epstein-Barr virus EBNA2 protein to its DNA responsive elements', *EMBO J,* 13(23), pp. 5633-8.

Wang, A., Welch, R., Zhao, B., Ta, T., Keles, S. and Johannsen, E. (2015) 'Epstein-Barr Virus Nuclear Antigen 3 (EBNA3) Proteins Regulate EBNA2 Binding to Distinct RBPJ Genomic Sites', *J Virol,* 90(6), pp. 2906-19.

Wang, D., Liebowitz, D. and Kieff, E. (1985) 'An EBV membrane protein expressed in immortalized lymphocytes transforms established rodent cells', *Cell,* 43(3 Pt 2), pp. 831-40.

Wang, F., Gregory, C. D., Rowe, M., Rickinson, A. B., Wang, D., Birkenbach, M., Kikutani, H., Kishimoto, T. and Kieff, E. (1987) 'Epstein-Barr virus nuclear antigen 2 specifically induces expression of the B-cell activation antigen CD23', *Proc Natl Acad Sci U S A,* 84(10), pp. 3452-6.

Wang, F., Kikutani, H., Tsang, S. F., Kishimoto, T. and Kieff, E. (1991) 'Epstein-Barr virus nuclear protein 2 transactivates a cis-acting CD23 DNA element', *J Virol,* 65(8), pp. 4101-6.

Wang, F., Tsang, S. F., Kurilla, M. G., Cohen, J. I. and Kieff, E. (1990) 'Epstein-Barr virus nuclear antigen 2 transactivates latent membrane protein LMP1', *J Virol,* 64(7), pp. 3407-16.

Wang, L., Wei, Shen, H., Nobre, L., Ersing, I., Paulo, J. A., Trudeau, S., Wang, Z., Smith, N. A., Ma, Y., Reinstadler, B., Nomburg, J., Sommermann, T., Cahir-McFarland, E., Gygi, S. P., Mootha, V. K., Weekes, M. P. and Gewurz, B. E. (2019) 'Epstein-Barr Virus Induced One-Carbon Metabolism Drives B-Cell Transformation', *Cell Metabolism*

Wang, L. W., Jiang, S. and Gewurz, B. E. (2017) 'Epstein-Barr Virus LMP1-Mediated Oncogenicity', *J Virol,* 91(21).

Wang, Q., Liberti, M. V., Liu, P., Deng, X., Liu, Y., Locasale, J. W. and Lai, L. (2017) 'Rational Design of Selective Allosteric Inhibitors of PHGDH and Serine Synthesis with Anti-tumor Activity', *Cell Chem Biol,* 24(1), pp. 55-65.

Warburg, O. (1925) 'The metabolism of carcinoma cells.', *Journal of Cancer Research,* 9, pp. 148-163.

Warburg, O. (1928) 'THE CHEMICAL CONSTITUTION OF RESPIRATION FERMENT', *Science,* 68(1767), pp. 437-43.

Weekes, M. P., Antrobus, R., Talbot, S., Hor, S., Simecek, N., Smith, D. L., Bloor, S., Randow, F. and Lehner, P. J. (2012) 'Proteomic plasma membrane profiling reveals an essential role for gp96 in the cell surface expression of LDLR family members, including the LDL receptor and LRP6', *J Proteome Res,* 11(3), pp. 1475-84.

Weekes, M. P., Tomasec, P., Huttlin, E. L., Fielding, C. A., Nusinow, D., Stanton, R. J., Wang, E. C., Aicheler, R., Murrell, I., Wilkinson, G. W., Lehner, P. J. and Gygi, S. P. (2014) 'Quantitative temporal viromics: an approach to investigate host-pathogen interaction', *Cell,* 157(6), pp. 1460-72.

Welz, T., Wellbourne-Wood, J. and Kerkhoff, E. (2014) 'Orchestration of cell surface proteins by Rab11', *Trends Cell Biol,* 24(7), pp. 407-15.

Wille, C. K., Li, Y., Rui, L., Johannsen, E. C. and Kenney, S. C. (2017) 'Restricted TET2 Expression in Germinal Center Type B Cells Promotes Stringent Epstein-Barr Virus Latency', *J Virol,* 91(5).

Wirtz, T., Weber, T., Kracker, S., Sommermann, T., Rajewsky, K. and Yasuda, T. (2016) 'Mouse model for acute Epstein-Barr virus infection', *Proc Natl Acad Sci U S A,* 113(48), pp. 13821-13826.

Woisetschlaeger, M., Yandava, C. N., Furmanski, L. A., Strominger, J. L. and Speck, S. H. (1990) 'Promoter switching in Epstein-Barr virus during the initial stages of infection of B lymphocytes', *Proc Natl Acad Sci U S A,* 87(5), pp. 1725-9.

Wolfe, A. L., Singh, K., Zhong, Y., Drewe, P., Rajasekhar, V. K., Sanghvi, V. R., Mavrakis, K. J., Jiang, M., Roderick, J. E., Van der Meulen, J., Schatz, J. H., Rodrigo, C. M., Zhao, C., Rondou, P., de Stanchina, E., Teruya-Feldstein, J., Kelliher, M. A., Speleman, F., Porco, J. A., Jr., Pelletier, J., Ratsch, G. and Wendel, H. G. (2014) 'RNA G-quadruplexes cause eIF4A-dependent oncogene translation in cancer', *Nature,* 513(7516), pp. 65-70.

Wolfson, R. L., Chantranupong, L., Saxton, R. A., Shen, K., Scaria, S. M., Cantor, J. R. and Sabatini, D. M. (2016) 'Sestrin2 is a leucine sensor for the mTORC1 pathway', *Science,* 351(6268), pp. 43-8.

Wood, C. D., Veenstra, H., Khasnis, S., Gunnell, A., Webb, H. M., Shannon-Lowe, C., Andrews, S., Osborne, C. S. and West, M. J. (2016) 'MYC activation and BCL2L11 silencing by a tumour virus through the large-scale reconfiguration of enhancer-promoter hubs', *Elife,* 5.

Wu, Q., Ishikawa, T., Sirianni, R., Tang, H., McDonald, J. G., Yuhanna, I. S., Thompson, B., Girard, L., Mineo, C., Brekken, R. A., Umetani, M., Euhus, D. M., Xie, Y. and Shaul, P. W. (2013) '27-Hydroxycholesterol promotes cell-autonomous, ER-positive breast cancer growth', *Cell Rep,* 5(3), pp. 637-45.

Wu, Y., Chen, K., Liu, X., Huang, L., Zhao, D., Li, L., Gao, M., Pei, D. and Wang, C. (2016) 'Srebp-1 Interacts with c-Myc to Enhance Somatic Cell Reprogramming', *Stem Cells,* 34(1), pp. 83-92.

Xiao, G., Chan, L. N., Klemm, L., Braas, D., Chen, Z., Geng, H., Zhang, Q. C., Aghajanirefah, A., Cosgun, K. N., Sadras, T., Lee, J., Mirzapoiazova, T., Salgia, R., Ernst, T., Hochhaus, A., Jumaa, H., Jiang, X., Weinstock, D. M., Graeber, T. G. and Müschen, M. (2018) 'B-Cell-Specific Diversion of Glucose Carbon Utilization Reveals a Unique Vulnerability in B Cell Malignancies', *Cell,* 173(2), pp. 470-484.e18.

Yang, H. S., Jansen, A. P., Komar, A. A., Zheng, X., Merrick, W. C., Costes, S., Lockett, S. J., Sonenberg, N. and Colburn, N. H. (2003) 'The transformation suppressor Pdcd4 is a novel

eukaryotic translation initiation factor 4A binding protein that inhibits translation', *Mol Cell Biol,* 23(1), pp. 26-37.

Yang, M. and Vousden, K. H. (2016) 'Serine and one-carbon metabolism in cancer', *Nat Rev Cancer,* 16(10), pp. 650-62.

Yang, T., Espenshade, P. J., Wright, M. E., Yabe, D., Gong, Y., Aebersold, R., Goldstein, J. L. and Brown, M. S. (2002) 'Crucial step in cholesterol homeostasis: sterols promote binding of SCAP to INSIG-1, a membrane protein that facilitates retention of SREBPs in ER', *Cell,* 110(4), pp. 489-500.

Yang, T. H., Bolten, C. J., Coppi, M. V., Sun, J. and Heinzle, E. (2009) 'Numerical bias estimation for mass spectrometric mass isotopomer analysis', *Anal Biochem,* 388(2), pp. 192-203.

Yang, W. S. and Stockwell, B. R. (2016) 'Ferroptosis: Death by Lipid Peroxidation', *Trends Cell Biol,* 26(3), pp. 165-176.

Ye, J., Mancuso, A., Tong, X., Ward, P. S., Fan, J., Rabinowitz, J. D. and Thompson, C. B. (2012) 'Pyruvate kinase M2 promotes de novo serine synthesis to sustain mTORC1 activity and cell proliferation', *Proc Natl Acad Sci U S A: Vol. 18*, pp. 6904-9.

Yeo, J. C., Wall, A. A., Luo, L. and Stow, J. L. (2016) 'Sequential recruitment of Rab GTPases during early stages of phagocytosis', *Cell Logist,* 6(1), pp. e1140615.

Yogev, O., Lagos, D., Enver, T. and Boshoff, C. (2014) 'Kaposi's sarcoma herpesvirus microRNAs induce metabolic transformation of infected cells', *PLoS Pathog,* 10(9), pp. e1004400.

Yoshino, H., Nohata, N., Miyamoto, K., Yonemori, M., Sakaguchi, T., Sugita, S., Itesako, T., Kofuji, S., Nakagawa, M., Dahiya, R. and Enokida, H. (2017) 'PHGDH as a Key Enzyme for Serine Biosynthesis in HIF2alpha-Targeting Therapy for Renal Cell Carcinoma', *Cancer Res,* 77(22), pp. 6321-6329.

Young, L. S., Arrand, J. R. and Murray, P. G. (2007) 'EBV gene expression and regulation'.

Yu, Y., Maguire, T. G. and Alwine, J. C. (2012) 'Human Cytomegalovirus Infection Induces Adipocyte-Like Lipogenesis through Activation of Sterol Regulatory Element Binding Protein 1', *J Virol: Vol. 6*, pp. 2942-9.

Yun, S. M., Kim, Y. S. and Hur, D. Y. (2019) 'LMP1 and 2A Induce the Expression of Nrf2 Through Akt Signaling Pathway in Epstein-Barr Virus-Transformed B Cells', *Transl Oncol,* 12(5), pp. 775-783.

Zeller, K. I., Jegga, A. G., Aronow, B. J., O'Donnell, K. A. and Dang, C. V. (2003) 'An integrated database of genes responsive to the Myc oncogenic transcription factor: identification of direct genomic targets', *Genome Biol,* 4(10), pp. R69.

Zeller, K. I., Zhao, X., Lee, C. W., Chiu, K. P., Yao, F., Yustein, J. T., Ooi, H. S., Orlov, Y. L., Shahab, A., Yong, H. C., Fu, Y., Weng, Z., Kuznetsov, V. A., Sung, W. K., Ruan, Y., Dang, C. V. and Wei, C. L. (2006) 'Global mapping of c-Myc binding sites and target gene networks in human B cells', *Proc Natl Acad Sci U S A,* 103(47), pp. 17834-9.

Zha, X., Hu, Z., Ji, S., Jin, F., Jiang, K., Li, C., Zhao, P., Tu, Z., Chen, X., Di, L., Zhou, H. and Zhang, H. (2015) 'NFkappaB up-regulation of glucose transporter 3 is essential for hyperactive mammalian target of rapamycin-induced aerobic glycolysis and tumor growth', *Cancer Lett,* 359(1), pp. 97-106.

Zhang, B., Zheng, A., Hydbring, P., Ambroise, G., Ouchida, A. T., Goiny, M., Vakifahmetoglu-Norberg, H. and Norberg, E. (2017a) 'PHGDH Defines a Metabolic Subtype in Lung Adenocarcinomas with Poor Prognosis', *Cell Rep,* 19(11), pp. 2289-2303.

Zhang, H., Gao, P., Fukuda, R., Kumar, G., Krishnamachary, B., Zeller, K. I., Dang, C. V. and Semenza, G. L. (2007) 'HIF-1 inhibits mitochondrial biogenesis and cellular respiration in VHL-deficient renal cell carcinoma by repression of C-MYC activity', *Cancer Cell,* 11(5), pp. 407-20.

Zhang, J., Jia, L., Lin, W., Yip, Y. L., Lo, K. W., Lau, V. M., Zhu, D., Tsang, C. M., Zhou, Y., Deng, W., Lung, H. L., Lung, M. L., Cheung, L. M. and Tsao, S. W. (2017b) 'Epstein-Barr Virus encoded Latent Membrane Protein-1 upregulates glucose transporter-1 transcription via the mTORC1/NF-κB signaling pathways', *J Virol*.

Zhang, L., Dai, F., Cui, L., Zhou, B. and Guo, Y. (2017c) 'Up-regulation of the active form of small GTPase Rab13 promotes macroautophagy in vascular endothelial cells', *Biochim Biophys Acta Mol Cell Res,* 1864(4), pp. 613-624.

Zhao, B., Mar, J. C., Maruo, S., Lee, S., Gewurz, B. E., Johannsen, E., Holton, K., Rubio, R., Takada, K., Quackenbush, J. and Kieff, E. (2011a) 'Epstein-Barr virus nuclear antigen 3C regulated genes in lymphoblastoid cell lines', *Proc Natl Acad Sci U S A,* 108(1), pp. 337-42.

Zhao, B., Maruo, S., Cooper, A., R Chase, M., Johannsen, E., Kieff, E. and Cahir-McFarland, E. (2006) 'RNAs induced by Epstein-Barr virus nuclear antigen 2 in lymphoblastoid cell lines', *Proc Natl Acad Sci U S A,* 103(6), pp. 1900-5.

Zhao, B., Zou, J., Wang, H., Johannsen, E., Peng, C. W., Quackenbush, J., Mar, J. C., Morton, C. C., Freedman, M. L., Blacklow, S. C., Aster, J. C., Bernstein, B. E. and Kieff, E. (2011b) 'Epstein-Barr virus exploits intrinsic B-lymphocyte transcription programs to achieve immortal cell growth', *Proc Natl Acad Sci U S A,* 108(36), pp. 14902-7.

Zhao, W., Prijic, S., Urban, B. C., Tisza, M. J., Zuo, Y., Li, L., Tan, Z., Chen, X., Mani, S. A. and Chang, J. T. (2016) 'Candidate Antimetastasis Drugs Suppress the Metastatic Capacity of Breast Cancer Cells by Reducing Membrane Fluidity', *Cancer Res,* 76(7), pp. 2037-49.

Zhou, H., Schmidt, S. C., Jiang, S., Willox, B., Bernhardt, K., Liang, J., Johannsen, E. C., Kharchenko, P., Gewurz, B. E., Kieff, E. and Zhao, B. (2015) 'Epstein-Barr virus oncoprotein super-enhancers control B cell growth', *Cell Host Microbe,* 17(2), pp. 205-16.

Zhu, Y., Li, T., Ramos da Silva, S., Lee, J. J., Lu, C., Eoh, H., Jung, J. U. and Gao, S. J. (2017) 'A Critical Role of Glutamine and Asparagine gamma-Nitrogen in Nucleotide Biosynthesis in Cancer Cells Hijacked by an Oncogenic Virus', *MBio,* 8(4).

Zhu, Y., Ramos da Silva, S., He, M., Liang, Q., Lu, C., Feng, P., Jung, J. U. and Gao, S. J. (2016) 'An Oncogenic Virus Promotes Cell Survival and Cellular Transformation by Suppressing Glycolysis', *PLoS Pathog,* 12(5), pp. e1005648.